The Performance Properties of Recycled Concrete in Road Pavement Materials

by
Zaandré Bredenkamp

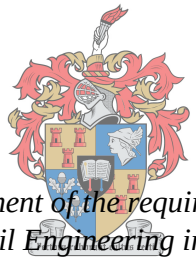

Thesis presented in fulfilment of the requirements for the degree of Master of Engineering in Civil Engineering in the Faculty of Engineering at Stellenbosch University

Supervisor: Mrs Chantal Rudman
Co-supervisor: Prof Kim Jenkins

March 2018

Plagiarism Declaration

By submitting this thesis/dissertation electronically, I declare that the entirety of the work contained therein is my own, original work, that I am the sole author thereof (save to the extent explicitly otherwise stated), that reproduction and publication thereof by Stellenbosch University will not infringe any third party rights and that I have not previously in its entirety or in part submitted it for obtaining any qualification.

Date: March 2018

Abstract

Due to a rise in population and industrialisation, the demand on infrastructure in developing countries have increased significantly. The world has been moving towards a more environmentally friendly and sustainable approach to provide the necessary infrastructure to sustain the economy. High quality natural aggregate is a finite resource with declining supply. It is therefore imperative that materials previously regarded as waste, should be recycled and reused. Large amounts of Concrete Demolition Waste (CDW) is created when old infrastructure is destroyed and this material placed in already constrained landfill sites. There has been a shift in perceptions of this material from being a waste to being a valued road construction material in recent years. Recycled Concrete and Masonry Aggregate are widely used in some developed countries, where good quality natural resources are scarce. However, in developing countries that have an abundance of good quality aggregate, but limited knowledge in the field of recycling, this material is often disregarded.

Builders' rubble that have been recycled, such as Recycled Concrete Aggregate (RCA), has shown to be an effective alternative material in structural pavement layers in other countries. In the South African industry, standards and guidelines towards the use of this material has not yet been developed and implemented.

The experimental design developed for this study, incorporated two different types of RCA material, the Unexposed material used from the crushing process, and Exposed material that has been treated with the aim to promote rapid self-cementation. In this study, laboratory triaxial tests, which included monotonic and permanent deformation tests were performed. The self-cementing potential of the material was investigated by using two different types of material. These materials were tested at different curing times to investigate the effect on the durability of the material.

It was found that RCA material, both Exposed and Unexposed, had large amounts of variability in terms of behaviour. The Exposed RCA more so than the Unexposed RCA. This can be attributed to the reduction in self-cementation potential and the variable dispersion of the cement particles left in the material after processing of the Exposed material. Both materials had very high shear strength parameter values (cohesion and friction angle). Results revealed that the shear parameters are not an indication of the material's ability to withstand permanent deformation, as was shown for the Exposed RCA material. The Exposed material exhibited similar shear parameters to the Unexposed material. However, the Deviator Stress Ratio for the Exposed material, where stable behaviour in the permanent deformation tests was observed, was much lower than that of the Unexposed material. This suggests that the material relies not only on the matrix of aggregate interlock, but possibly also on the cementitious bonds for shear strength and resistance to permanent deformation.

Using the results obtained from permanent deformation results, the best fit model could be identified. The critical parameters that influence the behaviour of RCA were identified as deviator stress ratio, moisture content and density. This has a direct effect on the magnitude of plastic strain in the material. The results from the permanent deformation tests were used to synthesise a transfer function for the Unexposed RCA material. This transfer function can be used to calculate the pavement life of RCA layers within a pavement structure.

Pavement analyses were performed on pavement structures that include RCA as either a base or subbase. These results were compared to three typical South African pavement structures. The transfer function that was developed was used to calculate the life for the pavement layers consisting of RCA materials. Although the DSR at which the material performs at satisfactory levels of permanent deformation is lower than that of standard granular materials used in pavement construction, the analysis yielded favourable results. Results showed that RCA material delivered reliable and achievable results for the use of this material in a pavement layer when compared to these standard pavements.

Opsomming

As gevolg van 'n toename in die bevolking en industrialisering, het die aanvraag na infrastruktuur eksponensieël gegroei. Veral in ontwikkelende lande is hierdie aanvraag noemenswaarding groot. Terselftertyd beweeg die wêreld na 'n meer omgewingsbewus en volhoubare aanslag om sodoende die nodige infrastruktuur te voorsien. Hoë kwaliteit aggregaat is 'n beperkte hulpbron met afnemende voorraad. Vir hierdie rede is dit van uiterse belang om materiaal wat van tevore beskou is as rommel, te herwin en hergebruik. Groot hoeveelhede Betonslopingsafval (CDW) word gegenereer met die afbreking van ou infrastruktuur. Tans word meeste van hierdie materiaal in stortingsterreine met reeds beperkte kapasiteit geplaas. In onlangse jare het die persepsie oor die materiaal geskuif van 'n materiaal wat gemors is tot 'n materiaal wat as 'n waardevolle padkonstruksiemateriaal gebruik kan word. In ontwikkelde lande waar hoë kwaliteit natuurlike aggregate 'n skaars hulpbron is, word materiaal soos Herwinde Betonaggregaat (RCA) en Herwinde Messelwerkaggregaat (RCM) reeds gebruik. Alhoewel, in ontwikkelende lande, waar daar baie keer 'n oorvloed van goeie kwaliteit materiaal is, maar 'n tekort aan kennis oor herwinning, word die materiaal dikwels oorsien.

Die gebruik van slopingsmateriaal soos RCA is bewys as 'n goeie alternatief vir beide die kroon- en stutlaag in ander ontwikkelde lande. In Suid-Afrika is standaarde vir die gebruik van die materiaal nog nie ontwikkel en geimplementeer nie.

Die eksperimentele ontwerp het twee tipes RCA materiaal ingesluit, naamlik die Onblootgestelde materiaal, wat direk na die opbreekproses gebruik word, en die Blootgestelde materiaal wat behandel word om die self-sementerings proses bevorder. In hierdie was triaksiale toetse, wat monotoniese en permanente vervormingstoetse insluit, uitgevoer. Die self-sementeringspotensiaal van die materiaal was ondersoek deur na verskillende kuurtydperke te kyk, omrede dit 'n direkte impak op die duursaamheid van die materiaal sal hê.

Dit was gevind dat beide die Blootgestelde en Onblootgestelde materiaal groot hoeveelhede variasie toon in terme van gedrag. Die Blootgestelde RCA het groter variasie getoon as die Onblootgestelde materiaal. Dit kan toegeskryf word aan die self-sementering en die veranderlike verspreiding van sement partikels in die materiaal. Albei die materiale het baie hoë skuifsterkte parameters opgelewer. Die resultate het ook gewys dat die skuifsterkte parameters nie gebruik word as 'n indikasie van die materiaal se weerstand tot permanente vervorming nie, en dit was spesifiek die geval met die Blootgestelde RCA. Die materiaal skuifsterkte parameters van die Onblootgestelde materiaal was vergelykbaar is met die van Blootgestelde materiaal. Tog is die hoeveelheid uitwykspanningsverhouding (DSR) waarby die Blootgestelde materiaal stabiele gedrag onderhewig aan permanente deformasie toetse getoon het baie laer as die van die Onblootgestelde materiaal.

Dit wysdat die materiaal moontlik nie slegs op die matriksvergrendeling staat maak nie, maar ook op die sementverbindings om weerstand te bied teen vervorming.

Deur gebruik te maak van die bevindinge uit die eksperimentele ontwerp, kan die beste pasmodel wat die langtermyn permanente vervormimgsgedrag van die materiaal voorspel, gevind word. Die kritiese parameters wat die gedrag van die materiaal beïnvloed is geïdentifiseer as die die DSR, voginhoud en die digtheid. Hierdie faktore het 'n direkte impak op die hoeveelheid plastiese vervorming wat in die materiaal ontstaan. Die resultate van die vervormingstoetse was gebruik om 'n ontwerpsfunksie te ontwikkel vir RCA materiaal. Die ontwerpsfunksie kan gebruik word om die plaveisellewe van RCA lae binne 'n plaveiselstruktuur te vind.

Plaveiselanalises was uitgevoer op plaveiselstrukture wat RCA materiaal as kroon- of stutlaag bevat. Die gedrag was dan vergelyk met drie tipiese plasveiselstrukture van Suid Afrika. Alhoewel die DSR waarby RCA materiaal voldoende funksioneer minder is as die van 'n granulêre materiaal, het die analises steeds gunstige resultate gelewer en die RCA materiaal betroubare en haalbare resultate toon.

Acknowledgements

I would like to extend my heartfelt gratitude to the following people, who have made an impact not only in my personal life but also in my academic future, without whom this Masters would not have been a success:

- My parents, Edna and Dutliff Bredenkamp, my mother who ensured my physical and emotional wellbeing during my academic career and father who passed on his analytical brain and love for engineering on to me
- My boyfriend Dian Page, who on many occasions motivated and supported me
- My study leader, Mrs Chantal Rudman and my co-supervisor Prof Kim Jenkins. Mrs Rudman that always had a solution in trying times and a word of motivation. Prof Jenkins for the calming force that he is and for the different angle he sees in every situation
- The N3TC for funding my studies
- The Laboratory technicians, Colin, Gavin and Eric for their guidance and assistance in the material preparation
- My office colleagues, Elaine Goosen, Nina Agnello, and Ricki-Lee Beardmore, better friends and a better support structure I could not have asked for during my Maters

The biggest thanks of all goes to the Lord who protects and guides us through every endeavour in life.

Table of Contents

List of Figures

Appendix A

Appendix C

Appendix D

List of Tables

Appendix B

Appendix E

List of Abbreviations

ASR	Alkali Silica Reaction
BSM	Bitumen Stabilised Materials
CSH	Calcium Silicate Hydrate
CDW	Construction Demolition Waste
EMS	Equilibrium Moisture Content
HVS	Heavy Vehicle Simulator
ICC	Initial Consumption of Cement
Kt	Kilo-Tonne
LVDT	Linear Vertical Displacement Transducer
MDD	Maximum Dry Density
MESA	Million Equivalent Standard Axles
Mt	Mega-Tonne
MTS	Material Testing System
OMC	Optimum Moisture Content
PD	Permanent Deformation
PPP	Public Private Partnership
PS	Plastic Strain
RA	Reclaimed Asphalt
RCA	Recycled Concrete Aggregate
RCM	Reclaimed Concrete and Masonry
RD	Relative density
RLT	Repeated Load Test
SAMPDM	South African Mechanistic Pavement Design Method
SANRAL	South African National Road Agency Limited
SAPEM	South African Pavement Engineering Manual
TRH	Technical Recommendations for Highways
UCS	Unconfined Compressive Strength
UGMs	Unbound Granular Materials

List of Symbols

Greek upper case letters

$\Sigma\Delta^2$	Sum of least squares

Greek lower case letters

α	Constants dependent on the Road category and Reliability for Granular material transfer function
β	Constants dependent on the Road category and Reliability for Granular material transfer function
$d\varepsilon_a$	Incremental strains in the axial direction
$d\varepsilon_h$	Incremental strains in the radial direction
$\varepsilon_{a,i}$	Axial strain corresponding to the i^{th} point on the stress-strain loop
$\varepsilon_{a,i+1}$	Axial strain corresponding to the $(i+1)^{th}$ point on the stress-strain loop
ε_t	Tensile Strain
ε_r	Recovered/Resilient Strain
$\varepsilon_{s,p}$	Permanent shear strain
$\varepsilon_{1,p}$	Axial permanent strain
θ	Sum of principal stresses
σ_1^a	Applied major principal stress for waterbound macadam stress ratio
$\sigma_{d,f}$	Deviator stress at failure
$\sigma_{d,i}$,	Deviator stress corresponding to the i^{th} point on the stress-strain loop
$\sigma_{d,i+1}$	Deviator stress corresponding to the $(i+1)^{th}$ point on the stress-strain loop
$\sigma_{1,f}$	Principle stress at failure
σ_1	Principal vertical stress
σ_3	Confinement pressure
Ø	Diameter
φ	Friction angle
ω	Moisture Content

Latin upper case letters

A	Area
A	Limit value for permanent axial strain (Equation 2-12 and 2-16)
A_1	Material and stress-strain parameter (

C	Cohesion
F	Shift Factor that is based on the stress ratio
L	Stress path length
N	Number of Cycles
N_{actual}	Number of cycles obtained from laboratory tests
$N_{transfer}$	Number of cycles obtained from the transfer function
$P_{d,f}$	Applied force at failure
R^2	Coefficient of determination
R_f	Constant relating to compressive strength to a limiting stress difference
S	Saturation
SR	Stress Ratio

Latin lower case letters

a,b,c	regression parameters
h	Height
i:	i^{th} point on the stress-strain loop
k_1, k_2	Material coefficients
m	Mass
m'	Static failure line slope
n	grading coefficient
p	Mean normal stress
p^o	Modified normal stress
p^*	Stress parameter for the intersection of the static failure line and the p-axis in p-q space
p_{max}	Maximum mean normal stress
q	Deviator stress
q^o	Modified deviator stress
q_{max}	Maximum deviator stress
w:	unit energy dissipated per cycle within the material

Chapter 1: Introduction

1.1 Background

South Africa is a country rich in natural resources such as gold, manganese, platinum and diamonds. As in many other countries, an often overlooked resource is the presence of high quality natural aggregates. The construction and civil industry is responsible for 60% of the world wide consumption of natural resources (Bribian *et al.*, 2011). Pavement construction is highly dependent on the availability and quality of natural aggregates and therefore these materials are mined from borrowpits or quarries. As South Africa continues to develop and construct infrastructure, the demand for natural aggregates will increase, placing pressure on the natural supply. Much like any non-renewable resource natural aggregate production cannot continue at the rate that is currently provided, and alternative solutions must be found.

The effect of shortages in good quality natural aggregates can be seen in various developed countries such as The Netherlands, Great Britain and Dubai. A good example is The Netherlands, a country which is not self-supporting in terms of aggregate production. To sustain the construction industry, up to 40 Million tons of aggregate per year must be imported (Meulen *et al.*, 2005). Importing materials can be very costly and alternative solutions to the aggregate shortage is important. Many first world countries have successfully researched and implemented the use of alternative materials in the construction industry to reduce the need for natural aggregates. The use of materials from existing road pavements such as asphalt and good quality aggregate is a sustainable and cost effective solution.

There are various materials that can be recycled and introduced in the road construction industry in order to decrease the demand for natural aggregates. Reclaimed Asphalt (RA) is a good example of an alternative material that has been introduced into the construction process. However materials such as Recycled Concrete Aggregate (RCA) and Reclaimed Concrete and Masonry (RCM) are also a possible solution. The recycling of construction material is a relatively irregular practice in South Africa and little is known about the performance constraints of the material. In developing countries such as South Africa, less construction demolition waste is produced when compared to developed countries. The fact that there is no accepted standard practice for the reuse of CDW materials in South Africa is a deterrent for the production thereof. If road authorities accepted the use of CDW in pavement structures, more awareness would be created regarding the value for this material and more sources would become available.

According to the National Waste Baseline Report, South Africa landfilled 98 million tons of waste of the total 108 million tons waste produced, resulting in only 10% recycling of generated waste (Department of Environmental Affairs, 2012). The landfilling of waste is problematic as current landfill sites are overflowing. Finding new areas to construct landfills is proving difficult and a costly exercise. The Solid Waste Management Department of the Municipality of Stellenbosch quotes a value $\mathrm{R}450/\mathrm{m}^3$ of material waste, whereas the City of Cape Town indicates a figure of $\mathrm{R}350/\mathrm{m}^3$ (Cleghorn, 2015). According to the Department of Environmental Affairs (2012) a total of 4,725 million tons of Construction Demolition Waste (CDW) was produced across South Africa in 2011, of which only 16% was recycled.

The introduction of CDW, with particular reference to RCA in a pavement structure is a relatively new practice in South Africa. However there are many developed countries that have successfully re-used this material. This experience should be utilised when investigating the use of such materials in a local context. The Netherlands is a country that has successfully used both RCA and RCM in the subbase layers during pavement construction. Table 1-1 shows the amount of CDW produced in The Netherlands in million tons. In 2012, of the 25.71 Mt produced, 94% was recycled and only 477 Kt was disposed of in a landfill (Deloitte, 2015). The Netherlands imposes a ban on landfilling material that can be reused or incinerated to ensure effective recycling.

Table 1-1: Construction demolition waste generation in The Netherlands (Deloitte, 2015)

CDW generation data	2010	2011	2012
Hazardous CDW (Mt)	1.47	1.33	1.48
Non-hazardous CDW (Mt)	23.06	23.07	24.22
Total (Mt)	24.53	24.41	25.71

To improve cost effectiveness of a project, many South African contractors are partially recycling materials from a demolition or rehabilitation project. Transportation and dumping of these usable materials is unsustainable and inefficient especially as there is a cost incentive to be achieved in recycling these materials. Currently the only use for RCA is crushing and using it as a granular material in sidewalks or concrete production for road barriers. Internationally, developed countries have proven the inherent value of a product previously seen as waste. There is undeniable proof that RCA performs very well, not only in laboratory testing but also in practice. Unfortunately, very little

research has been done on the application of RCA and RCM as road materials in a South African environment but this is starting to change.

In a time where greater importance is placed on green engineering and finding renewal alternatives, greater emphasis must be placed on reusing material rather than dumping it. As development in South Africa increases and a larger strain is placed on the transport infrastructure it will become vital to use recycled materials. As the development in urban centres increase and outlying areas are demolished to create space, more of this material will become available. With extensive quality control processes, material of such quality can be produced so that it can be used in both the subbase and possibly the base of the pavement structure.

The University of Stellenbosch, together with Green Cape has been the driving force behind the inclusion of RCA as an alternative pavement material. This thesis links with some of the research already performed in this field, and aims to improve the knowledge on the performance parameters of RCA, as well as the self-healing properties induced by the self-cementing process.

1.2 Objectives

The primary objective of this study is to gain insights into the unique engineering properties of RCA that can be compared against those of granular and cemented materials. This will assist in gaining a reliable understanding of key performance attributes and sustainable design models for RCA.

The secondary objectives of this study can be defined as follows:

- To investigate the strength of RCA compared to conventional pavement materials;
- To use triaxial testing in order to determine the critical performance parameters, such as cohesion, friction angle, and resistance to deformation;
- To use permanent strain rate in order to obtain material categories in terms of stable and unstable behaviour upon repetitive loading;
- To perform specialised intermittent triaxial testing, with a variable time scale and exposure. This allows for measurement of the performance after the material has been subjected to a certain initial cyclic loading. The same material (sample) is subjected to an additional loading after an identified lapsed time period and curing process.
- To create a function that describes the permanent deformation of the material in order to quantify the RCA performance.

1.3 Limitations

The following factors negatively impacted the outcome of this project:

- The availability of good quality concrete resulted in only one source of concrete being tested, namely from the rehabilitated N2 highway. To crush, sieve, cure and test the samples are challenging and time-consuming limiting the scope of the research to only one source of material;
- The availability of the machinery and material only allows for 1 permanent deformation test per confinement pressure, unless an unexpected result is obtained;
- The triaxial machine can only apply constant confinement pressures, the confinement pressures in a road varies depending on the applied load;
- The availability of water in a drought stricken Western Cape, as the triaxial machine uses 800l/h of water. Additional water recycling systems had to be developed;
- Field testing was not be performed in order to benchmark between laboratory and field data;
- The crushing process performed in the laboratory is on a very small scale cannot simulate the exact crushing conditions experienced in the field.

1.4 Report Structure

This thesis report will consist of 7 chapters. The content of each chapter is briefly discussed below:

- Chapter 1 includes an introduction to CDW and more specifically RCA. This chapter provides a brief background, application and demand for this material, as well as the objectives and limitations of the undertaken study;
- Chapter 2 is a literature review on RCA as pavement material. It includes the factors that will influence the performance parameters and a background of the testing method. Some information will also be presented on dissipated energy and the Shakedown Theory in order to aid with the classification of material categories;
- Chapter 3 gives an outline of the testing methodology that was followed to acquire the relevant results. The material preparation procedures such as the crushing, sieving and reconstitution is also outlined;
- Chapter 4 discusses the results of all the triaxial tests performed, including the assessment of various permanent deformation models;
- Chapter 5 contains the synthesis of a transfer function for RCA material as well as a sensitivity analysis.

- Chapter 6 a comparison between pavement including various variables investigated, such as pavement configuration, layer thickness, and subgrade quality in order to obtain the pavement life of a pavement structure containing a RCA layer;
- Chapter 7 concludes the research and discusses the outcomes of the project providing recommendations on using this material in a pavement structure.

Chapter 2: Literature Review

2.1 Introduction

This chapter discusses the literature review that has been performed. The aim of the Literature Review is to gain knowledge on RCA materials and the behaviour response as part of the layerworks in flexible pavements. The technology is relatively new and has not been implemented in a South African context. An opportunity exists to investigate the behaviour and performance of these materials within the context of global pavements. Some research states that RCA can be classified as an unbound granular material, however due to the self-cementing properties of the material, it might exhibit characteristics of both unbound granular and cemented materials. The deformation behaviour and factors affecting the permanent deformation of the material is of particular interest. Previous research has shown that this is the most likely mode of failure for this material (Van Niekerk, 2002). For this reason it is measured against unbound granular performance properties. In order to measure the properties of unbound materials triaxial tests are employed. This chapter discusses the performance of these materials within the pavement system, taking cognisance of previous research including that of unbound granular materials. Thereafter, the different test methods, including the monotonic, resilient modulus and repeated triaxial load test are explained. Of particular interest is the application of various mathematical models as this will form the basis of the material comparisons in this thesis.

2.2 South African Pavement Structure

The manner in which pavements are constructed in South Africa differ significantly from the approach followed in Europe and America. A pavement in the South African context is less reliant on a thick asphalt layer and more on a good quality base and subbase layer. This is partly due to the high quality of natural aggregates in South Africa. A large proportion of pavements are built according to the inverted pavement concept, in which a granular base is placed upon a lightly cemented subbase. Other technologies such as Bitumen Stabilised Materials (BSM) are also available, although not widely used as more conventional materials. For the purpose of this research granular and cemented materials will be briefly discussed in particular the performance of the material. A brief discussion of RCA as a pavement layer is also included.

2.2.1 Unbound granular layer

Unbound granular materials can be classified into three sub-categories, namely natural gravels, gravel-soils and graded crushed stones (SANRAL, 2014a). Only natural gravels and crushed stones are used in the construction of the upper structural layer of a pavement. Gravel soils normally make up the in-situ subgrade or selected subgrade layers. Graded crushed stones are used to construct

granular base layers and the materials are obtained from an established quarry operation. There are strict criteria and standard developed for crushed stone. Quarry operations are closely monitored and a high degree of quality control is applied. Natural gravels are usually obtained from borrowpits close to the construction site with less stringent quality control.

The mechanism of failure of a granular layer incudes deformation due to the densification of the material, which induces a gradual shear deformation under repeated loading (SANRAL, 2014b). The South African Mechanistic-Empirical Pavement Design Method (SAMPDM) which is accepted as standard practice for pavement design in South Africa, proposes certain steps within its procedure. To evaluate granular layers, the standard approach dictates that the principle vertical stress (σ_1) and the major confining pressure (σ_3) is determined in the middle of the layer, as can be seen in Figure 2-1. To obtain these critical parameters linear-elastic software such as MePADS or Bisar can be used. This approach is further discussed in Chapter 6:. The stresses obtained from these software packages can be used to determine the shear stress state of the layer and can be compared to the shear strength of the material using the Mohr-Coulomb Model. These critical parameters can be used in the transfer functions as developed by Theyse (1996) to calculate the structural life of the pavement layer.

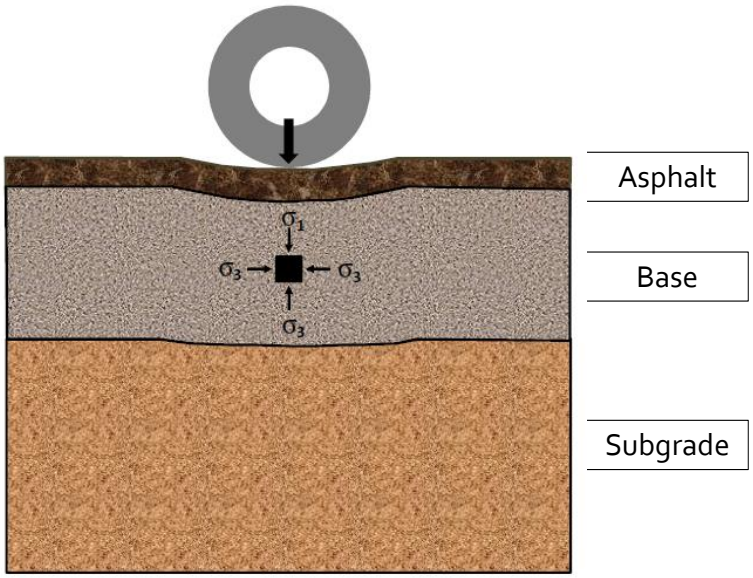

Figure 2-1 Critical evaluation parameters and locations within a granular layer adapted from SAPEM (2014b)

2.2.2 Bound cemented layer

In South Africa lightly cemented materials are mostly used in the subbase, as part of an inverted pavement. However, some examples of cemented base courses can be found as well. A lightly cemented material consists of natural gravel or crushed aggregate with a small percentage of added

cement. Cemented layers are classified by the notation C1-C4 with a reducing strength as the numerical value decreases. The Technical Recommendations for Highways (TRH) 14 (1985) specifies that at least a G6 material must be used to achieve a C3 or C4 quality stabilised material.

The failure mechanism and failure positions of a cemented layer is different to that of a granular layer. The most important factor to consider when looking at a cemented subbase, is the fatigue resistance. A cemented layer has two methods of failure, crushing at the top of the layer and fatigue at the bottom of the layer. The critical evaluation parameters are the major vertical stress (σ_1) at the top of the layer and the tensile strain (ε_t) at the bottom of the layer as shown in Figure 2-2."Although crushing is considered at the top of the cemented layer, and this is of particular interest when looking at bound base layers. Crushing is not considered a terminal condition for bound layers, and it is therefore not included in the critical layer calculations (Jenkins, 2016)."

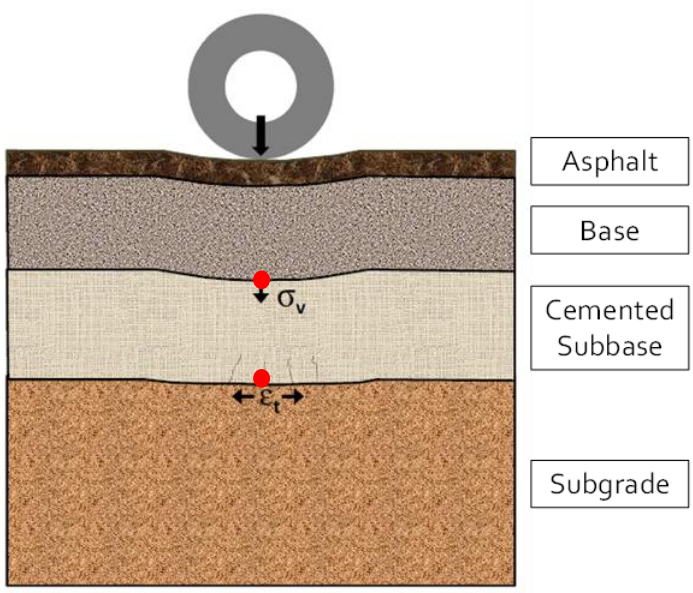

Figure 2-2: Critical evaluation parameters and locations within a cemented layer adapted from SAPEM (2014b)

The behaviour of a cemented layer changes over time as shown in Figure 2-3. A cemented material undergoes three phases during its life, namely the pre-cracked phase, effective fatigue life phase and the equivalent granular phase. A lightly cemented material is prone to cracks from various sources such as thermal cracking, fatigue cracking and shrinkage cracking. These mechanisms may cause microcracking throughout the layer. It is assumed (for design purposes) that when the material is loaded, cracks start predominantly at the bottom of the layer and propagate to the top of the layer. This is because of the probable stress situation, due to traffic for example, leading to a maximum vertical strain induced at the bottom after microcracks have formed throughout. Thicker layers will take longer for the cracks to propagate through the depth of the layer. The terminal condition is the

equivalent granular phase. This is when the material has cracked to such an extent that it is comparable to an unbound granular material according to Theyse (1996). The pre-cracked phase is short and is not included in the pavement life calculations. To calculate the pavement life for a cemented layer, a transfer function is used for both the second and third phase. The pavement life is calculated for the equivalent granular phase and this is added to the pavement life of the effective fatigue life to obtain the entire life of the layer.

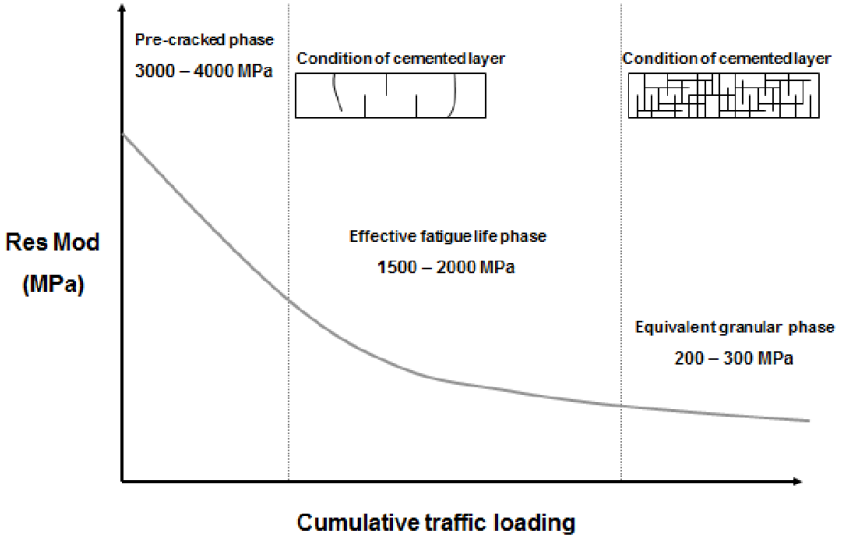

Figure 2-3: Long term behaviour of a cemented pavement layer (Jenkins, 2016)

2.2.3 Recycled Concrete Aggregate

The behaviour of RCA material under traffic loading is relatively unknown in a South African context. Due to the unknown behaviour of the material it is yet to be determined how RCA material performs within a pavement structure. RCA has been successfully implemented in several road construction projects in various countries, first as a drainage backfill material and as a bedding layer for footpaths, and later as a subgrade material (Nataatmadja & Tan, 2001). Although The Netherlands has successfully implemented the use of RCA in a pavement structure, it is important to note that the way in which they configure and construct pavements are significantly different from South Africa.

As previously mentioned RCA cannot with certainty be classified explicitly as a granular or cemented material. As a raw material RCA is utilised as a granular material, but once placed the latent cement in the RCA has the potential to significantly increase the strength of the material. In this case it might perform more like a lightly cemented layer. This potentially could be beneficial, but also, too much cementing could lead to challenges inherent to that of stabilised materials. The study of these potential concerns such as fatigue, cracking, shrinkage and carbonation, are not included in the scope of this research. It is still important that one is aware of the issues that may arise. Many researchers report on the self-cementing aspect particularly on the shear deformation and resilient properties.

However, in general, limited research has been performed and particularly the investigation on permanent deformation behaviour and classification of RCA. The most comprehensive of its nature is the research was performed by Van Niekerk (2002).

2.3 Deformation behaviour of Unbound Granular Materials

2.3.1 Stress state in Unbound Granular Material layers

At any given time, the stress state of a three dimensional material can be explained by 3 normal stresses and 6 shear stresses as shown in Figure 2-4 (a). It can be shown that for any general stress state, through any point in a body, three perpendicular planes exist on which there are no shear stresses (Werkmeister, 2003). In other words, it is possible to rotate the axes in such a way that there are no shear stresses acting on the cube. The resulting three normal stresses are known as the principal stresses $\sigma_1, \sigma_2, \sigma_3$ as shown in Figure 2-4 (b).The principal stresses are not dependent on the choice of co-ordinate system.

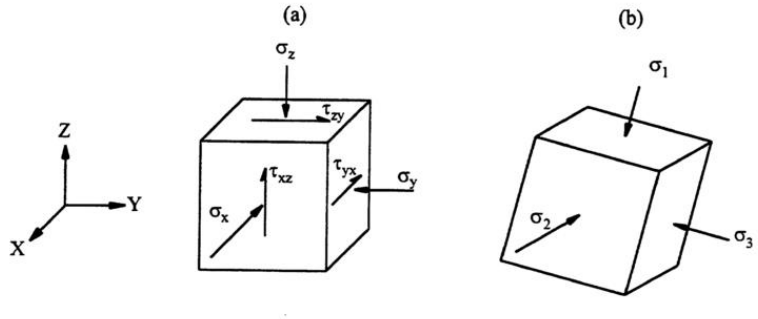

Figure 2-4: Stress components acting on an element (Lekarp & Dawson, 1997)

The rolling motion of a wheel causes a more complex stress situation than that described in Figure 2-4, due to the moving action of the load. A rolling wheel induces a stress pulse in the pavement structure. The stress pulse is made up of vertical, horizontal and shear stresses of fluctuating magnitudes. Figure 2-5 shows the stress pulse that is induced in the pavement structure. The shear stresses are reversed, and the principal axes are rotated as the wheel passes over the pavement. The principal stresses only act perpendicular to the surface of the cube directly beneath the wheel load.

The repeated load triaxial (RLT) is the most common way of simulating the real life loading conditions in the laboratory. The RLT can be used to simulate the vertical and horizontal loading conditions in a material, however it cannot simulate shear stresses or the principal axes reorientation that is induced in a pavement structure by a moving wheel. The force applied by the RLT is equivalent to the in-situ principal stresses directly under the wheel as seen in the middle of Figure 2-5 (Werkmeister, 2003).

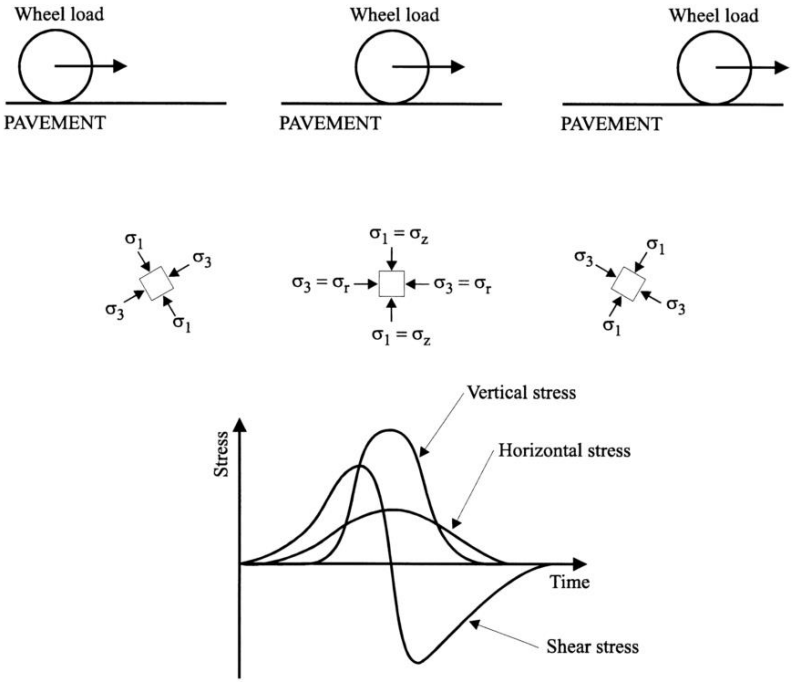

Figure 2-5: Stress induced in a pavement beneath a rolling wheel (Lekarp & Dawson, 1998)

The available literature on principal stress reorientation indicates that the reorientation results in larger permanent strains being induced to what is predicted by laboratory testing (Lekarp *et al.*, 2000a).

2.3.2 Deformation Characteristics of Unbound Granular Materials

Werkmeister (2003) concluded that the resistance to deformation of Unbound Granular Materials (UGMs) is a function of the applied stress. UGMs can experience strain hardening and strain softening and the type of behaviour is dependent on the magnitude of the applied stress (Figure 2-6).

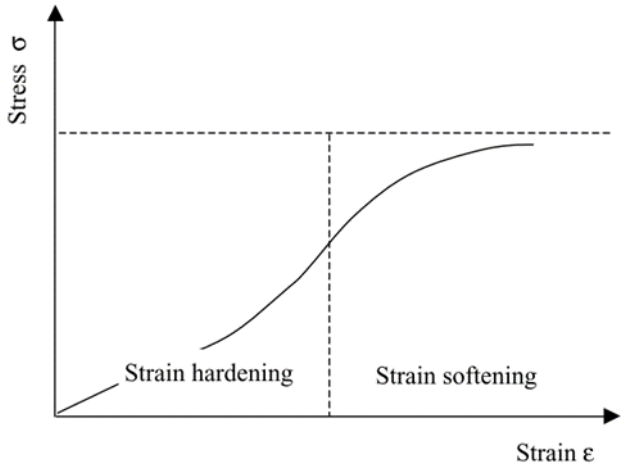

Figure 2-6: Stress-strain behaviour of granular materials (Werkmeister, 2003)

Strain hardening takes place at low levels of stress. The stiffness of the material increases as the applied load increases. Due to the applied force the particles of the UGMs are forced into new positions causing the material to be more densely packed and have a higher degree of aggregate interlock. If the stress increases in magnitude, to a level closer to failure, the material will undergo strain softening. During strain softening volumetric deformation will occur.

Due to the application of cyclic axle loads, granular materials undergo two phases of deformation, firstly resilient (elastic) strain and secondly permanent (plastic) strain as shown in Figure 2-7. Elastic strain is the deformation that is recovered at the end of the applied load, plastic strain is the component that is permanent and is accumulated as the amount of load cycles increases. Arnold (2004) found that the amount of permanent deformation will decrease as more load cycles are applied to the material.

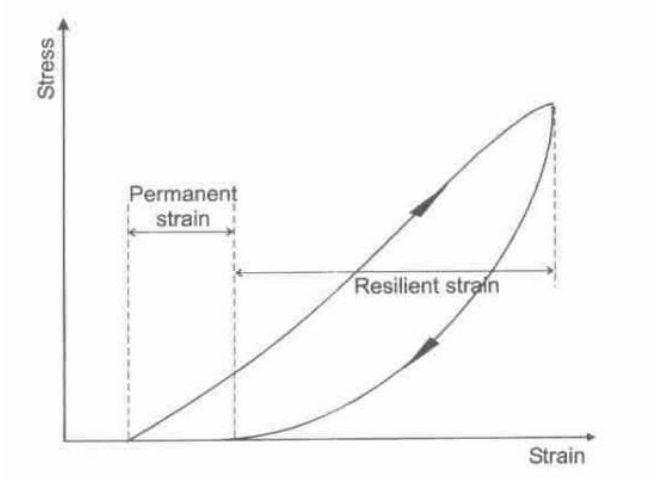

Figure 2-7: Resilient and Permanent strains in a pavement during one load cycle (Lekarp *et al.*, 2000b)

2.4 Deformation properties

There are various factors that influence the permanent deformation behaviour of unbound granular materials. Given that RCA can potentially exhibit properties of both granular materials as well as lightly cemented materials, the factors influencing the deformation properties of unbound granular materials is discussed in this section.

2.4.1 Physical properties

The permanent deformation behaviour of granular materials are affected by the physical properties of the aggregate particles, including the grain shape and the grain roughness (Werkmeister, 2003). The influences of grain shape and grain roughness will be discussed separately.

Grain Shape

The two main factors that affect the shape of the aggregate particles is the mineralogical composition of the parent material, as well as the method of crushing used to obtain the material. The origin of the material can be used to broadly define the particle shape into two different groups. The first group consists of natural sands and gravels and the second group consists of crushed materials. The natural gravels and sands have smoothed surfaces due to the transportation the material has undergone in riverbeds, beaches and deserts. Crushed aggregates can have very sharp surfaces due to the mechanical process used in the crushing procedure (Werkmeister, 2003). Allen (1973) investigated the plastic strain induced in different materials of the same density. He stated that rounded particles such as natural gravels and sands will undergo more plastic deformation than that of crushed particles. Barksdale and Itani (1989) identified four general groups of particles shapes; cubic, rod, disc and blade. They concluded that blade shaped crushed aggregate is slightly more susceptible to permanent deformation than other crushed aggregates. The data obtained by Barksdale and Itani (1989) compared with the conclusions made by Allen (1973), in that natural gravels are more susceptible to rutting. Van Niekerk (2002) developed a pictorial summary of the identification method to flatness, elongation and cubicity of a particles (when determined by a slot/bar sieve) as illustrated n in Figure 2-8. The shape of the particles not only affect the deformation properties but also the grading and density of the material (Van Niekerk, 2002).

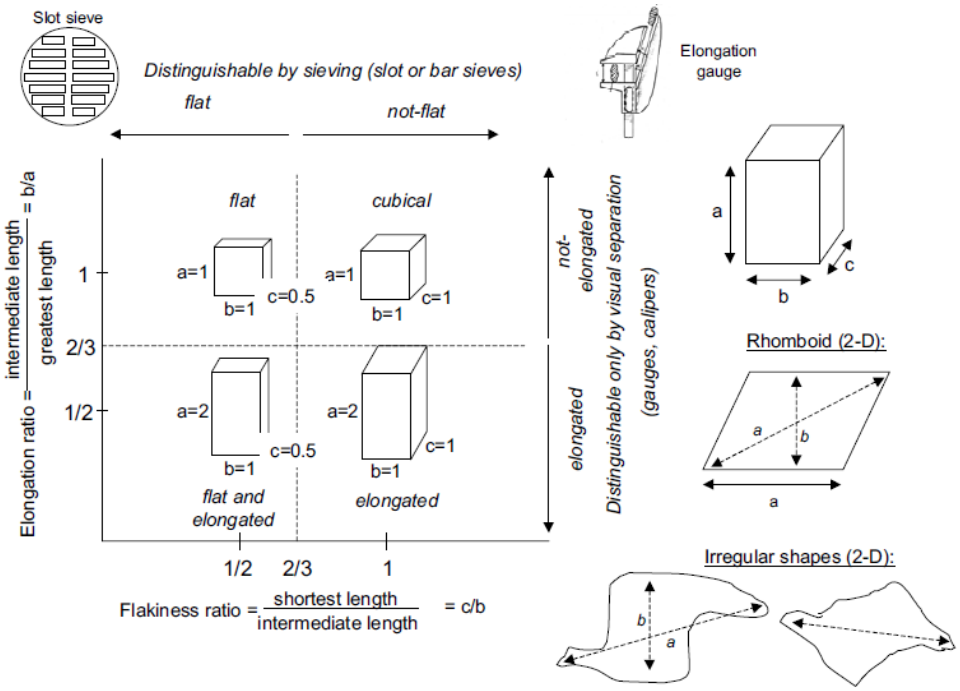

Figure 2-8: Flatness, elongation and cubicity of particles (Van Niekerk, 2002)

Grain Roughness

The grain roughness can be divided into micro and macro roughness. Micro roughness is the particle shape texture on a microscopic level (surface texture), whereas macro roughness is the particle angularity discernible through visual inspection. Tutumluer and Pan (2008) investigated the effect of angularity and surface texture on the permanent strains developed in a sample. They concluded that specimens which consisted of material with lower angularity and surface texture experience higher induced permanent strains, and that a rough surface texture is more beneficial during the initial shakedown or densification. The shakedown theory will be discussed further in Section 2.7. Shakedown occurs when no further deformation will occur in a material. The findings by Tutumluer and Pan (2008) agrees with findings by Thom and Brown (1989). They concluded that the macro surface roughness better relates to the material's ability to resist plastic strains. Werkmeister (2003) also found in her research that a sandy gravel with smooth surface had a lower permanent deformation resistance than crushed materials. Cheung (1994) explains that the reason for this is that the surface friction at contact points between particles affect the elastic deformation behaviour of the material. This is of particular importance when the applied load reaches the value where the particles start to slide over one another. A sandy gravel with smooth surfaces has lower amounts of surface friction and particles can easily slide over one another, resulting in a lower resistance to permanent deformation. Crushed materials have more angularity and will experience more friction between the particles which will results in higher resistance to permanent deformation.

2.4.2 Grading

The effect of grading and density on the permanent deformation is very closely linked to the amount of fines. The influence of the grading on the permanent deformation is in turn affected by the compaction and therefore the density of the material (Kotze, 2014). Kolisoja (1998) performed large scale triaxial tests and found that if the grading was adapted in such a way that the relative density was increased, the resistance to permanent strain would be increased. He also found that aggregates containing high percentages of filler (e.g. d<0.074mm >15%) showed a significant increase in permanent deformation, similarly with low fines content.

Uthus (2007) used five different grain size distributions as shown in Figure 2-9 to investigate the effect of gradation on the resilient modulus and permanent deformation of materials. The PPP line (a grading defined by Uthus used for a Public Private Partnership project in Norway) shows a well graded material. The results showed the interdependence of variables when investigating these parameters. Uthus (2007) found that the degree of saturation, the grading and the density play significant roles in

the resistance to permanent deformation. By comparing samples of the same degree of saturation, the effect of the grading is more prominent.

In her research, the material with a grading coefficient of n=0.5 showed significantly larger resilient moduli than the other two gradings. The materials with gradings PPP and n=0.35 showed similar behaviour for all deviator stress ratios even if the PPP sample has a higher density. Her work concluded that the resilient modulus is higher at drier states for the finer materials (n=0.35), however very sensitive as the degree of saturation increases. The permanent deformation showed the same trends in sensitivity to moisture whereby the material with a grading coefficient of n=0.35 rapidly declines in its resistance to elastic and plastic deformation when compared to a coarser material (n=0.5).

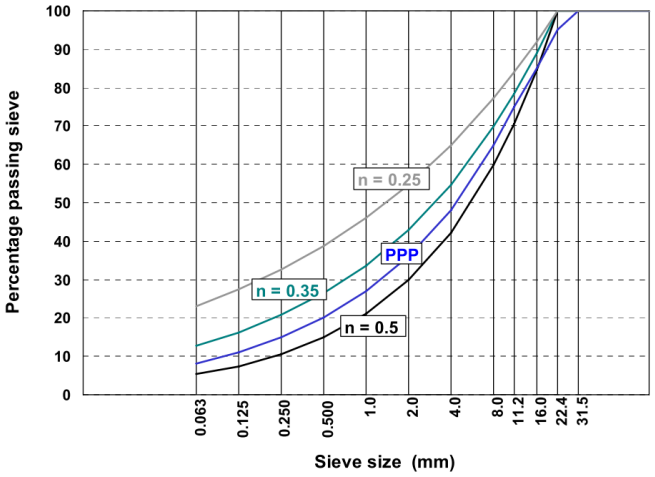

Figure 2-9:Grain size distribution of materials used by Uthus (2007)

The particle size distribution (gradation) is critical for the performance of unbound granular materials. Shear strength and load-spreading ability of an unbound granular material is determined by the friction between the material particles.

Thom and Brown (1988) concluded that as the size of the particle increases, the contact area between the particles decreases resulting in less permanent deformation and consequently higher stiffness. This means the impact of particle size distribution on permanent deformation relies on the level of compaction.

2.4.3 Filler Content

Various researchers have investigated the effect that the amount of filler (d<0.075mm), as well as the plasticity of the filler has on the permanent deformation of a material. Thom and Brown (1988), Barksdale (1989) and Uthus (2007) concluded that the resistance to permanent deformation decreases as the amount of filler is increased.

Barksdale and Itani (1989) investigated the effect of the plasticity of the filler by adding a predetermined percentage of either kaolinite or bentonite to the material. In the case of kaolinite it was observed that the permanent strain could increase as much as 3 times if the percentage of kaolinite in the fines was increased from 0 to 75%. Although plasticity will not be present in Recycled Concrete Aggregate, it could potentially be in Recycled Concrete Masonry and potentially considered as a variable that could have an influence on the performance. Most masonry bricks obtained from commercial sources are "fully baked in the production process" and plasticity in the fines absent. This might be different with more informal brick sources, particularly in the South African environment, for example bricks produced in more rural settings. In the case of construction demolition waste, the influence of fines and filler could also be significant as stated by Paige-Greene (2010). The influence of this is further discussed in Section 2.9.

2.4.4 Density

The achieved dry density of a material is dependent on various material properties such as grain size, shape and gradation as well as the amount of filler and/or fines and moisture content. The compaction method and compactive effort will also have an influence (Hoff *et al.*, 2003). Barksdale-(1972) investigated the permanent deformation of various granular materials and concluded that a material can experience up to 185% permanent axial strain if compacted to 95% and 100% of the maximum density, respectively. Thom and Brown (1988) investigated the influence of compaction and grading on the resistance to plastic strain in granular materials. As seen in Figure 2-10, material that was heavily compacted resulted in less permanent strain developing in the material, when compared with the lightly compacted or uncompacted material. They found that grading played a prominent role when the material was uncompacted compared to highly compacted materials. For highly compacted materials, all gradings performed similarly.

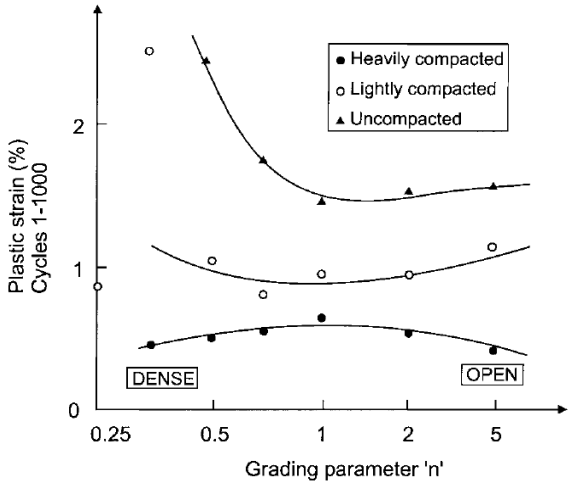

Figure 2-10: Effect of grading and compaction on the permanent deformation of granular materials (Thom & Brown, 1988)

2.4.5 Moisture content

There is always a certain amount of water present in UGMs. The correct amount of water allows for easier compaction and placement of particles. The amount of water needed to achieve the maximum dry density at a specific Proctor compactive effort is known as the optimum moisture content for that material (SANRAL, 2014a). If the optimum amount of water is present within a material it can have a beneficial result in terms of strength and stiffness. However, if the moisture content increases beyond the optimum level and saturation is neared, positive pore water pressure can develop under repetitive loading. Various researchers have concluded, from laboratory and field studies that at saturation level the pore water pressure increases and the effective stress decreases. This results in a lower stiffness as well as less resistance to permanent deformation (Lekarp *et al.*, 2000a). Figure 2-11 shows the permanent deformation triaxial test results of two samples. The one sample was allowed to drain (similar to in-situ conditions) and the other sample was kept at the original moisture content. The undrained sample experienced larger amounts of permanent deformation than the drained sample.

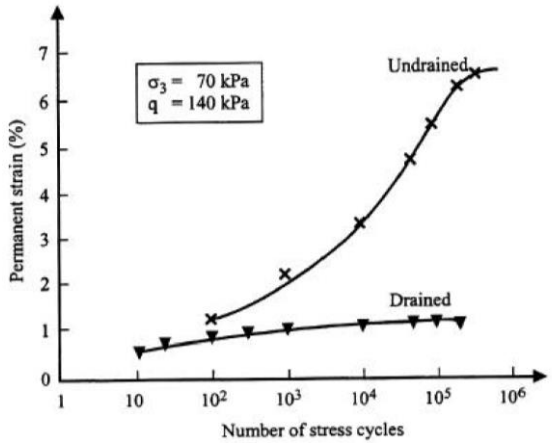

Figure 2-11: Influence of drainage on the development of permanent strain (Werkmeister, 2003)

Thom and Brown (1987) investigated the effect of moisture on the structural performance of road bases of crushed limestone. The study concluded that even a small increase in moisture content could result in a larger than anticipated increases in the permanent strain. They attributed this to the fact that a small increase in moisture would not necessarily result in excess pore water pressure forming, however the increase in moisture could act as a lubricant for material particles.

2.4.6 Number of Applied Cycles

The number of load repetitions, in conjunction with stress conditions, are one of the most important factors of UGMs affecting the resistance to permanent deformation. Here the Shakedown Theory can be incorporated to define the behaviour of the material. Although discussed briefly in the paragraphs that follow greater detail is provided in Section 2.7. Various researchers have reported

that the permanent deformation continuously increases with the number of applied load cycles, however, there are some conflicting opinions on the stabilisation of strain and when this occurs. One of the earliest studies by Morgan (1966) reported that permanent strain continued to increase after 2 million load cycles. Barksdale (1972) found a logarithmic relationship between the cumulative permanent deformation and the amount of load cycles. He cautioned that the plastic strain accumulation may exhibit a rapid and unpredicted increase. He argued that the permanent axial strain increases linearly with a logarithmic number of load cycles and this can be classified as Shakedown Theory Range B.

Paute et al (1996) found that the rate of increase of permanent strain in a granular material subjected to repetitive loading, decreases to the point that one is able to define a limit value for the accumulation of permanent strain. The curve representing the accumulated permanent strain will approach an asymptote with a limiting value. The number of load repetitions that has to be completed for a successful test, plays a significant role in the behaviour of the material. The findings by Paute et al (1996) also supports the finding that the material performs within Range B of the Shakedown Theory.

Kolisoja (1998) made two findings regarding the number of applied cycles for granular materials. Firstly, he found that samples that exhibited stable behaviour, stabilised after 80,000 cycles and performed in Range A behaviour of the Shakedown Theory as shown in Figure 2-12.

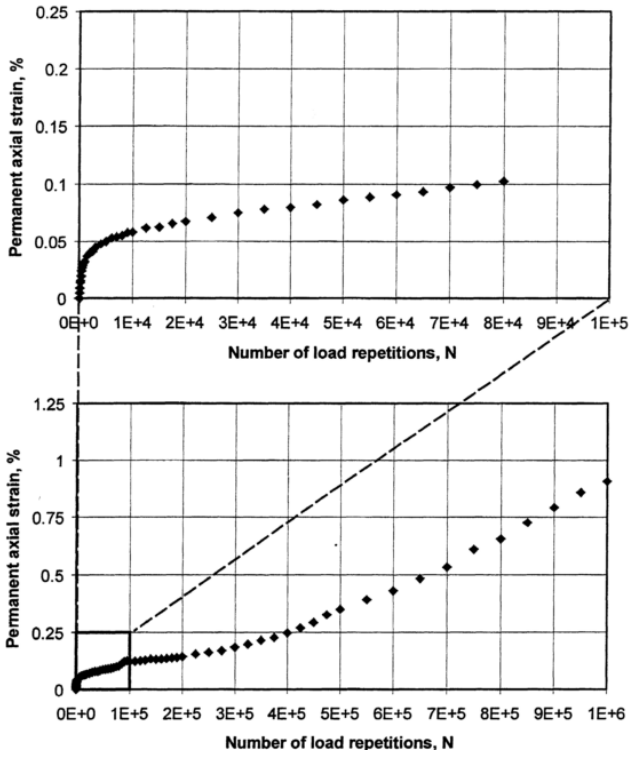

Figure 2-12: The effect the number of load cycles has on the permanent axial strain (Kolisoja, 1998)

However, with additional load cycles, a progressive linearity of the strain plot is observed for further permanent deformation as seen in Figure 2-12.

Secondly he concluded that development of the permanent strain may not be predicted using a simple function as a material may appear to be approaching a stable condition when it suddenly becomes unstable under additional loading, this is shown using Range C of the Shakedown Theory.

2.4.7 Stress History

The permanent deformation resistance of a granular material is directly dependent on the stress history. The stress history of a material is indicative of the order of magnitude of load applications. Brown and Hyde (1975) investigated the effect of stress history on granular materials by changing the magnitude and order of loads during triaxial testing. The study concluded that the induced permanent strain, from a gradually increasing stress level, is smaller than if the highest stress is applied immediately to the material as shown in Figure 2-13. During a repetitive loading test the effect of stress history result in the material stiffening caused by each applied load, which reduces the proportion of resilient to permanent strains (Lekarp *et al.*, 2000a).

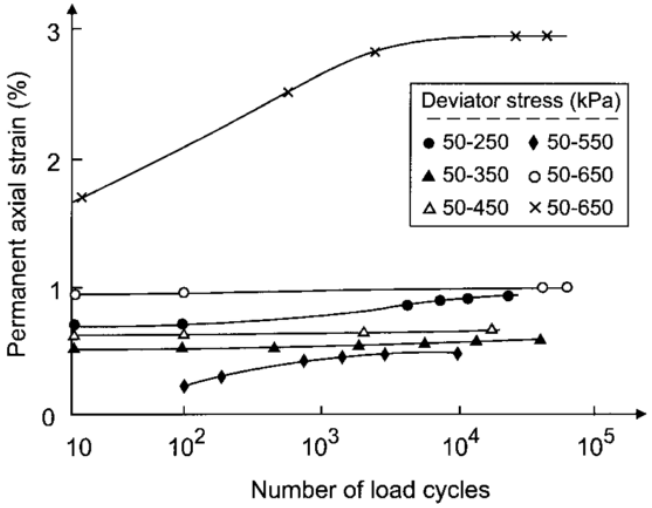

Figure 2-13: Effect of stress history on the permanent deformation of granular materials (Lekarp *et al.*, 2000a)

2.5 Triaxial Testing

The triaxial test is globally accepted as the most accurate way in which to simulate the effect of a moving vehicle on a pavement material. The triaxial test simulates the confined state in which the material is found in a pavement structure. The material is subject to three compressive stresses that

act perpendicular to each other. A confinement stress is applied by air pressure and principal stresses applied by means of an actuator. The triaxial apparatus is shown in Figure 2-14.

The triaxial testing technology has improved to such an extent that various tests can be performed using the same apparatus to obtain various material properties. Various sample sizes can be tested using this setup, with diameters ranging from 75 mm to 300 mm and heights varying from 150 mm to 600 mm (Kotze, 2014). Typically a rule of thumb is applied that the height of the sample should be twice the diameter of the specimen in order to get accurate results. The benefits of using a cylindrical sample are firstly that it simulates the column of compressed material under the wheel load. Secondly it allows for the maximum and minimum principal stresses (σ_2 and σ_3) to be equal to the confinement pressure which simplifies the analysis of results (Kotze, 2014).

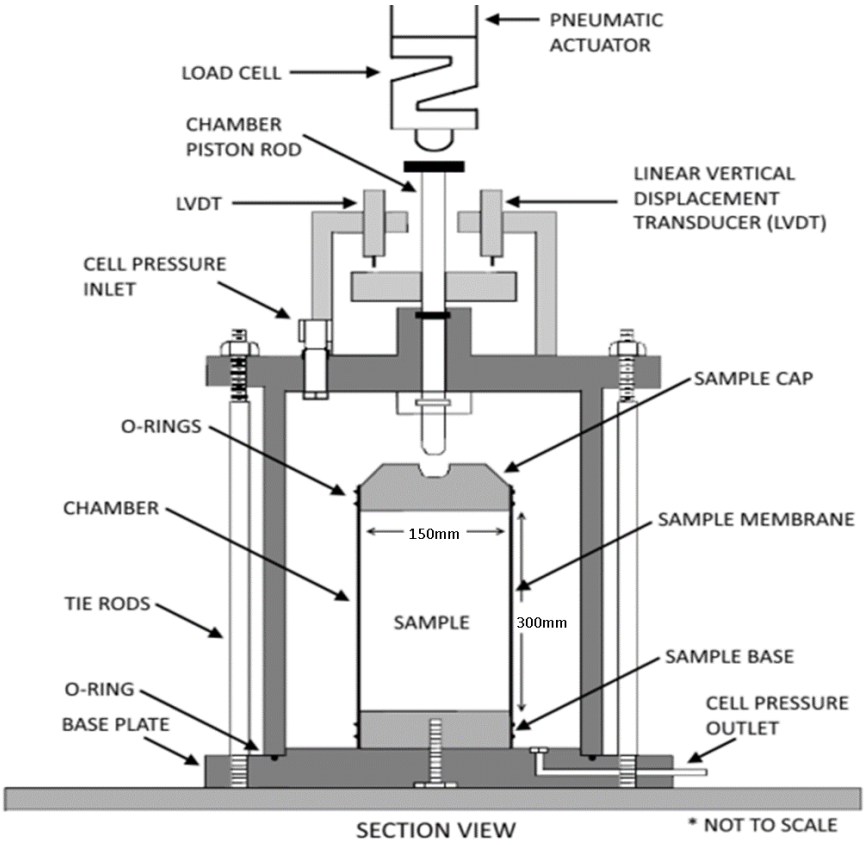

Figure 2-14: Schematic of the triaxial test apparatus, adapted from Munro & Mohajerani (2016)

To perform permanent deformation testing the movement of the wheel must be simulated using a force pattern that closely resembles the loading and unloading of a moving vehicle. The load that most accurately describes the motion of the wheel is identified as a haversine pulse, as shown in Figure 2-15. A force is applied to the sample for 0.1 second followed by a rest period of 0.9 seconds

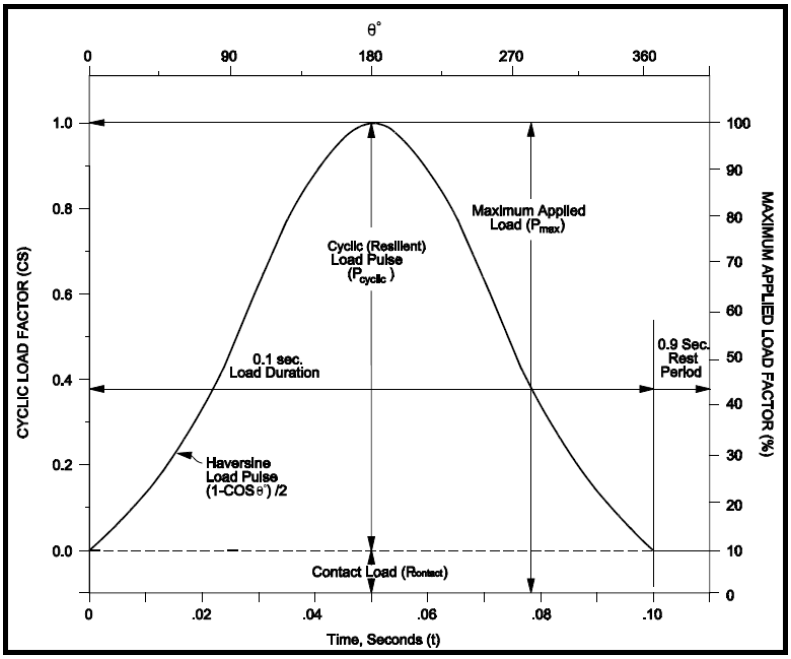

Figure 2-15: Haversine pulse used in triaxial testing (Federal Highway Administration Resarch and Technology, 2007)

The triaxial test setup can be used to perform three main types of tests and each test is used to obtain different material properties. The tests are as follows:

1. Monotonic Testing is when a sample is loaded with a force at a constant loading rate until the sample cannot withstand the applied force. This ultimate force is used to calculate the shear strength parameters of the material, i.e. the Cohesion (c) and Friction angle (φ);
2. Resilient Modulus Testing (M_r) is used to formulate an equation that can be used to determine the Resilient Modulus given a set of stress conditions. The shear parameters are used to obtain the deviator stress, the material is then loaded with forces that are increasing in deviator stress magnitude as well as at increasing confinement pressure;
3. Repeated Load Test (RLT) is used to evaluate the permanent deformation of material by applying a force in terms of a haversine pulse for a large number of cycles.

Only Monotonic and Repeated Load Tests are performed in this study, but all three are briefly discussed.

2.5.1 Monotonic Testing

During a Monotonic test the vertical axial load (force that induces the maximum principal stress (σ_1)) is applied to obtain a constant deformation or constant strain rate. For granular materials a sample is loaded at a rate of 3mm/min, and the maximum load is obtained when the material breaks. To obtain

the shear strength parameters at least 3 specimens are needed at different confinement pressures. However for reliability of results more tests are needed, as tests are performed at different confinement pressures ranging from 0 kPa to 200 kPa. Figure 2-16 shows the stress-strain graph for two samples, one was tested at a high confinement pressure and one was tested at a low confinement pressure. Similarly to what is experienced in road layer, a higher confinement pressure results in a higher failure load. Whereas a lower confinement pressure results in a lower failure load for the same material.

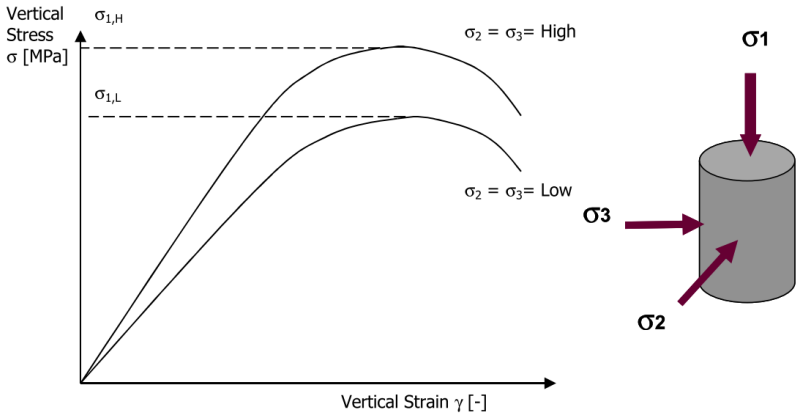

Figure 2-16 : Stress vs. Strain graph obtained from Monotonic testing (Jenkins, 2016)

The results obtained for the ultimate load of during the test can be reworked to provide the deviator stress $\sigma_{d,f}$. One should note that the conversion from the force results obtained from the triaxial test already includes the contribution of the confinement and therefore present the deviator stress ($\sigma_1 - \sigma_3 = \sigma_{d,f}$) the Monotonic test results can be plotted to obtain the Mohr Coulomb presentation as shown in Figure 2-17.

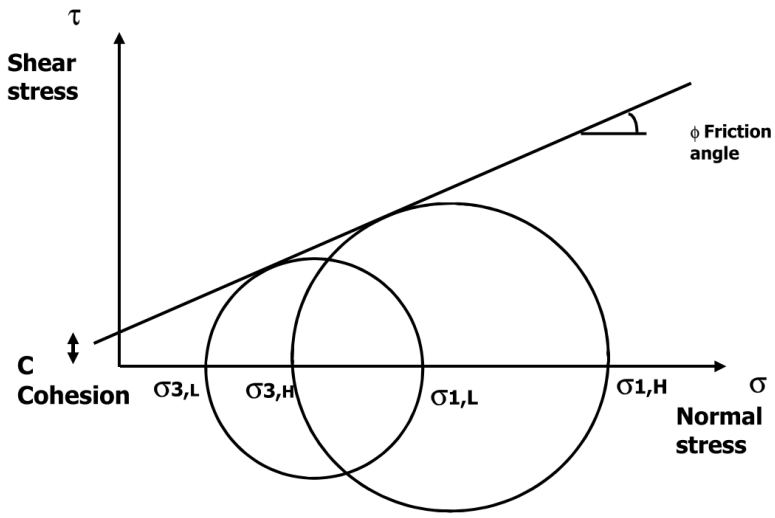

Figure 2-17: Mohr Coulomb plot for two monotonic tests (Jenkins, 2016)

The Mohr Coulomb Model uses the failure stress and the confinement pressure to plot a circle for each test. A straight line is drawn that is tangential to each circle to find the failure envelope. The slope of the line represents the friction angle (φ) and the intercept with the y-axis indicates the cohesion (c). The tangential line is known as the failure envelope as stress values above this line will lead to failure. The modelling of Monotonic Test results are discussed in Section 3.6.4.

2.5.2 Resilient Modulus Testing

During the Resilient Modulus Test the reaction of the specimen to various loads at increasing confinement pressures are tested. The same confinement pressures used for the Monotonic tests are used, and the applied loads are the deviator stress ratios as obtained using the shear stress parameters. The deviator stress ratio is calculated using the deviator stress divided by the deviator stress at failure for the same confinement pressure ($\sigma_d/\sigma_{d,f}$). In traditional approaches the elastic properties of materials are defined by the Modulus of Elasticity (E) and the Poisson's ratio (υ), for granular materials the Modulus of Elasticity is replaced by the Resilient Modulus (M_r) to indicate the non-linearity (i.e. the stress dependant behaviour) of granular materials (Lekarp *et al.*, 2000b). The M_r calculation and the graphical presentation is shown in Equation 2-1 and Figure 2-18, respectively.

$$M_r = \frac{\Delta(\sigma_1 - \sigma_{3)}}{\varepsilon_r} \qquad 2\text{-}1$$

Where:

σ_1: Major Principal Stress (kPa)

σ_3: Minor Principal Stress (kPa)

ε_r: Axial Strain to be recovered

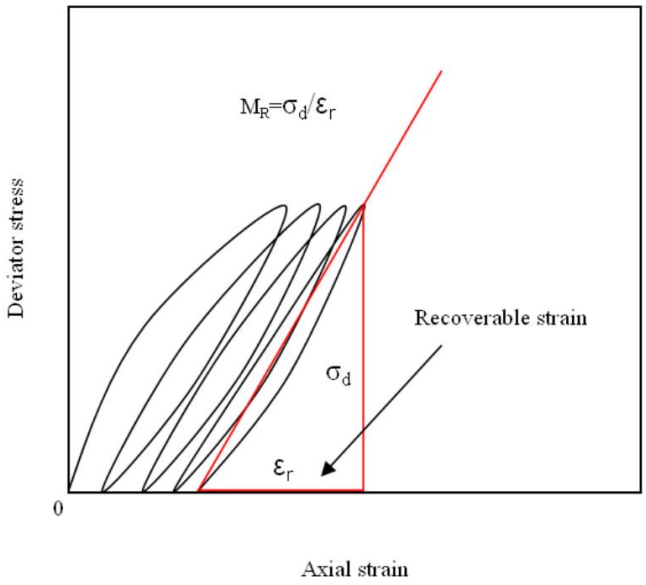

Figure 2-18: Graphic presentation of Resilient Modulus (Li *et al.*, 2010)

The simplest model used for Resilient Modulus calculations is the Mr-θ model. The results obtained from a triaxial test is plotted on a double logarhitmic scale to obtain a straight line as shown in Figure 2-19.The mathematical expression for the Mr-θ model is given by Equation 2-2 However, this simple model has been proven to be inaccurate as this straight line phenomenon is not observed during triaxial testing, there are various other models that are better suited but not explained futher within the scope of this study.

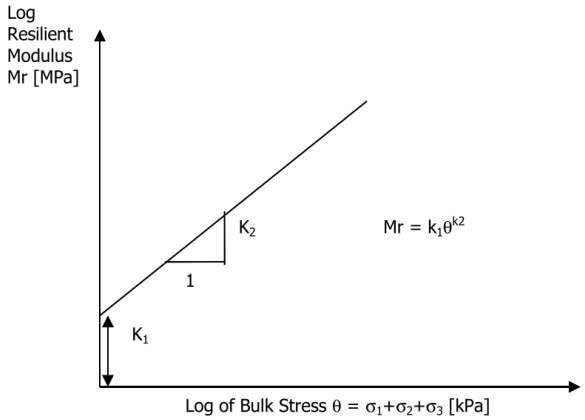

Figure 2-19: Mr- θ Model for the Resilient Modulus (Jenkins, 2016)

$$M_r = k_1 \theta^{k_2} \qquad 2\text{-}2$$

Where:

k_1, k_2: Material coefficients

θ: Sum of principal stresses (kPa)

2.5.3 Permanent Deformation Testing

The Permanent Deformation (PD) test is integral in predicting the plastic strain of a granular material. The application of the haversine pulse of a PD test simulates the repetitive movement of a wheel. To analyse the deformation response of a material various samples of the same material are tested at different deviator stress ratios and different confinement pressures. The samples are tested for a predetermined period of time, depending on the amount of cycles that must be completed and the frequency at which the load cycles are applied. During a PD test there is gradual accumulation of permanent strain with the number of load applications.

As shown in Figure 2-20, the shear parameters are used to draw the failure envelope, which in conjunction with the confinement pressure the deviator stress at failure ($\sigma_{d,f}$) can be found.

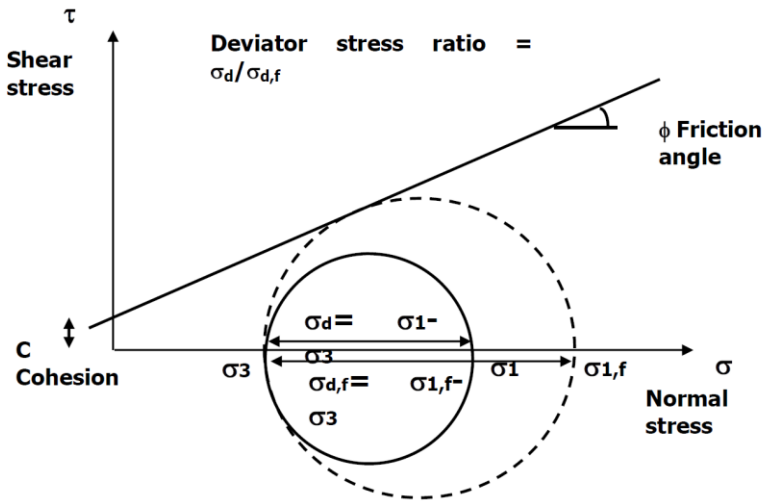

Figure 2-20: Deviator Stress Ratio (Jenkins, 2016)

Equations 2-3 to 2-6 can be used to calculate the deviator stress ratio. The deviator stress allows one to test the material at a percentage of the failure load.

$$\sigma_{1,f} = \frac{(1 + sin\varphi) \cdot \sigma_3 + 2Ccos\varphi}{(1 - sin\varphi)} \quad 2\text{-}3$$

$$\sigma_d = \sigma_1 - \sigma_3 \quad 2\text{-}4$$

$$\sigma_{d,f} = \sigma_{1,f} - \sigma_3 \quad 2\text{-}5$$

$$DSR = \frac{\sigma_d}{\sigma_{d,f}} \quad 2\text{-}6$$

As each load is applied to the sample, plastic strain and elastic strain is induced in the material as shown in Figure 2-7. The elastic strain is recoverable whereas the plastic strain is accumulated in the material. From Figure 2-21 the accumulation in plastic strain, and the changes in elastic strain during a PD can be seen. The changes in strain is used to calculate the axial deformation and classify the material according to the Shakedown Theory.

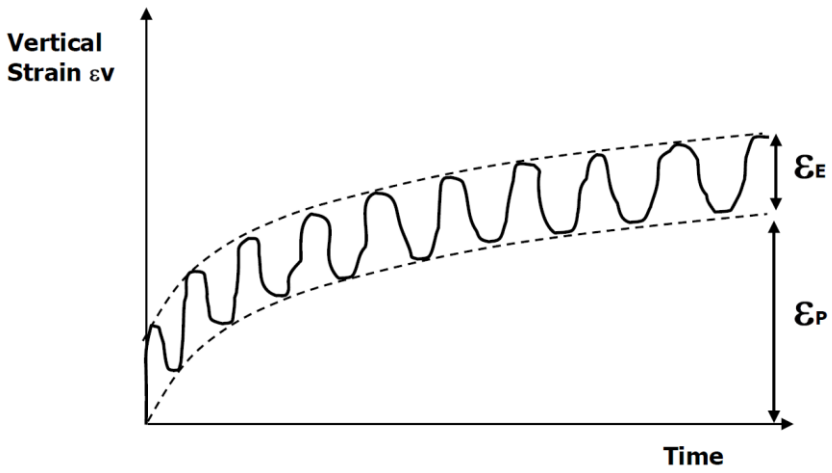

Figure 2-21: Permanent Deformation test results (Jenkins, 2016)

If the stress levels are low, the material will initially undergo a high amount of permanent deformation due to some compaction. The deformation will reduce as the number of load cycles are increased until a stable condition is reached as seen in Figure 2-22 (a). Given that all conditions stay the same the material can maintain this stable condition where the accumulated strain falls below a certain strain limit and the changes in strain approaches zero. At higher stress levels the accumulated strain continues to increase after the initial compaction and this will lead to the failure of the material as seen in Figure 2-22 (b)

.

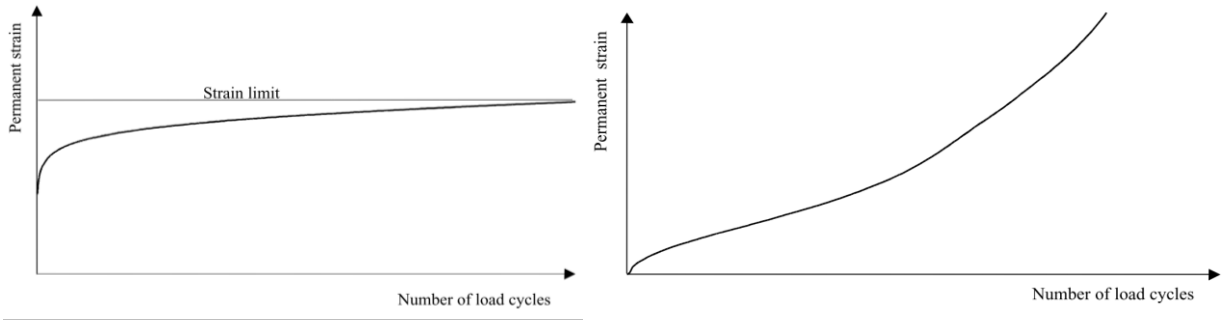

Figure 2-22: (a) Stable conditions at low stress (b) unstable conditions at high stress levels (Werkmeister, 2003)

2.6 Permanent Deformation Models

The purpose of modelling the long term dynamic response of materials is to find a relationship which best describes the gradual accumulation of plastic strain as a function of the number of load repetitions while emphasising the important role that the stress conditions play (Lekarp *et al.*, 2000a). The plastic deformation can be modelled in two ways, firstly with respect to the number of load cycles

and secondly with respect to the stress conditions. Lekarp (2000a) reviewed various models and these models are be discussed in the following sections.

2.6.1 Models in terms of Load Applications

Barksdale (1972) performed RLT on various base course materials to investigate the deformation behaviour and tested to 10^5 load cycles. He found that the accumulation of plastic strain was proportional to the logarithm of the number of load cycles, and followed the lognormal relationship in Equation 2-7.

$$\varepsilon_{1,p} = a + b\log(N) \qquad 2\text{-}7$$

Where:

$\varepsilon_{1,p}$: Axial permanent strain

a,b: Constants for a given deviator stress and confinement pressure

N: Number of load cycles

Veverka (1979) found a correlation between the elastic and plastic behaviour of granular materials. He proposed the simple relationship in Equation 2-8.

$$\varepsilon_{1,p} = a\varepsilon_r N^b \qquad 2\text{-}8$$

Where:

$\varepsilon_{1,p}$: Axial permanent strain

ε_r: Resilient strain

a,b: Constants for a given deviator stress and confinement pressure

N: Number of load cycles

Sweere (1990) studied the long term behaviour of unbound granular materials and sands in base courses and could not confirm the equations as stated by Veverka (1979) or Barksdale (1972). He performed repeated load tests applying 10^6 cycles and found the lognormal approach did not represent his data, and suggested that for larger number of load cycles a log-log approach would be more appropriate as in Equation 2-9.

$$\varepsilon_{1,p} = aN^b \qquad 2\text{-}9$$

Where:

$\varepsilon_{1,p}$: Axial permanent strain

a,b: Constants for a given deviator stress and confinement pressure

N: Number of load cycles

Khedr (1985) researched the permanent deformation development in crushed limestone at variable confinement pressures. Similar to Ververka (1997), the fundamental development of this model included consideration of both the plastic and elastic strain in the material. He concluded that the rate of permanent strain accumulation is inversely proportional to the logarithm of the load cycles as seen in Equation 2-10

$$\frac{\varepsilon_{1,p}}{N} = A_1 N^{-b} \qquad 2\text{-}10$$

Where:

$\varepsilon_{1,p}$: Axial permanent strain

A_1: Material and stress-strain parameter (function of the stress state and the resilient modulus)

a,b: Constants for a given deviator stress and confinement pressure

N: Number of load cycles

Wolff (1992) a South African researcher, performed full scale heavy vehicle simulator tests for millions of cycles. He identified two phases of strain build up in the material. For the initial 1,200,000 cycles a rapid increase in permanent strain was observed with a continuous decrease in the strain rate. The second phase consist of significantly slower strain development, and the strain approaches an asymptotic value. He found that the log-log approach was insufficient to predict the second phase of his findings. Wolff and Visser (1994) developed the stress-strain model in Equation 2-11. This research is based on South-African material and therefore is a better suited model to investigate.

$$\varepsilon_{1,p} = (cN + a)(1 - e^{-bN}) \qquad 2\text{-}11$$

Where:

$\varepsilon_{1,p}$: Axial permanent strain

a,b, c: Constants for a given deviator stress and confinement pressure

N: Number of load cycles

Paute (1996) suggested that the permanent strain approached an asymptotic value and the permanent strain after the first 100 cycles could be modelled using Equation 2-12. The permanent strain approaches a limit value denoted by A as the number of load cycles increase. Lekarp (1997) investigated this model and concluded that it is only valid at low deviator stress ratios.

$$\varepsilon_{1,p} = A\left(1 - \left(\frac{N}{100}\right)^{-b}\right) \qquad 2\text{-}12$$

Where:

$\varepsilon_{1,p}$: Axial permanent strain

A: Limit value for permanent axial strain

b: Constants for a given deviator stress and confinement pressure

N: Number of load cycles

Huurman (1997) found that many of the permanent deformation models were only applicable if the material exhibited stable behaviour. He added a second term to the log-log approach model developed by Sweere (1990) to better account for unstable behaviour as well as higher confinement pressures. Equation 2-13 can be used to model both stable and unstable behaviour. If a material exhibits stable behaviour the model will be governed by the first term. If the material exhibits unstable behaviour the first and second term will govern the behaviour.

$$\varepsilon_{1,p} = a\left(\frac{N}{1000}\right)^{b} + c\left(e^{d\left(N/1000\right)} - 1\right) \qquad 2\text{-}13$$

Where:

$\varepsilon_{1,p}$: Axial permanent strain

a, b, c, d: Constants for a given deviator stress and confinement pressure

N: Number of load cycles

2.6.2 Models in terms of Stress Conditions

Barksdale (1972) developed a relationship to model the permanent axial strain with respect to the deviator stress ratio and a constant confinement pressure. He based the model on the hyperbolic relationship given by Duncan and Chang for static triaxial tests, and found a relationship with the stress-strain curve of RLT (Lekarp & Dawson, 1998). He suggested that the change in permanent strain can be found using Equation 2.14.

$$\varepsilon_{1,p} = \frac{q/K \cdot \sigma_3^n}{1 - \left(\frac{(R_f \cdot q)/2(C \cdot cos\varphi + \sigma_3 \cdot sin\varphi)}{(1 - sin\varphi)}\right)} \quad 2\text{-}14$$

Where:

$K \cdot \sigma_3^n$: Relationship defining the initial tangent modulus as a function of the confinement pressure

q: Deviator stress

R_f: Constant relating to compressive strength to a limiting stress difference

Pappin (1979) investigated the permanent strain in crushed limestone for variable confinement pressures. He found that the permanent shear strain rate is a function of the length of the stress path in the p-q space (Lekarp & Dawson, 1998). He found a shape factor for the change in permanent strain due to the number of cycles and applied this to his model as seen in Equation 2-15.

$$\varepsilon_{s,p} = (fnN) \cdot L \cdot \left(\frac{q^0}{p^0}\right)_{max}^{2.8} \quad 2\text{-}15$$

Where:

$\varepsilon_{s,p}$: Permanent shear strain

fnN: Shape factor

L: Stress path length

q^0: Modified deviator stress $=\sqrt{2/3} \cdot q$

p^0: Modified normal stress $=\sqrt{3} \cdot p$

Paute (1996) defined an asymptotic value for the permanent strain (A) as seen in Equation 2-12. He found that A changes with the maximum shear stress ratio to yield Equation 2-16. In Equation 2-16 it can be seen that A increases as the maximum shear stress increases, and that the maximum shear stress has a limit value denoted by m for which A is infinite.

$$A = \frac{\frac{q_{max}}{(p_{max} + p^*)}}{b\left(m - \frac{q_{max}}{(p_{max} + p^*)}\right)} \quad 2\text{-}16$$

Where:

A: Limit value for permanent axial strain

q_{max}: Maximum deviator stress

p_{max}: Maximum normal stress

p^*: Stress parameter for the intersection of the static failure line and the p-axis in p-q space

m: Static failure line slope

Lekarp and Dawson (1998) found that none of the above models modelled their data to a satisfactory level, and found a new relationship between the accumulated permanent axial strain, the maximum shear stress ratio and the stress path length. The relationship is given in Equation 2-17.

$$\frac{\varepsilon_{1,p}(N_{ref})}{(L/p_0)} = a \cdot \left(\frac{q}{p}\right)^{b}_{max} \qquad 2\text{-}17$$

Where:

$\varepsilon_{1,p}(N_{ref})$: Accumulated axial permanent strain at any given number of load cycles (greater than 100)

$(q/p)_{max}$: Maximum stress ratio

q: Deviator stress

p: Mean normal stress

2.6.3 Summary

The permanent deformation can be modelled according to two criteria, namely the number of load applications and the stress conditions. In order to obtain a holistic view a summary in terms of both criteria are tabulated in Table 2-1 and Table 2-2.

Table 2-1: Summary of models for permanent deformation related to load cycles

Equation	Model	Reference	Parameters	Conclusion
1	$\varepsilon_{1,p} = a + b\log(N)$	Barksdale (1972)	a,b	Model only stable behaviour
2	$\varepsilon_{1,p} = a\varepsilon_r N^b$	Veverka (1979) [a]	a,b	
3	$\varepsilon_{1,p} = aN^b$	Sweere (1990)	a,b	
4	$\frac{\varepsilon_{1,p}}{N} = A_1 N^{-b}$	Khedr (1985) [a]	A_1, b	
5	$\varepsilon_{1,p} = (cN + a)(1 - e^{-bN})$	Wolff and Visser (1994) [b]	a, b, c	
6	$\varepsilon_{1,p} = A\left(1 - \left(\frac{N}{100}\right)^{-b}\right)$	Paute (1996)	A, b	
7	$\varepsilon_{1,p} = a\left(\frac{N}{1000}\right)^{b} + c\left(e^{d(N/1000)} - 1\right)$	Huurman (1997)	a, b, c, d	Model stable and unstable behaviour

[a] Models developed to include resilient and plastic strains [b] Modelled with South African Materials

Table 2-2: Summary of models for permanent deformation related to stress conditions

Equation	Model	Reference	Parameters
1	$\varepsilon_{1,p} = \frac{q/K \cdot \sigma_3^n}{1 - \left(\frac{(R_f \cdot q)/2(C \cdot cos\varphi + \sigma_3 \cdot sin\varphi)}{(1 - sin\varphi)}\right)}$	Barksdale (1972)	q, K, R_f
2	$\varepsilon_{s,p} = (fnN) \cdot L \cdot \left(\frac{q^0}{p^0}\right)^{2.8}_{max}$	Pappin (1979)	fnN, L, q^o,p^o
3	$A = \frac{\frac{q_{max}}{(p_{max} + p^*)}}{b\left(m - \frac{q_{max}}{(p_{max} + p^*)}\right)}$	Paute (1996)	b,m,p,q
4	$\frac{\varepsilon_{1,p}(N_{ref})}{(L/p_0)} = a \cdot \left(\frac{q}{p}\right)^b_{max}$	Lekarp & Dawson (1998)	a,b,L,p,q

Some of the attributes and shortcomings are discussed in the previous section. This includes some models describing the relationship of the evolution of plastic strain to that of the number of cycles differently. In addition, not all models can describe the various phases in the development of plastic strain equally well. These phases include the initial embedment (initial accelerated strain phase) after which the development of the plastic strain decreases in the second phase. In the second phase three scenarios can be observed and include (a) the plastic strain versus life cycles reaches an asymptotic value, (b) a gradual increasing gradient observed in the plastic strain versus life cycles or (c) a rapid increase in the development of plastic strain versus life cycles. It is in the second phase particularly, where some models are not able to describe all three types of behaviour.

Kotze (2014) illustrated how some models describe the behaviour of the material better than others. He concluded that it is important that more than one model is applied to the data in order to determine which models is the most appropriate to describe the behaviour of the material. Based on the comparison made here, the best models to predict the permanent deformation can be identified and used later in this research to model the permanent deformation behaviour of RCA. The identified models and process of prioritising the models to be used in this research is further discussed in Chapter 4.4.

2.7 Shakedown Theory

As previously discussed, a pavement structure under repeated loading undergoes a gradual accumulation of permanent deformation, causing material breakdown and ultimately leading to

incremental collapse. Alternatively, a load can be applied that initially causes permanent deformation, but after a number of cycles, the material behaves elastically and no further deformations are induced. In this case the material is said to have undergone shakedown and adapted. Sharp and Booker (1984) proposed applying the Shakedown concept (initially applied to structures) to pavements as distress (especially permanent deformation) in pavements have been known to decrease after a number of load cycles if the deviator stress ratio is sufficiently low.

The conventional Shakedown concept described the behaviour of structural elements and structures under repeated cyclic loading. The samples are subjected to repeat cyclic loading where the compression and tension loads are equal. The concept identifies four material response categories as seen in Figure 2-23. The categories are purely elastic, elastic shakedown, plastic shakedown and ratchetting (incremental collapse), respectively. Werkmeister *et al.* (2004) performed RLT on unbound granular materials in order to classify them with regards to the Shakedown Theory. She found that none of her test results exhibited purely elastic behaviour, and concluded that this behaviour does not occur in UGMs. Real pavement materials are not purely elastic and are subjected to resilient and permanent deformations.

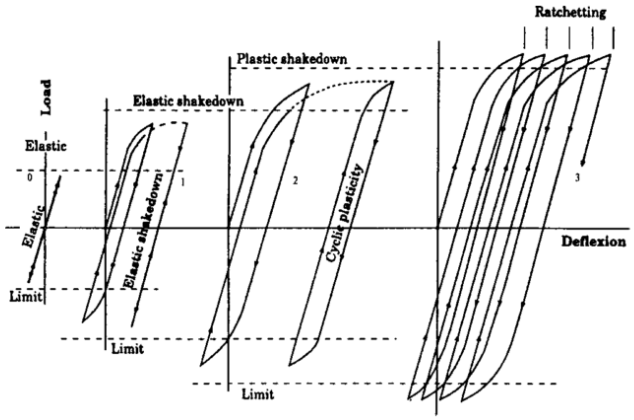

Figure 2-23: Elastic/plastic shakedown behaviour under repeated cyclic loading for structures (Werkmeister *et al.*, 2004)

Due to the differences between structural and pavement materials, it is seen that Figure 2-23 is not an accurate representation of UGMs. Instead Werkmeister *et al.* (2004) adapted this figure to describe the behaviour of pavement materials. Figure 2-24 shows the three categories of behaviour observed in UGMs, namely plastic shakedown (A), plastic creep (B) and incremental collapse (C).

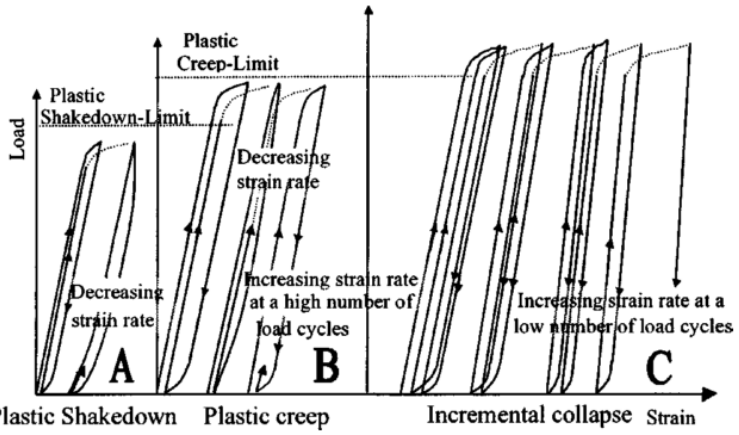

Figure 2-24: Behaviour of unbound granular materials under repeated cyclic loads (Werkmeister *et al.*, 2004)

A brief explanation of each behaviour range includes:

Range A: the material shows an initial plastic response for a number of load cycles before the material reaches a stable equilibrium response to the loading. No further plastic strain will develop and is referred to as shakedown behaviour. No further plastic strain will develop and the material is said to "shake down". The applied stress levels are sufficiently low and the material is in a stable condition. Range A is the ideal behaviour for pavement materials as only a small amount of permanent deformation will accumulate before equilibrium is reached.

Range B: this is an intermediate response between Ranges A and C. The material shows an initial plastic response, however the plastic strain rate decreases until a near constant value, the material will generally reach equilibrium. Kolisoja (1998) proved that although materials appear to stabilise after 100,000 cycles, unexpected failures could occur if the loading sequence continued for extended periods of time.

Range C: At high deviator stress levels the material response will have amounts of plastic deformation with only a small amount of elastic deformation, with each load application the accumulated plastic strain rapidly increases until incremental collapse occurs. Range C behaviour in pavement materials results in failure of the pavement layer due to shear deformation and rutting.

The described ranges are shown in Figure 2-25. It can be seen that Range A is stable with a low amount of plastic strain in the material as the equilibrium is approached. Range B has developed more plastic strain, but the strain rate is decreasing and the material is tending towards equilibrium.

Range C shows a sharp upward tendency in strain, which is the rapid accumulation of plastic strain that will lead to failure.

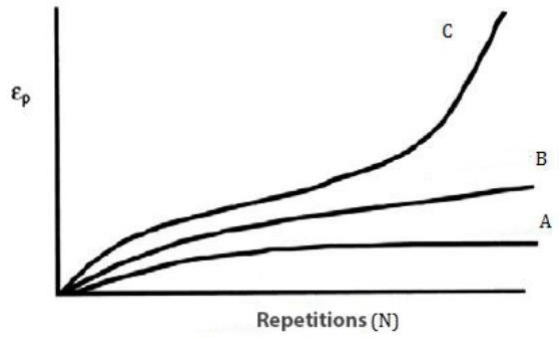

Figure 2-25: Material behaviour ranges as defined by the Shakedown Theory (Werkmeister, 2003)

Maree (1982) investigated the behaviour of gravels and crushed stone at a constant confinement pressure and found that the specimens stabilised below a certain applied deviator stress. He named this threshold stress level the maximum safe repeated deviator stress. He developed a design procedure based on this failure model that allows for the maximum stress to be kept lower than this maximum safe repeated deviator stress (Lekarp *et al.*, 2000a). Wolff (1992) investigated the elastoplasticity of granular materials and criticised this design procedure due to the fact that it does not include the non-linear stress-strain behaviour of UGMs.

Lekarp and Dawson (1998) proposed that the Shakedown Theory could also be used to model and classify the permanent deformation behaviour of UGMs. They found that none of the models based on the applied stress could accurately describe their test results, and developed a relationship based on the accumulated permanent strain and the number of load cycles. This relationship was discussed in Equation 2-17. A comparison between the measured and modelled values showed correlations between their values and the Shakedown Theory.

2.8 Dissipated energy

The Shakedown Theory as proposed by Werkmeister (2003) is mostly a subjective and unreliable approach, especially when approaching the boundary conditions between Ranges A,B and C. The dissipated energy concept is used to gain a better understanding of the material behaviour and to provide a more reliable and definitive answer than the shake down approach (Tao *et al.*, 2010). The dissipated energy model as described by Tao *et al.* (Tao *et al.*, 2010) can be used to describe the shakedown characteristics of recycled materials subjected to repeated loading. Two types of behaviour can be identified, namely stable and unstable behaviour the type of behaviour is

dependent on the type of material, deviator stress ratio and various other factors. The dissipated energy model is best used to describe the transitional phase from stable to unstable.

According to Tao *et al.* (Tao *et al.*, 2010) granular materials undergo both resilient and permanent deformations when subjected to each load cycle. The deviator stress (σ_d) is plotted against the vertical deformation for each load application to form a non-linear stress strain curve that is known as a hysteresis loop.

The area of the hysteretic loop defines the deformation work per volume on the material, or the dissipated energy caused by particle sliding or rolling within the material. Equation 2-18 can be used to calculate the dissipated energy per loading cycle (Tao *et al.*, 2010).

$$w = \int \sigma_i d\varepsilon_i = \int (\sigma_1 d\varepsilon_a + 2\sigma_3 d\varepsilon_h) = \int [\sigma_d d\varepsilon_a + \sigma_3(1-2\nu)d\varepsilon_a] \qquad 2\text{-}18$$

$$\approx \frac{1}{2}\sum_{i=1}^{N-1}\left(\sigma_{d,i} + \sigma_{d,i+1}\right)\cdot\left(\varepsilon_{a,i+1} - \varepsilon_{a,i}\right) + \frac{1}{2}(1-2\nu)\sum_{i=1}^{N-1}\left(\sigma_{3,i} + \sigma_{3,i+1}\right) \cdot \left(\varepsilon_{a,i+1} - \varepsilon_{a,i}\right)$$

Where:

w:	Unit energy dissipated per cycle within the material
$d\varepsilon_h$, $d\varepsilon_a$:	Incremental strains in the axial and radial directions
i:	i^{th} point on the stress-strain loop
σ_1, σ_3:	Major and minor principal stresses
N:	Total amount of points on the stress-strain loop
$\sigma_{d,i}, \sigma_{d,i+1}$:	Deviator stress corresponding to the i^{th} and $(i+1)^{th}$ point on the stress-strain loop
$\varepsilon_{a,i}, \varepsilon_{a,i+1}$:	Axial strain corresponding to the i^{th} and $(i+1)^{th}$ point on the stress-strain loop

The dissipated concept as described by Tao (2010), is proposed due to the challenge with identifying definitive boundaries between the different ranges of behaviour by Werkmeister (2003). According to Tao (2010), the classification of the different shakedown ranges as proposed by Werkmeister could lead to inconsistency in the definition of the boundaries between ranges. This is especially of concern between the "stable" and "unstable" range of the material. In the characterisation of Dissipated Energy two distinct phases are defined. Phase 1 is characterised by a rapid linear decrease of permanent strain rate and dissipated energy and occurs in the first load cycles. In Phase 2, a gradual non-linear reduction of permanent strain occurs. In Phase 1 the permanent strain rate decreases much faster than the dissipated unit energy. In Phase 2 material damage becomes more as a result

of the permanent deformation rate decreasing at a slower rate. The different ranges covering stable to unstable behaviour is defined as Range A, B and C, and to some degree similar to that of Werkmeister (2003). A Range A response can be expected when Phase 1 is predominant. This is due to non-sliding contacts or reversible contacts within the sample which dissipated the energy. To accommodate larger loading as the stress level increases, more irreversible sliding contacts will have to persist and Phase 2 will then become dominant. When Phase 2 is dominant, a Range C response will occur as the stress levels continue to increase. The transition process from Range A to C (Phase1 to 2) can be a gradual process and explains why defining these shakedown responses can be challenging at times.

Tao (2010) refers to the boundaries suggested by Werkmeister (2003) which includes that permanent strain rates larger than $1X10^{-5}$ defines the Range A-B boundary and permanent strain rates larger than $8X10^{-5}$ the Range B-C boundary. In his research he shows through the energy dissipated concept how materials rapidly become unstable but fails to propose guidelines to define these boundaries.

Dissipated energy as a measurement criteria holds potential but significant research is still needed, particularly related to its application in granular materials. Only then can this be implemented as a definitive tool to measure the response of the material.

2.9 Self-Cementing behaviour

Self-cementation is a mechanism whereby latent bonding of unhydrated cement occurs within the material composition. Self-cementation increases the stiffness of the material due to the pozzolanic reaction. This will have an influence on the long term performance of the material (Rudman & Jenkins, 2015). To understand the process of self-cementation, the hydration process of Portland cement must be investigated.

Cement consists of the following 5 major compounds:

- Tricalcium silicate (C_3S)
- Dicalcium silicate (C_2S)
- Tricalcium aluminate (C_3A)
- Tetracaclium aluminoferrite (C_4AF)
- Gypsum (CSH_2).

During the hydration process water is added to the cement and 4 complex reactions occur. The hydration of tricalcium silicate produces lime, and Calcium Silicate Hydrates as shown in Equation 2-19. The CSH compound creates short fibre structures that contributes a large proportion of the strength of the cement.

$$2C_3S + 6H \rightarrow C_3S_2H_3 + 3CH \quad \text{2-19}$$

The Belite (dicalcium silicate) also undergoes hydration to form calcium silicate hydrates. The CSH contributes to the strength of the cement paste. The reaction as shown in Equation 2-20 proceeds at a slower rate, but it will increase in strength continuously.

$$2S + 4H \rightarrow C_3S_2H_3 + CH \quad \text{2-20}$$

There are two reactions that occur during the hydration of C_3A. The first reaction shown in Equation 2-21 , takes place very quickly, whereas the second reaction shown in Equation 2-22, takes place at a significantly slower rate. Gypsum is added to prevent flash set, which causes the cement paste to set within minutes of mixing. The release of calcium and sulphate ions from the gypsum results in C_3A to undergo the second reaction. The product of Equation 2-22 is called ettringite which consist of long crystalline chains that do not contribute to the strength of the cement paste.

$$2C_3A + 21H \rightarrow C_4AH_{19} + C_2AH_8 \rightarrow 2C_3AH_6 + 9H \quad \text{2-21}$$

$$C_3A + 3CSH_2 + 26H \rightarrow C_6AS_3H_{32} \quad \text{2-22}$$

Tetracalcium alumina ferrite reacts in a similar way to C_3A, but the reaction is significantly slower. The ferrite undergoes two progressive reactions with gypsum. The first reaction as shown in Equation 2-23, is where the ettringite reacts with the gypsum to form ettringite, lime and alumina hydroxides. The ferrite further reacts with the ettringite to produce garnets as shown in Equation 2-24

$$C_4AF + 3CSH_2 + 3H \rightarrow C_6(A,F)S_3H_{32} + (A,F)H_3 + CH \quad \text{2-23}$$

$$C_4AF + C_6(A,F)S_3H_{32} + 2CH + 23H \rightarrow 3C_4(A,F)SH_{18} + (A,F)H_3 \quad \text{2-24}$$

From the reactions shown, it is clear that the hydration process of cement is a complex procedure, but that each of the compounds play an important role.

Poon (2006) showed that even after significant processing of RCA and RCM, the C2S and $C_3H_2S_3$ (C–S–H) compounds are still present. The C2S is a less reactive compound compared to C3S and takes a significantly longer time to hydrate. Figure 2-26 illustrates the results of research performed by Poon (2006) which shows that the <0.15 mm fraction of RCA and RCM could be a potential cause of the self- cementing properties, as this fraction contained the highest amount of C2S. The C2S was not present in the larger fractions as can be seen from Figure 2-26.

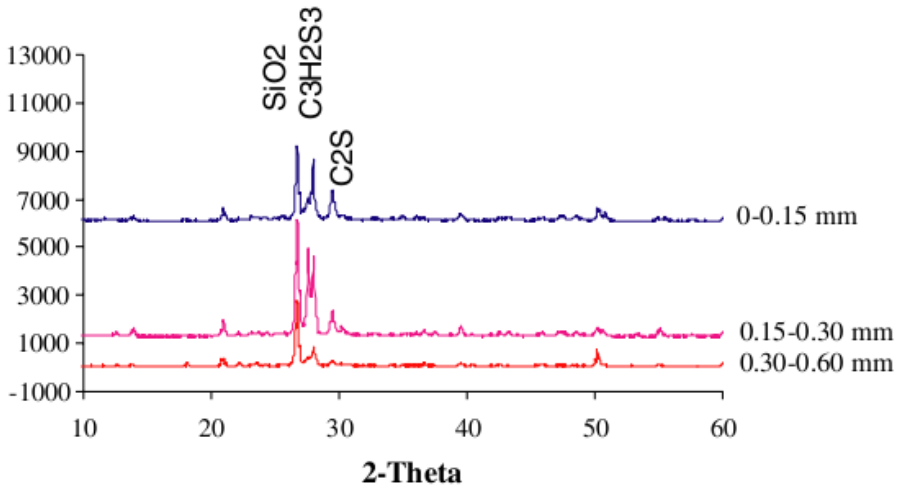

Figure 2-26: X-Ray defraction patterns on various fractions of RCA (Poon & Chan, 2006)

According to Rudman and Jenkins (2015) the self-cementing properties of RCA are not included in in the traditional design approach, as the current accepted assumption is that RCA material behaves as an unbound granular material and the traditional design applied accordingly (Van Niekerk, 2002) as discussed in Chapter 2. These models used in the pavement design do not allow for the gradual stiffening of the material due to self-cementation, and due to the lack of knowledge on the phenomenon it is not yet applied explicitly in road construction. It is however important to understand the mechanisms that control self-cementation and the effect it will have on the material, as well as the long-term performance. The increase in stiffness can have both beneficial and detrimental effects on performance. An increase in stiffness will lead to a stronger layer, however with the increase in strength potential durability issues can manifest such as shrinkage cracks and carbonation.

When considering self-cementation, the hydration process is not the only contributing factor. Environmental factors such as the temperature and availability of water as well as material properties play a role. There have been contrasting views on the mechanism of self-cementation and the initiation thereof. Karlsson (1998) found that there was no significant increase in the cementation of old concrete that was crushed and ground. Paige-Green (2010) found that the finer aggregate (<0.15mm) had a larger surface area, and contained the largest amount of C_2S which can react with water resulting in an increase in the hydration potential, increasing the strength and stiffness. He found that recycled cement stabiliser formed second generation cementitious bonds.

Self-cementation is potentially a major benefit for the use of RCA and RCM. A number of studies have been performed by various researchers that show how the performance aspects such as shear parameters and resilient modulus values increase with "curing" time of the material. Arm (2000)

investigated the self-cementing behaviour of RCA in both laboratory and field conditions. She tested the resilient modulus of different material types at different time intervals (incrementally between 1 and 90 days) to ascertain the effect of self-cementation. Figure 2-27 indicates the difference in the increase rate of resilient modulus for granite at 1 and 90 days to that of crushed concrete. Arm (2000) assigns the increase in stiffness to the self-cementation phenomenon. The increase of the resilient modulus of the crushed granite could be attributed to consolidation of the granular materials as a result of traffic loading. However, the significant gradient of increase of the crushed concrete over this time period suggests self-cementation

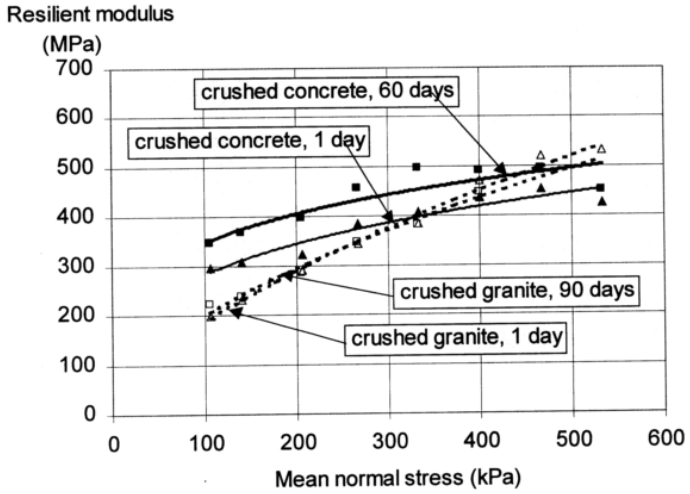

Figure 2-27: Comparison of the Resilient Modulus for RCA and Granite at varying time frames (Arm, 2000)

Van Niekerk (2002) also showed significant increases in the stiffness with time as can be seen in Figure 2-28. Here a 10 –fold increase (at the least) in the resilient modulus is observed over 13 weeks.

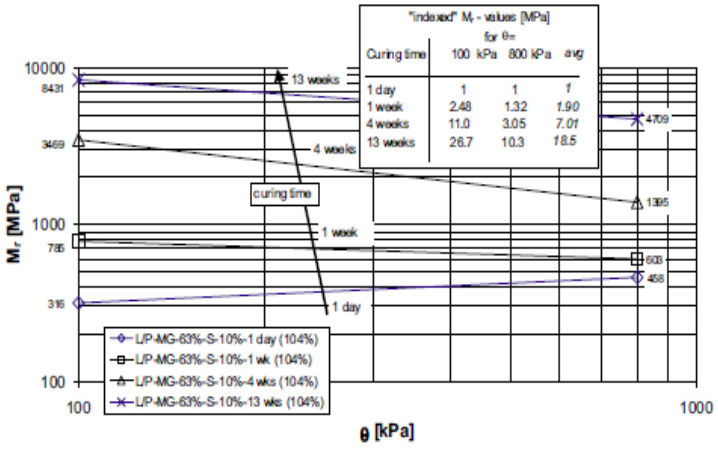

Figure 2-28: Resilient Modulus results for blends of 63% RCA and 27% RCM with curing times of 1 day and 1, 4, 13 weeks (Van Niekerk, 2002)

The self-cementing potential present in these type of materials also manifest in blends of RCA and RCM. Rudman and Jenkins (2015) performed a limited study showing how the Unconfined Compressive Strength (UCS) of different blends of concrete change over time as presented in Figure 2-29. The nomenclature used in this figure includes blends either of a 70% concrete and 30% masonry mix (70C:30M) or 30% concrete and 70% masonry (30C:70M) by mass. The notation 4% or 8% after the mix composition (30C:70M:4%) refers to the amount of filler (<0.075mm) in the material.

The results of this study revealed a noticeable increase in the failure load over a 21 day period. In all cases the largest increase is observed between 0 and 7 days.

Rudman and Jenkins (2015) also compared these results to standard cemented materials. This is depicted as C3 and C4 standard stabilised materials as used in South Africa and defined in SAPEM (2014a). It is clear from this figure that these materials are comparable to that of typical cemented materials, when measured by the UCS test as measurable.

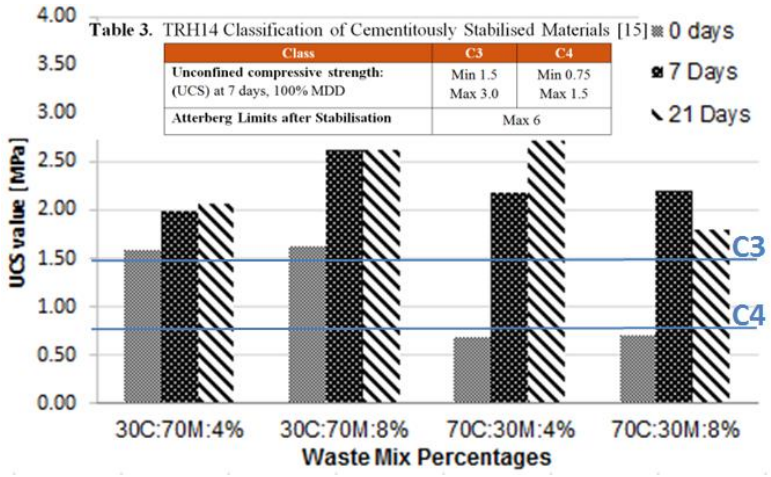

Figure 2-29: UCS results of various blends of RCA and RCM (Rudman & Jenkins, 2015)

The shear parameters are also significantly increased with curing time. Rudman and Jenkins (2017) reported on studies that they have performed on two different sources. They compared these studies with typical cohesion values of a representative granular material and studies performed at Curtin University (Leek, 2010). As can be seen in Table 2-3, all RCA sources exhibit high cohesion values. These values increase significantly after 28 days of curing, with an average increase of between 25 to 105% as a result of self-cementation.

Table 2-3: Shear parameter results from various sources of concrete (Rudman & Jenkins, 2017)

Research/Type	C [KPa]		ϕ° [°]	
	1 Day	28 Days	1 Day	28 Days
van Zyl (2014) G2	158,0	-	47,8	-
Leek (2010)	58,4	86,5	56,9	62,6
RCA (Source 1) - Old	119,0	244,1	52,8	51,8
RCA (Source 2) - New	252,1	317,6	51,0	61,0

There are many factors that play a role in the order of self-cementing that can occur. Some of them are briefly discussed here:

a. Moisture in hydration process

The water to cement ratio affects the hydration of cement and the amount of water available for hydration. The forces acting on each of the articles and the availability of water determines the physio-chemical behaviour at all stages of the hydration (Paige-Green, 2010).

b. The Effect of Fineness (Specific Surface) and amount of fines and filler

The fineness of cement will influence the hydration process. Finer particles have larger surface area which can react simultaneously with water. This effect is larger at early ages, until the structure becomes increasingly dense and this rate of reaction then decreases (Paige-Green, 2010).

Paige-Greene (2010) states that in the context of construction demolition waste, this would increase the number of contact surface areas within a grading and would therefore increase the amount of rehydration potential and ultimately increase the strength and stiffness. The same principle is also applicable for the amount of filler (<0.75mm) and fines (0.425mm). Increasing this amount will results in increased surface area.

c. The Cement Composition and Age

In terms of the C_3S/C_2S ratio in cement, the C_3S provides a significant contribution to strength at early ages whilst the C_2S contributes to strength at a slower rate.

Other factors are also at play. For example the rate of reaction of C_3S increases if there is an increased content of C_3A present. This effect of C_3A increases with time and reaches a maximum at an age of about 28 days. C_3A makes little contribution to strength.

At early ages, the quantity of alkali in cement (Na+ and K+) also affects the hydration process. With an increase in the alkali content accelerating the hydration process for C_3S and C_2S and reduces the formation of ettringite (Poon & Chan, 2006). This is an important characteristic to consider and should be evaluated in the micro-level testing, especially in the aftermath of received demolitions from site.

One process to consider includes potential alkali silica reactions (ASR) that could have occurred in the original concrete (before re-using). As a result of the gel interactions within the latent cement bonds, swelling could potentially occur. When the material is processed and compacted into a pavement layer, additional problems could manifest. Although their research did not include explicit use of recycled concrete in a pavement material, Gottfredsen and Thogersen (1994) investigated the possible effect ASR could have on the reuse of concrete. The volume change characteristics associated with their findings showed that the material could still develop a potential distress mechanism that should be considered.

d. The Effect of Temperature

Temperature plays a significant role during the reactions between the cement and water. The curing temperature will increase the rate of reaction (Sharp, 1997).

e. The Effect of Carbonation

Carbon dioxide can also react with the hydration of products of cement, which can lead to a risk of counteracting the benefits of chemical stabilisation. Potentially this can result in a reduction of strength. For the long term development of bond-formulation this could have a significant effect.

To use RCA as a pavement material, more research must be completed on the self-cementing phenomenon and how it affects the performance of RCA materials. A fine balance must be found between the beneficial characteristics of self-cementing and the detrimental effects it can have. More insight is also required on the behaviour of RCA and whether it is classified as a bound or unbound material.

Limited research is available particularly on the durability aspects concerning RCA as a new construction material. South Africa, unlike The Netherlands, do not have formalised processes in place where stockpiles are stored for a time period and the material is likely to have less potential for self-cementing. Here it is very likely that demolished RCA could be used immediately after it has been crushed. It is in light of these challenges that these durability aspects are investigated in this research as discussed in later chapters.

2.10 Summary of Literature

The main objective of the literature review was to gain insight and gather information on RCA materials and permanent deformation behaviour. This provides a departure point upon which decisions can be based before laboratory testing can be undertaken. Some of the aspects covered in the literature will not be used in the remainder of the study and included towards a holistic understanding of the challenges faced with these materials.

Due to the lack of research on the RCA materials, the literature study focused on the behaviour of unbound granular materials. UGMs are subjected to a variety of load combinations that induces certain stresses and strains in the material. The stress and strain in the material causes resilient and permanent deformation in the material. Various material factors such as grain shape, fine content, moisture content, stress history and grading affect the amount of permanent deformation in the material.

The performance of RCA material will vary depending the amount of time that has elapsed since placement. Initially. RCA material will exhibit similar stress conditions to unbound granular materials. Once self-cementation has taken place it may exhibit some behaviour that is similar to that of a lightly cemented materials. This does not imply that it will fully perform as a bound material, but some of the characteristics associated with stabilised materials may partly manifest.

Self-cementation is a phenomenon that occurs with RCA material, but relatively little information is available. Self-cementation has the ability to be a major benefit for the use of RCA in pavement structure as it increases the strength and stiffness of the material. However, the degree of self-cementation could lead to durability issues as discussed earlier in this chapter.

Triaxial testing is used to best simulate the loading conditions experienced in the pavement layers. The three different triaxial tests, namely monotonic tests, resilient modulus tests and the permanent deformation tests are briefly discussed. For each test the material characteristics obtainable and the calculations to obtain them are discussed. In this research only monotonic and permanent deformation tests will be performed.

Various researchers have developed mathematical models that model the amount of permanent deformation given a certain number of load applications. Each of these models have their own shortcomings as well as advantages. Based on the findings of previous researchers the best models to predict the permanent deformation will be identified and used later in this research to model the permanent deformation behaviour of RCA.

The behaviour of granular and RCA materials and the evolution of damage with load repetitions can be described using different theories such as the shake down approach or the dissipated energy model. The Shakedown approach is very popular as it is an easy method to apply to measured data, however it can be very subjective and unreliable. The dissipated energy model is more reliable and accurate but contains complex mathematical calculations.

Chapter 3: Methodology

3.1 Introduction

In this chapter the experimental design and methodology that was followed to achieve the objectives are discussed. The main testing equipment that was used is the Material Testing System (MTS) machine. This machine can be used to perform a variety of tests but it will only be used for monotonic and permanent deformation tests in this study. In this chapter the material source, the preparation of the two types of materials, the preparation of the samples as well as the experimental plan and procedure, together with the modelling of the data obtained from the laboratory tests will be discussed.

3.2 Project overview

The project overview is presented in a schematic diagram as shown in Figure 3-1. The diagram illustrates the steps that were completed in order to achieve the objectives set out in Chapter 1.2.

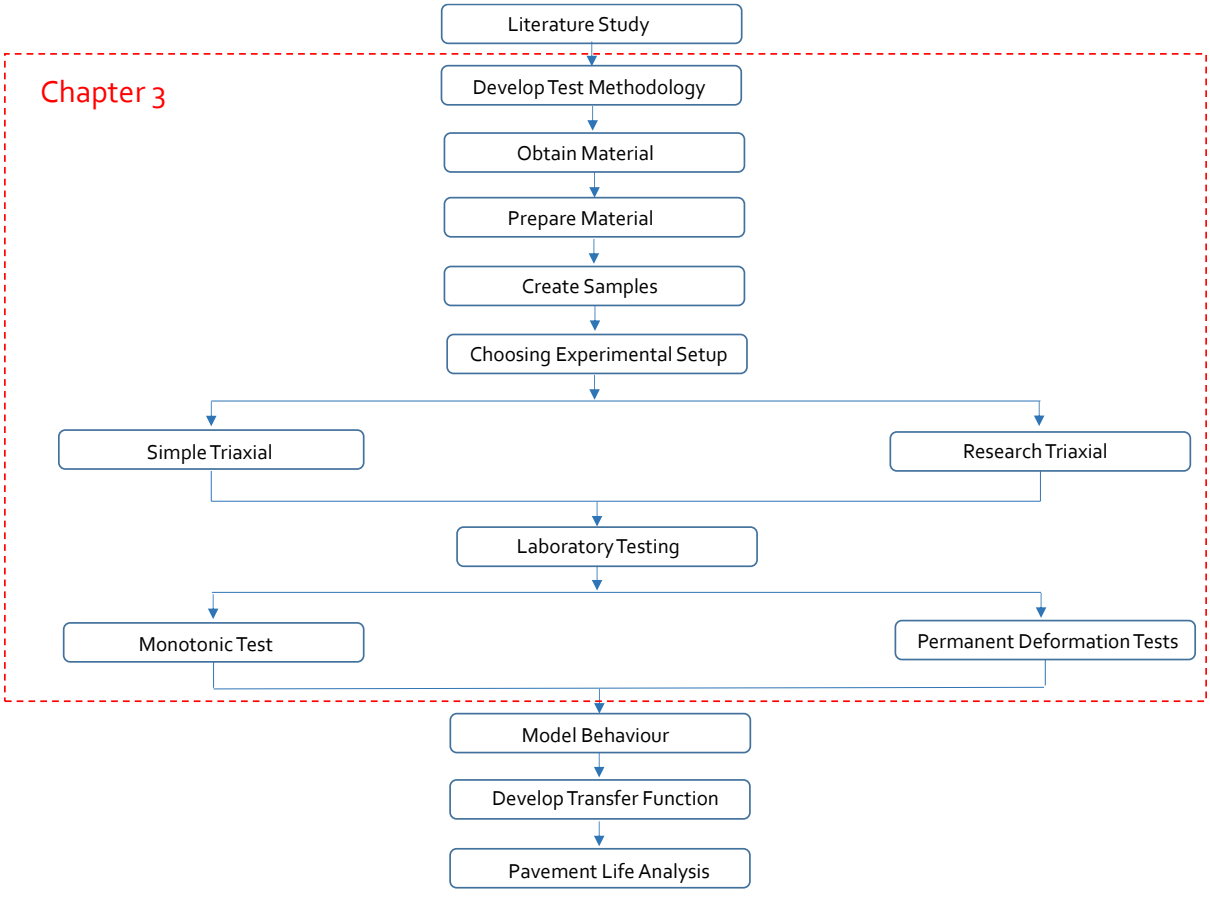

Figure 3-1: Schematic diagram showing the project overview

The project overview consists of the development of the experimental design. The material acquisition, sample preparation, followed by the investigation into which triaxial setup would yield

the best results is included in the steps. There is a choice between using the simple triaxial setup from Wirtgen and using the research triaxial setup, these setup configurations is further discussed in Chapter 3.6.2.An explanation particularly of the simple triaxial setup is provided in Annexure A. Once the appropriate test setup was identified, monotonic tests to determine cohesion and friction angle and permanent deformation (ε_p-N) tests were completed and the results modelled. The modelled results were used to create a transfer function and analyse the pavement life of an RCA layer. The methodology for the transfer function and the pavement life analysis is discussed in Chapter 5 and 6, respectively.

3.3 Experimental Design

The triaxial machine was used to conduct two types of tests, namely monotonic and permanent deformation tests. As discussed in the project overview the methods used for material and samples preparation are discussed in further detail in this chapter. Once the samples were made they were subjected to two different curing processes. Two types of materials were tested and two types of tests were completed on each material type. The first material is the Unexposed material which is used directly after the crushing and sieving process. The second type of material was "cured" for 14 days in its separate fractions. These fractions were submerged in water containers and a set at 40°C and high humidity to promote self-cementation. This is called the Exposed material. The material preparation is discussed in Section 3.4. The specimens used for monotonic testing were created and cured for one day before they were tested. The permanent deformation specimens were cured for one day and then tested. After the initial test completion of 100 000 cycles, the samples were sealed and cured for one month before being tested again for another 100 000 cycles. These tests are referred to as intermittent tests. The samples were sealed in plastic bags and cured at a constant temperature of 25 °C.

Figure 3-2 shows the experimental plan for monotonic testing, with two samples being tested at each confinement pressure. The breaking force for each sample can be used to calculate the shear strength parameters, namely cohesion and the friction angle. Figure 3-3 shows the experimental plan for the Permanent Deformation (PD) tests. Each test is performed twice, with the first sample being loaded for 250000 load repetitions (basic PD), and the second sample being loaded for 100000 load repetitions. The latter is then sealed and stored for 1 month and then tested for a further 100000 load repetitions (intermittent PD). The choice of 1 month was based on a reasonable time period to allow for latent self-cementation to occur so that realistic comparisons could be made between different variables if preloading was applied. The aim is not to simulate site conditions but rather evaluate the change in performance properties.

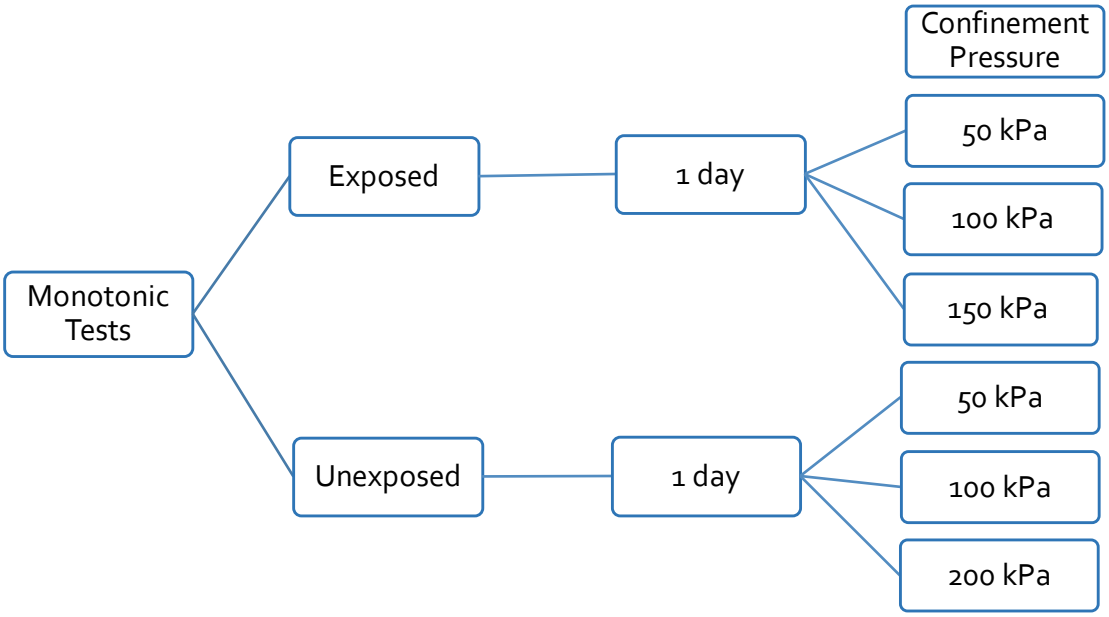

Figure 3-2: Experimental design for Monotonic Tests

The maximum confinement pressures at which the two types of materials were tested differ (i.e. 150kPa and 200 kPa, respectively). Typically tests at higher confinement pressures would lead to higher failure loads of the sample. The testing procedure includes performing the tests with the lowest confinement pressures first. At this point it is postulated what the maximum failure loads would be at 200kPa. If these values are above the machine capacity, the confinement pressure at which the follow-up tests are performed is lowered. Although tests were performed at different confinement pressures for the two types of materials, the results are still comparable as the monotonic tests are based on a statistical regression analysis calculated using the Mohr-Coulomb Method.

The choice in DSR ratios as shown in Figure 3-3 are two-fold. This includes firstly to be able to obtain representative data in the stable and unstable domain of the material. As these ranges could differ slightly between confinement pressures for the same material, choices were made to establish reasonable representative DSR values, based on preliminary permanent deformation tests performed. These choices are maintained for the remaining of the other confinement pressures for that same material (Exposed or Unexposed). Secondly, there is a considerable difference between the choices of DSR percentages of Exposed and Unexposed. At the start of the experimental programme, results revealed that the transition between stable and unstable behaviour of the

Exposed material is much lower than that of the Unexposed materials. The choice of DSR percentages for this material was made accordingly.

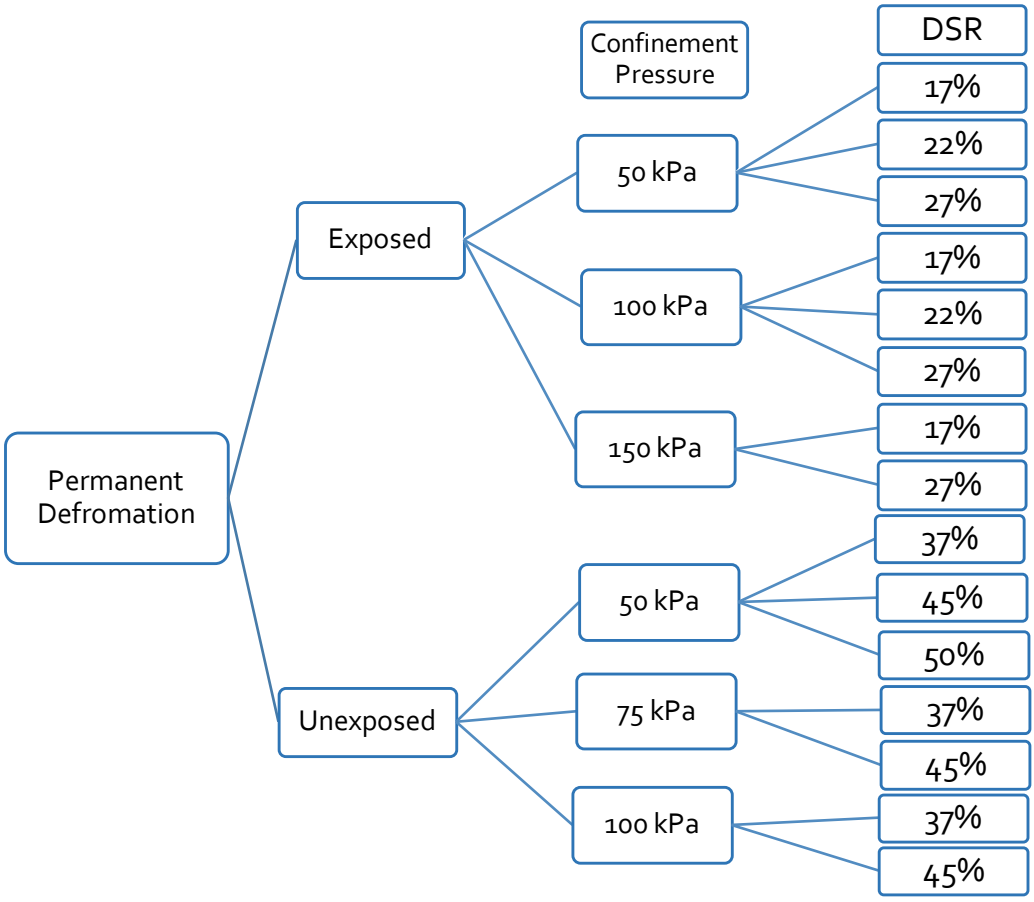

Figure 3-3: Experimental design for Permanent Deformation Tests

3.4 Materials

The RCA material used in this study originated from the N2, Borcherds Quarry and Swartklip interchange in Cape Town. It was originally used as a concrete layer of a road that had approximately 82000 vehicles travelling on it per day (Western Cape Government, 2016).The original road comprised of Jointed Unreinforced (Plain) Concrete Pavement (JCP) constructed between 1971 and 1972 (Strauss, 1989).

Severe surface cracking was observed along the contraction joints shortly after the construction of the road. It was identified that Alkali Silica Reactions (ASR) has manifested, which resulted in excessive expansion within the slab. It was concluded that detrimental chemical reaction between the alkalis and certain mineral constituents in the Malmesbury Group hornfels aggregates, occurred.

In 1986, some mitigation measures were applied to limit further expansion of joints. This included replacing severely damaged contraction joints and additional sealing of the entire concrete with a

bitumen rubber single seal, including a bitumen rubber open graded asphalt surfacing. The objective was to prevent any further ASR to occur

According to Western Cape Government (2016), the SANRAL Pavement Management System (PMS) has identified that the road has deteriorated sufficiently to warrant an investigation. This ultimately led to periodic maintenance of the road to restore the integrity of the road for a period of ten years.

The crushed and sieved material is used in two different capacities for the experimental design. The first material is the Unexposed RCA and is used as is after the crushing and sieving procedure. The second material is the Exposed RCA, which is the RCA that has been cured for 2 weeks using water and a high humidity room to reduce the self-cementing potential. The material is cured in its fractional state by adding water to keep the material and keep the material submerged. The moist conditions together with the humidity allows for the hydration of latent cement to take place at an increased rate and therefore reducing the self-cementing potential of the material (i.e. less latent cement is present when the sample is made). This course of action is followed to investigate the effect that self-cementation has on the durability of the RCA material.

When conducting the monotonic tests on Unexposed specimens that had been cured for 1 month, the capacity of the machine was reached before the material had shown signs of failure. At a low confinement of 50 kPa an axial force of 86 kN was recorded when the machine reached an interlock and stopped. This challenge was attributed to the self-cementing potential of the material. This finding further necessitated the need for the investigation of both the Exposed and Unexposed RCA in order to quantify the effect of self-cementation on the durability and performance of the material.

As discussed in earlier sections the informal nature of this industry could very well lead to material being used as soon as it has been demolished leading to a material comparable to an Exposed material. On the other hand, the material to be used in the pavement layer might have been tested at early ages but then be lying on a stockpile for quite a while before being used. These two cases present potentially examples including the worst and best scenario these materials would have to perform under. This research would aim, through this approach in testing the Unexposed and Exposed material, to gain better insight on how performance could differ. It will also provide insight on how contractors and consultants should prescribe processing, testing and handling of these materials on site. It does not necessarily mean the inclusion of extra procedures but rather the quality process that must be implemented to achieve reliable performance originally anticipated.

3.5 Specimen Preparation

The RCA material obtained from the N2 rehabilitation project was broken down into manageable pieces before being transported to Stellenbosch University, great care was taken in ensuring no cross contamination between RCA material and other granular layers in the pavement. The material was then crushed in a jaw crusher to obtain the correct size material, which was used to achieve the desirable grading as described in Section 3.5.1. Figure 3-4 shows the material crushing, sieving and grading process. The first image as shown in Figure 3-4 a) shows the raw material that was obtained from the contractor. The material was then crushed and sieved into fractions as shown in Figure 3-4 b) and the fractions were reconstituted to form a specimen with determined grading as shown in Figure 3-4 c).

Figure 3-4: a) Raw RCA b) Crushed and sieved Fractions of RCA c) Reconstituted fractions of RCA

3.5.1 Sieving and Material grading

The grading of the material plays a big role in the interlocking of particles and so to the strength of the final sample. The crushed material was sieved into the following fractions (retained sieve sizes): 13.2 mm, 9.5 mm, 6.7 mm, 4.75 mm, 2.36 mm, 1.18 mm, 0.6 mm, 0.425 mm, 0.3 mm, 0.15 mm, 0.075 mm and < 0.075mm (pan) and then reconstituted into a specific grading. It was decided that the material should satisfy the requirements of a G2 material, and therefore the ideal grading was obtained using the COLTO (1998) specifications for a G2 material using as guidelines the upper and lower limit grading limits allowed for the material. The G2 grading was used so that the material conforms to the specifications of good quality quarried aggregates that are used in the base course of South African pavements. The mass of each fraction to obtain the ideal grading is shown in Table 3-1 and the grading of the RCA mix compared to the COLTO (1998) specifications is shows in Figure 3-5 COLTO (1998) specifies a grading envelope with the upper and lower bounds as shown in the red

and blue lines of Figure 3-5 respectively. The grading was chosen as to fit as closely as possible to the average of this grading envelope. This reconstitution process is important to keep the grading consistent across all the specimens and tests performed.

Table 3-1: Grading of the RCA mix

Retained Size (mm)	% Retained fraction	% Passing fraction	Mass (kg)
19	22	78	2.750
13.2	11	67	1.375
9.5	7	60	0.875
6.7	8	52	1.000
4.75	7	45	0.875
2.36	10	35	1.250
1.18	9	26	1.125
0.6	6	20	0.750
0.425	2.5	17.5	0.313
0.3	2.5	15	0.313
0.15	4.5	10.5	0.563
0.075	2.5	8	0.313
Pan	8	0	1.000
Total	100	100	12.5

The maximum particle size allowed in a triaxial specimen is 19mm due to the size of the compacting mould, limiting the size of larger particles. The diameter of the sample is 152 mm, using particles of 19 mm would distort the packing of the material within the mould, and therefore a process known as scalping is used. This is based on the finding that the maximum particle size to diameter of the mould should not exceed a 1:7 ratio (Sweere, 1990). All the material retained on the 19 mm sieve is excluded and it is replaced with 13.2 mm material in the grading. Although this process changes the grading curve, it provides the most practical and representative performance results of different alternatives as was investigated by Van Zyl (2014).

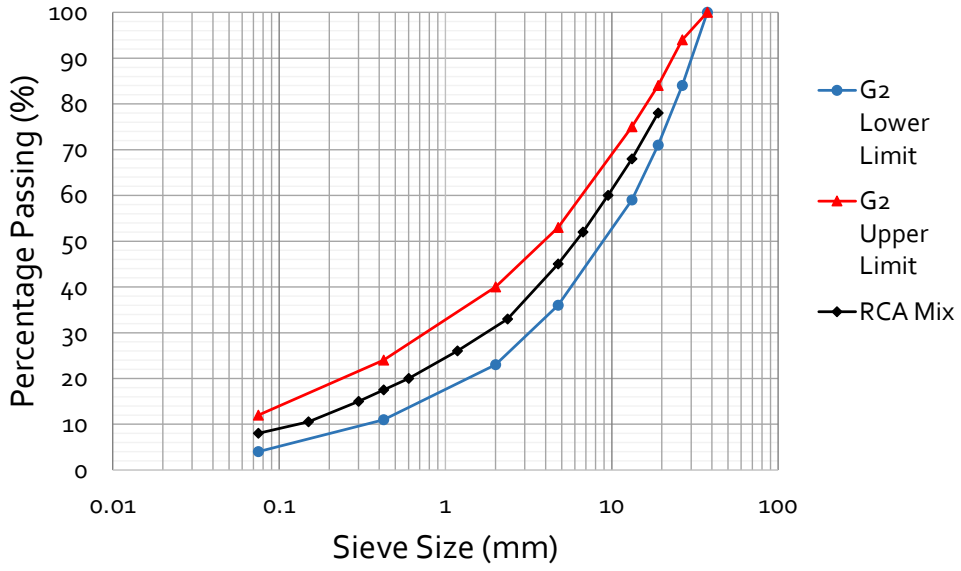

Figure 3-5: Designed grading compared to COLTO (1998) G1-G3 envelope

3.5.2 Optimum Moisture Content (OMC)

There are two ways of obtaining the OMC for a given material, firstly the Modified AASHTO compaction method can be used (which is commonly used in laboratories) or the vibratory hammer compaction method that has been developed at Stellenbosch University. It was decided to use the vibratory hammer compaction as this gives a more accurate presentation of the compactive effort that occur on site, using heavy vibratory steel-drum rollers. The following steps were followed to obtain the OMC and the maximum dry density (MDD):

1. Calculate the mass of material needed at a chosen dry density of 2500 kg/m^3 to fill the small vibratory compaction mould (Ø=152 mm x 120 mm);
2. Using the grading as calculated in Chapter 3.5.1, constitute 6 samples for the OMC testing. Add enough material to the calculated mass to allow for a hydroscopic moisture test (an additional 1 kg to the 5.5 kg specimen);
3. Each sample must be tested at a different moisture content namely 5, 6, 7, 8, 9 and 10% of the dry mass. These moisture contents may vary depending on the grading and type of material. Add the calculated water to the material and mix thoroughly;
4. Prepare the vibratory hammer mould, by greasing the inside and also lining the bottom with filter paper. The specimen must be compacted in two layers of equal weight, for a time of 1 minute per layer in order to ensure that the material is compacted to refusal. The surface between the two layers must be scarified to allow for interlocking of aggregate between the two layers;
5. Once compacted, remove the mould and record the height and weight of each sample;

6. Using Equation 3-1 calculate the dry density for each sample :

$$MDD = \frac{m_{after\ compaction}}{1+\omega} \cdot \frac{1}{Area \cdot H_{after\ compaction} \cdot 1000} \qquad 3\text{-}1$$

7. Plot a graph using the calculated dry densities in conjunctions with the moisture contents as shown in Figure 3-6. The Maximum Dry Density (MDD) is read off from the graph at the highest point and the corresponding water content is then used as the optimum moisture content. .

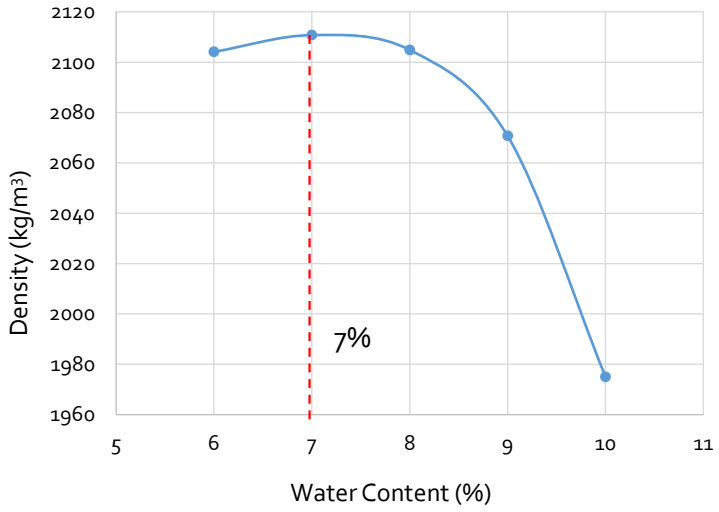

Figure 3-6: Maximum Density at added moisture contents

3.5.3 Mixing of material

The fractions of raw material is weighed out according to Table 3-1 to constitute a sample. A total weight of 12.5 kg is used, which is calculated using the maximum dry density and the volume of the big compaction mould (Ø=152 mm x 300 mm), and additional 1 kg of material is added for the hygroscopic moisture test. The material is weighed after reconstitution to ensure accuracy in the weighing process. Thereafter, the amount of water corresponding to the water content that was read off on the graph in Figure 3-6 is measured out.

The material and the water is mixed together using an electronic pan mixer as shown in Figure 3-7 a). The material must be mixed thoroughly until no dry material can be seen and all fractions are evenly distributed. The material is weighed off into 5 plastic bags of equal weight, the bags must be sealed to ensure no moisture loss. The remaining material can be transferred into an oven pan, and the mass recorded before being put into an oven at 110 °C for 24 hours. This is used to calculate the hygroscopic moisture of each sample.

3.5.4 Compaction of samples

Before compaction, the correct preparation of the mould and machine must take place. A split mould as previously described of diameter 152 mm and height of 300 mm must be used. The inside of the mould is lined with a lubricant (i.e. Spray and Cook) to prevent the sample from sticking to the mould. The mould must be placed on the pedestal and tightened with the clamps. Two layers of filter paper is placed inside the mould on the pedestal. It is very important to ensure all pieces of the setup is clean to prevent cross contamination.

The sample is compacted in 5 layers using the material previously weighed out into plastic bags. The Wirtgen Vibratory hammer, as seen in Figure 3-7 b) is used to compact each layer to a height of at least 60mm, the sample is compacted to refusal, meaning the maximum density will be reached. Each layer is compacted for a time of 45 seconds. Once a layer has been compacted the surface is scarified to ensure interlocking of aggregates between layers. This process is repeated for the following 4 layers.

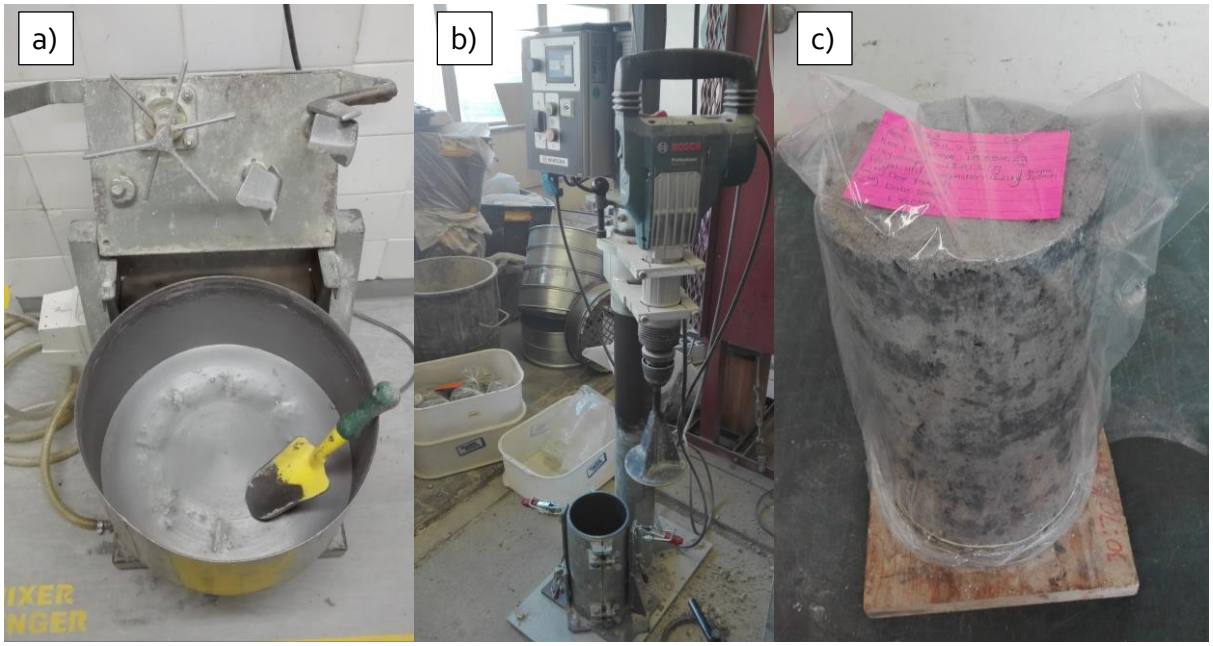

Figure 3-7: a) Mixing of Sample b) Compacting the sample c) Curing the sample

Once the sample has been compacted the mould is loosened and the sample can be removed, care should be taken as to not damage the sample during this process. The sample is weighed and the height as indicated by the Wirtgen machine should be recorded. The sample is placed on a wooden base plate and covered with a plastic bag and sealed using elastic bands to prevent excess moisture loss during the curing process.

3.5.5 Curing of samples

The samples must be cured for different periods of time, but at the same conditions. The samples that are to be tested at 0 months must be cured for 1 day and samples to be tested at 1 month must be cured for 30 days. The samples are covered with plastic bags to limit moisture loss, and are placed in a room with a constant temperature of 25 °C. A fully prepared and covered sample is shown in Figure 3-7 c).

3.6 Triaxial Testing

The triaxial test is performed using the Material Testing System (MTS 810, Model 318.10) at the Stellenbosch University Pavement Laboratory. To simulate real life conditions the material must be loaded axially, but must also have confinement pressure around the entire specimen. The MTS machine uses air pressure to provide confinement stress. The MTS machine at Stellenbosch University has certain capabilities and constraints shown in Table 3-2. These constraints are important due to the fact that RCA behaviour lies somewhere between a granular and a cemented material. If self-cementation has taken place the strength of the material at high confinement pressures could be higher than the 100 kN maximum vertical load that can be applied. At this point the capacity of the machine will be insufficient and no result of the sample can be obtained. This was the case when testing samples of Unexposed RCA that had been cured for 1 month. Table 3-2: MTS Machine testing capabilities (Cleghorn, 2015)

Item	Level
Controlled Channels	1 Vertical Load Actuator of 100 kN maximum
Controlled Method	Displacement or Force
Controlled Temperature	From 0°C up to 60°C
Confinement Type	Air
Confinement Method	Manual
Maximum Vertical Load	100 kN
Maximum Confinement	250 kPa

3.6.1 Rubber Membranes

A rubber membrane is made using liquid latex and the machine shown in Figure 3-8. To make the membrane the plastic cylinder (Ø=150 mm x 400 mm) is rolled through the liquid latex and all air

bubbles are removed from the layer. The machine continues to rotate until the layer of latex is dry. This takes between 3 and 4 hours. Once the layer has dried sufficiently, another layer can be added. The membranes used consisted of three layers of latex. It is important that the membrane is neither too thin nor too thick as both scenarios have a negative effect on the accuracy of the tests. A membrane that is too thin will tear easily, and a membrane that is too thick may unintentionally provide additional confinement to the material during the testing procedure.

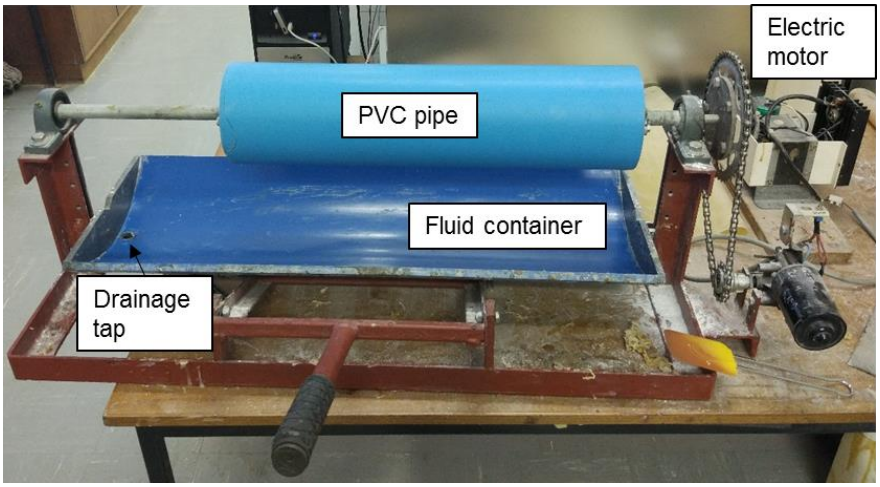

Figure 3-8: Equipment for latex membrane production

3.6.2 Triaxial Setup

There was a choice between using the standard research triaxial setup or the Wirtgen simple triaxial Setup (2 resilient modulus test were run using the different setup procedures to ascertain which setup would be better). The Wirtgen simple triaxial setup was developed by BSM laboratories in Kwazulu-Natal and has applications in both pavement and geotechnical engineering. The method simplifies the setup of the triaxial test saving time and effort. The setup is explained further in Annexure A.

However, when comparing the results obtained from sample Resilient moduli tests performed by van Tonder (2017), it was observed that the simple triaxial setup allowed air to be pushed back into the system due to repeated dynamic cyclic loads. This was as a result of inefficient sealing capability of the one-way valve providing the pressure in the first place. This effectively reduced the air pressure in the cell below the desired level. Although the results were comparable between the simple and research triaxial for monotonic testing, there were concerns regarding the reliability about its extended application in the continuous dynamic load application. It was decided to use the research triaxial setup for both monotonic and permanent deformation tests. Even in the research triaxial setup, it is important to take care during the assembling procedure to ensure that all air leaks are sealed and a constant air pressure is maintained.

3.6.3 Preparation of Sample

The preparation and setup of the sample for triaxial testing is important and can be directly linked to the reliability of results achieved. Firstly, ensure that all equipment and components are clean. The membrane plays a very important role in the triaxial tests as it seals the sample from air so that no air can enter the sample pores. The membrane allows for equilibrium to be maintained between the sample and the sealed cell. Although the membrane lends some confinement to the sample this is considered to be negligible, it is for this reason that the membrane should not be too thick. To seal the top and the bottom of the sample an additional strip of latex is used, this has no bearing on the results as it only covers a very small part of the sample. A cylindrical membrane applicator as seen in Figure 3-9 a) is used to expand the membrane diameter so that it can be placed over the sample as seen in Figure 3-9 b) and c). Ensure that there are no holes or tears in the membrane after the sample is covered.

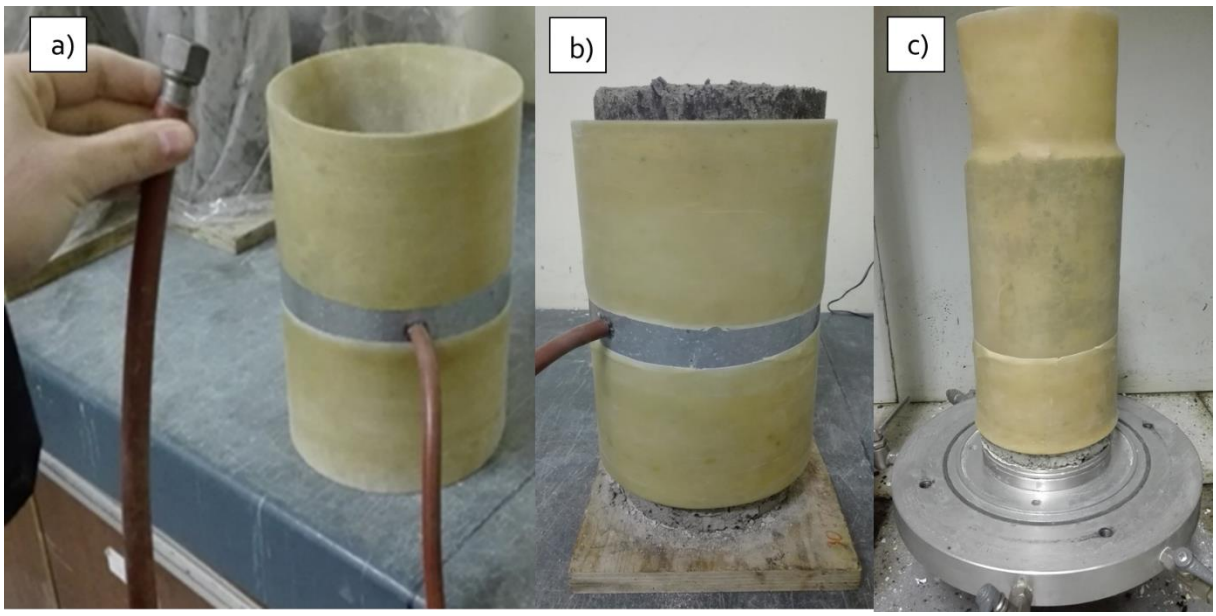

Figure 3-9: a) Membrane applicator b) Membrane applied to sample c) Sample with membrane placed on loading plate

The sample is placed on the base plate and the membrane is folded double, a double O-ring is used to seal the membrane to the base plate at the bottom of the sample. At the top of the sample a loading plate is placed and the membrane is folded over the plate and again secured with double O-rings. The entire membrane application process is shown in Figure 3-10. It is important that the sample is placed in the middle of the base plate and that the centre of the loading plate coincides with the centre of the sample. This will ensure that the sample is not loaded eccentrically.

Figure 3-10: Double O-ring application process

The frame, Perspex cylinder and lid can be placed to make up the triaxial cell. Ensure that the loading ram is placed in the centre of the loading plate before attaching the frame and lid using rods and nuts. The complete triaxial setup can be seen in Figure 3-11.

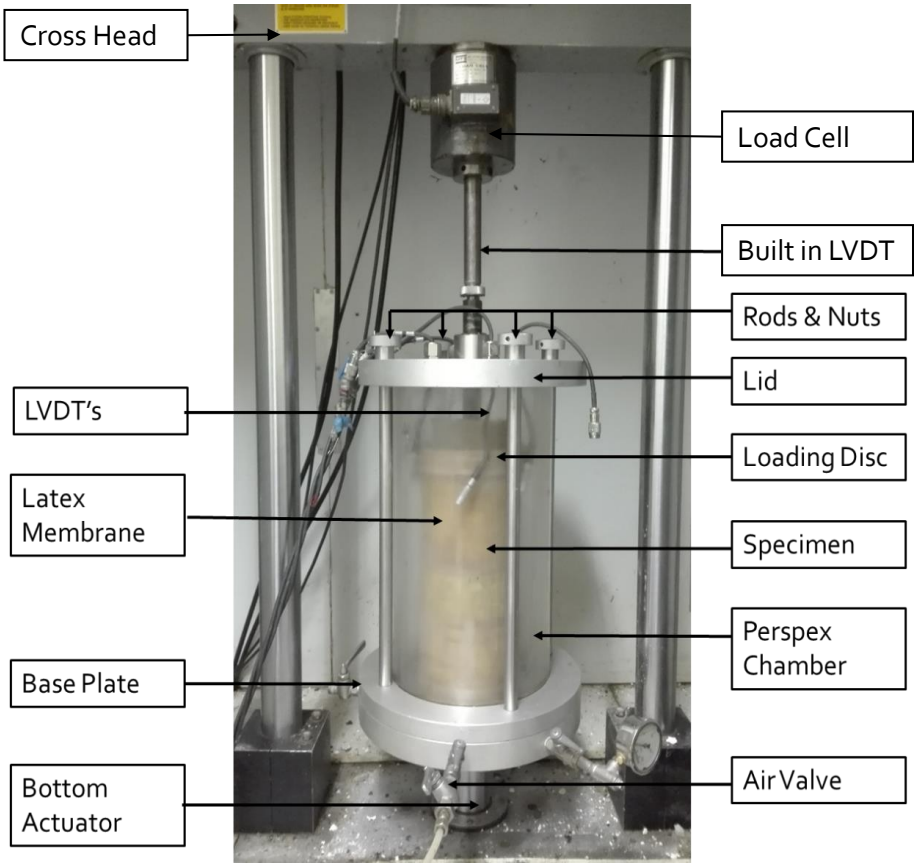

Figure 3-11: Complete triaxial setup

Once the setup is completed the air pressure can be connected and the Perspex chamber should be checked for air leaks. The air can then be turned off. To ensure no pressure build up within the sample itself occurs, a visual inspection ensuring a tight fit between membrane and sample is performed. The actuator can be lowered until it makes contact with the loading ram. The triaxial setup is now completed and the sample is ready to be tested.

3.6.4 Monotonic Testing

The monotonic tests are performed to determine the shear parameters such as the cohesion (c) and the friction angle (φ) for the RCA material. The shear parameters can in turn be used to determine the failure stress at any given confinement. The failure stress is used to determine the force at which to test for the permanent deformation.

During the monotonic testing three results at different confinement pressures are needed to draw the normal versus shear stress graph. This graph is used in conjunction with the Mohr-Coulomb method to obtain the failure envelope as well as the shear strength parameters. In order to ensure statistical accuracy more monotonic tests are advisable. All the specimens must be created and cured at the same conditions. The samples are prepared following the instructions in Section 3.5.3 to 3.5.5. When performing the monotonic testing no Linear Vertical Displacement Transducers (LVDT's) are used, as the actuator provides sufficient and accurate data to determine the shear parameters. Two specimens were tested at each of the three confinement pressures, namely 50 kPa, 100 kPa and 200- kPa for Exposed RCA. The confinement pressures differ slightly for the Unexposed RCA, namely 50- kPa, 100 kPa and 150 kPa. The reason for this difference is explained in Section 3.3. Two samples were tested at each confinement to ensure statistical accuracy and repeatability of results. Samples were loaded at a constant displacement rate equal to 1% of the axial length (i.e. 3mm/min).Tests were terminated when the applied force reached a peak value and is unloaded at the same displacement rate until 80% of the failing force is reached.

The principle of Mohr-Coulomb is used to plot the reworked data to form Mohr circles. The failure force can be used to determine the failure stress and with the known confinement the axial stress can be calculated. These two normal stress values are plotted on a graph that compares normal stress and shear stress and the failure line which is tangent to all three Mohr circle can be found. The shear strength of the material is obtained using the Mohr Coulomb failure criteria as shown in Equation 3-2. The y-intercept of the failure line indicates the cohesion, and the slope of the tangent line indicates the friction angle. The Mohr Coulomb graph for monotonic tests are shown in Figure 3-12.

$$\tau_f = c + \sigma \cdot \tan(\varphi) \qquad 3\text{-}2$$

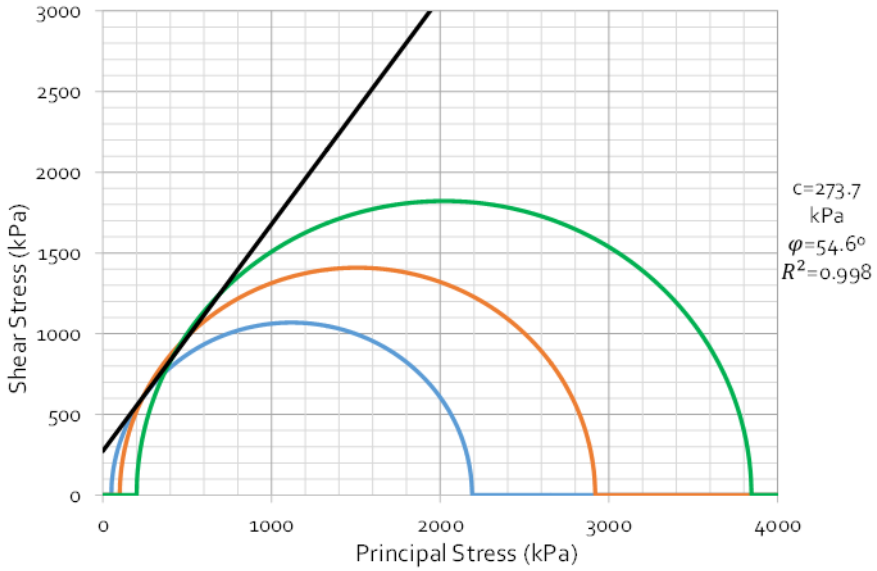

Figure 3-12: Mohr-Coulomb graph for RCA shear parameters

3.6.4.1 Modelling of monotonic results

The maximum force that resulted in the failure of the material during the monotonic test is known as the failure force (P_{df}). The conversion of this force to a stress, already presents the deviator stress at failure. Using Equation 3-3, the failure force can be converted to the deviator stress. Once the deviator stress at failure is obtained Equation 3-4 can be used to calculate the principal stress at failure.

$$\sigma_{d,f} = \frac{P_{d,f}}{A} \qquad 3\text{-}3$$

Where:

$\sigma_{d,f}$: Deviator stress at failure (kPa)

$P_{d,f}$: Applied force at failure (kN)

A: Area of the specimen (m^2)

$$\sigma_{1,f} = \sigma_{d,f} + \sigma_3 \qquad 3\text{-}4$$

Where:

$\sigma_{1,f}$: Principle stress at failure (kPa)

σ_3: Confinement pressure (kPa)

The relationship between the principal failure stress and the confinement pressure within the cell can be modelled using Equation 3-5 (SANRAL, 2011). The values of A and B are determined using linear regression analysis on three combinations of $\sigma_{1,f}$ and σ_3 values. Equation 3-6 and 3-7 (SANRAL, 2011)

can be rewritten in terms of c and φ to obtain the shear parameters of the RCA material. This results in Equation 3-8 and 3-9 (SANRAL, 2011)are obtained:

$$\sigma_{1,f} = A \cdot \sigma_3 + B \quad 3\text{-}5$$

$$A = \frac{(1 + sin\varphi)}{(1 - \sin\varphi)} \quad 3\text{-}6$$

$$B = \frac{(2c \cdot cos\varphi)}{(1 - sin\varphi)} \quad 3\text{-}7$$

$$c = B \cdot \frac{(1 - sin\varphi)}{2cos\varphi} \quad 3\text{-}8$$

$$\varphi = \sin^{-1}\left(\frac{A - 1}{A + 1}\right) \quad 3\text{-}9$$

3.6.5 Permanent Deformation Testing

A permanent deformation test is used to determine the relationship between the cumulative permanent axial strains induced in the material for increasing amount of load cycles at a specific set of stress conditions.

The samples are prepared following the instructions in Section 3.5.3 to 3.5.5. For the permanent deformation test the main LVDT measured over the full height was used as measurement of the vertical deformation. LVDT's placed on the specimen itself (so that only the middle third of the displacement during loading is measured) was initially considered but not implemented. On-sample LVDT's allow for the exclusion of the frictional effect, through boundary condition improvement, caused by the loading plates (Erkens, 2002). However the length over which these LVDT's measure displacements are significantly smaller and any error that occur potentially large (in ratio) in comparison to the original reading. Weighing these limitations it was decided to use the main LVDT readings in this research.

Two types of permanent deformation tests was performed for this research. The basic permanent deformation test includes samples that were subjected to 250 000 load cycles at a given set of stress conditions. The intermittent permanent deformation test was included to investigate the magnitude of the self-healing and self-cementing properties of the material. These samples were subjected to 100 000 cycles, upon which the sample was sealed and cured at 25°C for a duration of 1 month. Once

the time has elapsed the sample was again tested for 100 000 cycles. All stress conditions were therefore investigated twice, once during a basic test and once during an intermittent test.

The confinement conditions at which tests were performed included 50, 75 and 100 kPa and each Unexposed sample was subjected to an applied vertical stress of 37%, 45%, and 50% of the deviator stress at failure. The Exposed samples had to be tested at lower DSR's due to the reduction in strength as will be discussed in Chapter 4: When testing samples at 50% deviator stress ratio it is shown that the material cannot withstand such a high applied stress and it was decided not to include 50% at the higher confinement pressures.

The samples were firstly subjected to 1000 cycles that serve as a conditioning phase. The axial force and axial displacement of the actuator records output at 256 Hz for the last 5 cycles of each 1000 completed cycles. This is done in order to minimise the amount of data output received by the machine, whilst still recording enough data to accurately model the material behaviour. A Haversine load with a 0,1 second pulse and 0,9 second rest period was applied (SANRAL, 2011).

3.6.5.1 Modelling of Permanent deformation results

The axial displacement of the actuator is used to calculate the cumulative permanent strain at each load cycle and can be plotted against the number of load cycles. Excel's Solver function is used to fit the observed data to the behavioural models. The Solver function is used to determine the regression correlation (R^2) between the measured data and modelled data. The aim is to get this is as close as possible to one, while minimising the sum of the squared errors. Equation 3-10 shows the regression parameters, x and can interchangeably denote the coefficient a, b, c or d. The regression parameters are used in the models as shown in Equation 3-11 and Equation 3-12, this is merely an example and other will be fitted and discussed in further detail in Chapter 4.

$$X = x_1 \left(\frac{\sigma_1}{\sigma_{1,f}} \right)^{x_2} \quad 3\text{-}10$$

$$\varepsilon_p = A \left(\frac{N}{1000} \right)^{B} \quad 3\text{-}11$$

$$\varepsilon_p = A \left(\frac{N}{1000} \right)^{B} + C \left(e^{D\left(\frac{N}{1000}\right)} - 1 \right) \quad 3\text{-}12$$

As discussed in Chapter 2.6, there are various models that are used to model the permanent deformation behaviour of an unbound material. In Figure 3-13 and Figure 3-14 examples of models

used in this study is presented. Both graphs show the difference between actual measured data and various fitted models. It can be observed, considering both Figure 3.13 and 3.14, that the model developed by Huurman (1997), shows the most accurate and appropriate simulation (when measured against both stable and the unstable behaviour). However as stated by Kotze (2014), more than one model should be applied in research studies as to ensure the most accurate fit. The same approach was followed in this study. The models that were prioritised for use in this study is further explained in Chapter 4.

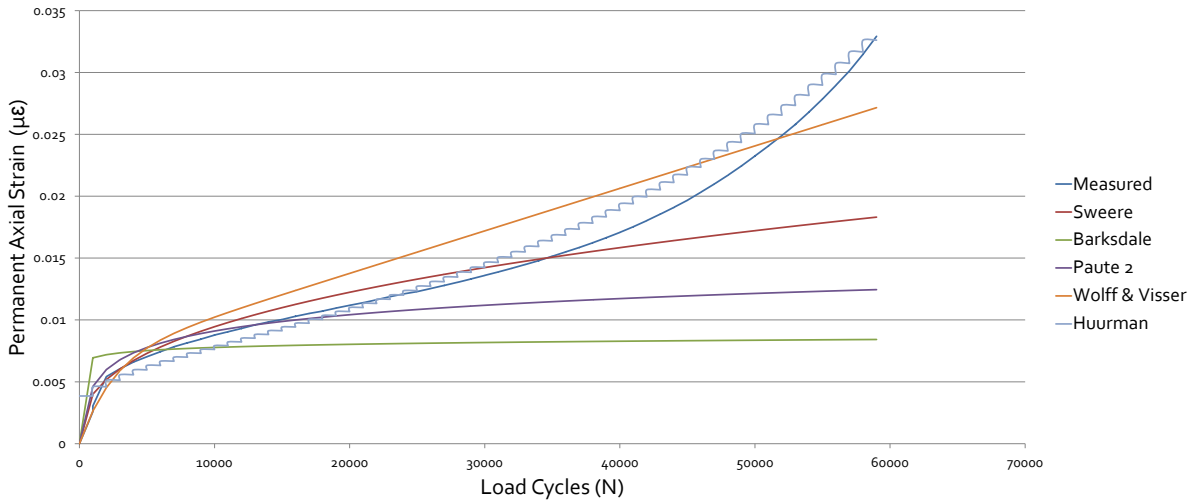

Figure 3-13: Measured and Modelled graphs of unstable Permanent Deformation behaviour

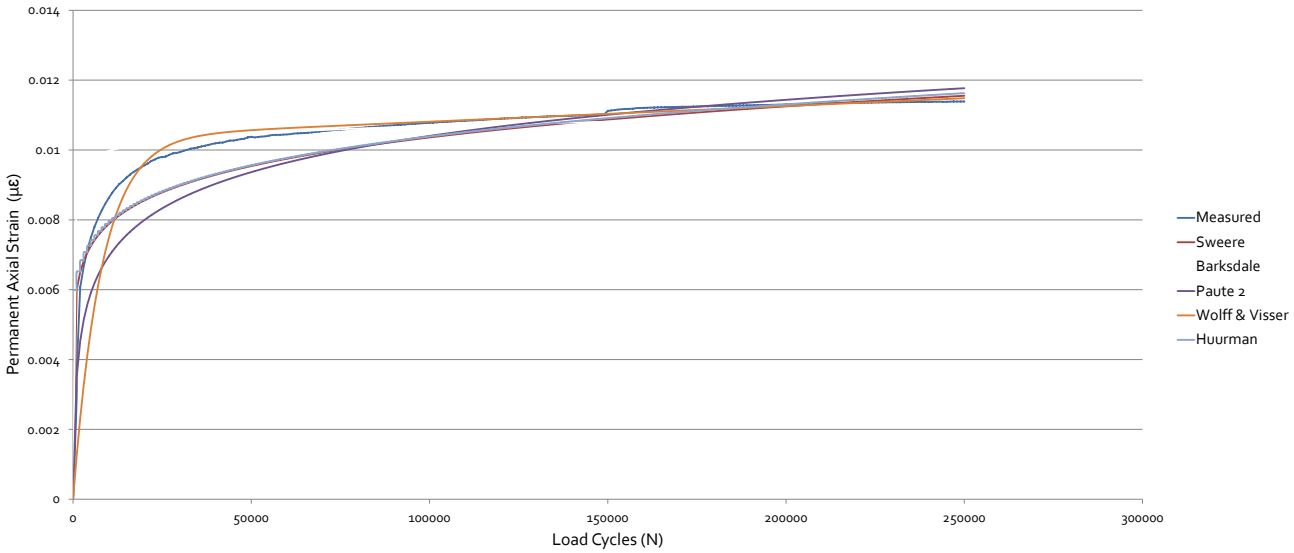

Figure 3-14: Measured and Modelled graphs of stable Permanent Deformation behaviour

3.7 Transfer Function Synthesis

The modelled permanent deformation data was used to create a transfer function in order to predict the pavement life of the RCA material. Various factors that influence the permanent deformation resistance of the material was identified and these factors were included in the transfer function. The basic form of the RCA transfer function is based on a granular transfer function. The variables considered in the Waterbound Macadam are similar to that to be considered for RCA. Therefore the Waterbound Macadam transfer function, as developed by Theyse (2000), was used as a point of departure in the development of a RCA transfer function. The format as well as the calibration of the transfer function will be discussed in Chapter 5:

3.8 Pavement Analysis

A pavement analysis is performed in order compare the structural life of pavements including RCA to that of standard South African Pavements. The transfer function that was developed for RCA material was used as a basis for the pavement life calculations of RCA base and subbase layers. The transfer functions as stated in SAPEM (2014b) was used to calculate the pavement life of other pavement layers. The methodology of this pavement analysis is discussed in further detail in Chapter 6 and the results presented thereafter.

3.9 Summary

The methodology was setup in order to reach the objectives of this research thesis. Initially, it was decided to perform monotonic and permanent deformation triaxial tests on a RCA material obtained from the road demolition project on the N2 highway near the Cape Town International Airport. The main objective for performing these tests were to gain information on the performance of the material. This will enable the development of a preliminary transfer function that can be further calibrated as more research becomes available. It is important to state that the experimental design and the methodology changed as the tests were performed and the material behaved unexpectedly. Due to the high strength and good quality of the material, it was decided to test at lower confinement pressures and to introduce an Exposed branch of testing, to consider comparatively the durability challenges that could be experienced.

The methodology discussed all aspects of the testing procedure ranging from the material preparation to the testing procedure. All the equipment that was needed to prepare and compact the material was discussed and illustrated. The preparation for the specimen as well as the test procedure for each method of testing was discussed. Once the data was obtained it could be reworked to determine the permanent deformation behaviour for the RCA material.

Numerical models were used to model the permanent deformation behaviour, and to obtain full data sets for the synthesis of transfer functions. Lastly comparisons between standard South African and pavements including RCA layers were performed.

Chapter 4: Results

4.1 Introduction

This chapter presents the results obtained from the monotonic and permanent deformation tests performed in this study. The objective was to investigate the permanent deformation behaviour of the material for increasing load cycles, curing times, applied stresses and different exposure conditions. Two types of materials were tested, firstly the Unexposed material that was obtained from the investigation site. Secondly, the Exposed material which consists of the Unexposed material that was treated with water for 14 days and allowed to cure. Once the permanent deformation results were obtained, various numerical models were used to model the behaviour and a model identified that best fits the overall behaviour of the test set. A comparison of the models were performed and the influence of each variable on the model completed.

A summary of this chapter is given in Figure 4-1. The objectives of the various aspects of the results are reported in order to put the research project into context. Objectives 1 and 2 are addressed in this chapter. Objective 3 is only addressed in the following chapters where the transfer function is synthesised followed by pavement analyses. The sections that the results are presented in are indicated next to each major level of the diagram in Figure 4-1. An elaboration on the objectives as shown on the schematic in Figure 4-1 is as follows:

1. Compare and discuss the difference in behaviour and performance of granular materials and RCA materials;
2. Compare the difference in performance of Exposed and Unexposed RCA materials to provide an indication of the durability of the material;
3. Model Permanent Deformations in order to create a transfer function which will allow the prediction of the pavement life.

The results reported here is divided into two sections and includes the Unexposed material (Chapter 4.2) and the Exposed material (Chapter 4.3). The reason for discussing the results in different subchapters is due to the potential for self-cementation that could lead to different behavioural characteristics between the two materials.

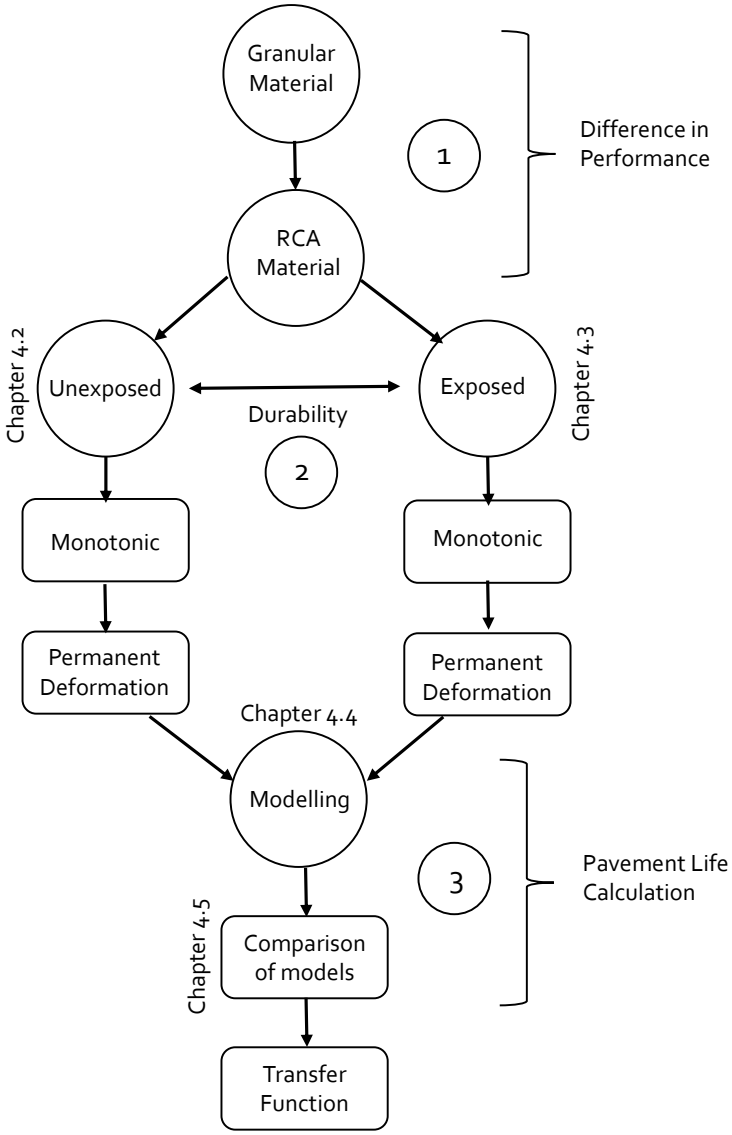

Figure 4-1: Summary of results chapter and the objectives

4.2 Unexposed Material

The Unexposed material was taken directly from the investigation site and prepared for testing as explained in Chapter 3.

4.2.1 Shear Behaviour

4.2.1.1 Monotonic Results

The shear strength of the Unexposed RCA material is determined using 6 monotonic tests. The tests were executed as outlined in Chapter 3.6.4. The results obtained from the 6 monotonic tests are summarised in Table 4-1. The table includes the maximum axial force at failure, as well as the maximum deviator stress. The deformation behaviour at each confinement pressure is illustrated in Figure 4-2. Here it can be seen that the strength of these materials are directly dependent on the confinement pressure applied.

Table 4-1: Results obtained for 6 monotonic Unexposed RCA tests

Specimen	MU1	MU2	MU3	MU4	MU5	MU6
Confinement (kPa)	50	50	100	100	200	200
Maximum Deviator stress (kPa)	2138.3	2127.8	2818.3	2780.8	3644.3	3632.2
Maximum Force (kN)	38.80	38.61	51.14	50.46	66.13	65.91
Maximum Displacement (mm)	9.48	9.4	9.13	9.22	10.04	10.20

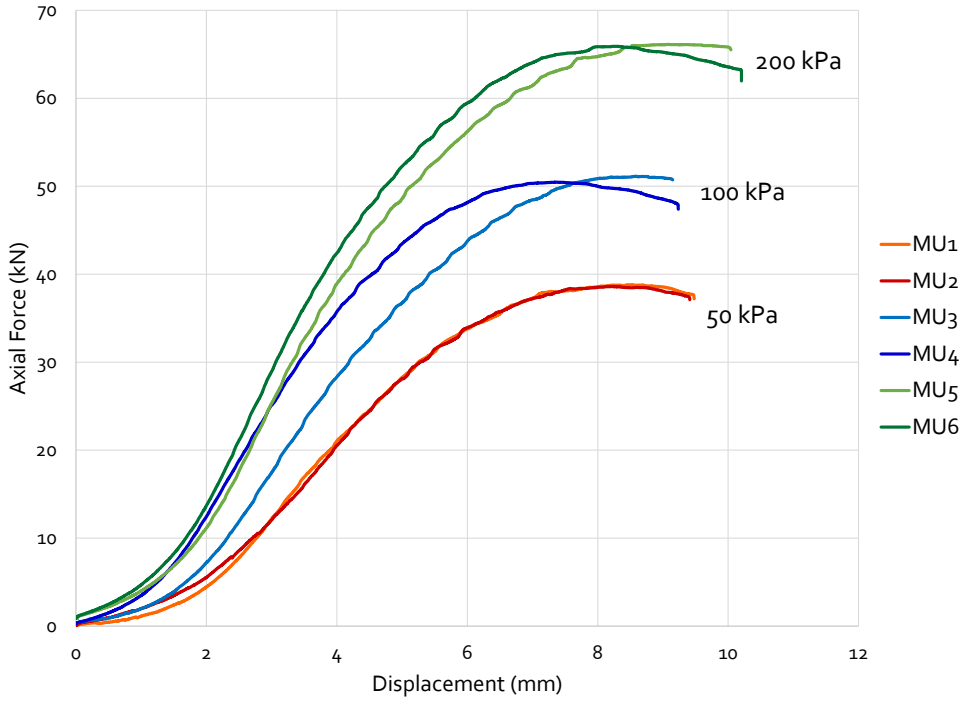

Figure 4-2: Axial force versus the axial displacement for the Unexposed Monotonic tests

The maximum applied force can be used to calculate the deviator stress at failure ($\sigma_{d,f}$) and in turn can be used to calculate the principal stress at failure. The principal failure stress is related to the shear strength parameters of the material. Table 4-2 shows the principal failure stress for each test as well as the calculated shear strength parameters for the RCA Unexposed material.

Table 4-2: Principal stress at failure and shear strength parameters for Unexposed RCA material

Data Point	σ_3 (kPa)	$\sigma_{d,f}$ (kPa)	$\sigma_{1,f}$ (kPa)	C (kPa)	Φ (°)	R^2
1	50	2138.3	2188.3			
2	50	2127.5	2177.5			
3	100	2818.3	2918.3	273.7	54.6	0.98
4	100	2780.9	2880.9			
5	200	3644.5	3844.5			
6	200	3632.1	3832.1			

The principal stress at failure and the confinement stress is plotted to obtain Figure 4-3. A straight line of best fit is plotted and the obtained line parameters can be used to obtain the shear parameters according to the A-B model as explained in Chapter 3.6.4.1.

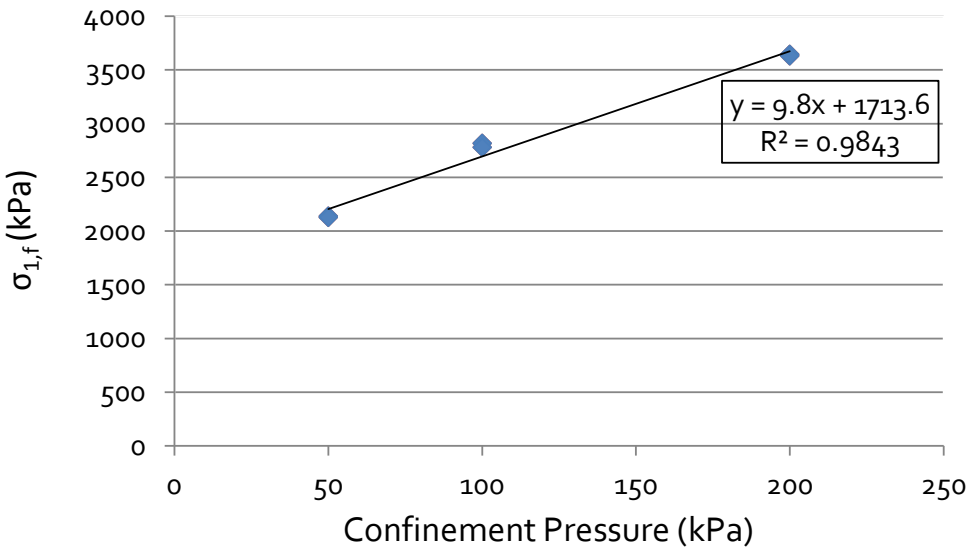

Figure 4-3: Principal stress at failure versus confinement pressure

It is important to note that the R^2 value of the data points is very high. This indicates a strong correlation between the data points. If any data points did not fit the trend or the R^2 was low, it would be advisable to redo these tests as the monotonic tests and the shear parameters form the basis of the calculations for the permanent deformation tests to be performed. It should also be noted that the friction angle and cohesion is inordinately high. This is discussed in the following section.

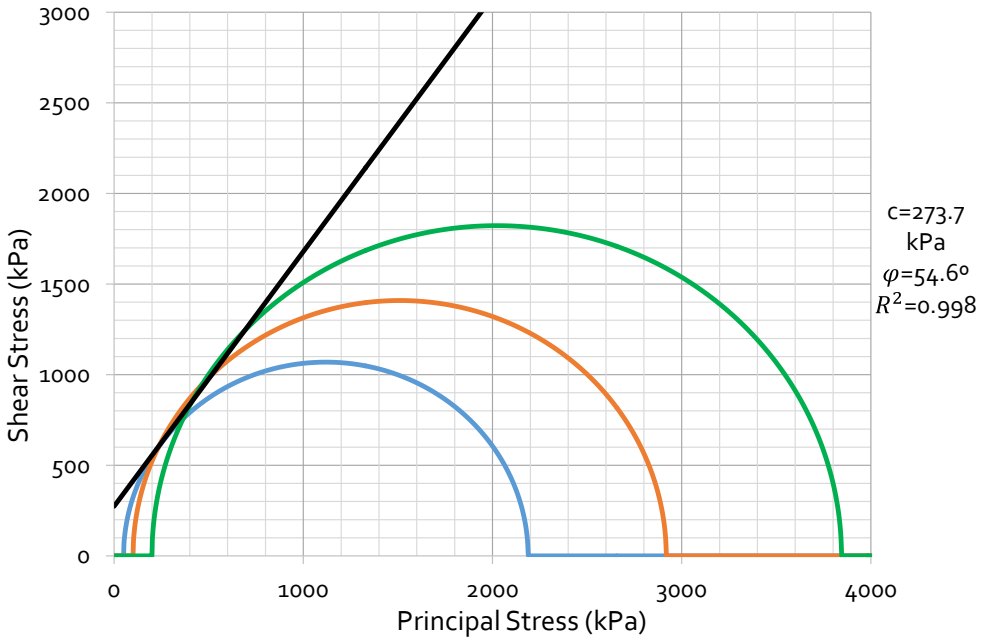

Figure 4-4: Mohr-Coulomb plot for Unexposed RCA material

4.2.1.2 Discussion of Monotonic Results

To establish the validity of the obtained monotonic results and shear parameters, it is beneficial to investigate the shear parameters obtained by other researchers. Rudman and Jenkins (2015) and van Zyl (2015) both completed previous studies concerning the behaviour of RCA studied at Stellenbosch University. Rudman and Jenkins investigated the performance of newly crushed concrete, whereas van Zyl investigated the performance of older crushed concrete. Cameron *et al.* (2013) and Arulrajah *et al.* (2014) are researchers from Australia that investigated the viability of RCA as base or subbase layer substitute. A summary of the shear parameters of the above mentioned researchers are shown in Figure 4-5.

In most cases, with the exception of Arulrajah (2014) and Cameroon (2013), gradings were kept consistent. This allows for reasonable comparisons between these materials, but at the same time one must be aware that grading can have a significant influence on results.

When comparing the data obtained for the Unexposed RCA to that from other studies it can be seen that this material has the highest cohesion and friction angle. The shear strength parameters for a G2 granular material is obtained from SAPEM (2014b). When comparing the granular material and the RCA material, the cohesion of the RCA material is 223 kPa larger than that of the granular material, and the friction angle of RCA is 2° higher. Arulrajah *et al.* (2014) obtained a cohesion of 0, which is highly unlikely due to the cementitious nature of RCA material. His results are therefore not comparable to that obtained in this research. Cameron *et al.* (2013) obtained values of cohesion and

friction angle that are comparable to the values obtained by Rudman and Jenkins(2015). Van Zyl (2015), that investigated old concrete obtained a low cohesion of 119 kPa and normal friction angle of 52.9°.

The lower cohesion may be attributed to the fact that he tested old concrete and the self-cementing potential in this material was lower. The results obtained in this thesis correlates with that obtained by Rudman and Jenkins (2015), who tested newly crushed concrete. New concrete has a very high potential for self-cementing as there are still high contents of latent cement present within the matrix, the fact that the current Unexposed RCA shows similar cohesion and friction angles to that of Rudman (also a new concrete) and may be suggest that this material has a very high self-cementing potential as well.

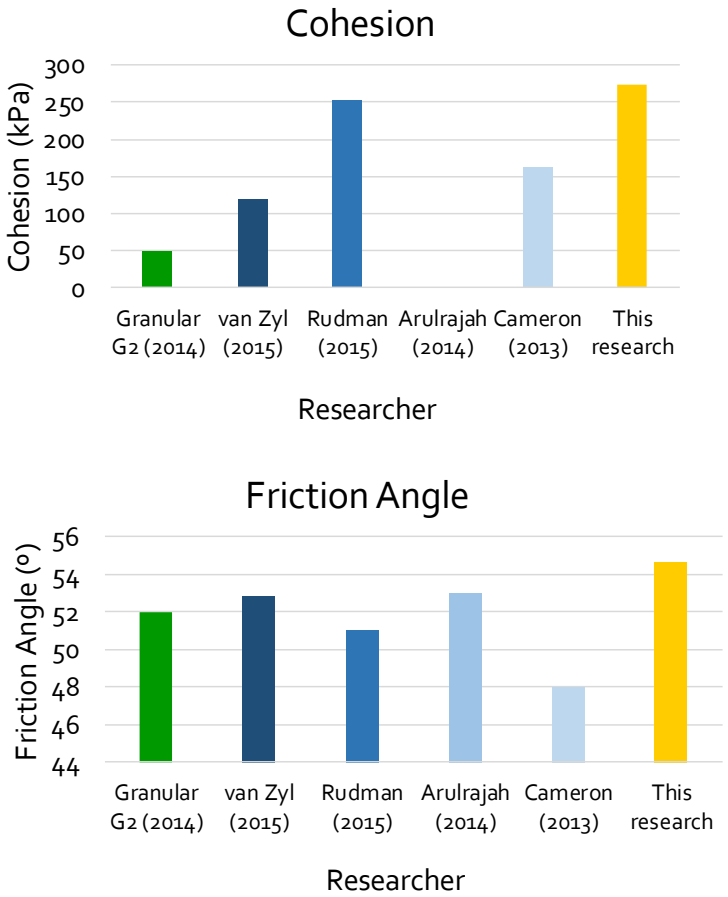

Figure 4-5: Summary of shear parameters for Unexposed RCA materials at 0 months of curing

According to Leek and Siripun (2010) the cohesion of a RCA material should be between 20 and 150 kPa. If the cohesion is less than 20 kPa the material will ravel. If the cohesion is above 150 kPa it will result in brittle behaviour of the material. The cohesion for the Unexposed RCA is significantly larger than this range. This means the material is very stiff and could result in an unexpected mode

of failure (i.e. not permanent deformation). The friction angle of a RCA material should be higher than 45° (Leek & Siripun, 2010). The Unexposed RCA material has a higher friction angle than the prescribed value.

It was attempted to perform monotonic tests at 28 days of curing, on the same Unexposed material, however this material has cemented to such an extent that the material was too stiff and strong and exceeded the capacity of the MTS machine at Stellenbosch University. Due to the cementation of the material it was not possible to perform permanent deformation tests on the Unexposed samples that were cured for 1 month. Figure 4-6 provides some context on the magnitude of such an increase caused by an extended period of curing. Van Zyl (2015) showed a 105% increase in the cohesion, and Rudman (2015) showed a 26% increase.

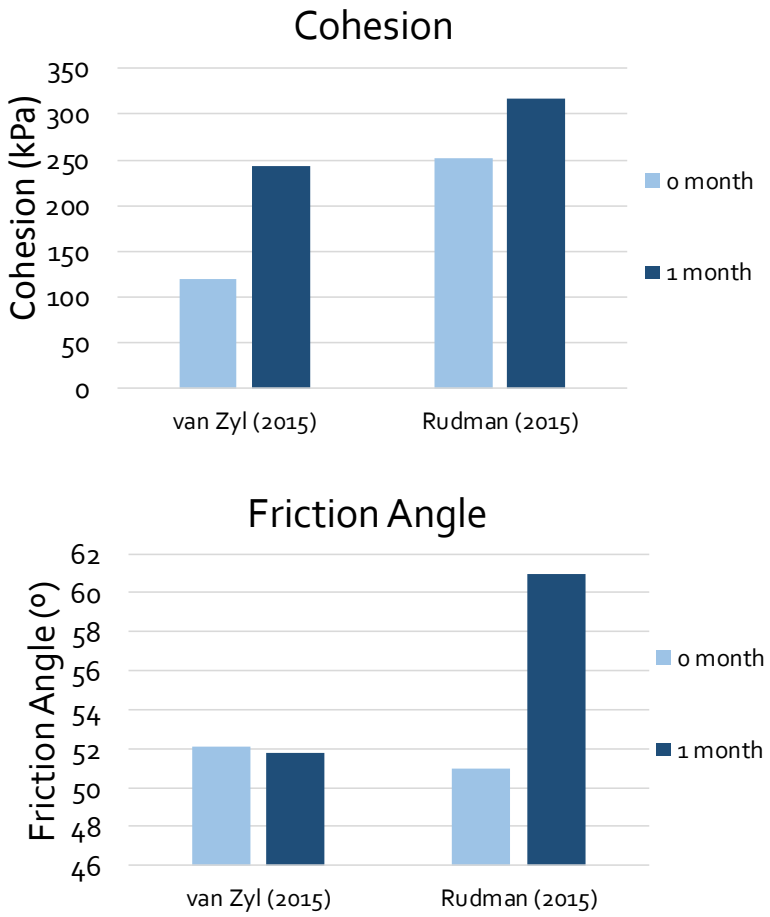

Figure 4-6: Summary of shear parameters for Unexposed RCA materials at 1 month of curing

The increase in cohesion could be attributed to the latent cement in the material, however no clear relationship between concrete type and growth can be found from these results. It should be noted that the cohesion and friction angle increase over time. This which will affect the material, due to an increase in strength, when intermittent permanent deformation tests are performed. It was still

possible to perform permanent deformation tests, even with the increase in strength as the deviator stress values tested were much lower than that of failure.

4.2.2 Permanent Deformation Test Results

Permanent deformation tests were performed at three confinement pressures, 50 kPa, 75 kPa, and 100 kPa. Convention would have the monotonic tests and the permanent deformation tests performed at the same confinement pressures, however this is beyond the capability of the MTS machine at Stellenbosch University. The MTS machine has a maximum loading capacity of 100 kN, which is limited to 90 kN in order to protect the integrity of the machine. If the material was to be tested at 50% of the failure stress at 200kPa for extended dynamic periods of time this could result in damage to the machine. The material was therefore tested at 50 kPa, 75 kPa, and 100 kPa with a deviator stress ratio of 37% and 45%, 50%. Two types of tests were performed, including basic permanent deformation tests to a limit of 250 000 load cycles. Intermittent permanent deformation tests were tested to a limit of 100 000 cycles, before they were removed and cured for 1 month, thereafter, another 100 000 cycles were applied. The monotonic test results and calculated failure forces for each confinement pressure for both Exposed and Unexposed RCA can be found Annexure-B. When referring to a specific test the nomenclature of x/y is used (x denotes the confinement pressure and y denotes the percentage deviator stress ratio).

4.2.2.1 Basic Permanent Deformation Results

Seven basic performance tests were performed at different confinement pressures. The seven tests consisted of the longer loading schedules, i.e. 250 000 loading cycles at different confinement pressures. The permanent axial displacement of the specimens were limited to 25mm of the total height of the sample or 8% permanent axial strain. The limit allowed for the test to be stopped before the material disintegrates. The results obtained from the basic permanent deformation tests are summarised in Figure 4-9.

The stress levels, comprising of the deviator stress and confinement stress is one of the most important factors influencing the development of permanent deformation in granular materials. In granular materials, the accumulation of permanent axial strain is directly proportional to the deviator stress and inversely proportional to the confinement pressure. This means that, as the deviator stress increases the amount of permanent deformation increases, and as the confinement pressure increases, the amount of permanent deformation decreases (Lekarp *et al.*, 2000a). However, this behaviour was not observed in the permanent deformation results for RCA material. It can be seen in Figure 4-9 that as the deviator stress increases for the same confinement the amount of permanent

deformation increases which is in line with the expected behaviour. Although as the confinement pressure increase the amount of permanent deformation in the material increases.

The reason for this behaviour may possibly be attributed to the self-cementing process that takes place within the material. The latent cement in the material reacts when the water is added to the specimen, this results in cement bonds forming within the material. The high strength of the material can be attributed to these bonds. At low confinement pressures, the loading force (force applied to induce the needed deviator stress) is of a low enough in magnitude that the material is compacted but the cement bonds within the material stay intact. The material at low confinement pressures can rely on the matrix interlock as well as the cement bonds to withstand the applied loads. The cement bonds at this level possibly also provide resistance to deformation in the vertical and horizontal direction, thereby "assisting/contributing" to the effect of the confinement pressure. It therefore performs well at low confinement pressures. The vertical stress applied at higher confinement pressures is much higher even if there is only a change of 50KPa in confinement (and attributed to the high friction angle). Possibly at these higher confinement pressures the cement bonds break down and it relies only on the matrix interlock with no "extra positive contribution" to the confinement either. Further studies are needed to investigate this theory and the influence of the applied stress on the specimen. In this research it shows that confinement plays a role in the behaviour of the material, but it is necessary to ascertain whether it is the magnitude of the applied stress that causes the unexpected behaviour. The applied stress and the confinement pressure are directly dependent on another. The increase in the applied stress for each confinement may be of such an extent that it plays the governing role in the behaviour of the material.

When the confinement pressure is increased, the force possibly becomes of such a high magnitude that the material is not only compacted, but the cement bonds within the material are broken down. Once the cement bonds are broken, the applied vertical force is only carried by the matrix interlock, resulting in a higher amount of permanent deformation at high confinement pressure. This behaviour can be seen in Figure 4-7. The first phase is the material before testing, the second phase is as the confinement and deviator stress is applied, the material is compacted. Possibly, formed clusters of lightly cement bonds, stay intact. Also, cement bonds do not necessarily form uniformly throughout the sample, but probably more as these clusters. During the third phase at high confinement pressures, where high applied vertical stresses are applied, the material is not only compacted but the cement bonds are possibly broken down.

.

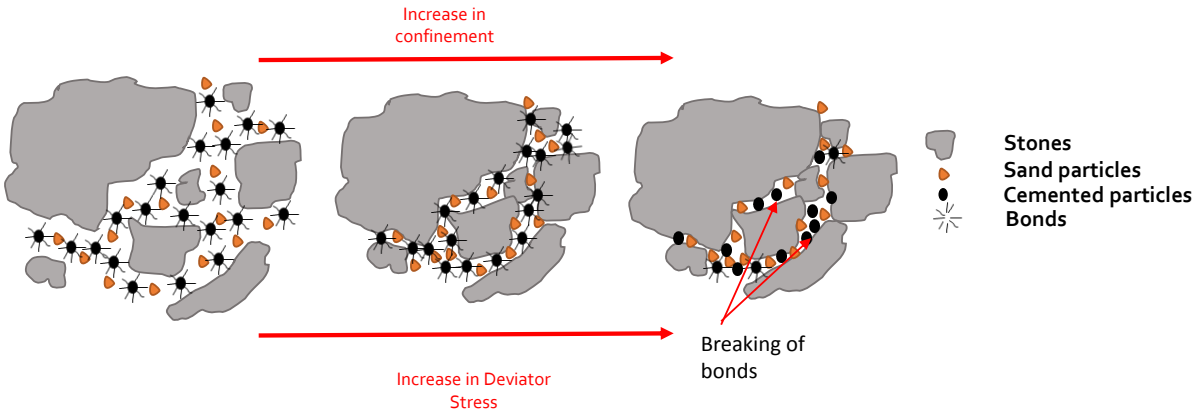

Figure 4-7: Behaviour of RCA material with increasing confinement and deviator stress

Figure 4-9 shows the results for seven basic tests, with the red lines representing a confinement pressure of 50 kPa, the blue lines representing a confinement pressure of 75 kPa and the black lines representing a confinement pressure of 100 kPa. Figure 4-8 can be used to discuss the results obtained from the permanent deformation results. As explained in Chapter 2 the shakedown approach can be used to classify the behaviour of the material. Below the plastic shakedown limit is Range A, between Plastic creep limit and plastic shakedown limit is Range B and Range C is static failure. As the confinement pressure and deviator stress ratio increases the material behaviour changes from stable to unstable behaviour.

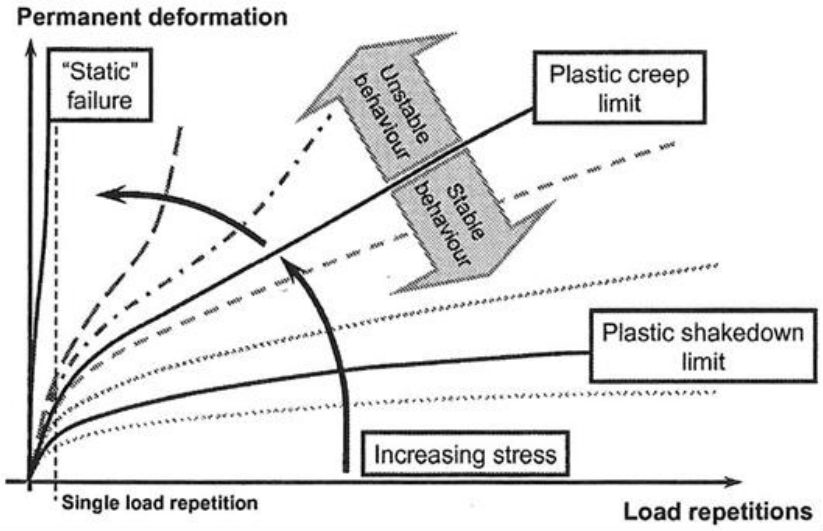

Figure 4-8: Annotated diagram of the Shakedown Theory (Theyse et al., 2007)

For a confinement pressure of 50 kPa, three stress ratios are tested namely 37%, 45% and 50%. The results obtained for 37% and 50%, exhibit similar behaviour of reaching a limiting value of permanent deformation of 1.2%. The rate of increase in permanent deformation is approaching 0% axial strain, and the material falls below the plastic shakedown limit, in Range A. The results obtained for 45%

stress ratio, shows slightly different behaviour, with the accumulation of permanent deformation still happening towards the end of the test. This means that the material has exceeded the plastic shakedown limit and falls with Range B. This specimen still exhibits stable behaviour, although there is a chance of unexpected failure. The fact that the specimen at 50% stress ratio performed better than the specimen at 45% stress ratio can be attributed to variability of the material and means it is an outlier. Due to material constraints and the availability of the current source of material this test was not retested. RCA material has a high degree of variability even in terms of compaction and moisture content and the performance of some samples. Even though lab preparation is highly controlled. The initial hygroscopic moisture of the material differs considerably within the same source. In latent cement bonds in the materials might also be a cause of high variability.

For a confinement pressure of 75 kPa, two stress ratios namely 37% and 45% were tested. Initially both tests exhibit similar behaviour, but towards the end of the test, it can be seen that the specimen tested at 37% stress ratio stabilises and will fall within Range A, whereas the specimen subject to 45% stress ratio continues to accumulate permanent deformation and will fall within Range B. Both samples exhibit stable behaviour for the duration of the test.

For a confinement pressure of 100 kPa, two stress ratios were tested namely 37% and 45%. Both tests at 100 kPa confinement pressure exhibits rapid increase in permanent deformation development, at 37% stress ratio the material initially performs satisfactorily, but towards the end of the test the amount of permanent deformation is increasing rapidly. For the specimen tested at 45% stress ratio, static failure in Range C is observed, and the specimen fails rapidly after the commencement of the test, it only lasts 50 000 cycles of the total of 250 000.

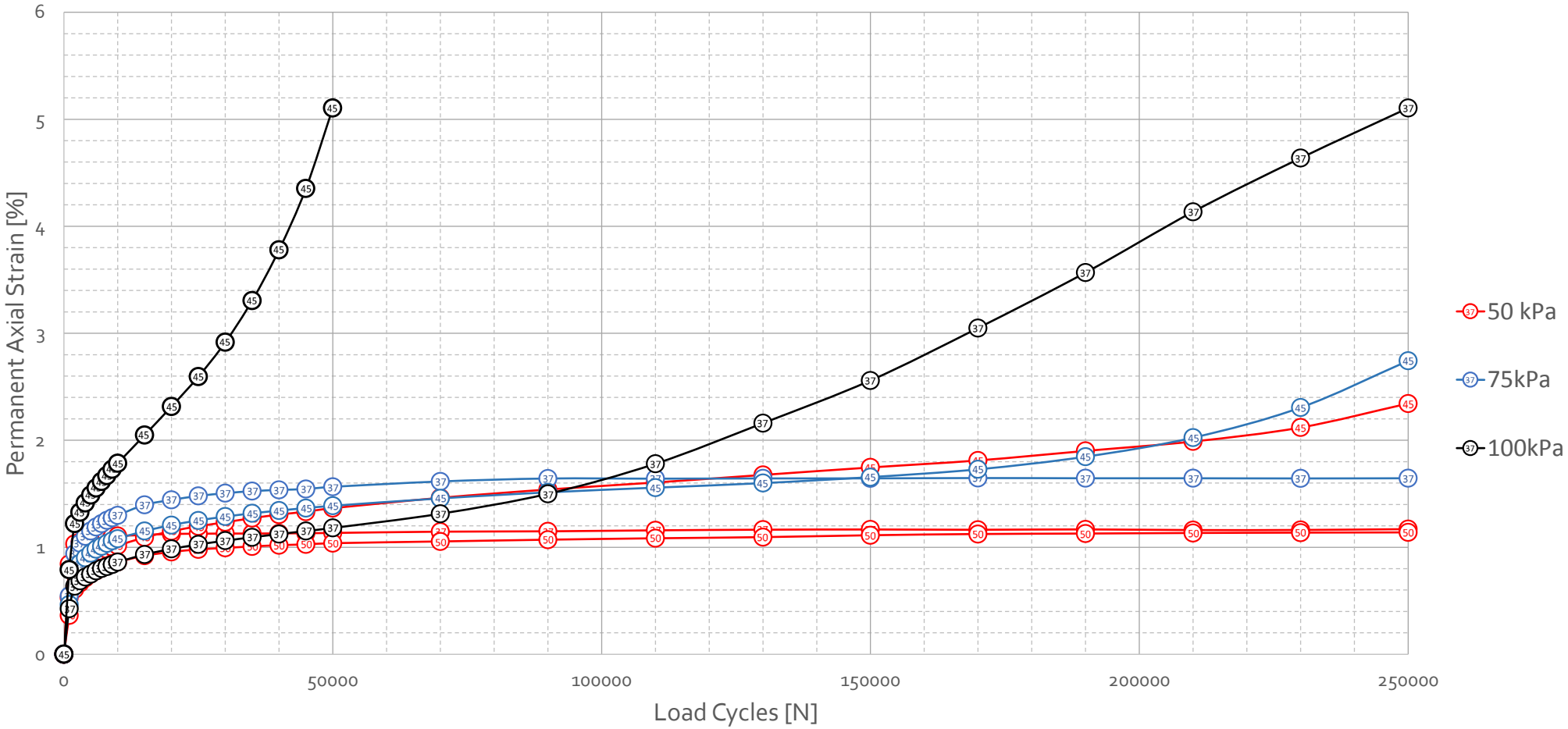

Figure 4-9: Summary of Basic Permanent Deformation test results for Unexposed RCA material at 0 months of curing

4.2.2.2 Intermittent Permanent Deformation Results

The Intermittent Permanent Deformation tests are specialised tests that have been completed to gain insight into the self-healing potential of RCA material. Due to the self-cementing phenomenon of RCA, the material has the potential to create bonds which can fix small cracks or deformities in the fine matrix. Very limited research is available on the self-healing potential of RCA materials. The intermittent tests are completed by testing a specimen for 100 000 cycles at 1 day of curing, and then removing it from the machine, sealing and curing it for 1 month before testing the specimen again for 100 000 cycles at the same confinement pressure and deviator stress.

The results of the permanent deformation tests are shown in Figure 4-11 and Figure 4-12. Figure 4-11 shows the results for the first cycle of tests that are completed at 1 day of curing, and Figure 4-12 shows the results for the second cycle of tests that are completed at 28 days of curing. In order to preserve the sample and prevent disintegration, the maximum axial displacement was limited to 20 mm of the total height of the sample or 6.67% permanent deformation. This limit allows for a sample that show Range C behaviour (defined as unstable), i.e. a rapid increase in the vertical displacement, to be removed in one piece and be further tested as part of intermittent samples. It is possible for the sample to have reached this point but not yet reached terminal condition of the sample as defined here and still be cured and retested at the intermittent 100 000 cycles

The importance of this set of tests are to compare the change in behaviour from 0 month to 1 month. The behaviour exhibited at 0 months, for a reduced loading period is similar to what was discussed for the basic permanent deformation tests regarding confinement pressure. The graphs that compare the change in behaviour for the intermittent samples between 0 month and 1 month of curing (i.e. 1 day and 28 day curing periods) are shown in Annexure C. One of these graphs are shown in Figure 4-10, to explain the difference in behaviour. During the first round of testing the specimen tested at 100 kPa confinement at a stress ratio of 37%, showed unstable behaviour and resulted in Range C behaviour according to the Shakedown Theory. The sample could only withstand 50 000 cycles before the specified vertical displacement limit placed on the machine. It was then removed from the machine, sealed and cured, before being tested for a second run of 100 000 cycles. A sample that previously showed unstable behaviour (typical Range C behaviour), now showed stable behaviour. In this example only 0.26% percent permanent deformation is induced in the sample after 1 month of curing, this is a 88.8% reduction from the initial 2.325% permanent deformation.

For all specimens tested after 1 month of curing, the percentage permanent deformation has decreased and the average percentage varies between 0.2-0.6% strains. One outlier test was observed with strains of 1.6%. This is due to the higher vertical displacement in the initial cycles of

the intermittent testing of this particular test. Possibly because of a large stone moving and coming to rest within the aggregate matrix. If these initial cycles are not taken into account the material would exhibit the same trend in terms of percentage strain. This shows a clear improvement between the percentage strain for the 0 and 1 month samples.

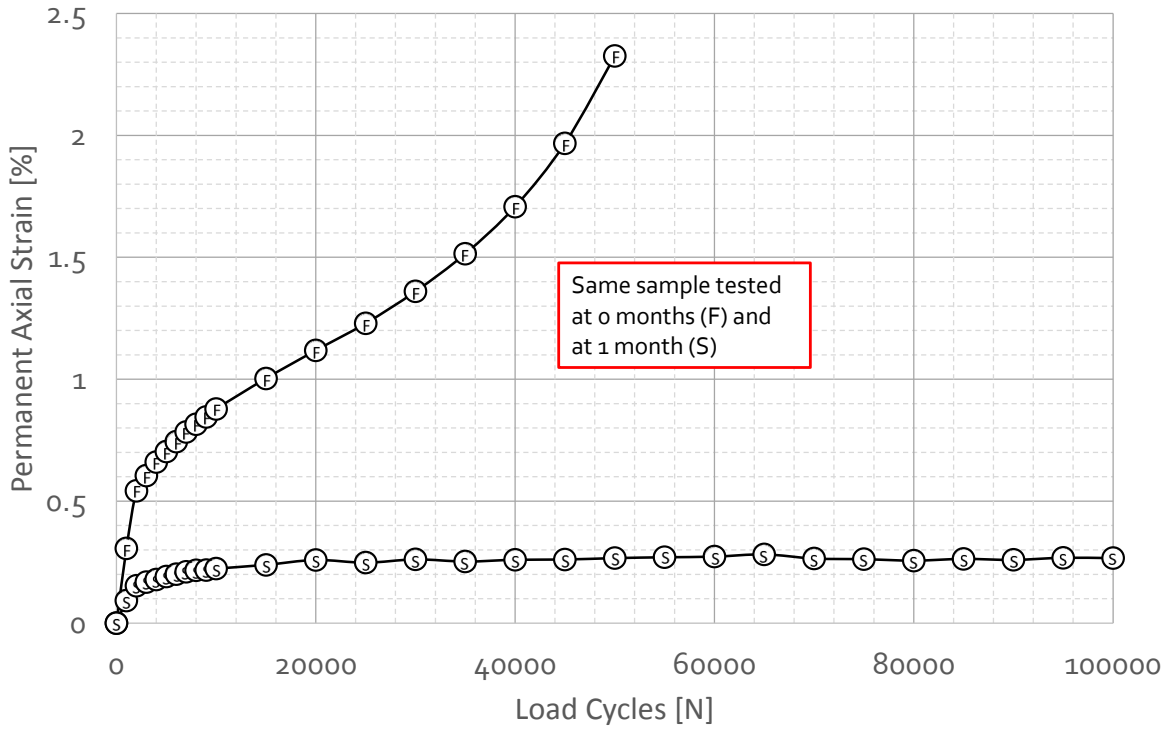

Figure 4-10: Behaviour change in RCA due to curing time at 100 kPa confinement with a 37% deviator stress ratio

This improved behaviour was exhibited for all tests that were tested at 0 and 1 month curing time. This finding holds a key piece of information in terms of the trafficability of RCA material. This shows that RCA material once placed in the road structure can undergo some loading as a results of construction vehicles, and through intermittent resting periods (not necessarily the long resting periods tested here), will result in markedly higher strength and a significantly lower permanent deformation accumulation within the material. One should realise though, that the material might have moved into an entirely different region of behaviour. After 1 month curing the material may be more lightly cemented and in a transitional area between bound and unbound. As has been shown, the intermittent results that indicate stable behaviour for both 37% and 45% stress ratio. However, it is important to remember that this deviator stress ratio at 1 month testing is based on the 0 month shear parameters of the Unexposed RCA. The shear parameters for 1 month is not known, and this might have shown a reduction in deviator stress ratio.

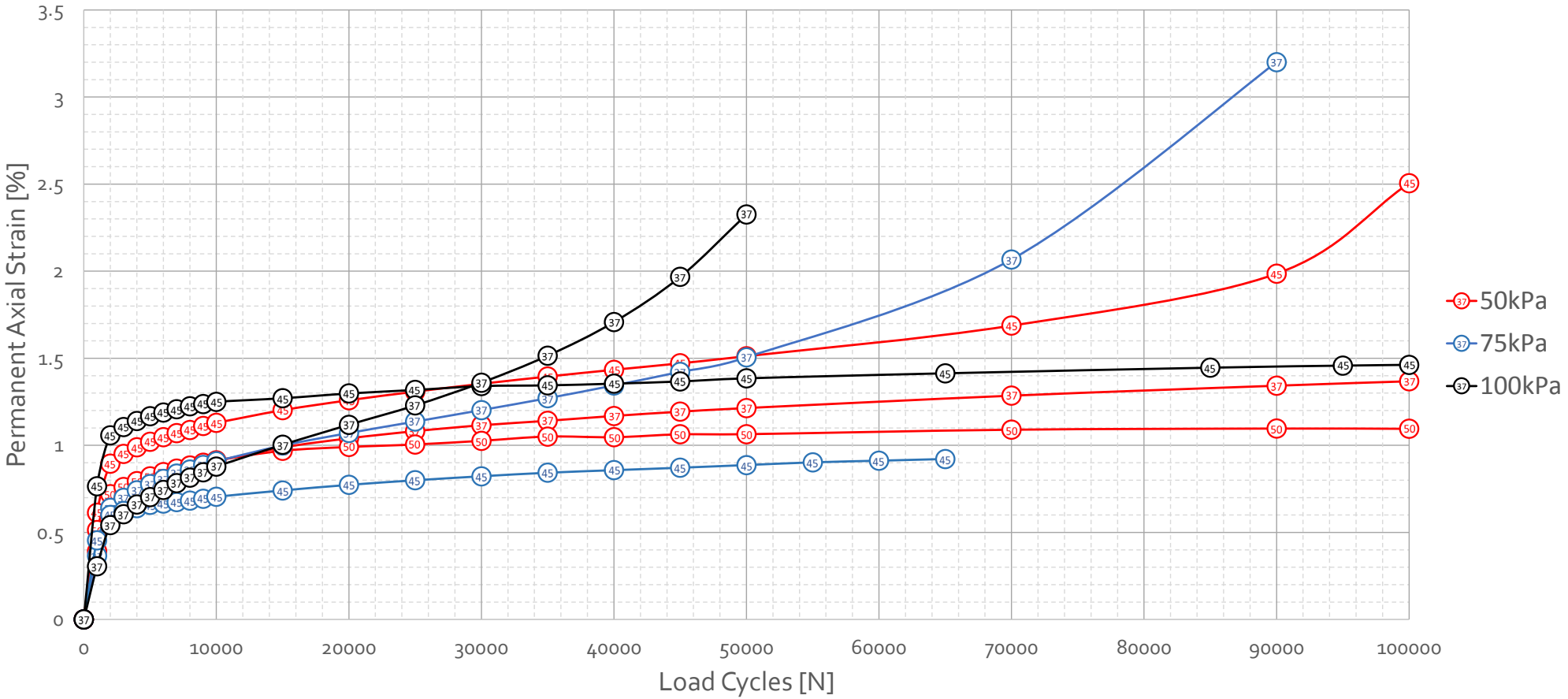

Figure 4-11: Summary of Intermittent Permanent Deformation test results at 0 months of curing for Unexposed RCA

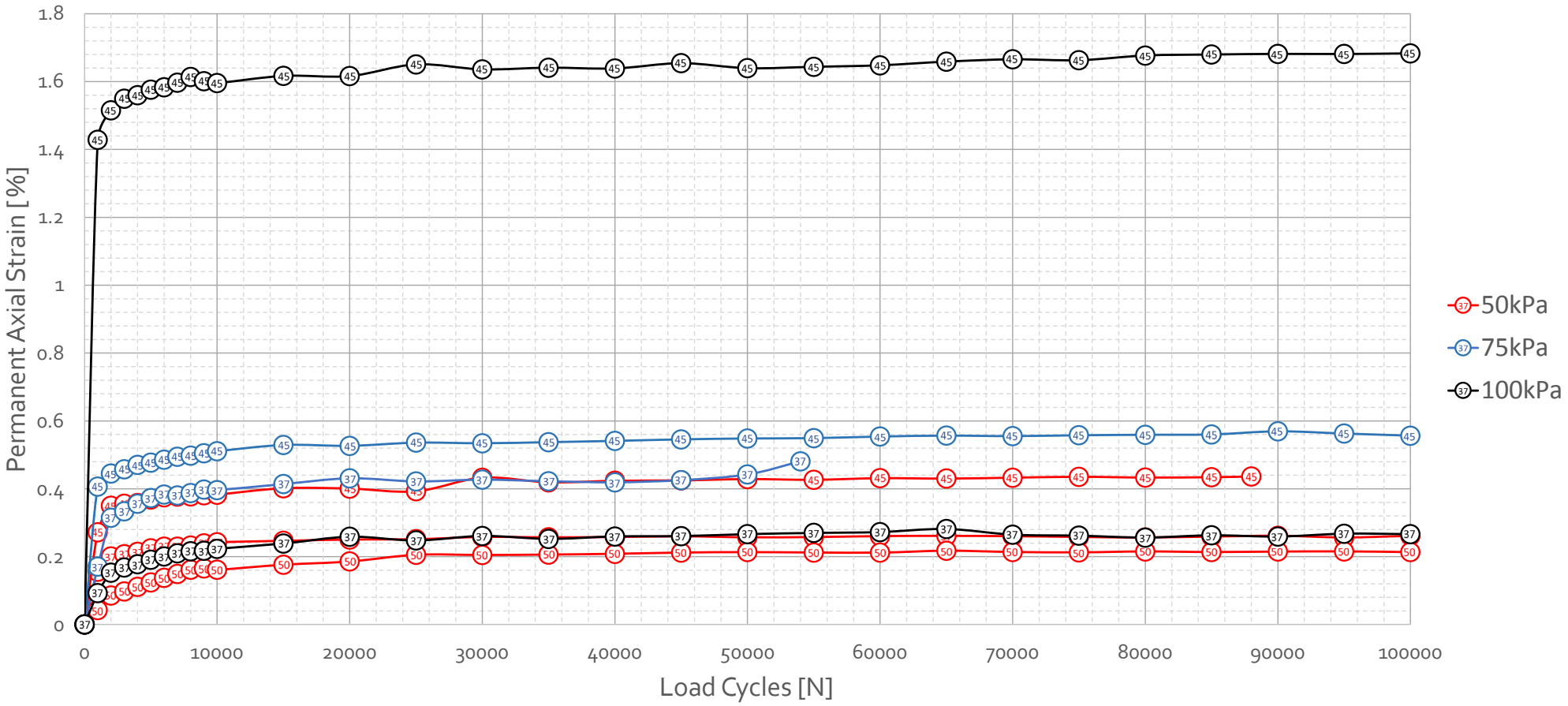

Figure 4-12: Summary of Intermittent Permanent Deformation test results at 1 month of curing for Unexposed RCA

4.3 Exposed Material

Previous results reported in this study on the behaviour of Unexposed RCA shows the dependence of the behaviour of the material on the self-cementing process. With this benefit one should consider what will happen if the material does not have the potential or if this potential is diminished, and this leads directly to durability concerns. Due to the variable sources of this material, it is difficult to predict the self-cementation potential of the material, and it is therefore important to investigate the behaviour of the material if the self-cementation potential is negligible. This will be the worst case scenario. The self-cementing process, could lead to the material behaviour of a lightly cemented material. Depending the dominating behaviour, this could potentially lead to increase in shrinkage cracks and other problems such as carbonation. Many researchers have investigated the performance of RCA, but very little research has been done on the durability aspect of the material. In order to investigate the impact that self-cementing will have on the material, and in turn the durability in terms of performance for RCA material, two types of materials were tested. The Unexposed material is used as is from the site, whereas the Exposed material, is cured using additional water and humidity to reduce the self-cementing potential of the material. The water added during the curing process will result in the hydration of latent cement, the humidity will also accelerate this reaction. By forcing the hydration reactions the amount of latent cement in the material should decrease. It is believed that the Exposed material will have a lower self-cementing potential, and the material will therefore perform more like a granular material. This is a very important factor to investigate, as there is a high possibility that the RCA material will be stockpiled and will be exposed to some water on a construction site. The results obtained for Exposed RCA materials will be presented and discussed here.

4.3.1 Shear Behaviour

4.3.1.1 Monotonic Test Results

The shear strength of the Unexposed RCA material was determined using 6 monotonic tests. The tests were executed as outlined in Chapter 3.6.4. A high degree of variability was observed in the test results of the Exposed RCA material. Therefore 9 monotonic tests were performed and outlier data was eliminated as the shear parameter calculations are very sensitive to the variability in test results. It was also found that the machine does not have the capacity to apply the vertical forces at 200 kPa and was decided to replace the 200 kPa confinement with 150 kPa confinement. The results obtained from the 9 monotonic tests are shown in Table 4-3. The deformation behaviour at each confinement pressure is illustrated in Figure 4-13. Similarly to the previous monotonic test results the strength of the material is dependent on the confinement pressure.

Table 4-3: Results obtained for 9 monotonic Exposed RCA tests

Specimen	ME1	ME2	ME3	ME4	ME5	ME6	ME7	ME8	ME9
Confinement (kPa)	50	50	50	100	100	100	150	150	150
Maximum Deviator stress (kPa)	2100.8	2164.7	2002.8	2680.0	2707.0	2553.2	2938.4	3072.9	3219.5
Maximum Force (kPa)	38.12	39.28	36.34	48.63	49.12	46.33	53.32	55.76	58.42
Maximum Displacement (mm)	12.17	11.02	8.29	13.63	14.42	8.23	11.41	10.15	9.77

When comparing Figure 4-2 and Figure 4-13, which include the monotonic test results for the Unexposed and Exposed material, it can be seen that the Exposed material shows higher degrees of variability in the smoothness of the graph than compared to that of the Unexposed material. This can be seen by the difference in the line of the curve, they are not smooth as was the case for Unexposed RCA montonic tests. This can attributed to the fact that there is non-uniform distributions of cement bonds (or clusters as earlier referred to) throughout the Exposed RCA material. The repeatibility of the results are not as consistent as the monotonic results obtained for the Unexposed material.

Figure 4-14 shows the principal failure stress for each test as well as the calculated shear strength parameters for the Exposed RCA material. In order to calculate the shear parameters two graphs must be drawn. The principal stress at failure and the confinement stress is plotted to obtain Figure 4-14. A straight line of best fit is plotted and the obtained line parameters can be used to obtain the shear parameters according to the A-B model as explained in Chapter 3.6.4.1. The Mohr-Coulomb plot of the results are shown in Figure 4-15.

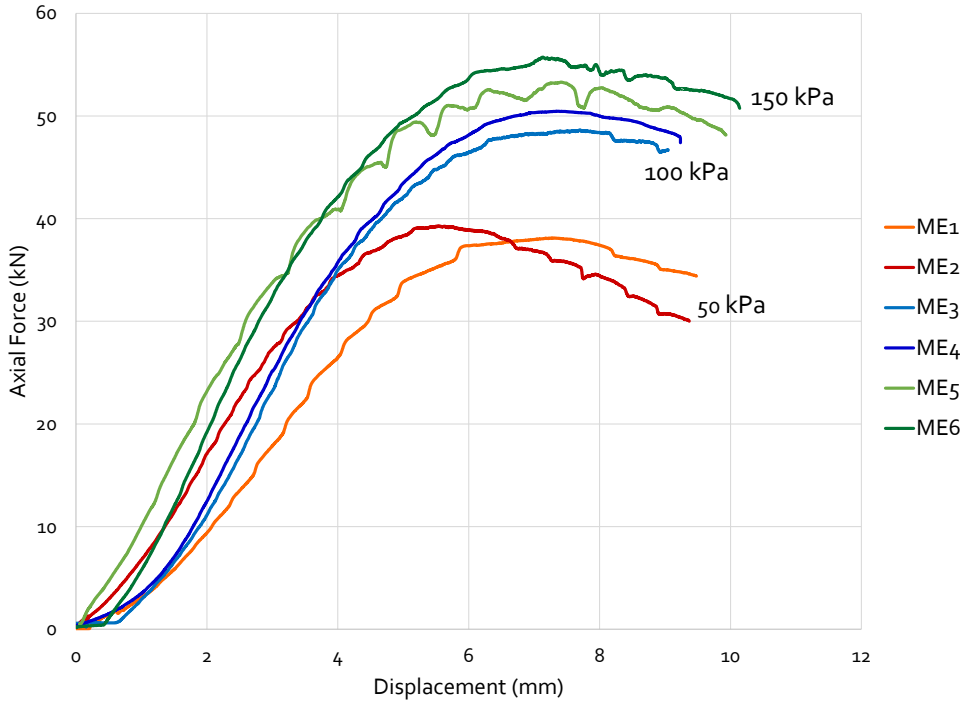

Figure 4-13: Axial force versus the axial displacement for the Exposed Monotonic tests

Table 4-4: Principal stress at failure and shear strength parameters for Exposed RCA material

Data Point	σ_3 (kPa)	$\sigma_{d,f}$ (kPa)	$\sigma_{1,f}$ (kPa)	C (kPa)	Φ (°)	R^2
1	50	2100.8	2150.3			
2	50	2164.7	2214.7			
3	100	2680.0	2780.0	294.1	52.6	0.960
4	100	2707.0	2807.0			
5	150	2938.4	3088.4			
6	150	3072.9	3222.9			

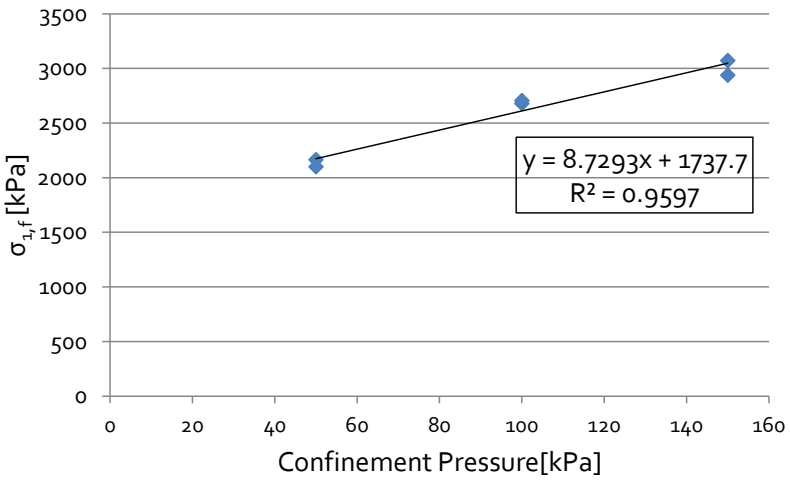

Figure 4-14: Principal stress at failure versus confinement pressure

In order to keep the correlation coefficient as high as possible and to find the line of best fit through the data points, only the 6 data points with the strongest correlations were used. RCA material has a high variability and it is important to take this variability into account, but to not compromise results as a result of variability.

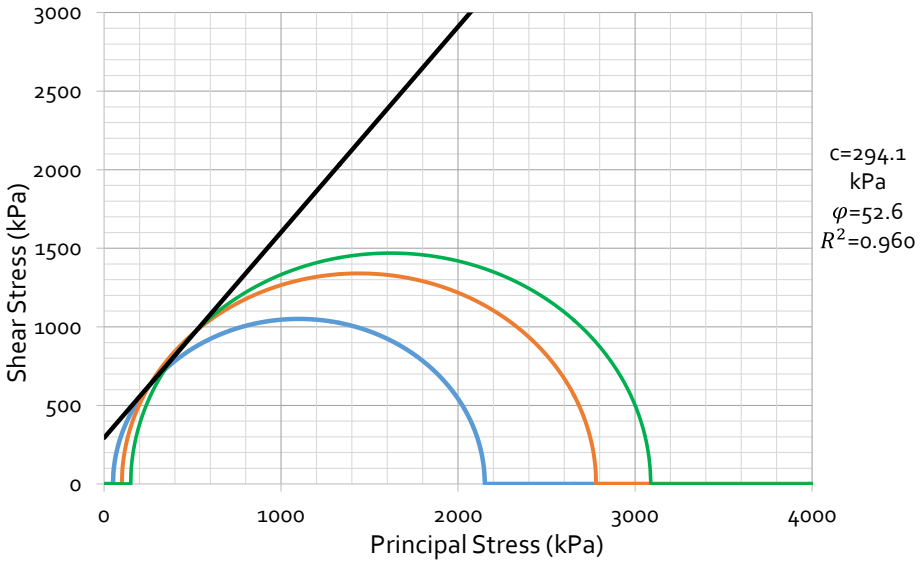

Figure 4-15: Mohr-Coulomb plot for Exposed RCA material

4.3.1.2 Discussion of Monotonic Test results

No literature could be found on researchers that have investigated the exposing of RCA material, and the effect this will have on the self-cementing properties or the performance of the material. Van Tonder (2017) at Stellenbosch University used the same material as this research, and investigated the different factors that affect the shear strength of RCA materials. One of the variables he

investigated was the exposure of RCA material. The results obtained by van Tonder (2017) research is shown in Figure 4-16 , together with the results of exposed material in this research.

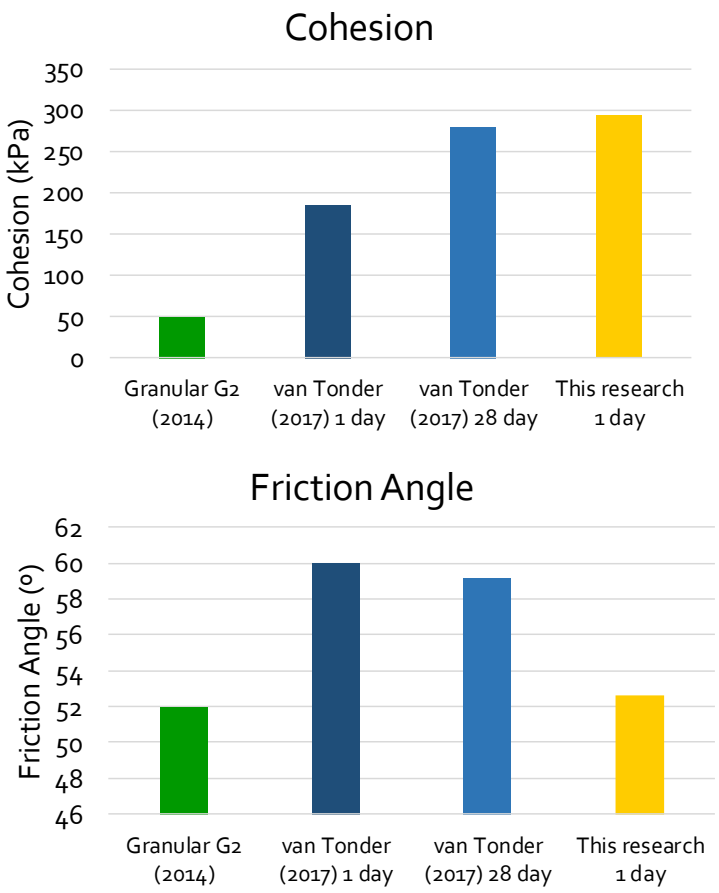

Figure 4-16: Summary of shear parameters for Exposed RCA materials

The results obtained by van Tonder (2017) differs from what was obtained in this research, especially when considering the friction angles. As previously mentioned, the self-cementing process allows for high degrees of variability in the material which is increased during the exposure process. His results should also be considered realistically as Van Tonder (2017) only performed three tests in his Monotonic Testing. With three samples it is not possible to identify outliers as was done for the Monotonic results in this research. It was found that the deviator force at failure he obtained at 1 day curing for 150kPa confinement pressure was 63.71 kN, which is significantly larger than the 53kN-to-58 kN range that was obtained for this study. A small difference in the failure force results in a large increase in friction angle and decrease in cohesion as shown in Figure 4-17. In this study the friction angle after 1 day of curing is 52.6°, whereas the friction angle found by van Tonder (2017) was 60°.

Again, this friction angle and cohesion for this research is high and very comparable to that of high quality granular materials. It is understandable that the friction angle would remain high even after the exposure process due to shape of the parent rock typical used in original concrete mixes. With the many fractured faces in the stone used in concrete mixes, it is quite possible that it could provide the dense matrix interlock. However, surprisingly, is the high cohesion values that the material exhibits. The cohesion of the material is a parameter that one would expect would be influenced by the latent self-cementing properties of the material. The Exposed material went through a regime in order to promote some of the self-cementing prior to testing, yet the values obtained for cohesion still is inordinately high.

Comparisons between the Unexposed and Exposed materials are made in Section 4.5 of this chapter.

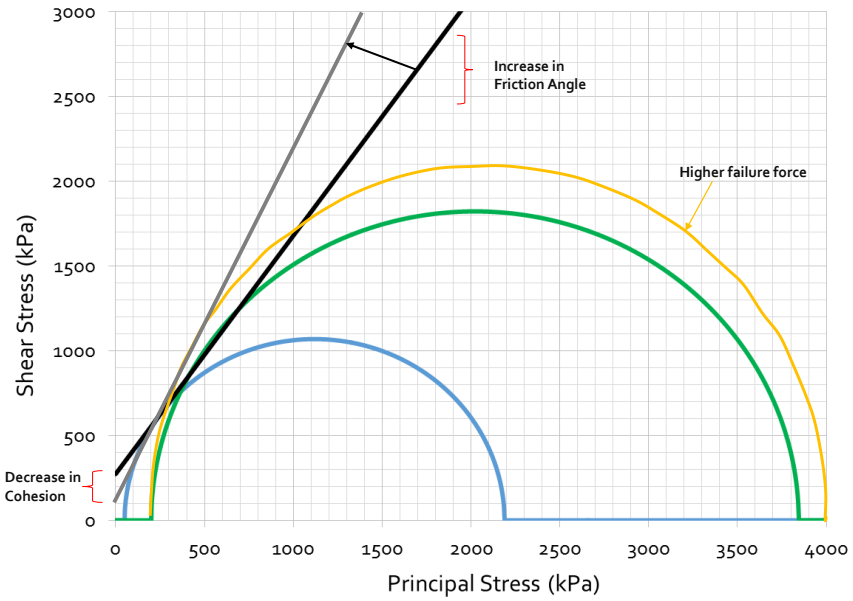

Figure 4-17: Shortcomings of Mohr-Coulomb calculations

4.3.2 Permanent Deformation results

Initially the same testing regime was to be used for Exposed and Unexposed RCA material, in order to best discuss the changes in behaviour of the material due to the curing process. The monotonic test of the Unexposed RCA showed high shear strength parameters with cohesion values higher than 250kPa.As will be discussed when comparing the Unexposed and Exposed shear strength results, the cohesion and friction angles remained more or less similar to each other (within a reasonable range, accounting for variability). This was not expected, however it was later observed that this similarity did not hold for the permanent deformation tests. Here, the Exposed material could not withstand

the high deviator stresses that was applied to the Unexposed material. At 37% deviator stress the specimen failed and disintegrated almost immediately after the commencement of the test. It is believed that due to the lower self-cementing potential, the Exposed material forms less cement bonds, which results in the material not being able to withstand high failure forces (especially when repeated loading is applied), the material can only rely on matrix interlock for strength. Although variability of the material could play a large role, possibly, the type of behaviour measured between the two types of tests (Monotonic vs. Permanent Deformation) here is another potential cause for the reason. The monotonic testing and the application of the Mohr-Coulomb's method is applied to measure shear parameters with one single terminal. The permanent deformation applies continuous dynamic loading. The manner in which the presence of cemented bonds would respond is different in these two different tests.

Even though one would attribute the cohesion increase to the self-cementing potential, depending on the variability of the results it is important to recognise that the mathematics is structured in such a way that the cohesion and the friction angle do not work independently from one another. This is a very important finding in terms of RCA material behaviour. The material cannot be judged solely on the shear performance, permanent deformation tests are vitally important. It was therefore decided to complete the testing the Exposed material at lower deviator stress ratios namely 17%, 22% and 27% (after some preliminary testing to identify reasonable values). Due to availability of material as well as the capacity machine only intermittent permanent deformation tests are performed on Exposed RCA material.

4.3.2.1 Intermittent Permanent Deformation Results

The intermittent permanent deformation tests for Exposed material were performed in the same manner as that of the Unexposed materials. The objective was to investigate the self-healing potential of RCA material due to the self-cementing phenomenon. It was expected that thee Exposed material has a reduced amount of active latent cement present due to the curing process. Although this theory was not supported by the monotonic test results. When the permanent deformation tests were executed it could be seen that the exposing had an effect on the self-cementation. The Exposed RCA did not withstand the same deviator stress ratios as the Unexposed RCA when continuous dynamic loads were applied. In order to preserve the integrity of the specimens, the maximum axial displacement was limited to 20mm or 6.67% permanent axial strain. Despite this counter-measure, two of the samples failed and disintegrated during the first phase of testing which resulted in no available samples for the second phase of testing. The intermittent permanent deformation results for Exposed material for 0 month and 1 month of curing are shown in Figure 4-19 and Figure 4-20, respectively.

From Figure 4-19 it can be seen that at a deviator stress ratio of 27%, the Exposed material becomes unstable and enters Range C of the Shakedown for all confinement pressures tested. At 50 kPa and 150 kPa, the material undergoes static failure and shortly after the commencement of the test, at 100 kPa the material continues to show an increase in the accumulation of permanent strain, but does not fail before the end of the test, this can be classified as Range B behaviour. Due to the nature of the failure of the sample at 50 kPa confinement with 27% DSR and 150 kPa confinement with 27% DSR, they are not eligible for curing and 1 month testing. From these two test results it would be expected that the sample tested at 100 kPa confinement with a 27% DSR ratio would show the same behaviour, however this was not the case. This sample showed behaviour in Range B of the Shakedown Theory and did not fail, this could possibly be contributed to the variability of the material.

At 17% and 22% deviator stress ratio, regardless of the confinement pressure, the material exhibits stable behaviour and falls within Range A of the Shakedown approach. This suggests that maximum applied deviator stress ratio should not exceed 25% for the Exposed material. Overall, the Exposed material shows a similar trend to the Unexposed material in terms of confinement pressure and permanent deformation relationships. It seems that there is a certain trend forming where the amount permanent deformation in the material increases as the confinement pressure increases and similarly for the deviator stress ratio. This is true for most cases but in some cases such as with the 100kPa results which are lower than the 50kPa at two DSR's results show contradictions. This possibly could be due to variability experienced as a results of the material and therefore a definitive conclusion cannot be drawn. However the general trends suggest further investigation into this in future research.

From Figure 4-20 it can be seen that at 1 month testing after the curing period the Exposed material shows stable behaviour for most confinement pressures and deviator stress ratios. Here the relationship between permanent deformation and confinement pressure can be seen. The 50 kPa specimens has the lowest amount of induced permanent deformation, the 100 kPa follows the 50 kPa tests with a slightly higher amount of permanent deformation, and lastly followed by the 150 kPa specimen. The results obtained for the test at 100 kPa confinement tested at 27% deviator stress seems to be outlier and does not fit this trend, however this could possibly be due to the high amount of compaction during the conditioning phase, which can be seen by the high amount of permanent deformation induced at the first marker (observation of the first 1000 cycles of the test). Here a markedly higher permanent strain compared to the other materials were observed. The most probable reason could have been unintentional variability through preparation or possibly the inherent variability that seems to be a characteristic of the nature of the Exposed material. For the

test run at 150 kPa confinement at 17% deviator stress ratio, a system error occurred and the compressor stopped supplying air to the MTS machine. This resulted in the abnormal results obtained, as shown in Figure 4-18. Due to the lack of air pressure, the specimen no longer had the correct confinement of 150 kPa, which resulted in the applied load causing more damage than it would have. This is shown by the solid green line. The data up to that point was taken, and extrapolated, so that the entire test was not wasted, this is shown in the dashed green line.

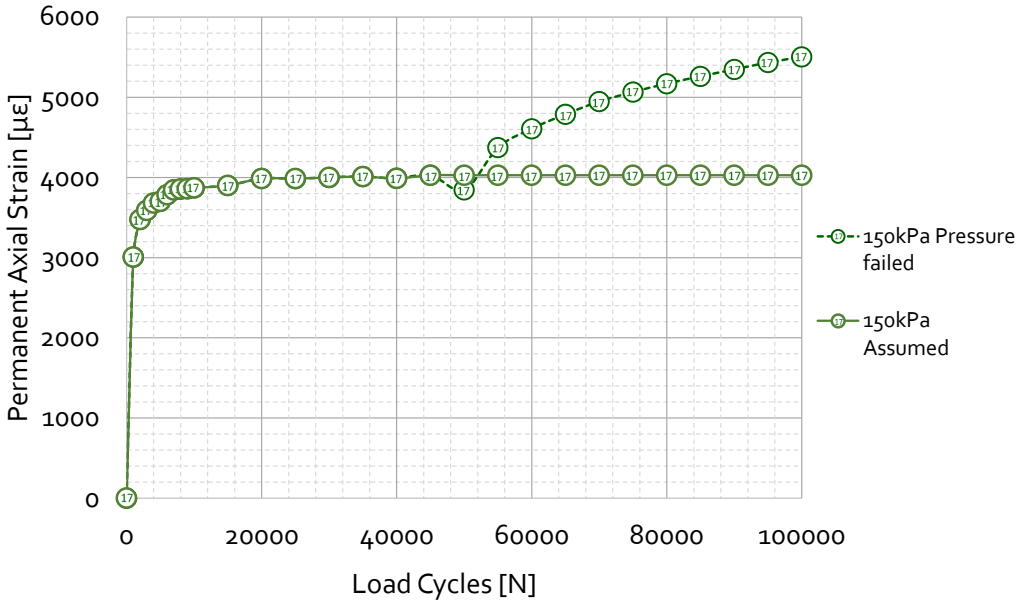

Figure 4-18: Lack of air pressure for specimen tested at 150 kPa confinement at a 17% DSR

Tredoux (2017) also investigated the effect of moisture content on this Exposed material, and the effect it would have on the permanent deformation. Tredoux concluded that by lowering the moisture content from 6.8% (OMC) to 6% the amount of permanent deformation induced in the material at the same confinement pressure and deviator stress ratio was significantly lower. Moisture has a pronounced effect, so that at the lower moisture content the material could again be tested at higher deviator stress ratios without the excessive collapse initially encountered. The Exposed RCA material shows significantly more variability in term of the tests results and this can be attributed to the non-uniform distribution of cement bonds. The same anomaly in terms of confinement pressure that was found for the Unexposed RCA material, was observed in the Exposed RCA material during the second phase of testing. The 100/17 test showed unexpected behaviour but this is probably due to the variability of the material. The tests at 150 kPa shows the problematic behaviour the best, as both tests performed worse than their counterparts that are completed at 50 kPa and 100 kPa, respectively.

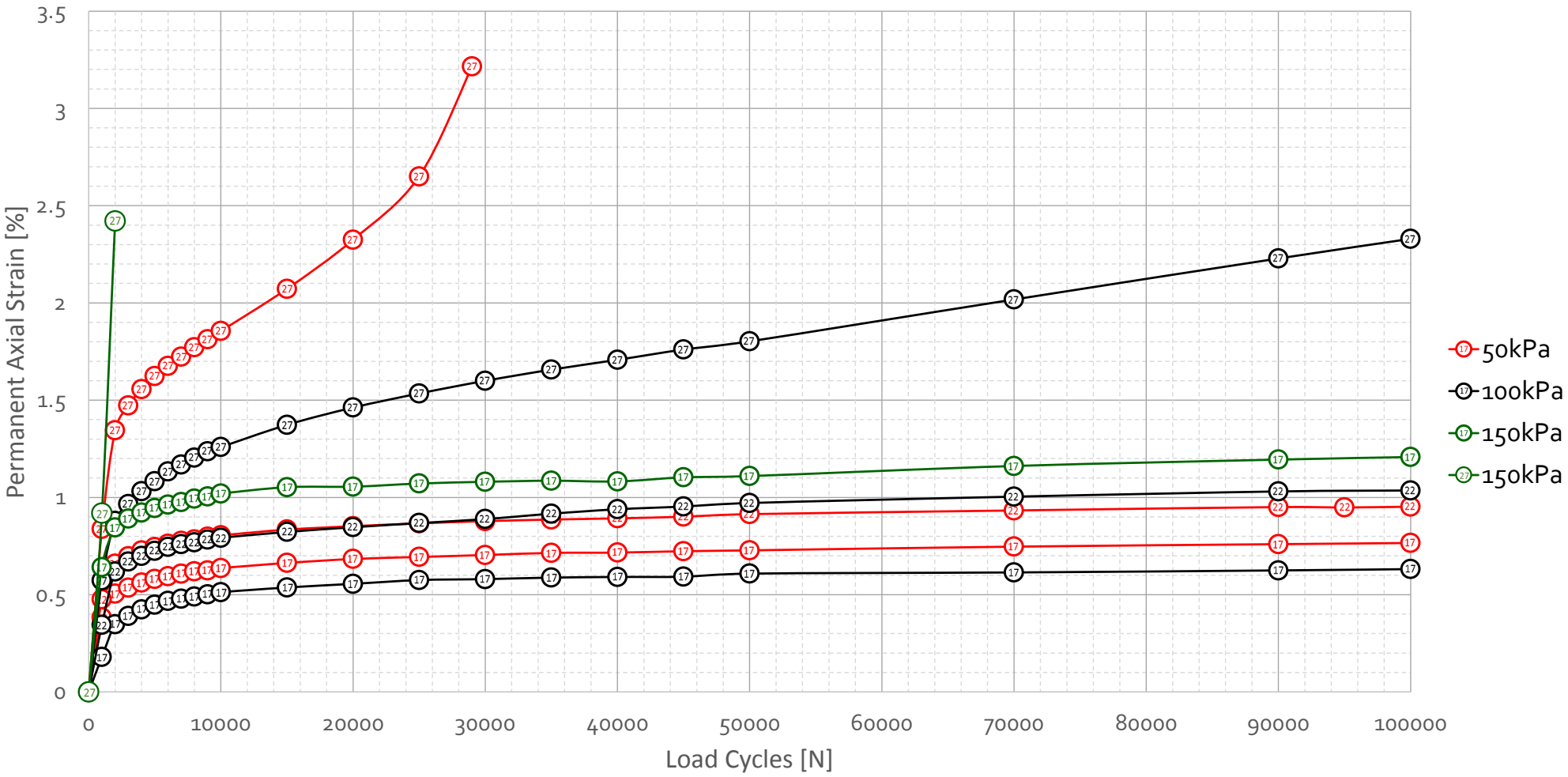

Figure 4-19: Summary of Intermittent Permanent Deformation Test Results at 0 months of curing for Exposed RCA

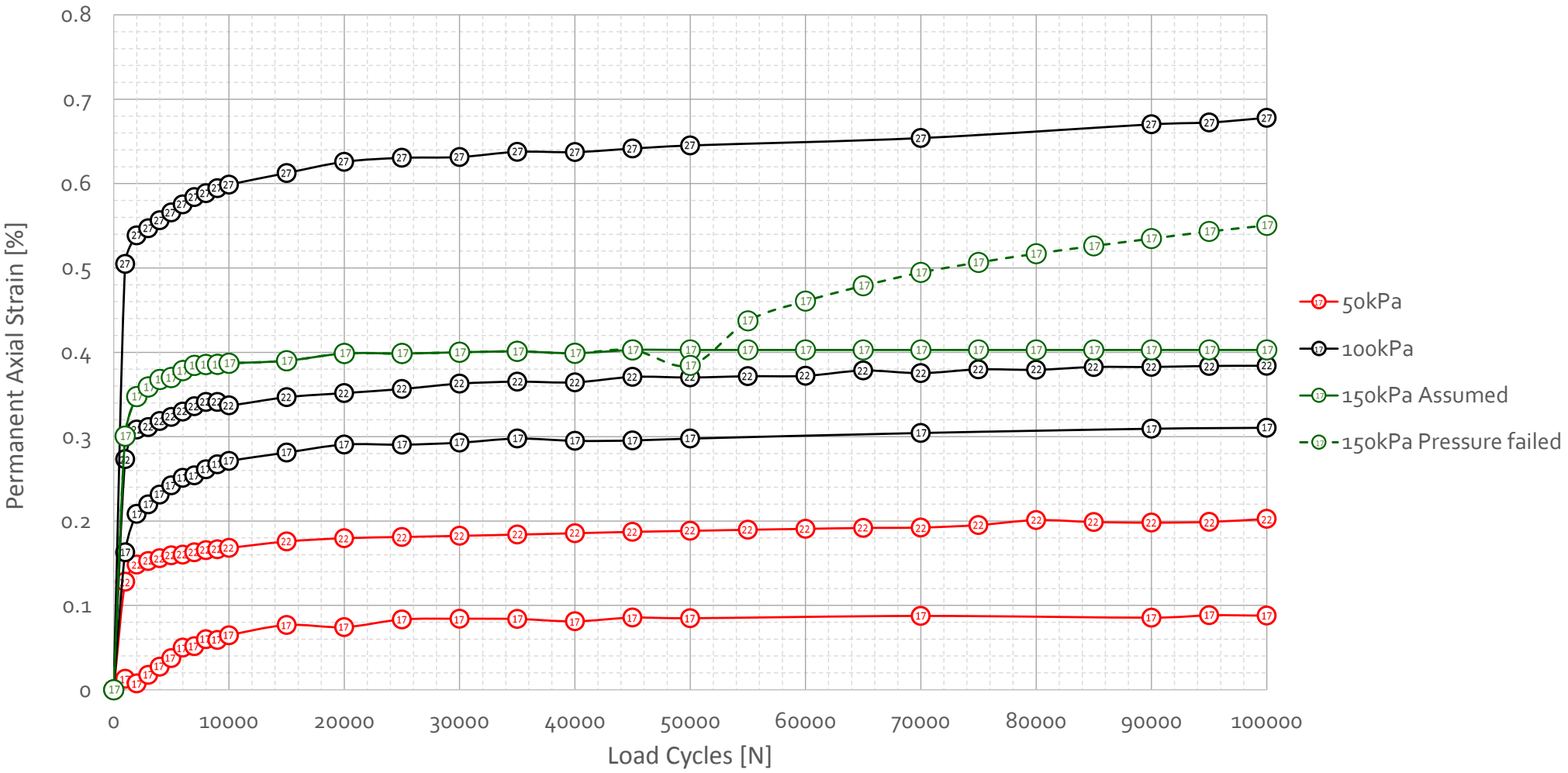

Figure 4-20: Summary of Intermittent Permanent Deformation Test Results at 1 month of curing for Exposed RCA

4.4 Triaxial Test Modelling

4.4.1 Introduction

The triaxial tests are only performed for 100 000 and 250 000 cycles respectively. The number of cycles designed for exceeds well over a million. It is not plausible to perform laboratory testing to simulate this number of cycles. It is therefore necessary to fit models that can predict beyond the last cycle number that was tested. Previous research has shown that in most cases realistic behaviour for further use in the fitting of models can be obtained when lab tests are run between these number of cycles (Kotze, 2014). For future investigation into a longer life this information is imperative. It is also needed to develop a transfer function for the material. In postulating possible behaviour larger than was tested in the current experimental plan, this information is imperative. It is also needed to develop a transfer function for the material. As discussed in Chapter 2, some models are more applicable in certain cases than others, and depends on the response behaviour of the material. It is for these reasons that various models were investigated and the most applicable model identified. It is for these reasons that various models are investigated and the most applicable model is identified. The triaxial test data can be modelled using current permanent deformation models as discussed in Chapter 2.6.

The permanent deformation behaviour is modelled using 5 models developed by researchers, as shown in Table 4-5. The fit of the models compared to the measured data are investigated to determine which model best describes the permanent deformation behaviour of the test under certain loading conditions.

In order to choose the best model that represents the data, three criteria are identified as and taken as the baseline for decision making of the most appropriate model. The three criteria are; the coefficient of determination (R^2), the sum of least squares ($\Sigma\Delta^2$) and the visual fit. To determine the best fit model, the coefficient of determination should be as close as possible to 1, the sum of least squares should be as close as possible to 0. Initially preliminary guidelines values were set as limits but it became apparent that it was not realistic to maintain all three methods limitations simultaneously, considering the three-fold approach. The coefficient of determination is in line with values obtained in Van Niekerk (2002). However, it should be noted that all three criteria were offset against each other to determine the most acceptable solution.

Table 4-5: Permanent Deformation models

Equation	Model	Reference	Parameters	Shakedown Ranges
1	$\varepsilon_{1,p} = a + b\log(N)$	Barksdale (1972)	a,b	A & B
2	$\varepsilon_{1,p} = aN^b$	Sweere (1990)	a,b	A & B
3	$\varepsilon_{1,p} = (cN + a)(1 - e^{-bN})$	Wolff and Visser (1994)	a, b, c	A & B
4	$\varepsilon_{1,p} = A\left(1 - \left(\frac{N}{100}\right)^{-b}\right)$	Paute (1996)	A, b	A & B
5	$\varepsilon_{1,p} = a\left(\frac{N}{1000}\right)^b + c\left(e^{d(N/1000)} - 1\right)$	Huurman (1997)	a, b, c, d	A, B & C

Only models defined in terms of load applications were considered in this study. Of these models those that related both the plastic deformation and resilient response to the material were excluded (and this included the Ververka (1997) and Khedr (1995) Model). The reason for this is that even from fundamental principles these two were not developed to describe the unstable behaviour due to the fundamental formulation that includes the plastic and resilient part. The focus of in the development of such a model is in the initial stages of the evolution of permanent deformation. Although some of the models considered for this study are not able to describe behaviour in the unstable region either, it is not necessarily because of the fundamental parameters considered.

According to Kotze (2014), the best fit model depends on the range in which the data falls according to the Shakedown Theory. For ranges A and B, which constitutes stable behaviour the best model is Barksdale (1972). The only model that is able to describe range C behaviour is Huurman (1997). His model consists of two terms, the first term as defined by Sweere (1990), which describes stable behaviour, and the second term which is used to describe the unstable behaviour of the material. According to Lekarp (1998) the best model for permanent deformation is that of Paute (1996). Lastly the model by Wolff and Visser (1994) was used as his data and results are based on South African

materials. It is important to note that all of the above models are developed for granular materials, there are no models developed for RCA material.

4.4.2 Summary of Modelling Results

The models as shown in Table 4-5 were used to model the permanent deformation results. The full set of graphical results, where the models are fit to the measured permanent deformation results for each test of Exposed and Unexposed measured results can be found in Annexure D. A summary of the top three models for each test, with the coefficient of determination, the sum of least squares and the model parameters will be presented in this chapter. It is important to note that the models that best describe the behaviour of RCA materials will differ for the two types of permanent deformation tests. In order to remain consistent one model must be chosen to model the 1 day curing results as well as the 28 day curing results. Although some models better fit different shakedown ranges, in order to simplify the problem and to get a consistency across all tests one model must be decided upon. The best model is chosen from the three criteria listed, a maximization of the coefficient of determination, a minimisation of the sum of least squares and visually the best fitting model.

4.4.2.1 Unexposed Modelling Results

Table 4-6. The two models that best describe the measured permanent deformation results are Wolff and Visser (1994) for stable behaviour and Huurman (1997) for unstable behaviour.

Table 4-6: Summary of modelling results for Basic Permanent Deformation Unexposed results

Test Type	Best model in order	R^2	$\Sigma\Delta^2$	Best Model	a	b	m	c	d	Shakedown Range
50/37	Paute	0.920	9.46E-06	Paute	0.012	0.566	2.45467E-09			A
	Wolff & Visser	0.871	5.38E-05		0.011	0.001				
	Huurman	0.751	2.21E-04		0.011	0.002		7.77E-06	1.81E-04	
50/45	Wolff & Visser	0.979	3.61E-04	Wolff & Visser	0.011	0.000	4.31028E-08			B
	Huurman	0.953	5.77E-04		0.005	0.253		7.12E-01	4.61E-06	
	Sweere	0.948	7.99E-04		0.005	0.265				
50/50	Wolff & Visser	0.928	3.34E-04	Wolff & Visser	0.010	0.0001	4.48357E-09			A
	Paute	0.921	6.26E-04		0.620	0.002				
	Huurman	0.880	7.54E-04		0.006	0.119		4.12E-05	4.05E-03	
75/37	Wolff & Visser	0.923	7.30E-04	Wolff & Visser	0.015	0.0001	7.37103E-09			A
	Paute	0.801	1.81E-03		0.396	0.006				
	Barksdale	0.798	6.42E-04		0.007	0.002				
75/45	Huurman	0.977	3.93E-03	Huurman	0.007	0.138	4.91702E-08	3.33E-04	1.51E-02	B
	Wolff & Visser	0.891	2.63E-03		0.011	0.000				
	Sweere	0.762	7.70E-03		0.007	0.173				
100/37	Huurman	0.987	2.49E-02	Huurman	0.002	0.359	1.67072E-07	8.67E-03	6.82E-03	C
	Wolff & Visser	0.948	2.61E-02		0.007	0.001				
	Sweere	0.795	7.68E-02		0.005	0.359				
100/45	Huurman	0.991	2.68E-03	Huurman	0.008	0.176	7.79885E-07	1.26E-02	2.76E-02	C
	Wolff & Visser	0.952	4.03E-03		0.011	0.001				
	Sweere	0.850	9.85E-03		0.009	0.375				

The results obtained for the intermittent permanent deformation results are shown in Table 4-7. The model that best describes 0 month and 1 month curing times, differ due to the difference in

behaviour. During the 0 month curing tests, many tests showed stable behaviour in Range B of the Shakedown approach or unstable behaviour in Range C of the Shakedown approach. Whereas with the 1 month results, all tests showed stable behaviour that falls within Range A of the Shakedown approach. For the 0 month curing tests, Paute (1996) modelled the stable behaviour test better whereas the unstable tests were better modelled using Huurman (1997). For 1 month curing tests all samples showed stable behaviour and the majority of the tests were best modelled by Paute (1996).

Table 4-7: Summary of modelling results for Intermittent Permanent Deformation Unexposed results

				0 month						
Test Type	Best model in order	R^2	$\Sigma\Delta^2$	Best Model	a	b	m	c	d	Shakedown Range
50/37	Paute	0.992	7.25E-05	Paute	0.028	0.091				A
	Sweere	0.982	3.55E-05		0.006	0.193				
	Huurman	0.984	2.08E-04		0.006	0.193		5.53E-07	1.09E-06	
50/45	Huurman	0.984	8.46E-04	Huurman	0.007	0.192		2.60E-04	3.57E-02	C
	Wolff & Visser	0.941	5.87E-04		0.011	0.001	1.03E-07			
	Sweere	0.843	1.31E-03		0.007	0.192				
50/50	Paute	0.983	8.88E-06	Paute	0.015	0.205				A
	Barksdale	0.938	5.37E-05		0.001	0.002				
	Wolff & Visser	0.918	8.00E-05		0.009	0.001	2.43E-08			
75/37	Huurman	0.986	6.55E-03	Huurman	0.003	0.360		5.68E-04	3.76E-02	C
	Wolff & Visser	0.908	5.29E-03		0.007	0.001	1.72E-07			
	Sweere	0.776	7.45E-03		0.005	0.358				
75/45	Huurman	0.981	2.46E-05	Huurman	0.005	0.131		3.44E-04	3.54E-05	B
	Sweere	0.983	7.00E-06		0.005	0.131				
	Wolff & Visser	0.947	1.86E-05		0.007	0.001	3.34E-08			
100/37	Huurman	0.986	1.98E-03	Huurman	0.004	0.218		3.54E-03	3.45E-02	C
	Wolff & Visser	0.910	2.19E-03		0.007	0.000	3.43E-07			
	Sweere	0.811	5.89E-03		0.004	0.373				
100/45	Paute	0.964	6.19E-05	Paute	0.017	0.272				A
	Wolff & Visser	0.951	6.82E-05		0.012	0.001	2.30E-08			
	Huurman	0.927	1.62E-04		0.010	0.092		5.72E-04	6.51E-05	
				1 month						
50/37	Paute	0.937	1.14E-06	Paute	0.0027	0.4286				A
	Wolff & Visser	0.936	1.87E-05		0.0025	0.0002	6.60E-10			
	Huurman	0.723	2.88E-05		0.0020	0.0578		1.89E-05	1.28E-06	
50/45	Paute	0.911	3.75E-06	Paute	0.0046	0.3892				A
	Wolff & Visser	0.893	6.42E-06		0.0037	0.0010	8.27E-09			
	Huurman	0.895	1.08E-05		0.0034	0.0535		2.44E-04	2.75E-05	
50/50	Paute	0.940	1.27E-05	Paute	0.0032	0.1485				A
	Barksdale	0.890	1.36E-05		0.0002	0.0004				
	Huurman	0.840	1.00E-04		0.0013	0.1096		1.17E-03	1.80E-04	
75/37	Wolff & Visser	0.920	5.00E-06	Wolff & Visser	0.0040	0.0006	6.87E-09			B
	Paute	0.875	1.39E-05		0.0047	0.4139				
	Huurman	0.707	1.51E-05		0.0034	0.0680		2.70E-05	1.85E-06	
75/45	Paute	0.973	6.26E-06	Paute	0.0060	0.4401				A
	Huurman	0.931	2.30E-05		0.0041	0.0719		6.46E-07	1.39E-02	
	Sweere	0.926	1.39E-05		0.0041	0.0787				
100/37	Paute	0.940	2.02E-05	Paute	0.0026	0.5972				A
	Wolff & Visser	0.919	8.66E-06		0.0025	0.0002	1.86E-09			
	Huurman	0.753	3.01E-05		0.0020	0.0631		4.26E-05	3.38E-06	
100/45	Barksdale	0.883	1.72E-05	Barksdale	0.0109	0.0012				A
	Huurman	0.879	3.78E-04		0.0144	0.0347		5.24E-04	6.89E-05	
	Sweere	0.875	2.65E-05		0.0144	0.0347				

4.4.2.2 Exposed Modelling Results

The results obtained for the intermittent permanent deformation tests are shown in Table 4-8. It can be seen that there is a significantly higher degree in variability between the best fitting models when

compared to the Unexposed RCA material results. The stable behaviour is best modelled using the model by Paute (1996) if the material fell in Range A of the Shakedown approach, and Wolff and Visser (1994) if the material exhibited Range B behaviour. The unstable behaviour is best modelled using Huurman (1997).

Table 4-8: Summary of modelling results for Intermittent Permanent Deformation Exposed results

					0 month					
Test Type	Best model in order	R^2	$\Sigma\Delta^2$	Best Model	a	b	m	c	d	Shakedown Range
50/17	Paute	0.995	1.73E-06	Paute	0.010	0.226				
	Wolff & Visser	0.954	1.57E-04		0.007	0.0002	1.07E-08			A
	Huurman	0.946	2.65E-04		0.005	0.077		7.10E-13	5.45E-12	
50/22	Paute	0.974	1.03E-04	Paute	0.010	0.468				
	Barksdale	0.949	1.59E-05		0.002	0.002				A
	Huurman	0.934	3.14E-04		0.007	0.079		6.48E-11	3.17E-10	
50/27	Wolff & Visser	0.973	1.63E-04	Wolff &	0.013	0.001	5.14E-07			
	Huurman	0.956	1.17E-04		0.008	0.359		2.98E-04	1.40E-02	C
	Sweere	0.923	5.66E-04		0.008	0.359				
100/17	Wolff & Visser	0.949	7.30E-05	Wolff &	0.006	0.0002	4.78E-09			
	Paute	0.917	4.33E-05		0.012	0.105				A
	Huurman	0.857	2.77E-04		0.005	0.060		5.68E-09	7.58E-11	
100/22	Paute	0.970	3.33E-05	Paute	0.028	0.068				
	Barksdale	0.966	8.37E-05		0.000	0.002				A
	Huurman	0.954	7.08E-04		0.006	0.128		8.92E-08	2.07E-09	
100/27	Huurman	0.993	4.44E-04	Huurman	0.005	0.302		9.91E-07	7.40E-02	
	Sweere	0.985	4.24E-04		0.005	0.302				B
	Wolff & Visser	0.963	1.13E-03		0.014	0.000	9.44E-08			
150/17	Wolff & Visser	0.948	9.94E-05	Wolff &	0.010	0.000	2.10E-08			
	Paute	0.940	2.63E-04		0.034	0.065				B
	Huurman	0.925	1.54E-04		0.008	0.097		4.30E-14	2.28E-05	
150/27	Paute	0.999	1.03E-03	Paute	0.010	8.989				
	Barksdale	0.998	1.07E-03		0.000	0.003				C
	Wolff & Visser	0.998	1.99E-06		0.301	0.000	1.71E-04			
					1 month					
50/17	Wolff & Visser	0.974	6.31E-07	Wolff &	0.001	0.0002	8.10E-10			
	Paute	0.831	2.49E-06		0.008	0.017				A
	Barksdale	0.824	5.01E-06		0.000	0.000				
50/22	Paute	0.978	1.34E-05	Paute	0.010	0.034				
	Barksdale	0.977	9.08E-07		0.0000	0.0004				A
	Huurman	0.972	1.50E-06		0.001	0.082		8.27E-11	3.95E-10	
100/17	Wolff & Visser	0.952	8.58E-06	Wolff &	0.003	0.0003	2.56E-09			
	Paute	0.895	3.94E-05		0.014	0.037				A
	Huurman	0.868	3.42E-05		0.003	0.044		6.53E-09	8.97E-11	
100/22	Paute	0.984	2.22E-05	Paute	0.005	0.189				
	Barksdale	0.975	5.88E-07		0.001	0.001				A
	Huurman	0.969	4.50E-05		0.003	0.054		1.01E-07	2.39E-09	
100/27	Paute	0.967	2.99E-05	Paute	0.008	0.265				
	Huurman	0.964	1.21E-04		0.005	0.059		1.04E-06	3.94E-08	A
	Sweere	0.965	2.44E-06		0.005	0.059				
150/17	Huurman	0.903	1.49E-04	Huurman	0.004	0.033		2.40E-05	4.03E-02	
	Sweere	0.684	2.35E-04		0.004	0.033				B
	Barksdale	0.670	2.34E-04		0.003	0.0003				

4.4.3 Discussion of Models

With the fitting of the coefficients in the previous section the eligibility of each model must be investigated and the best model is chosen based on the three criteria listed earlier. The general findings of each model will be briefly discussed, in terms of the advantages and disadvantages of the model in order to illustrate the decision making process in terms of the three criteria.

Figure 4-21 can be used to determine which part of the permanent deformation graph, affect certain predetermined criteria. These criteria that determine the best fit model was determine in study and will be used to determine applicability of certain models. In order to maximize the coefficient of determination, the embedding part of the modelled data, must be fit to the permanent deformation graph. Models with the ability to adjust the embedment shape and height will yield higher R^2 values, and will visually fit the measured data better. The stabilising part (behaviour of interest) of the graph will affect the sum of the least squares, if the model has the ability to move the tail end of the graph up and down, or change the shape in cases of unstable behaviour the sum of least squares will be lower and the model will visually fit the data better.

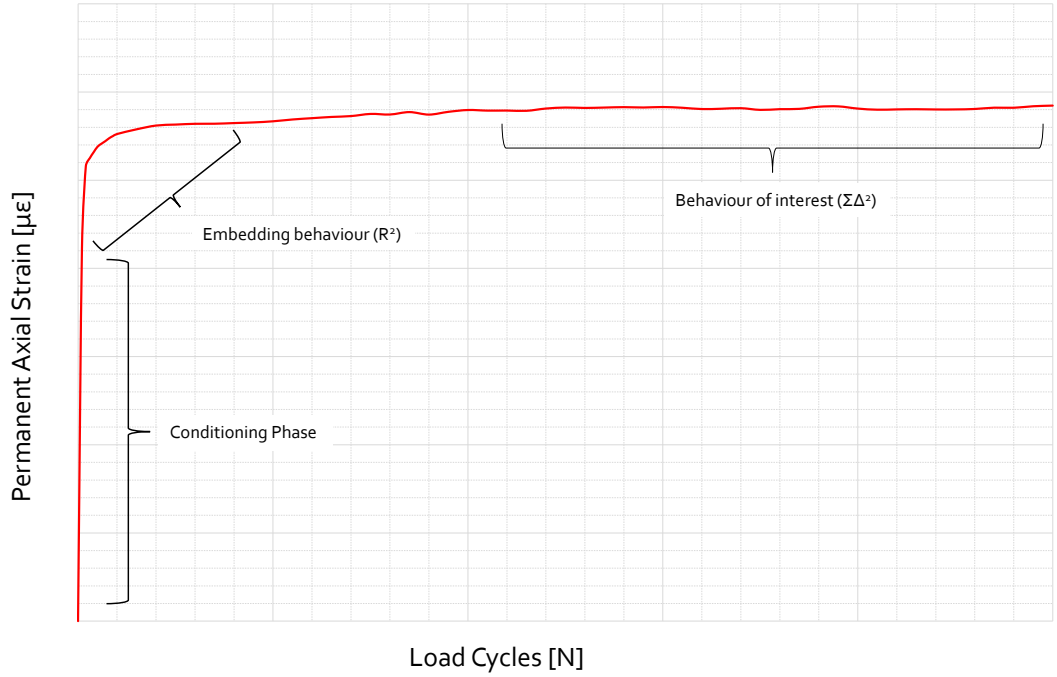

Figure 4-21: Parameters of interest during modelling

Werkmeister (2003) defined the micromechanical processes within a granular material, and found that there are three different phases of deformation behaviour:

- Phase I: After compaction in shakedown Ranges A,B and C
- Phase II: Stable behaviour in Ranges A, B and C
- Phase III: Collapse in Ranges B and C

The different phases of deformation behaviour as identified by Werkmeister (2003) was used in to classify the models and applicability of each model to predict the behaviour of the three ranges of the Shakedown Theory.

4.4.3.1 Model 1: Barksdale (1972)

Model 1 as seen in Table 4-5 shows that the amount of permanent deformation is proportional to the logarithmic number of load applications. The model constants a and b are dependent on the failure stress and the confinement pressure. Equations 4-1 and 4-2 are used to determine a and b , variables a_1 , a_2, b_1, b_2 are changed in order to best fit the model to the measured data. Using Figure 4-22 the effect of each of the parameters on the model curve is shown.

$$a = a_1(\sigma_1/\sigma_{1,f})^{a_2} \qquad 4\text{-}1$$

$$b = b_1(\sigma_1/\sigma_{1,f})^{b_2} \qquad 4\text{-}2$$

From the modelled data it was found that this model can only be used to describe the deformation behaviour of Phase I and Phase II as determined by Werkmeister (2003). The model cannot be used to represent the unstable behaviour represented by Phase III. Due to the variability in the compaction phase and the resultant instability that was found for RCA materials, it is seen that the model as defined by Barksdale (1972) does not accurately predict the deformation behaviour of RCA materials. In addition, the embedment of RCA is variable, and this model does not allow for big changes in the embedment phase of the graph.

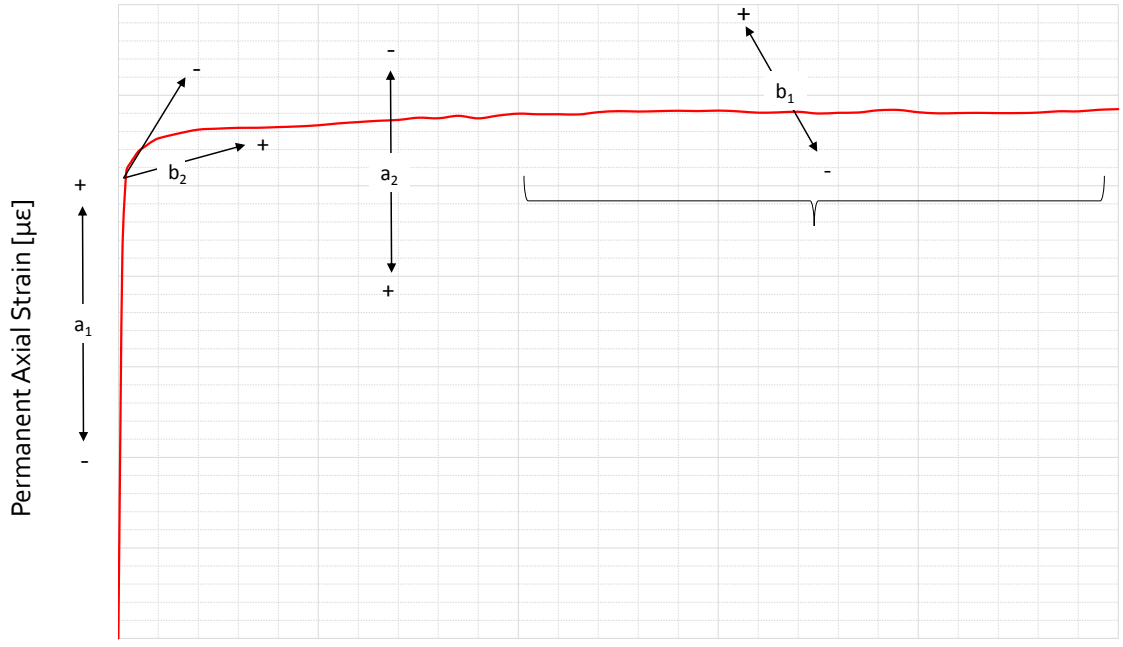

Figure 4-22: Behaviour of modelling coefficients for Barksdale (1972)

4.4.3.2 Model 2: Sweere (1990)

Werkmeister (2003) adapted and used the model as defined by Sweere (1990) to model the permanent deformation of materials for Phase I and II behaviour. This model shows a linear increase in the permanent deformation with increasing load cycles, if a log-log approach is used. Werkmeister (2003) adapted the model by determining the permanent deformation with respect to the deformation at 1000 cycles. This model is investigated as the adapted version forms part of the model as defined by Huurman (1997). This model is unable to model unstable behaviour as in Phase III, as this is an exponential behaviour shape, and this model is only able to model linear accumulation.

Figure 4-23 shows the effect of each parameter on the model curve. The model by Sweere (1990) does not accurately predict the behaviour of RCA material, this is due to the fact that this model has the same shortcomings as that of Barksdale (1972). The inability to shift or change the shape of the embedment of the modelled graph does not model the variable behaviour of RCA material sufficiently.

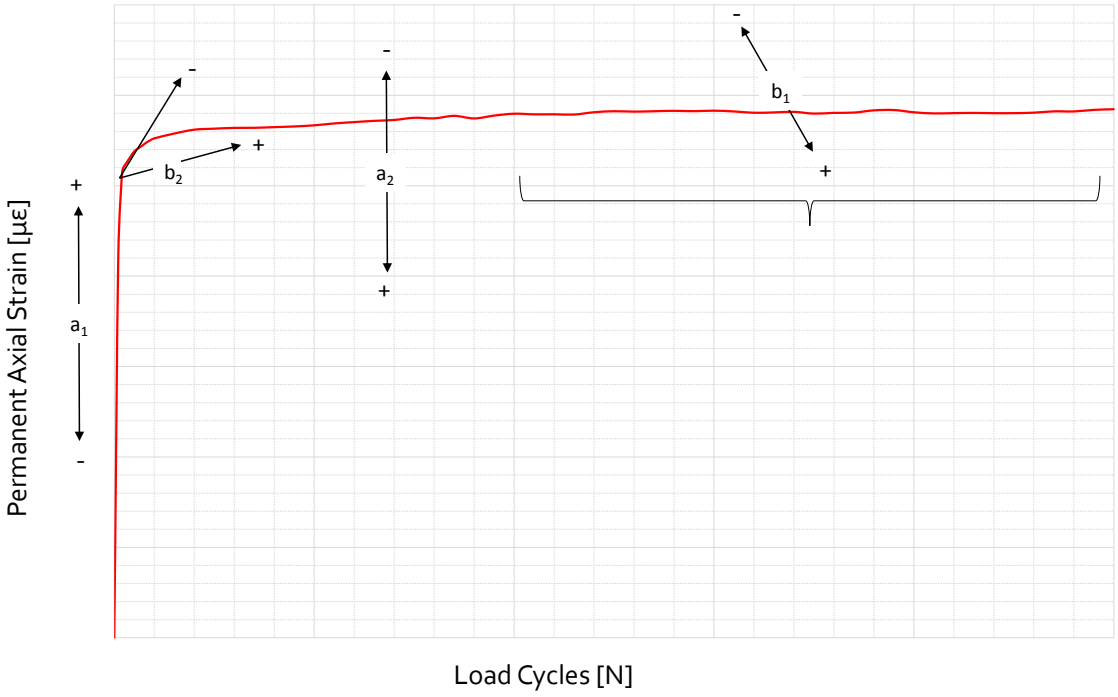

Figure 4-23: Behaviour of modelling coefficients for Sweere (1990)

4.4.3.3 Model 3: Wolff and Visser (1994)

Wolff and Visser (1994) investigated the applicability of the model as defined by Sweere (1990) using a Heavy Vehicle simulator at high amounts of load applications. They came to the conclusion that the permanent deformation behaviour can be divided into two phases based on the amount of load applications. They found the first phase consists of the first 1.2 million cycles, rapid permanent

deformation takes place, but the accumulation of permanent deformation is decreasing as the amount of load cycles increase. For the second phase the accumulation of permanent deformation is rapidly decreasing until it reaches a constant value. The model as developed by Sweere(1990) does not take into account the permanent deformation at very large load applications. Wolff and Visser (1994) therefore the developed the model as stated in Table 4-5. The behaviour of the model parameters can be seen in Figure 4-24.

The m-parameter in the Wolff and Visser (1994) model, allows for a gradient change of the tail of the modelled graph, which creates the ability to approximate unstable behaviour. It is unable to model the exponential behaviour of unstable materials, but it can roughly approximate this with a straight line. The b-parameter also allows for the change in shape and position of the embedment sector for the graph, which allows for the modelling of the variability in the compaction phase of the material. This specific function of the model is an improved capability when compared to Huurman (1997) and the benefits are weighed off against each other and will be discussed in the decision making process later in the section. The model as defined by Wolff and Visser (1994) is found to be the best model to use if the material falls within Range B of the Shakedown Theory.

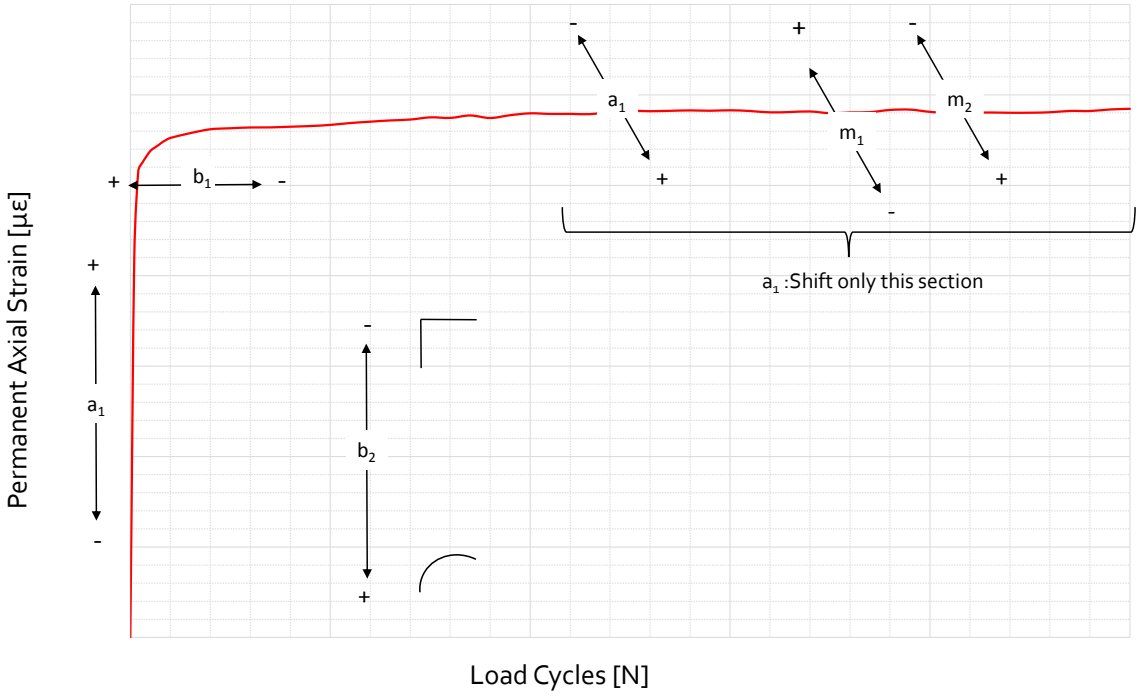

Figure 4-24: Behaviour of modelling coefficients for Wolff and Visser (1994)

4.4.3.4 Model 4: Paute (1996)

The model by Paute (1996) has a limiting parameter A, which limits the accumulating permanent axial deformation when the load applications approach infinity. According to Kotze (2014) , if B is

negative or very small, it must be considered as a practical value for the limitation of cumulative permanent axial deformation. In practice the A value is compared to twice the cumulative permanent deformation after 20 000 cycles, if the A value is bigger this should be seen as the practical limiting value. Figure 4-25 shows the behaviour of the coefficients for the model.

It was found that this model can only be used to describe the behaviour of Phase I and Phase II, and is not suitable for Phase III behaviour. However, if the RCA material showed stable behaviour in Range A of the Shakedown approach this is the best model to use. This is due to the fact that the shape of the embedment can be changed.

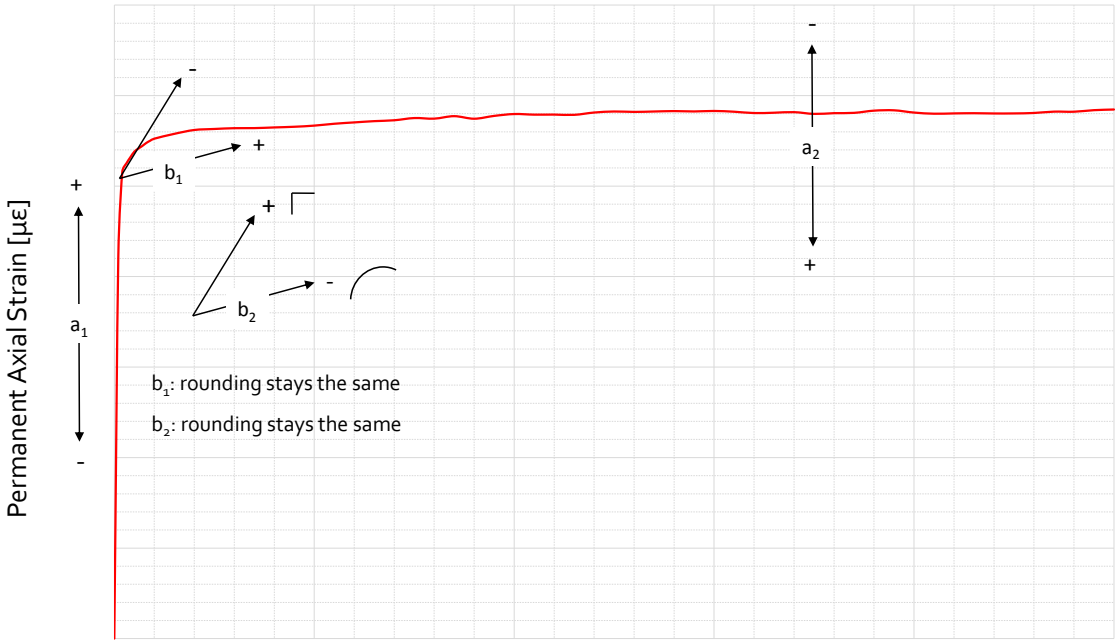

Figure 4-25: Behaviour of modelling coefficients for Paute (1996)

4.4.3.5 Model 5: Huurman (1997)

Huurman's (1997) model consist of two terms, the first term as defined by Sweere (1990) and adapted by Werkmeister (2003) and the second term as defined by Huurman . This is the only model that can accurately model the unstable behaviour experienced during Phase III. The extra modelling parameters c and d are calculated in the same way as were shown in Equation 4-1, with the parameter being dependent on the confinement pressure and the principal stress at failure. New research on the model has shown that the applied stress ratio $\sigma_d/\sigma_{d,f}$ might yield more accurate results as the original principal stress ratio. However, it was decided to continue the modelling using the original definition of the model parameters. Figure 4-26 shows the behaviour of the coefficients for the model.

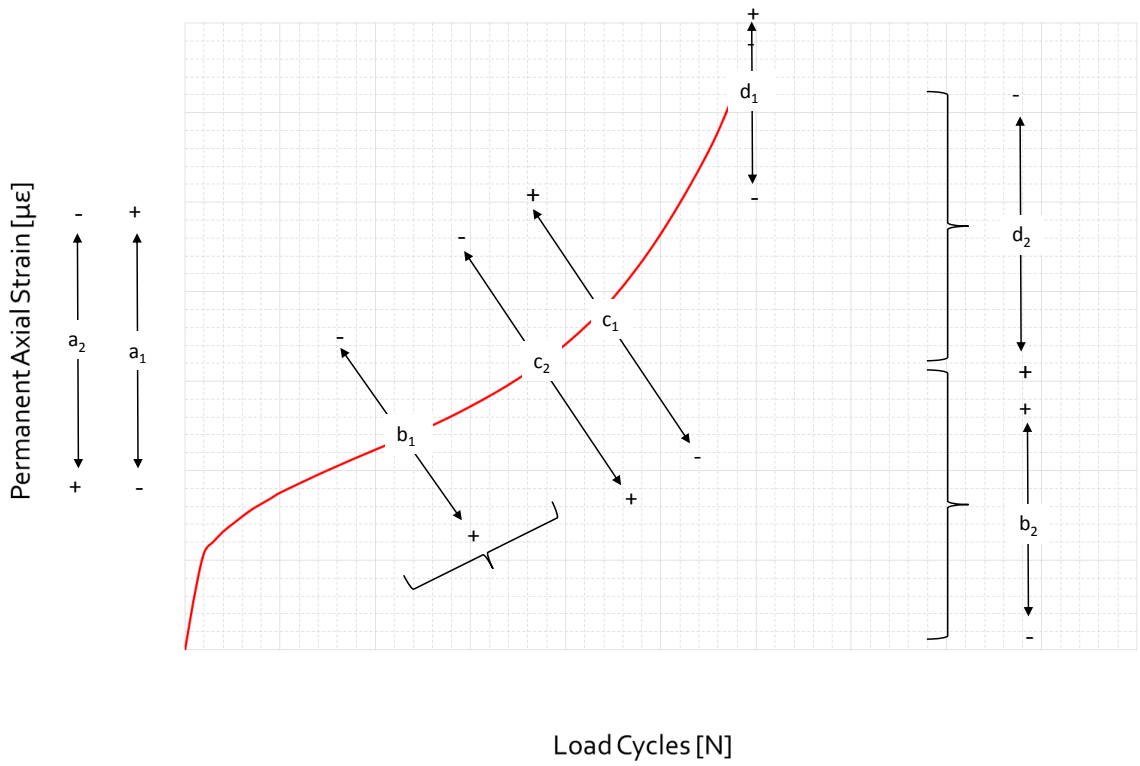

Figure 4-26: Behaviour of modelling coefficients for Huurman (1997)

4.4.4 Conclusion

Once the Exposed and Unexposed RCA material is modelled using the five chosen models as shown in Table 4-5, the best model for each behaviour range can be identified. By comparing the measured data to the modelled data and looking at the Shakedown approach ranges, the following conclusion was reached, as seen in Table 4-9 .

Table 4-9: Best fit model according to Shakedown range

Shakedown Range	Best Fit Model
A	Paute (1996)
B	Wolff and Visser (1994)
C	Huurman (1997)

However, in the interest of consistency when using modelled data to produce a transfer function, one model must be identified and used. It is decided to use the model as proposed by Huurman (1997), as it is the only model that is able to model unstable behaviour even when the benefits regarding the embedment movement of the Wolff and Visser (1994) model is taken into account. Although it is not the best model for stable behaviour, it does predict stable behaviour accurately enough that the margin of error will be negligible. The coefficient of determination for all tests of Exposed and

Unexposed RCA material for Huurman's model is shown in Figure 4-27. It can be seen that the R_2 for Huurman's model, is relatively high, with only 1 test falling below 65%, out of 35 tests performed 21 shows an R_2 of above 90%. The embedment phase of the modelling plays a significant role in the values obtained for the coefficient of determination but in reality the embedment phase is only a limited proportion of the entire pavement life or test cycle. Therefore, a lower R^2 caused by the embedment modelling is not a concern as in an entirety the model is still applicable. Even for a low R^2 of the overall model one could predict the part after the embedment phase accurately. This is where the weighing of the other two criteria are equally important. Similar to van Niekerk (2002), all three criteria were considered to determine the coefficients. This allows that errors due to statistical formulation do not govern the prediction in the behaviour in its entirety. In his findings he showed that considering only one criteria could underestimate or overestimate the prediction of the behaviour.

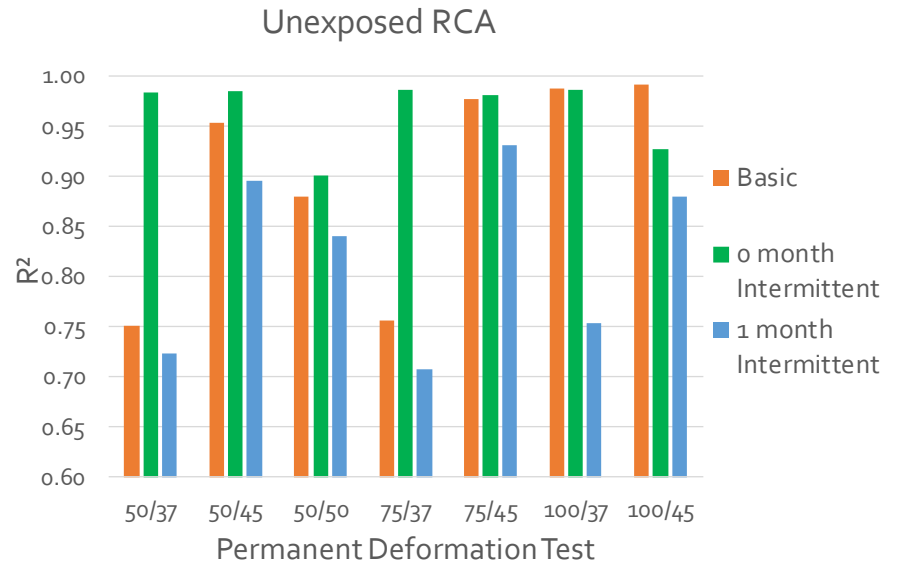

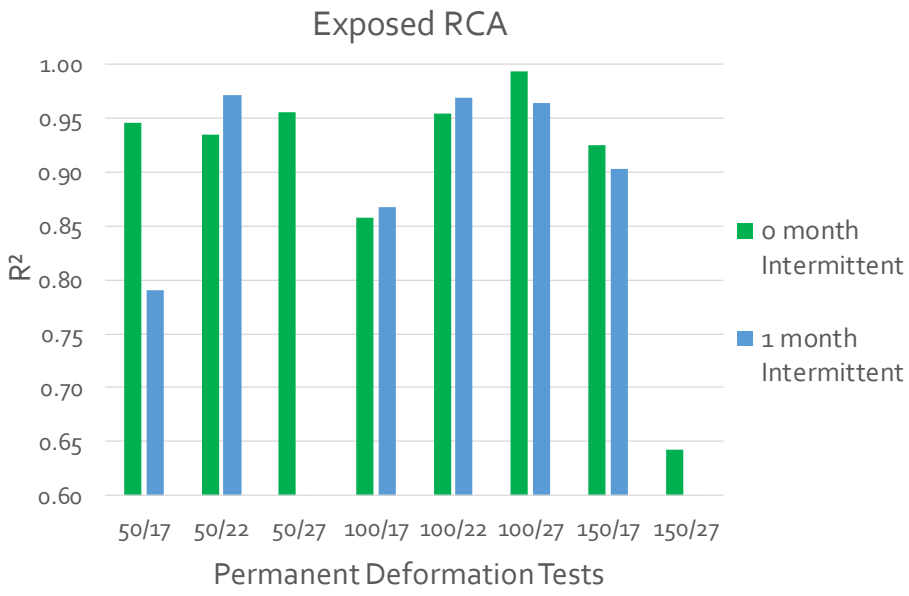

Figure 4-27: R^2 for Huurman's model for Exposed and Unexposed RCA

4.5 Comparative behaviour

4.5.1 Monotonic Test Results

The discussion in this section will compare the behaviour of the Exposed and Unexposed RCA material. The RCA material is exposed to investigate the effect of self-cementation on the performance of the material. The shear results obtained for the Unexposed and Exposed monotonic results are shown in Table 4-10.

Table 4-10: Unexposed and Exposed Monotonic Test results

Material	Cohesion (kPa)	Friction Angle (º)
Unexposed	273.7	54.6
Exposed	294.1	52.6

It was previously believed that the self-cementing potential of the material is the cause of the high observed cohesion in the RCA material. According to Leek and Siripun (2010) a cohesion above 150-kPa would result in brittle behaviour of the material. With the exposure of the material it was believed that the cohesion would be reduced due to the reduction in self-cementing potential. However, this was not the case. The cohesion for the Exposed RCA material resulted in a higher cohesion and a lower friction angle. The Exposed material only shows a small reduction in failure load compared to that of the Unexposed material, resulting in the unexpected behaviour. Agnello (2017) performed Initial Consumption of Cement (ICC) tests on the Exposed and Unexposed RCA material used in this research. She found that the Unexposed RCA had a pH of 12.83, and the Exposed RCA had a pH of 9.45. This is significant as the pH for cement is 12.4, it can be seen that the Unexposed RCA has nearly the exact pH of cement, indicating the high amount of latent cement present. Taking into account that pH is a log measurement, the Exposed RCA has a significantly lower value, which indicates that the attempt to reduce the self-cementing potential of the material was successful.

The shear parameters of the Exposed and Unexposed materials are very similar, but still larger than that obtained by other researchers. With this anomaly in behaviour, it can be seen that the Monotonic test results are not sufficient to make predictions about the performance and behaviour of RCA materials. For this reason it is very important to investigate the resilient modulus (not done in this study) and the permanent deformation of the material.

4.5.2 Permanent Deformation Results

It is important to compare the permanent deformation results obtained for the Exposed and Unexposed RCA material. A problem exists in doing so as the two materials could not be tested at the same deviator stress ratios. The Unexposed material is tested at 37%, 45% and 50%, deviator stress ratio, but the Exposed material failed at the 37% deviator stress ratio, and therefore lower DSR had to be chosen. Comparisons must be made between the 50 kPa and 100 kPa intermittent results. Due to the fact that the values differ it can be beneficial to compare the shape of the permanent deformation graphs of the material on a macro-scale without considering exact values. Table 4-12 shows the results obtained for the 50, and 100 kPa confinement pressure intermittent permanent deformation tests.

Table 4.11 shows a qualitative summary of the factors that affect the performance and behaviour of RCA material when comparing unexposed and exposed materials. This allows a holistic view on which factors change considerably, but also how these factors influence the material in its exposed and unexposed state. A general concept is that the downward arrow refers to a negative effect on a performance criteria and an upward arrow a positive contribution. Moisture content plays a significant role in the permanent deformation behaviour of the material and therefore it is denoted by two arrows. Although intuitively it would also have a large effect on the unexposed material, but as it was not tested explicitly not reported here. The change in moisture results in a change in the allowable (value where material changes from Range B to C) DSR ratio, which plays the largest role in the behaviour of the RCA materials and thus it is denoted by three arrows.

Table 4.11: Summary of properties that affect the behaviour of RCA

Properties	Unexposed	Exposed
Increase in Moisture Content	-	↓↓
Response to Confinement	Same response	Same response
Increase Deviator Stress Ratio	↓↓	↓↓↓*

- Refers to general tends. More tests will have to be performed to confirm this.

One of the findings when comparing the results in Table 4-12 is regarding the stability of the specimens after 1 month of curing. All tests performed after 1 month of curing resulted in a more stable material that is better able to withstand the accumulation of permanent deformation, which falls within Range A of the Shakedown approach. A clear reduction in the amount of permanent deformation can be seen from tests performed after 1 day of curing and tests performed after 1 month of curing. These reductions are quantified in Table 4-13.

Table 4-12: Comparison of Exposed and Unexposed Intermittent Permanent Deformation results

Unexposed RCA			Exposed RCA		
σ_3	DSR	Permanent Deformation	σ_3	DSR	
50 kPa	37%	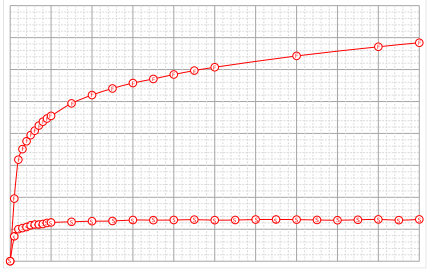	50 kPa	17%	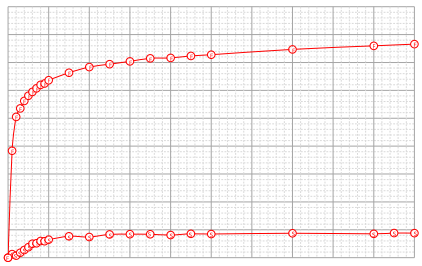
	45%	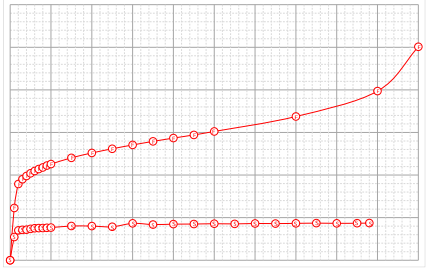		22%	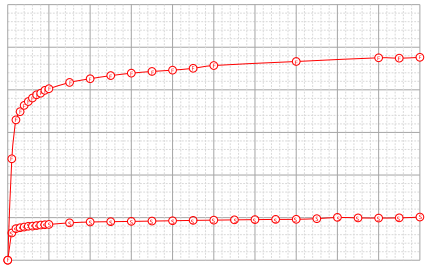
	50%	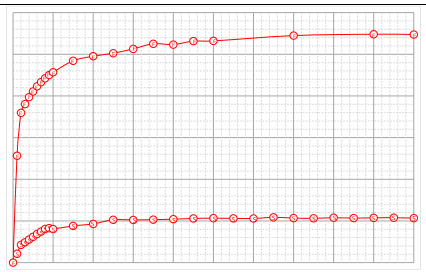		27%	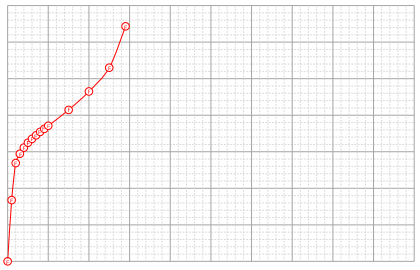
100 kPa	37%	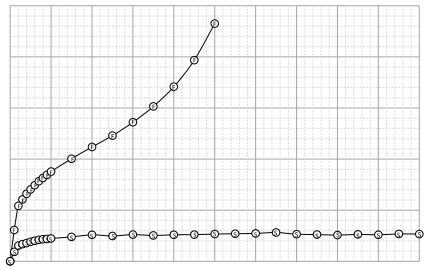	100 kPa	17%	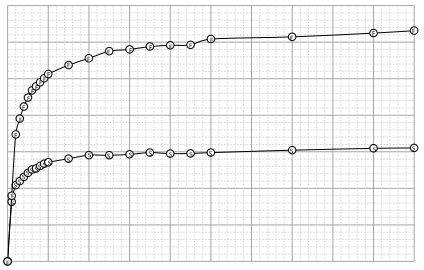
	45%	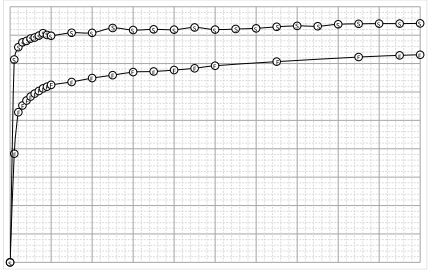		22%	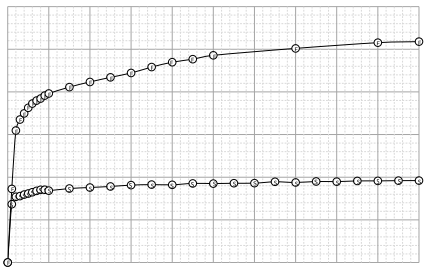
				27%	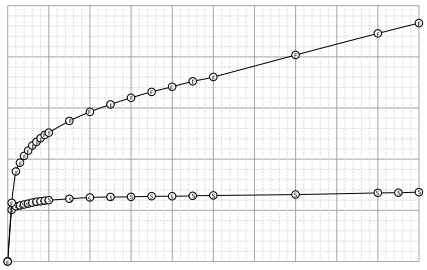

For samples that failed during the test procedure, the maximum percentage axial strain at that point of failure was taken. From this it can be seen that the permanent axial strain in the Unexposed material is reduced by 80.5% to 88.6% when comparing samples that are tested at 1 day of curing compared to 1 month of curing. All samples showed this behaviour barring one outlier that resulted in an increase in strain. This was due to excessive deformation taking place during the conditioning phase of the second phase testing. The reduction in permanent axial strain for Exposed material varies between 50.8% to 88.5% when comparing samples that are tested at 1 day and 1 month of curing. From these results is can be seen that the Exposed material has increased variability in the material when compared to Unexposed material. This can be attributed to the fact that during the curing process, some of the latent cement reacted, but only the latent cement that was exposed to water. There are thus aggregate pieces that contain no or very little latent cement, whereas other still have high amounts of latent cement present. The performance of the specimen is dependent on the amount of latent cement within it.

Table 4-13: Percentage permanent axial strain for Exposed and Unexposed RCA observed during Intermittent Permanent Deformation tests

Unexposed RCA				
σ_3 (kPa)	Month	Deviator Stress Ratio		
		37%	45%	50%
50	0	1.367	2.505	1.095
	1	0.261	0.436*	0.213
	% Reduction	80.9	82.6	80.5
100	0	2.325*	1.462	N/A
	1	0.266	1.683	
	% Reduction	88.6	-15.1	
Exposed RCA				
σ_3 (kPa)	Month	Deviator Stress Ratio		
		17%	22%	27%
50	0	0.766	0.952	3.215*
	1	0.088	0.203	Failed
	% Reduction	88.5	78.7	
100	0	0.632	1.036	2.33
	1	0.311	0.384	0.678
	% Reduction	50.8	62.9	70.9

* Maximum percentage strain taken at the point of failure

4.6 Summary

RCA material was tested in the laboratory, to gain insight into the performance of the material. During this experimental procedure various findings are made regarding the behaviour of the material. Two types of materials, namely Exposed and Unexposed RCA were tested to investigate the effect of latent cement on the performance of the material. Monotonic tests were performed in order to obtain the shear parameters of the material. Cohesion and Friction Angle results showed that Exposed material has a higher degree of variability, as the values for the monotonic tests do not correlate as well as for the Unexposed material. Therefore, additional monotonic tests had to be performed. The shear parameters of Exposed and Unexposed materials are very similar. It is concluded that an informed decision on the performance of RCA cannot be made based on monotonic tests alone.

Two types of permanent deformation tests were performed, i.e. basic and intermittent tests. Basic permanent deformation tests were performed for 250 000 cycles, and gives an indication of the long term behaviour of the material. Intermittent tests were performed for 100 000 cycles, before curing the sample for 28 days and testing it again for 100 000 cycles. Intermittent tests were performed to investigate the self-healing potential of RCA. The second finding is that RCA material does not behave entirely like a granular material. The third finding is that after 28 days of curing a specimen that has become unstable, showing Range B or C behaviour of the Shakedown Theory, retesting has shown the specimen to exhibit stable behaviour. This highlights the importance of curing RCA material if used as pavement layer. The initial loads applied by construction traffic can cause damage to the material, but with a sufficient curing period the material will be allowed to cement, and result in stable behaviour.

In order to obtain data that can be used in the development of a transfer function, the permanent deformation data must be modelled. To do this 5 models are identified and used, and the best model is chosen on the 3 criteria, the coefficient of determination must be as close as possible to 1, the sum of least squares must be as close as possible to 0 and the model must fit visually. For each range of the Shakedown approach a different model was found to be better fit to model permanent deformation. For Range A the model as suggested by Paute (1996), for Range the B the model by Wolff and Visser (1994) and for Range C the model as developed by Huurman (1997) was found to best describe the behaviour. The Huurman (1997) model was used in the remaining calculations of this report, as it is the only model that can accurately describe the unstable behaviour of RCA materials as well as the stable behaviour to an acceptable degree of accuracy.

Chapter 5: Transfer Function Development

5.1 Introduction

In order to express the influence of different variables on the pavement life, it is necessary to develop a transfer function that combines the influencing variables. The transfer function can then be used to determine the pavement life in terms of number of load applications for the pavement material that it has been developed for. The format of the transfer function was designed to incorporate the proportional influence of the variables (through calibration of coefficients) that affect the material in comparison to one another and therefore describes the typical behaviour of the material. The transfer function is based on the failure mechanism for the given material, and include various factors that affect the pavement life.

A distinction is made based on the transfer function development done here and those found in manuals and design methods in terms of the evolution process of such a design function. In this case the transfer function is based on laboratory results as opposed to a design function which is based on information gathered from materials within a pavement structure. A good example is the current design functions for all granular materials, cemented material, and asphalt are encapsulated in SAPEM(2014b). These functions have been developed through a process of initial design functions (based on laboratory results) which were then calibrated using data obtained from in-situ sections. Recognising this iterative process in order to reach an improved transfer function, the objective of this chapter is the preliminary development of a design function for RCA used in the South African condition. This can serve as a basis for further upscaling and calibration when more laboratory results become available. Subsequently, when the coefficient values of the material have been calibrated for various laboratory results, the same procedure process can be applied to performance results obtained from constructed pavements.

The failure mechanism for RCA depends on the extent of self-cementation that has been allowed to take place. For a low amount of self-cementation the failure mechanism will be similar to that of granular materials, which is shear failure manifested as permanent deformation. As discussed earlier, the failure of RCA material could also possible manifest as a combination of the failure mechanisms of granular and cemented materials. In this case, due to the self-cementation process the material could be dependent on both the matrix interlock and the tension elements formed through the self-cementing process as discussed in Chapter 4. For this RCA transfer function development it was assumed that the 0 month material will have the same failure mechanisms as that of an unbound granular material. This assumption is substantiated by the evaluation of the variables in the previous chapter.

The transfer function for waterbound macadam is used as departure point for the synthesis of the RCA transfer function. The waterbound macadam transfer function was used as this function contains important parameters that is critical for granular materials. From unpublished research performed at Stellenbosch University it was found that the waterbound macadam transfer function is applicable to materials that share properties with granular materials but are considered as variants of the original material such as RCA and BSM. This function is based on the bearing capacity of the material in terms of the number of load repetitions the material can handle before a set amount of plastic strain is induced in the material. The development of the transfer function for waterbound macadam will be discussed hereafter. Initially the transfer function used in the SAMPDM (2011) was considered. However, these transfer functions do not distinguish as clearly between different intrinsic variables of the material and the waterbound macadam function was deemed more appropriate.

A transfer function is synthesised using the waterbound macadam transfer function as a guide. The results obtained in Chapter 4 will be used to develop a laboratory based transfer function with the various influencing factors incorporated. Once the transfer function is developed, it must be calibrated and sensitivity analysis must be completed. Transfer functions will only be synthesised for the Unexposed RCA material. The reason for only doing the Unexposed RCA material is that the recycling of RCA material still remain very informal in the South African industry. The most representative situation assumed is that material will be used and processed shortly after demolishing. In addition, the increased variability reported in the results of the Exposed material also contributes to not developing a transfer function for this material. More laboratory tests for Exposed material must be performed in order to develop these coefficients.

5.2 RCA Transfer Function Methodology

The following section will include the methodology followed to obtain the transfer function for RCA material. Here the transfer function for waterbound macadam will be discussed, as well as the form and assumptions for the transfer function for RCA in particular. The calibration process of the transfer function, after the coefficients have been determined is also discussed.

5.2.1 Waterbound Macadam Transfer Function

The RCA material after 1 day of curing, had a very small window of opportunity to undergo self-cementation, and therefore the material will have some cementitious bonds but it will perform and fail like a granular material as found during the laboratory tests. The transfer function for the 0 month Unexposed material will be based on that of waterbound macadam (granular material).

The transfer function for waterbound macadam is shown in Equation 5-1.The formula calculates the amount of load repetitions the material can withstand before a predetermined amount of plastic

strain is induced in the material (Theyse *et al.*, 2000). This function was based on laboratory tests that included triaxial and heavy vehicle simulator (HVS) tests for the material waterbound macadam.

$$logN = 1.891 + 0.075RD - 0.009S + 0.028PS - 1.643SR \quad 5\text{-}1$$

Where:

N: Number of standard axles allowed before a predetermined plastic strain value is reached

RD: Relative Density (%)

S: Saturation (%)

PS: Predetermined Plastic Strain limit as a percentage of the layer thickness (%)

SR: Stress Ratio as defined in Equation 5-2

Equation 5-2 can be used to calculate the stress ratio for the waterbound macadam transfer function, when used in design. This stress ratio differs from usual, which includes the stress at failure and the confinement pressure, as it is a function of the shear parameters of the material, the load intensity and the pavement layer structures. For granular materials the shear parameters can be taken from the laboratory results for the material, if this is unknown the material property table for granular materials in SAPEM (2014b) can be used. For RCA material the shear parameters can only be based on laboratory testing as SAPEM does not include standard material properties for RCA.

$$SR = \frac{(\sigma_1 - \sigma_3)}{\sigma_3\left[\left(\tan^2\left(45 + \frac{\varphi}{2}\right) - 1\right)\right] + 2C\tan\left(45 + \frac{\varphi}{2}\right)} \quad 5\text{-}2$$

Where:

σ_1: Applied major principal stress (kPa)

σ_3: Minor principle stress acting in the middle of the granular layer (kPa)

φ : Friction Angle (°)

C: Cohesion (kPa)

Theyse *et al.* (2000) developed a model to obtain the friction angle of waterbound macadam. This model relates the friction angle to the relative density and the saturation of the material. The relative density and the saturation is expressed as a percentage of the apparent density and the inter-particle voids respectively. The friction angle can be calculated using Equation 5-3.

$$\varphi = -26.38 + 1.021RD - 0.171S \quad 5\text{-}3$$

5.2.2 RCA Transfer Function Format

By using the transfer function of waterbound macadam as a basis, a preliminary transfer function is developed as reported in Equation 5-4. The transfer function for RCA will be dependent on four properties of the material, namely the relative density, the moisture content (expressed as a percentage), the plastic strain limit and the deviator stress ratio. The density as measured at compaction is used as a percentage of the maximum vibratory hammer density. The vibratory hammer density is used in place of the conventional MOD AASHTO as it provides a better representation of the achievable density on site. A predetermined plastic strain limit is set, and the plastic strain is the amount remaining in the material, i.e. the amount of the plastic strain that can develop before the material reaches this predetermined limit. In the integration of the results to develop the coefficient variables, the DSR results were based on the monotonic results performed for this material.

$$logN = A + B\ (P_{vib}) - C(MC) - D(DSR)^F + E(PS) \qquad 5\text{-}4$$

Where:

N: Number of load cycles to accumulate a predetermined amount of plastic strain

P_{vib}: Density expressed as a percentage of the maximum vibratory hammer density (%)

MC: Moisture Content (%)

DSR: Deviator Stress Ratio

PS: Predetermined amount of plastic strain that may accumulate in the material before failure (%)

The unknowns, namely A, B, C, D, E, F in Equation 5-4 are constants that are used to develop the transfer function coefficients. During the initial phase of the transfer function synthesis these values were assumed arbitrary to have a starting point for the process. These values are then reiterated to obtain more suitable values. The seed values are assumed based on the perceived influence each variable had on the results of the triaxial tests and the architecture of the transfer function. For example moisture content and density were perceived to play a smaller role in the failure than the DSR. The seed values are shown in Table 5-1.

Table 5-1: Initial seed values for transfer function constants

Constant	Value
A	1
B	0.001
C	0.001
D	60
E	0.1
F	3

The negative and positive symbols in the equation are derived using sound engineering knowledge, however allowing for a potential change during the simulations of the transfer function. A good example can be found in Equation 5-4, where the density has a positive symbol, meaning an increase in density would be beneficial to the pavement life of the material. This variable could behave counterintuitively, due to the self-cementing potential of the material.

In Equation 5-1 the saturation has a negative symbol, which indicates that as the degree of saturation of the material increases, the number of load cycles decreases. In Equation 5-4 the same convention is applied, as an increase in the moisture content of the material, would reduce the shear capacity of the material causing a reduction in the pavement life. Here it is important to set a minimum value for the moisture content(at which is applicable) as it would seem (due to the structure of the formula) a moisture content of 0% would be beneficial, but in actual fact 0% moisture content would be detrimental as the material would not be compactable or able to react. A minimum value of 6% moisture content was set as this is a reasonable lower limit expected for OMC.

The term describing the effect of the DSR has a negative symbol, this is intuitive as the deviator stress ratio increases the applied load on the material increases which will cause a reduction in the pavement life. The DSR term has an unknown power coefficient. The objective of this coefficient is to increase the significance of the DSR variable if necessary on the pavement life. The significance of the power and the investigation to determine the correct value will be discussed later. The deviator stress ratio of a material is dependent on a variety of factors:

- The load applied to the material or pavement structure, an increase in the applied load with all other conditions such as confinement remaining stable will result in an increased DSR. The standard transfer function for waterbound macadam was developed for 80kN axles.
- The shear properties of RCA material is variable due to the self-cementation, as the friction angle or cohesion increase the Mohr failure envelope changes. If the failure envelope is elevated, the failure stress increases resulting in a lowered DSR.
- Due to the self-cementation that takes place RCA will potentially be a stiff material which will affect the load spreading ability of the pavement structure. The research completed by Arm (2000) shows the progression of stiffness of RCA and granular materials over time.
- Pavement structure and the placement of the RCA layer within the pavement structure will also affect the DSR.
- Curing period will affect the DSR, as the material cures and becomes stiffer the failure load increases which means the shear properties have increased; this will reduce the DSR.

- It should be noted that at higher DSR values, the vertical forces applied to the specimen increases. This applied force has a large influence on the behaviour of the material as a force with a large magnitude seems to break the cemented bonds within the material which results in a weaker material that becomes unstable. As discussed in Chapter 4 the material shows high variability and more tests must be performed to substantiate this conclusions explicitly.

5.2.3 RCA Transfer Function Calibration

The methods used to develop the coefficient values for the transfer function are discussed in this chapter. The data obtained in the laboratory tests must be modelled to obtain usable data to base a transfer function on. To fit the predicted values from the transfer function to the values obtained from the modelled data the transfer function must be solved by finding values for A, B, C, D, E and F in Equation 5-4. A mathematical function can be found to describe each of the tests performed in the laboratory perfectly. However, this would not be useful as it only describes one situation and would therefore be limiting in the application thereof. The transfer function must be calibrated for all the data obtained, this will result in a function that does not describe the data perfectly, but it will have far greater power in predicting a variety of situations.

The input values for the transfer function, such as the DSR, the density and percentage moisture content are measured for each triaxial test performed in the laboratory and recorded. The intermittent and basic triaxial tests for the Unexposed RCA material is modelled using the Huurman (1997) model to obtain the data used to calibrate the transfer function.

5.2.3.1 Laboratory Data to Modelled Data

The basic and intermittent triaxial tests are used as data sources for the transfer function. This poses a challenge as the basic tests are performed for 250 000 cycles and the intermittent tests for 100 000 cycles. In terms of a pavement life these values are extremely small and ideally the strains at larger load applications up to 40 million load cycles would be preferable. The laboratory test data is thus taken and modelled and using a simplified version of Huurman's (1997) model as identified by Werkmeister (2003) so that the strains at large load applications can be found. Equation 5-5 is used to model the laboratory data as discussed in Chapter 4.4.3.2.

$$\varepsilon_{1,p} = a\left(\frac{N}{1000}\right)^{b} \qquad 5\text{-}5$$

Where:

$\varepsilon_{1,p}$: Axial permanent strain accumulated

a, b: Constants for a given deviator stress and confinement pressure

N: Number of load cycles

To calibrate the transfer function a maximum allowable permanent strain of 5% of the layer thickness in the RCA is chosen. Traditionally the model in Equation 5-5 uses the number of load applications to determine the amount of plastic strain that has developed in the material, however with the predetermined strain limit, it is needed to calculate the number of load applications needed to achieve each amount of plastic strain. The equation is thus rewritten in terms of the number of load applications in Equation 5-6.

$$N = 1000 \cdot \left(\frac{\varepsilon_{1,p}}{a}\right)^{\frac{1}{b}} \qquad 5\text{-}6$$

For each of the basic and intermittent test the constants a and b are already known from the modelling completed in Chapter 4.4.2.1. Equation 5-6 can be used to determine the N_{actual} for the plastic strain values up to 5%. Bierman (2017) explained why the Huurman model is better to use for the development of plastic strain than a linear approach as seen in Figure 5-1. A linear approach will over estimate the amount of plastic strain, especially in the stabilising phase of permanent deformation behaviour. The architecture of the Huurman model is based on an exponential function and is able to better model the stabilising phase of the permanent deformation behaviour. Due to the second part of the Huurman equation it is also able to model the unstable behaviour. The latter part including unstable behaviour is not applicable to the development of the transfer function, however the data obtained from the laboratory tests further prove this point as it follows an exponential curve for stable behaviour of RCA.

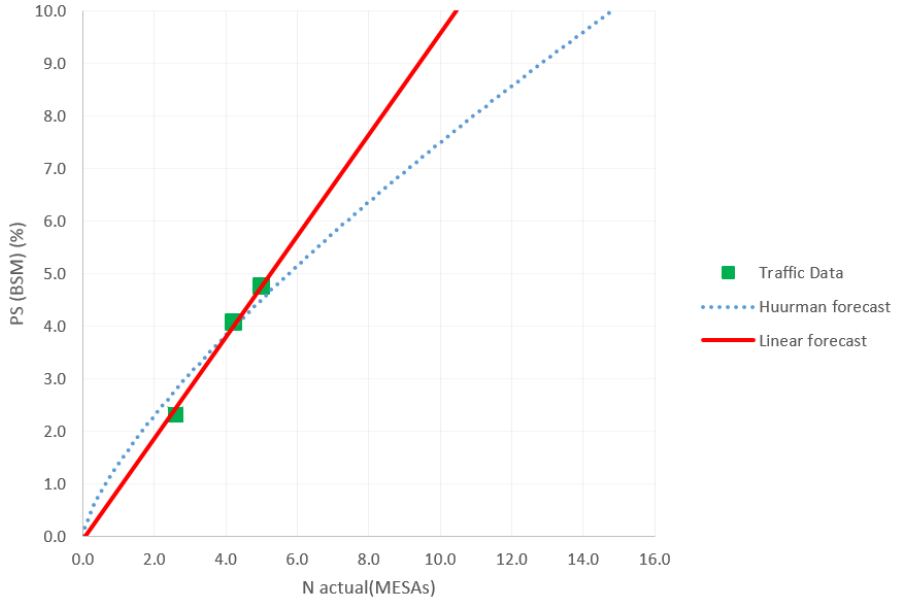

Figure 5-1: Extrapolation of plastic strain using linear relationship and Huurman model (Bierman, 2017)

One of the limitations of the transfer function is that the transfer function can only predict stable logarithmic behaviour. This is the reason why the second the term of the Huurman (1997) model was not used in the synthesis of the transfer function. Referring to Figure 4-9 and Figure 5-2 it can be seen that unstable behaviour occurs above45% deviator stress and at confinements of 100 kPa and above. One of the assumptions made in the synthesis of this transfer function is that unstable behaviour occurs above 45% DSR, at DSR lower than this value such as 43% or 44% the behaviour will have the same form as 37% DSR line in Figure 5-2, but the gradient will be significantly steeper. The line will have a very steep gradient, and the limit of 5% plastic strain will be reached within a small amount of load cycles but the behaviour will be stable falling in Range B of the Shakedown approach. The transfer function will thus have definitive limitations. This limitation does not mean that the 45% DSR results that were obtained in Chapter 4 were not used in the calibration of the transfer function.

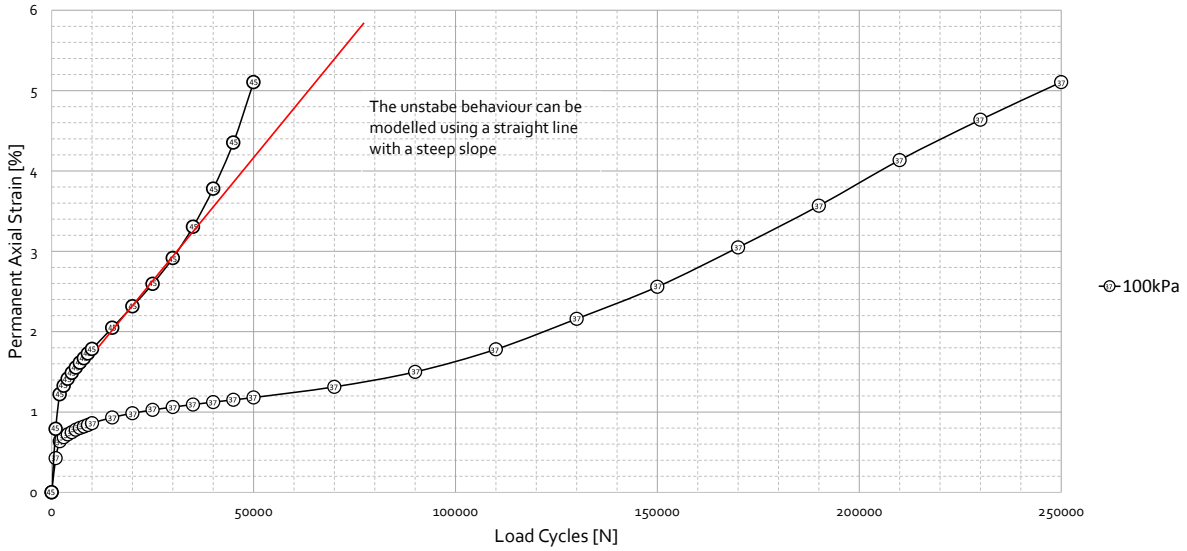

Figure 5-2: Explanation of assumption made regarding unstable behaviour

5.2.3.2 Relating the transfer function to actual traffic

The transfer function is used to calculate the remaining number of load application the material can withstand based on the amount of plastic strain remaining in the material. The maximum amount of plastic strain is limited to 5% for this transfer function as explained before. However, based on other RCA materials and triaxial testing, a designer may choose to change this limiting value.

With triaxial tests as well as in a pavement structure in the field ,the amount of plastic strain increases as the number of load applications increase on the layer, as seen in Figure 5-3 for granular materials. As the RCA at 0 month of curing is assumed to show granular material behaviour this simplifies the expected behaviour of the material

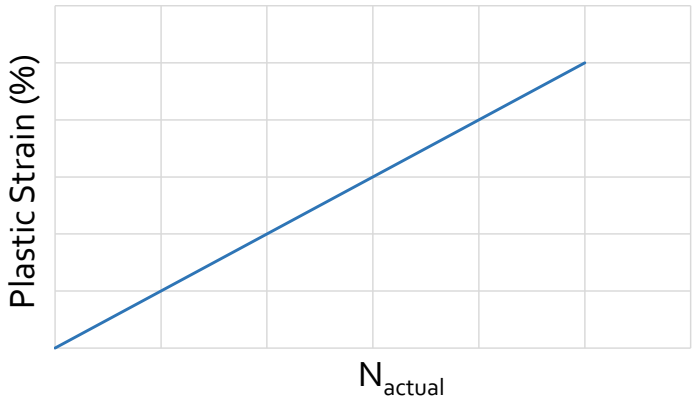

Figure 5-3: Development of plastic strain with traffic accumulation

This trend is not found when using the transfer function as seen in Figure 5-4. As the plastic strain increases the allowable number of load repetitions decreases to the terminal conditions. In order to compare the number of load applications that actually take place with the number of load applications predicted with the transfer function, the plastic strain value will have to be changed. Instead of using the actual amount of plastic strain in the material, it is necessary to use the amount of allowable plastic strain remaining in the material. It is for this reason that a limit value must be chosen so that the remaining plastic strain can be calculated. In this situation at the beginning of the pavement life the material will have 5% of plastic strain remaining and at failure the material will have 0% remaining. The N_{actual} at a given plastic strain should be compared to the $N_{transfer}$ at the plastic strain limit minus the given plastic strain. When looking at a plastic strain value, the term N_{actual} refers to the amount of load cycles the material can withstand based on the Huurman (1997) model which is based on the actual measured data. At the same plastic strain the term $N_{transfer}$ refers to the number of load cycles the material can withstand based on the transfer function.

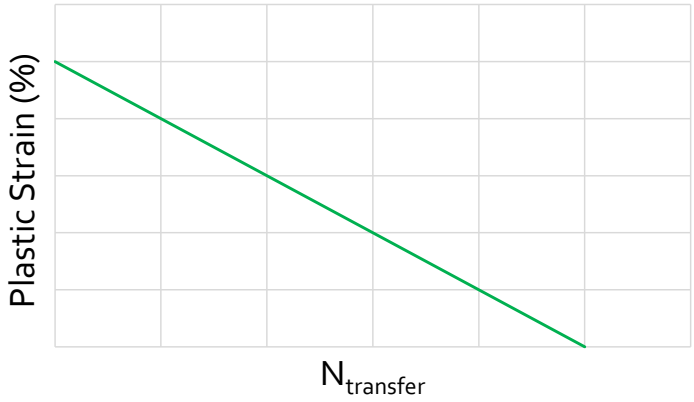

Figure 5-4: Development of plastic using the transfer function

In order to calibrate the transfer function the N_{actual} values and the $N_{transfer}$ values should be plotted on the same graph as shown in Figure 5-5. This creates a comparison mechanism for the two data sets.

When calibrating the function, there are two main criteria, firstly to minimise the sum of least squares and secondly to have the slope of the N_{actual} and the $N_{transfer}$ as close as possible to one.

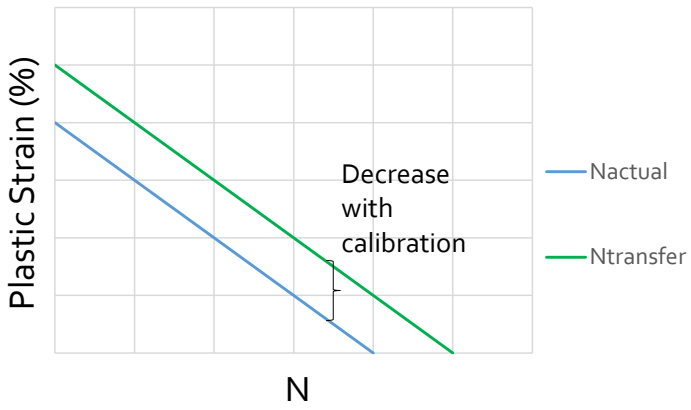

Figure 5-5: N_{actual} compared to $N_{transfer}$

5.2.3.3 Calibration of the transfer function with regression

The objective of the calibration is to find values for A, B, C, D, E and F so that the transfer function yields values as close as possible to the modelled data. A graphical representation of the problem can be created by plotting the N_{actual} and the $N_{transfer}$ on a single graph as shown in Figure 5-6. The calibration process is complete when the slope of the line approaches 1 and the R^2 of the function is as close as possible to 1. The regression parameter gives an indication to accuracy of the function. The sum of least squares can also be used to investigate the accuracy however the values that are obtained are so large that this parameter can be very deceiving.

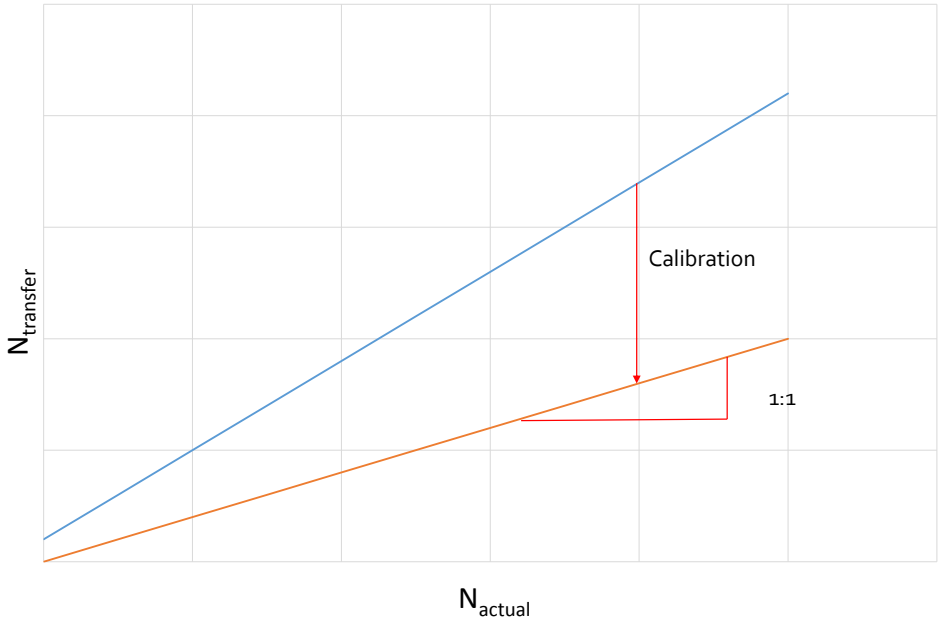

Figure 5-6: Conceptual calibration of the transfer function

In order to find the values of the unknown constants, the Solver function in Excel is used. The evolutionary solving method is used to change the values of the 6 constants in order to obtain a slope of 1 or the N_{actual} / $N_{transfer}$ plot and the highest R^2 value. The objective of the Solver function on Excel is the slope of the line comparing the actual and transfer function values, the constraints of the function are set and changed to converge the slope. The results and the development of the different steps of this will be discussed hereafter. It should be noted that these values of the parameters should not be readily accepted after the solving method, one should consider whether the values make sense in the context of the results obtained in the laboratory. This will become apparent as the solving process to obtain the unknown constants are re-iterated in the following sections.

5.3 Transfer Function of Unexposed RCA

To calibrate the transfer function, the density, moisture content and DSR for each test had to be identified, as these are some of the variables of the transfer function. The properties for each test are shown in Table 5-2. As discussed earlier, a limitation was set to 45% DSR and therefore tests at 50% DSR are disregarded. The nomenclature for this chapter was used so that 50/37, denoted a sample that was tested at 50 kPa confinement pressure at a 37% deviator stress ratio. The B or I denotes the type of performed with B being a basic test consisting of 250 000 cycles and I an intermittent test with 100 000 load cycles.Table 5-2: Summary of input value for the transfer function from laboratory tests.

Test	DSR (%)	Density (%)	Moisture content (%)
50/37 B	37	106.74	10.05
50/45 B	45	106.90	9.74
75/37 B	37	105.94	10.73
75/45 B	45	106.05	10.29
100/37 B	37	105.99	11.04
100/45 B	45	106.49	11.95
50/37 I	37	106.23	10.09
50/45 I	45	106.53	10.01
75/37 I	37	105.76	10.71
75/45 I	45	106.13	11.37
100/37 I	37	106.14	12.15
100/45 I	45	105.84	11.26

5.3.1 Calibration of Transfer Function to modelled data

The transfer function is calibrated by comparing the development of permanent strain using modelled data and that of the transfer function. The transfer function is calibrated to accurately

predict the number of load repetitions that are required to induce a certain level of plastic strain within the material. The transfer function is dependent on 4 input parameters, namely density, moisture content, DSR and plastic strain.

Three of the four parameters are given in Table 5-2 and are determined during the preparation of the specimens. The fourth variable is the controlling variable of the function and is the permanent strain in the material. As previously discussed plastic strain is a measurement of the remaining deformation that the layer can withstand before a predetermined value is reached and failure occurs. For the calibration of this transfer function the maximum plastic strain is limited to 5% of the RCA layer thickness. This means at the start of the pavement life when no loading has occurred and no deformation has occurred the material has 5 % plastic strain remaining. At the end of the pavement life, the layer would have accumulated 5 % plastic strain, and would have 0% plastic strain remaining, this means the material is on the verge of failure.

5.3.1.1 Initial analysis of transfer function

The simplified Huurman model is used to calculate the number of load repetitions at plastic strains ranging from 5% to 0% in constant increments. The remaining life of each laboratory test can then be calculated using the transfer function and an initial seed values of the constants are used. This provides an initial set of data to compare with one another. As in Figure 5-6 the number of load cycles yielded by the transfer function can be compared to the number of load cycles obtained from the model. Using Equation 5-7 and the initial constant values in Table 5-1 the first iteration of the transfer function can be completed.

$$logN = A + B\ (P_{vib}) + C(MC) + D(DSR)^F + E(PS) \qquad 5\text{-}7$$

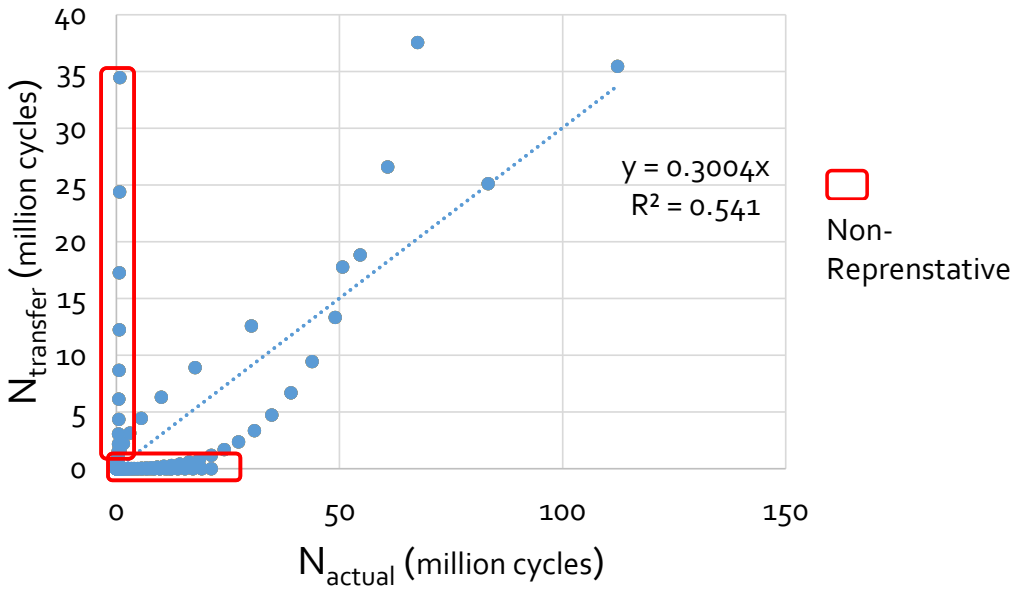

Figure 5-7: $N_{transfer}$ vs. N_{actual} with initial constants assumed

Using the initial seed values it can be seen that the transfer function does not predict the overall behaviour of the RCA material well. Using the estimated constant values the $N_{transfer}$ and N_{actual} are plotted as seen in Figure 5-7. The regression line that best fits the data has an equation of $y = 3.004x$ and the R^2 value is 0.541 .The slope of the regression is relatively low at 0.3 this slope indicates that in most cases the transfer function underestimates the number of load repetitions. The coefficient of determination is average indicating that the form of the transfer function does not represent the data very well. The transfer function has a low level of reliability.

Non-representative data as shown by the red squares in Figure 5-7, in other words areas where the transfer function completely fails to predict the behaviour is circled in red. In some cases the transfer function predicts an extremely low pavement life as seen by the values on the x-axis and in some cases the transfer function predicts extremely large values as seen on the y-axis. The values on the y-axis are values that the transfer function returns as positive results. However, the pavement is at the end of its life. These values are normally obtained when the plastic strain is at 0%. This should be when the transfer function determines the number of load repetitions to failure, after the layer has theoretically already failed. These values to do not represent an accurate situation and it is beneficial to remove them from the calibration process.

The transfer function must now be further calibrated in order to obtain a 1:1 slope for the regression line. As previously stated a relationship N_{actual}/ $N_{transfer}$ line with a slope of 1 indicates that the transfer function describes the known data without overestimating or underestimating the data. Various scenarios were investigated in the calibration process. The first scenario was where the exponent of the DSR term was taken as a constant with a value of three. Bierman (2017) found that for a BSM the influence of the DSR should be powered by three. The second scenario is where the exponent of the DSR term is allowed to vary. The third scenario is considered where the tests that resulted in non-representative data is removed to investigate the effect this will have on the reliability.

5.3.1.2 Scenario 1 Calibration

For the first scenario the exponent of the DSR term is kept constant at 3, this is the recommended value from the research completed on BSM by Bierman (2017). Excel Solver is used to find values for the constants A, B, C, D and E in order to obtain a 1:1 relationship or as close as possible to it. The linear estimation tool is used to find the slope, the coefficient of determination and the residual sum of squares of the graph comprising of $N_{transfer}$ vs. N_{actual}. The objective is to find the smallest sum of residual squares by changing the values of the constants. It is aimed to achieve a slope of between 0.95 and 1.05.

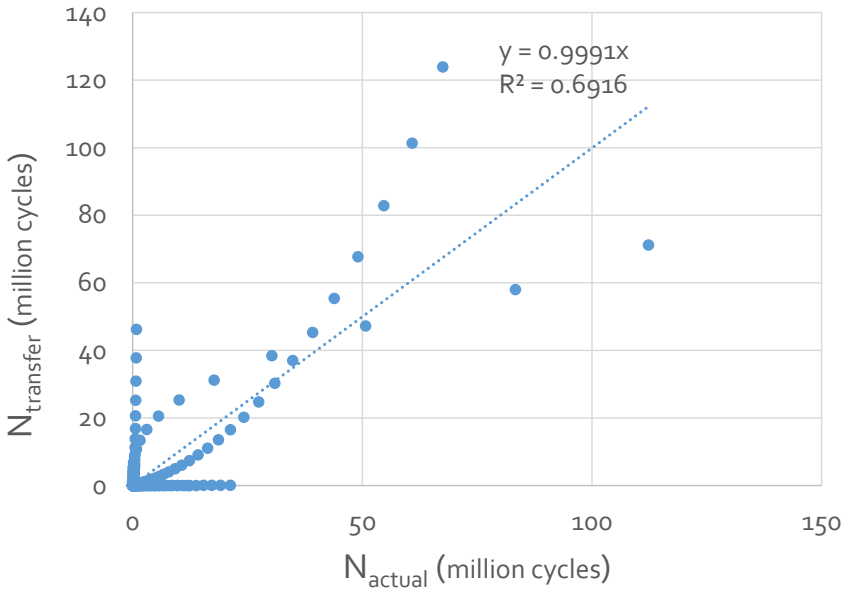

Figure 5-8: $N_{transfer}$ vs. N_{actual} calibrated to a 1:1 relationship with a constant exponent of DSR

Figure 5-8 shows the relationship between the $N_{transfer}$ and N_{actual} obtained using a constant exponent for the DSR term. The trend line with the linear relationship that best fits the data can be described by the equation $y = 0.9991x$ with a correlation coefficient of $R^2 = 0.6916$. Once the Excel Solver is complete the values for the constants are determined and shown in Table 5-3.

Table 5-3: Calibrated coefficients for transfer function with constant exponent of DSR

Constant	Value
A	57.4686
B	-0.0409
C	-0.5520
D	-93.4965
E	0.8746

During the calibration process the objective is to obtain a trend line with a slope that is equal to 1. The slope of this trend line indicates that the transfer function predicts the actual data to a satisfactory standard. By fitting the transfer function to this slope, the function predicts the pavement life with no safety factor. There are two challenges associated with this statement, firstly the function is based on laboratory results and therefore it cannot be used as a design function without further investigation, and secondly a design function should have a reliability of 90% for important roads such a Category B roads. The initial calibration process only aims to describe the observed data and not to create a function suitable for design.

The coefficient of determination for this scenario is 0.6916, which shows an average relationship between the plastic strain development and the new transfer function. As discussed earlier, with the addition of more laboratory tests. This value could probably increase. However, considering the

variability of the material this could possibly also decrease. . The correlation coefficient is not used as an indication of accuracy but rather just to describe the precision of the transfer function.

Although the slope of the line is good and close enough to the 1:1 relationship, if the graph is visually assessed and a few problems can be identified. This transfer function still has non-representative data, this can be attributed to the fact that samples that were unstable were modelled using a steep gradient as shown in Figure 5-2 , when the number of load cycles that are being analysed approaches these large values such as 10 million and above the tests fail so rapidly that they are not a clear representative of the data sample. The transfer function cannot accurately predict this behaviour. The second challenge is that above 50 million load repetitions the transfer function does not accurately predict the behaviour of the material as seen by the exponential nature of the points. However one should consider how realistic an approach is where a granular material can withstand 50 million load cycles. This challenge will be addressed later in the chapter.

It is valuable to note that in this scenario the density has a negative impact, albeit very small. This is an anomaly and counteracts what would be expected. It is expected that at a higher density the material should perform better when exposed to repeated loading, but with some RCA material this seems to not be the case. A possible reason for this is that the self-cementitious bond as are broken if the material is compacted to a high density which is counterproductive for the material.

RCA material is extremely variable, and due to the limited data set that only consists of 12 tests the variability of the results is pronounced. To increases the reliability of this transfer function, many more specimens and must be tested and added to the data set.

5.3.1.3 Scenario 2 Calibration

During the second scenario the exponent of the DSR term was allowed to vary to between 2 and 4. The exponent becomes another constant that must be solved using the Excel Solver. The calibration is done to obtain a 1:1 relation between the $N_{transfer}$ vs. N_{actual}. Similar to the previous scenario the slope is constrained between 0.95 and 1.05 and the objective of the solution is to obtain a residual sum of squares that is as small as possible. Once the Excel Solver is complete the values for the constants are determined and shown in Table 5-4.

Table 5-4: Calibrated coefficients for transfer function with varying exponent of DSR

Constant	Value
A	6.809
B	0.02284
C	-0.4468
D	-21.105
E	0.8203
F	3.357

Figure 5-9 shows the relationship between the $N_{transfer}$ and N_{actual} obtained using a varying exponent for the DSR term. The trend line plotted through the data points to obtain a line of best fit can be described by the equation $y = 1.0002x$ with a correlation coefficient of $R^2 = 0.7009$. The values obtained for the constants used in the transfer function can be found in Table 5-4.

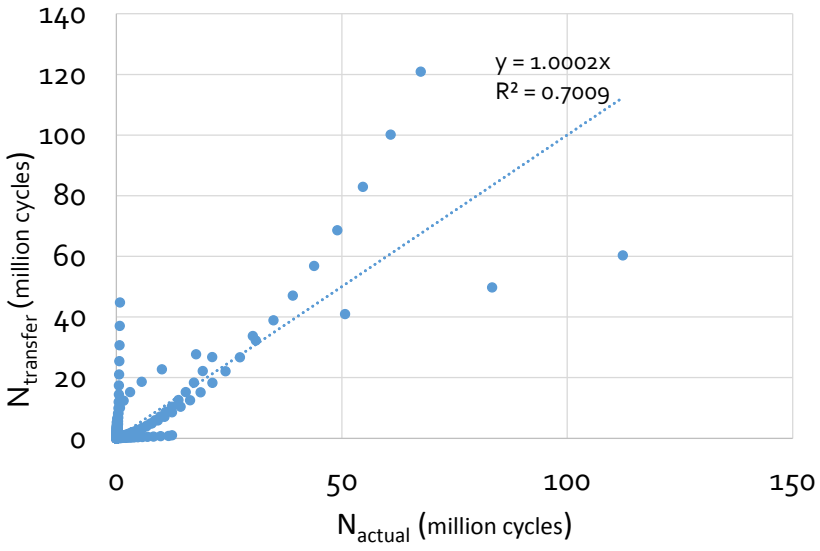

Figure 5-9: $N_{transfer}$ vs. N_{actual} calibrated to a 1:1 relationship with a varying exponent of DSR

When comparing the results obtained in the two scenarios with the constant and varying exponents it can be seen that the results are very similar. By allowing the exponent of the DSR term to vary the iterative process resulted in a 3.357 value, and for the constant exponent a value of 3 was chosen. The slope of both trend lines are very similar, for Scenario 1 the transfer function slightly underestimated the number load of repetitions whereas for Scenario 2 the transfer function slightly overestimated the number of load repetitions. The correlation coefficient for both of the scenarios are very similar.

It can be seen that for Scenario 2 the transfer function becomes inaccurate after 40 million load cycles, this is consistent with what has been seen in the first Scenario. It would be beneficial to place a load repetitions limit on these transfer functions to in order to err on the side of caution.

5.3.1.4 Scenario 3 Calibration

Two of the results from the permanent deformation tests, namely 100/37B and 100/45B are tests that become unstable, and are estimated with a very steep sloped line. As previously discussed, at high number of load repetitions the transfer function cannot represent these tests. It is decided to remove these test from the data set, with the provision of creating limitations on the transfer function as to not completely disregard the data and the shortcomings of this transfer function. The exponent of

the DSR term is allowed to vary during this Scenario as it is seen that it does not make a significant difference but it does count slightly in the favour of the transfer function. Similar to the previous Scenario the slope is constrained between 0.95 and 1.05 and the objective of the solution is to obtain a sum of least squares that is as small as possible.

The values obtained for the transfer function constants can be found in Table 5-5. The relationship between the $N_{transfer}$ and N_{actual} is shown in Figure 5-10. The DSR exponent was allowed to vary in order to the accuracy of the function. The trend line plotted through the data points to obtain a line of best fit can be described by the equation $y = 1.0077x$ with a correlation coefficient of $R^2 = 0.7896$.

Table 5-5: Calibrated coefficients for transfer function excluding unstable tests

Constant	Value
A	6.800
B	0.01933
C	-0.44118
D	-21.753
E	0.8929
F	3.358

From Figure 5-10 and the corresponding trend line values, it can be seen that the best fit to the data points are achieved in Scenario 3. Scenario 3 has a gradient that is very close to 1, and also has the highest regression coefficient. As previously stated it is necessary to limit the extent of the transfer function in terms of the amount of load cycles it is able to predict accurately. In this figure it shows that the transfer function becomes inaccurate when N_{actual} exceeds 40 million load cycles. It is therefore beneficial to limit the predictive ability of the transfer function at 40 million.

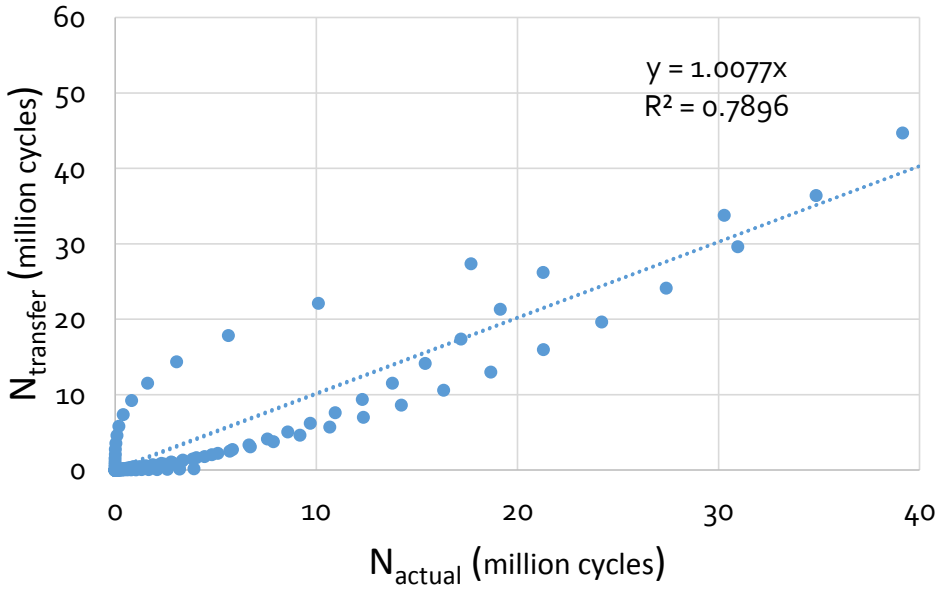

Figure 5-10: $N_{transfer}$ vs. N_{actual} calibrated to a 1:1 relationship excluding unstable tests

Figure 5-11 shows the data set and the trend line if the transfer function is limited to 40 million. Here it can be seen that the data points that were exponentially travelling away from the trend line has been removed. The data points are now situated closer to the trend line and the amount of non-representative points are reduced. The coefficient of regression has improved to 0.833, although the slope of the line is reduced to 0.940. The benefits of the limitation on the load application can be seen in the proximity of the data points to the trend line. The constants as shown in Table 5-5 are still valid for this function even though the limitation has been introduced.

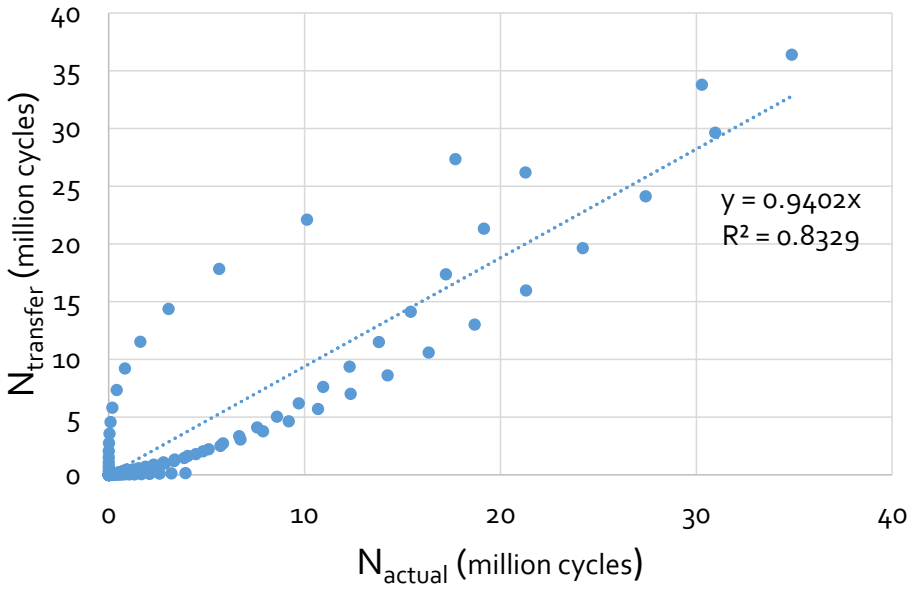

Figure 5-11: $N_{transfer}$ vs. N_{actual} calibrated to a 1:1 relationship excluding unstable tests and limited to 40 million load cycles

It is still worthwhile to note that the even though the transfer function has been improved, it still does not sufficiently describe the data to an accuracy that would be needed to use this a design function. In order to improve the transfer function and fit of the data, more tests must be completed so that more data is available to base the function on.

The final transfer function can be expressed as Equation 5-8, where the number of load cycles is limited to 40 million, the deviator stress ratio is limited to 45% and the moisture content must be more that 6%. The exponent is allowed to vary, and solved to a value of 3.35 which is very close to the initial assumed value of 3.

$$logN = 6.8 + 0.01933\,(P_{vib}) - 0.44118(MC) - 21.753(DSR)^{3.358} + 0.8929(PS) \qquad 5\text{-}8$$

5.4 Sensitivity Analysis

The transfer function is calibrated completing different scenarios and the final transfer function is given in Equation 5-8. The results of the transfer function are influenced by 4 main factors, namely density, moisture content, deviator stress ratio and the amount of plastic strain. The effect of these four factors and the extent in which they influence the transfer function will be investigated in this section. The sensitivity analysis is a means of quantifying the influence of the various factors on the transfer function.

5.4.1 Sensitivity to Deviator Stress Ratio

From Figure 5-12 to Figure 5-14 the significant effect that stress ratio plays in the transfer function can be seen. The transfer function is developed to be sensitive to changes in DSR, as the deviator stress is what causes the most significant damage. An important finding that concurs with the general damage equation used in practice shows that an increase in the axle above the standard axles load increases the damage in the pavement exponentially. The transfer functions response to the changes in DSR reflects the material's sensitive behaviour to an increased stress ratio.

After a 35% deviator stress ratio, the transfer function yields values that indicate a very rapid decline in pavement life. This is in line with the expected behaviour of RCA materials. The fact that the deviator stress after 35% causes rapid decrease in pavement life further likely supports the potential that RCA materials can manifest behaviour of granular and cemented materials. At a stress ratio of 50%, especially when looking at the moisture content and plastic strain sensitivity a low pavement life is obtained and the predictive ability of the transfer function is very low.

As the DSR increases a rapid decrease of the pavement life is returned by the transfer function. It is important to note that at DSR's of lower that 25% the transfer function returns very high values for the pavement life. The stress ratio of a pavement layer is influenced by various factors such as the shear parameters, the pavement configuration and the load applications. It is important to use the most accurate values available when looking at DSR as this is the factor that carries the most influence in the transfer function, due to the nature of the exponential function.

Figure 5-12 to Figure 5-14 is used to investigate the sensitivity of the transfer function to various factors such as the percentage moisture, plastic strain and density. In each of these analyses the deviator stress ratio is the independent variable that is change in order to visually illustrate the change in number of load cycles. Figure 5-12 shows the sensitivity top plastic strain, here it is seen that with an increase in deviator stress ratio the life of the pavement decreases. This trend is true for the other two parameters that are investigate das well. The influence that the deviator ratio has is dependent on the parameter that is being investigated. The deviator stress ratio and the parameter

being investigated is dependent on one another in terms of the effect that they have on the pavement life.

5.4.2 Sensitivity to Plastic Strain

The transfer function developed in this study was used to investigate the sensitivity of the function to allowable plastic strain as shown in Figure 5-12.The DSR is a governing factor in the sensitivity of the transfer function, and thus the plastic strain is varied over a range of different deviator stress ratio's in order to investigate the sensitivity. Figure 5-12 shows the number of load repetitions over a range of stress ratios for varying allowable plastic strains of 1%, 5%, 10% and 15%. The plastic strain is taken as a percentage of the height of the layer of RCA, or the total height of the specimen, and indicates the amount of plastic strain that can develop in the material before failure. It is expected that for a small allowable plastic strain the number of load repetitions would be reduced, if a larger plastic strain can be induced the specimen would be able to withstand more load cycles.

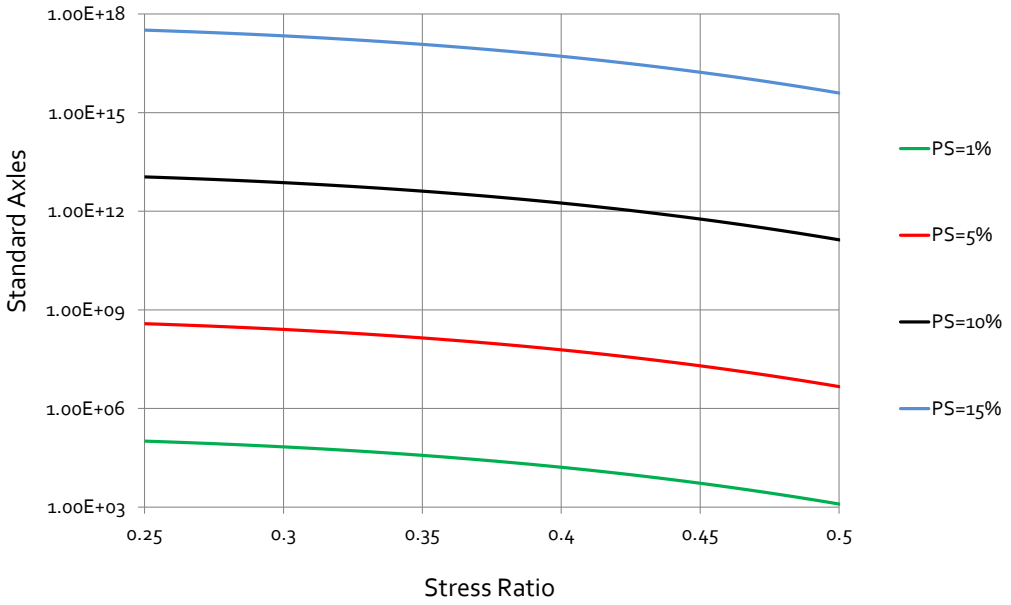

Figure 5-12: Sensitivity of the transfer function to Plastic Strain

The number of load applications in Figure 5-12 is plotted on a logarithmic scale. In order to complete the sensitivity analysis some of the variables must be constant. The moisture content was kept at 10% and the density at 100% of the vibratory hammer density. The effect of different plastic strains on the transfer function as the deviator stress ratio increases were investigated.

As expected, the number of load repetitions increased significantly as the amount of allowable permanent strain in the specimen increases. The amount load cycles for 10% allowable plastic strain compared to 1% allowable plastic strain is greatly increased, this can be seen by the magnitude of the values on the y-axis and the difference between each curve. This is the expected behaviour in granular

materials, as the allowable deformation of a pavement layer is increased, the number of load cycles that the layer can withstand before failure will also increase. The transfer function thus follows the logical conclusion in terms of allowable plastic strain in the material. It is important to remember that at low remaining plastic strains the transfer function can become inaccurate.

5.4.3 Sensitivity to Moisture Content

Moisture is needed in a granular materials in order to ease the process of placement and compaction. If too little moisture is added the material will not compact to its full ability and a low density will be encountered, whereas too much moisture will reduce the shear strength of the material. Figure 5-13 shows the effect that moisture content has on the transfer function for a range of DSR's plotted on a logarithmic scale.

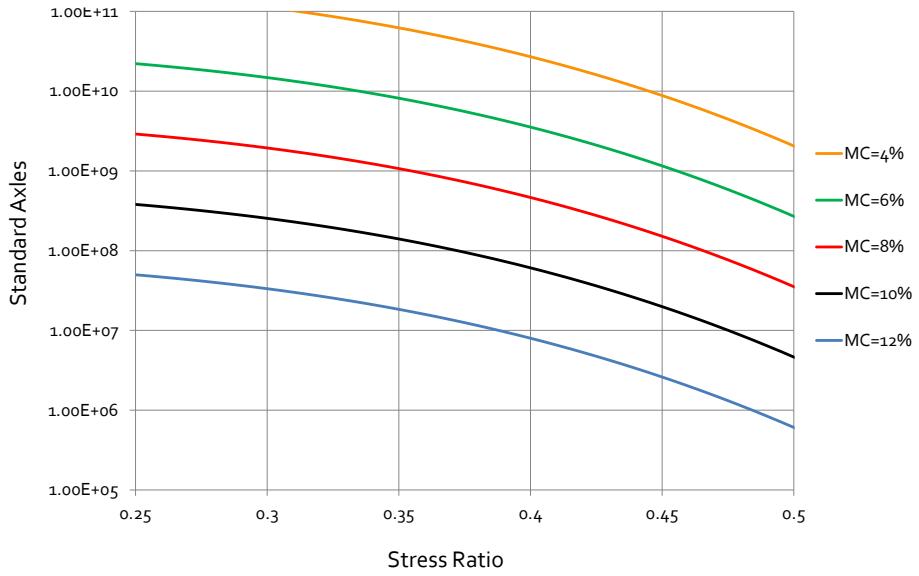

Figure 5-13: Sensitivity of the transfer function to Moisture Content

For the transfer function a minimum moisture content of 6% was specified. This is only a preliminary limitation until more tests can be performed and this value refined. Typical OMC values could range higher than this result due to the potential of the porosity of the material. This would imply that a value of 6% is too conservative. In addition the current architecture of the function is limited, for now, to this one source. When further tests are performed it would make logical sense to change this value to a percentage of OMC rather than the percentage OMC of the material. However, it might even be necessary to consider two values considering the moisture variable. The benefit of providing a percentage moisture content rather than a percentage of OMC could provide some insight on how much water absorption (because of porosity) could be present (if a person was experienced in typical values of OMC for RCA). Only considering percentage of OMC could potentially lead to a value that look acceptable. On the other hand only considering the percentage moisture; could make calibration

and accurate predictions of the transfer function challenging, if variable sources of RCA is considered. It is expected that as the moisture content increases the strength of the material will decrease and the number of load repetitions will be reduced.

From Figure 5-13 it can be seen that as the moisture contents increase from 4% to 12% as the amount of load repetitions decrease. Here it can be seen that moisture content does not play as a significant role in the number of load repetitions when compared to a factor such as plastic strain. The effect on the magnitude is significantly less pronounced than what is seen for plastic strain. The transfer function follows conventional thoughts when looking at moisture content. From Figure 5-13 it can be seen that for a 4% moisture content the transfer function yields a higher number of load repetitions, however this is not possible. If a material is placed at a lower than OMC it will affect the compaction which in turn will affect the number of load repetitions the layer can withstand. This is a shortcoming of the transfer function and thus a limit of 6% moisture content will be applied in order to circumvent this problem. It is necessary to also place an upper limit on the moisture content, as an increase in moisture will result in a decrease in standard axles, however may also result in unstable behaviour of the material. Further research should be done on the influence of moisture contents on the behaviour of RCA material before a definitive limit can be enforced.

5.4.4 Sensitivity to Density

The density is calculated as a percentage of the maximum vibratory hammer density as determined in the preparation phase of testing. From Figure 5-14 the number of load applications the transfer function yields for a constant plastic strain of 5% and a constant moisture content of 10% with varying densities.

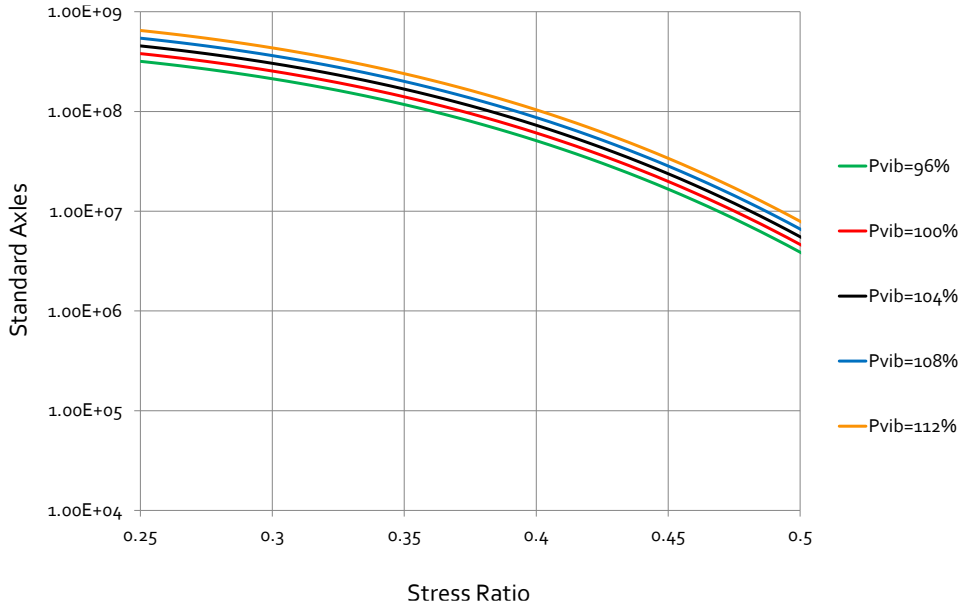

Figure 5-14: Sensitivity of the transfer function to Density

It can be seen that an increase in density will result in more load repetitions, however the effect that density has on the life is very small. This can be deduced by looking at the proximity of the various curves to one another as well as the difference in values of the curves. The trend that is expected is proved by the transfer function and it follows a logical argument.

Again it should be reiterated that this is only one source of RCA and this can possibly change with various sources of the material.

5.5 Reliability Adjustment

Once the transfer function has been calibrated it is needed to introduce certain levels of reliability. As previously stated, the calibrated transfer function is developed to describe the observed trends. In order to use a transfer function for design purposes it is necessary to introduce levels of reliability. The transfer function is changed to incorporate these levels of reliability by adjusting the constant A, or the shift factor in this case. The other constants in Equation 5-7 that describe the variable are kept constant. If the constants B, C, D, E, and the exponent were changed it would affect the significance of the effect on the transfer function results.

$$logN = A + 0.01933\ (P_{vib}) - 0.44118(MC) - 21.7525(DSR)^{3.3589} + 0.8929(PS) \qquad 5\text{-}9$$

Where:

A= calibrated for 50%, 80%, 90% and 95%

In order to calibrate the function for a specific reliability the values obtained by the transfer function is compared to the value calculated by the Huurman (1997) model. If the value yielded by the transfer function is higher than that calculated by the model it is assigned a value of 1. If the value calculated by the transfer function is lower than that calculated by the model it is assigned a value of 0.The average of all the values are found and this is taken as the reliability of the function. The value A can then be changed, while all other variables are kept constant in order to improve this reliability. The reliability indices are chosen to correspond with the four road categories in South Africa. These categories and their respective reliabilities is stated in SAPEM (2014b): Category A (95% reliability), Category B (95% reliability), Category C (80% reliability), Category D (50% reliability). Reliability in the transfer function is measured as a percentage of the predicted data by the transfer function that has a smaller value than the observed data. This means that the transfer function with a reliability added will predict the traffic in a conservative way, in order to ensure that a certain percentage of the data points are less than the actual data.

The process followed to adjust the transfer function predicted values to a certain reliability level can be seen in Figure 5-15. In this figure the transfer function is calibrated to a 90% reliability, which means that 90% of the values would be smaller than the actual data. The transfer function would return smaller values with the same input values compared to the original calibrated transfer function. This process is used to obtain values at reliability levels of 50%, 80%, 90%, and 95%.

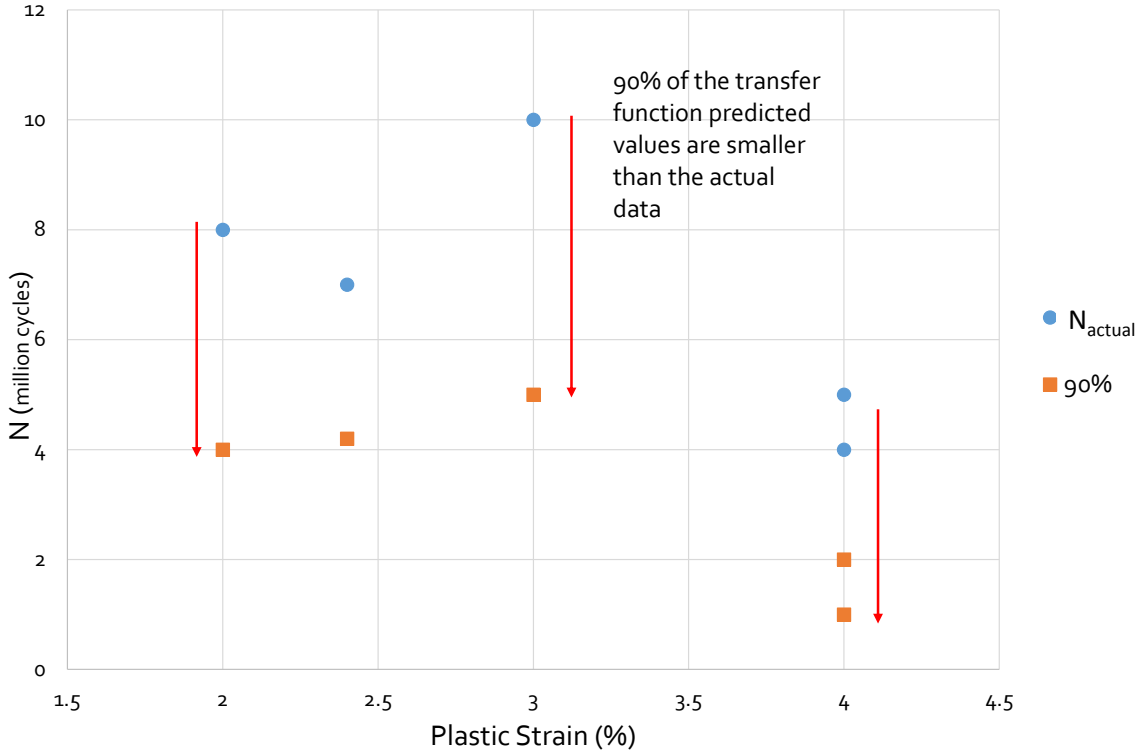

Figure 5-15: Method used to reduce the value predicted by the transfer function to a reliability index

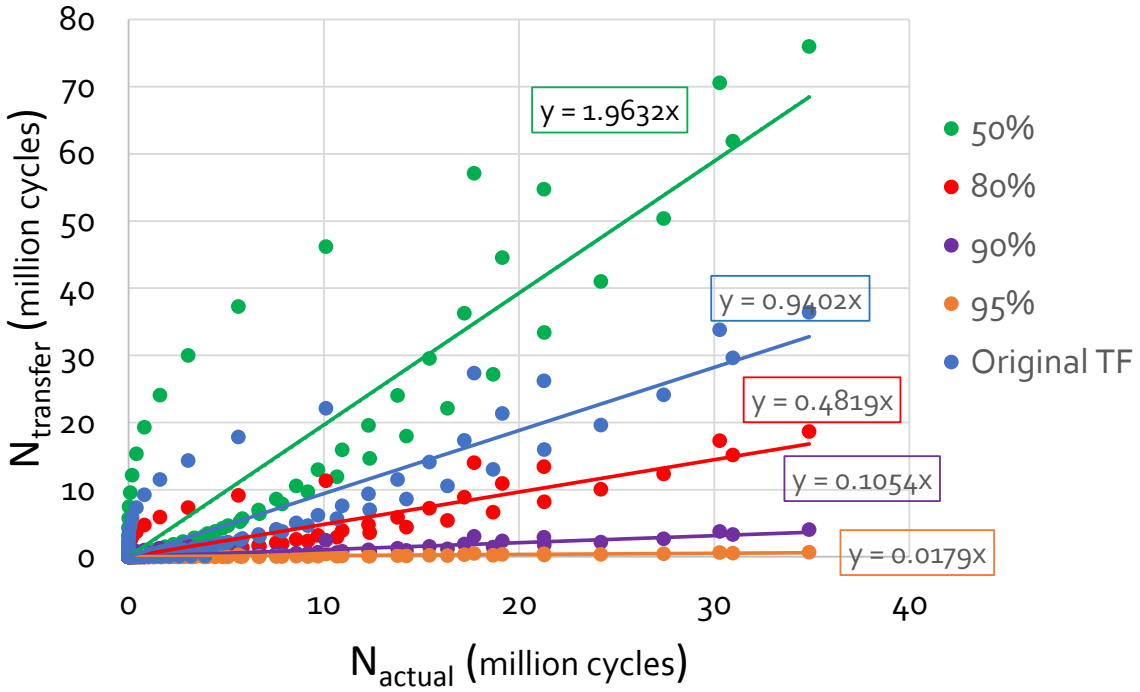

Figure 5-16: Transfer function reliability adjustments

Figure 5-16 shows the reliability adjustment for the transfer function compared to the original transfer function. Here it is worthwhile to note that the original transfer function has a reliability of 72%. This means that reliability adjustments of below this value, will mean the function is performing worse than it originally did. In Figure 5-16 the original transfer function can be seen in blue, the green line and accompanying dots are the values for the 50% reliability adjustment. The green values are above the blue value indicating a decline in the performance of the transfer function. For reliabilities above the 72% of the original transfer function the values as indicated in red, orange and purple are below the blue values of the transfer function.

In order to gain a full understanding of the effect of the reliability adjustment Table 5-6 is presented. The table includes the variable A, the slope and the regression coefficient of the transfer function. Reliability indices are investigated every 5% from 50% to 95% .It can be seen that the regression coefficient stays the same regardless of the reliability adjustment, although it has a pronounced effect on the slope of the best line, which is to be expected as the values of the transfer function are lowered.

Table 5-6: Summary of reliability adjustments for transfer function

Reliability (%)	A	Slope	R^2	Actual Reliability (%)
Original	6.8002	0.940	0.833	71.83
50	7.12	1.963	0.833	49.70
55	7.07	1.747	0.833	55.09
60	7	1.489	0.833	59.28
65	6.93	1.268	0.833	64.072
70	6.82	0.984	0.833	70.06
75	6.75	0.838	0.833	74.25
80	6.51	0.482	0.833	79.64
85	6.22	0.247	0.833	84.43
90	5.85	0.105	0.833	89.22
95	5.08	0.0179	0.833	94.61

In order to place this table and the values within context it is beneficial to calculate the number of standard axles predicted by the transfer function compared to the number of standard axles measured for each reliability index. From this table it can be seen that at 50% reliability the transfer function over predicts the number of load repetitions when compared to the actual values, for the

reliability indices of 80%, 90%, and 95% the transfer function underestimates the load repetitions when compared to the measured values. As the reliability improves the amount by which the transfer function underestimates the values increases.

Table 5-7: Summary of the load repetitions yielded by the transfer function for each reliability index

N_{actual}	$N_{transfer}$			
	50%	80%	90%	95%
100 000	165 781	40 694	8 903	1 512
500 000	514 639	126 328	27 638	4 694
1 000 000	856 438	210 231	45 993	7 811
3 000 000	2 517431	617 956	135 194	22 959
10 000 000	11 033470	2 708396	592 532	100 626
20 000 000	30 655486	7 525030	1 646 297	279 581
30 000 000	59 680250	14 649764	3 205 019	544 290

5.6 Summary

The waterbound transfer function macadam (Theyse *et al.*, 2000) was used as a departure point for the transfer function in this study. It is assumed that RCA will exhibit more prominent characteristics of a granular material than that of a cemented material.

During the synthesis process three different scenarios were investigated. The exponent of the deviator stress ratio was allowed be constant or varied. In addition the rapid failure of specimens at 100 kPa confinement were removed to improve the predictive ability of the transfer function. During this process various limitations and shortcomings of the transfer function were identified and are as follows:

- The transfer function cannot simulate unstable behaviour as seen in Range C of the Shakedown approach. This is circumvented by applying explicit limitations to the transfer function;
- To make the laboratory data applicable the transfer function is limited to a DSR of 45% and a confinement pressure of 100kPa. Above these values the transfer function will not be valid;
- Remaining plastic strain values of below 3% results in unrealistic values from the transfer function. Therefore this function is not good at predicting 1 month behaviour with very low amounts of strain;

- The number of applications is limited at 40 million, as beyond this point the transfer function yields unrealistically high or low values, and the relationship follows an exponential curve and no longer a linear relationship.
- A limitation is placed on the minimum percentage of moisture. As discussed earlier, this might change as the transfer function is calibrated for more laboratory tests. More important however is, that consideration should be given on how to express that contribution of water as a variable. This variable in future research must be able to distinguish the proportional value between for example hygroscopic moisture and that for percentage moisture content.

In order to use the transfer function as a design function reliability indices must be developed. The original calibration process of the transfer function is only aimed at describing the observed trend. By adjusting the shift factor (A) a measure of reliability can be added to the transfer function. The objective of the reliability adjustment is to reduce pavement life calculated by the transfer function so that a certain amount of the pavement life values fall below observed data. The original reliability of the function was found to be 72%, any value below this would result in the transfer function performing worse and over-estimating the value. Whereas if a higher reliability is used the transfer function would under estimate the amount of load repetitions which is the conservative approach.

Chapter 6: Pavement Analysis

6.1 Introduction

In this chapter pavement analyses are performed to compare RCA with that of standard materials. The main objective is not to make explicit conclusions on the pavement life as would be used for typical pavement design purposes. Instead the aim of this chapter is to provide some comparisons between using RCA as a pavement material to that of standard pavements. As the main objective is not to perform an analysis towards a standard pavement design, not all procedures followed were as per the standard SAMPDM. However, this was still used as the main framework and basis for analysis and comparison. Where standard procedures were not followed, this was explained.

A pavement structure is made up of different layers which can comprise of various material types and quality. The layers must accommodate the traffic and spread the load to the deeper layers. The load spreading ability of a pavement structure is a function of the stiffness of the material as well as other strength properties. In South Africa, a flexible pavement system is built typically comprising of a thin wearing course or seal, a base course consisting of high quality unbound natural aggregate, a subbase made of lightly cemented material and the subgrade. This is known as an inverted pavement, as the stiffness of the pavement increases with depth. This concept is based on providing a strong anvil as a subbase layer, in order to provide stability and strength for the upper layers of the pavement structure.

The materials used for pavement layers must have strict performance requirements. The physical and mechanical properties of aggregates such as the grading, shape, amount of fines and resistance to crushing are all indicators of the material's performance ability. It is for this reason that mechanical testing such as monotonic testing, resilient modulus testing and permanent deformation tests is needed to measure the material's damage behaviour when exposed to dynamic cyclic loading.

The mechanical properties of the material such as the shear parameters (C and ϕ) as well as the resilient parameters (M_r and υ) are important in the mechanistic design of flexible pavements. The shear parameters are used to calculate the resistance to shear deformation of the material whereas the resilient parameters provide the response under repeated loading (Barisanga, 2014). Theyse and Muthen (2000) proposed a schematic diagram as seen Figure 6-1 to explain the South African Mechanistic Empirical design method.

To model the pavement structure, multi-layer linear-elastic software is used. The Mr-θ model is used in multi-layer linear-elastic pavement analysis. However, the shortcoming of this model is that it yields a continuous increased resilient modulus as the bulk stress ($\sigma_1 + \sigma_2 + \sigma_3$) increases this means

that when stress-softening at higher DSR's occur the model would overestimate the stiffness of the material. This shortcoming means that this model is not usable in non-linear pavement modelling. For the pavement analysis mePADS is used, which is a multi-layer linear-elastic software and the Mr-θ model was used.

As discussed earlier, the pavement analysis will provide a comparison between standard pavements and pavements with a RCA layer. This will be achieved by executing a stress-strain analysis for each pavement layer within the pavement structure. Then for standard materials used in South Africa the transfer functions developed by Theyse (1996) will be used. For layers including RCA the developed transfer function in this study will be used.

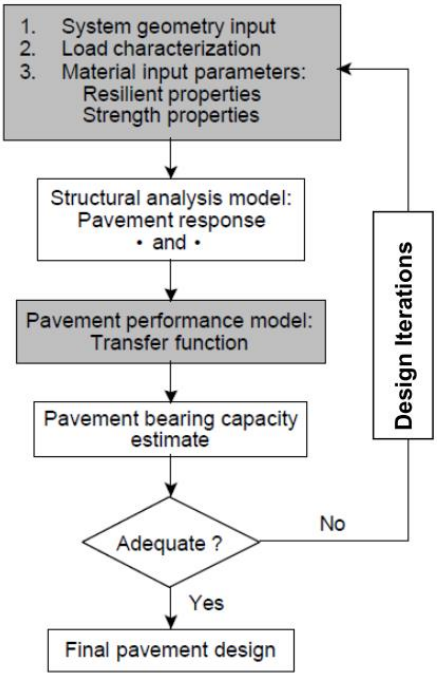

Figure 6-1: Flow diagram showing the Mechanistic Empirical Design Method (Theyse & Muthen, 2000)

6.2 Pavement Structure

As previously stated, the pavement structure in South Africa varies from what is encountered in developed nations in Europe and in America. The most commonly used pavement structure for high volume roads consists of an inverted pavement, however there are multiple variations on this structure. For this analysis a Category B road (90% reliability) will be designed for. A seal of approximately 10 mm will serve as surfacing, however this will not be analysed as its contribution to the load spreading ability of the pavement structure is negligible.

Three reference pavements will be analysed which comprise of traditional unbound aggregates and cemented materials. This is to create a basis for comparison for the pavements that include RCA

material. Reference Pavement A consists of G1 unbound granular base course, followed by a G5 unbound granular subbase layer that is placed on a G7 subgrade. According to SAPEM (2014b) modular ratio higher than 3 is an indication of an unbalanced pavement. If considering these original typical moduli, the base and subbase ratio is certainly unbalanced. Between the subbase and subgrade a modular ratio of 2.8 is calculated which is still quite high. However it is noted that the modular ratio concept is applied to bring the stiffness down. So that unrealistic stiffness values are not chosen as representative. Although not part of the standard procedure the modular ratio allows for realistic decisions to be made in terms of these stiffnesses due to factors such as different support conditions. Typical representative values are G7 has 120 MPa stiffness, a G5 has a 360 MPa stiffness and a G1 has a 700 MPa stiffness.

A G5 subbase is used and will provide a good indication as to how the RCA performs with a weaker support layer. The thickness of the layer as well as the elastic moduli of the layers are given in Figure 6-2. The red dots indicate the analysis points for each layer. Depending on the material, the layer is comprised of, the analysis points will vary. For example a granular layer the stresses are obtained in the middle of the layer, for a subgrade the vertical strain at the top of the layer is needed Theyse (1996). It is assumed that for RCA the analysis points are the same as for a granular layer. The division of the granular layer into three sublayers is also not prescribed by the standard SAMPDM. SAMPDM prescribes one layer analysis for the granular base layer and stresses are taken in the middle of that layer. However, granular materials are stress dependent and it is more realistic to evaluate the stresses at different points in the layer as the maximum stress might not occur in the middle of the layer.

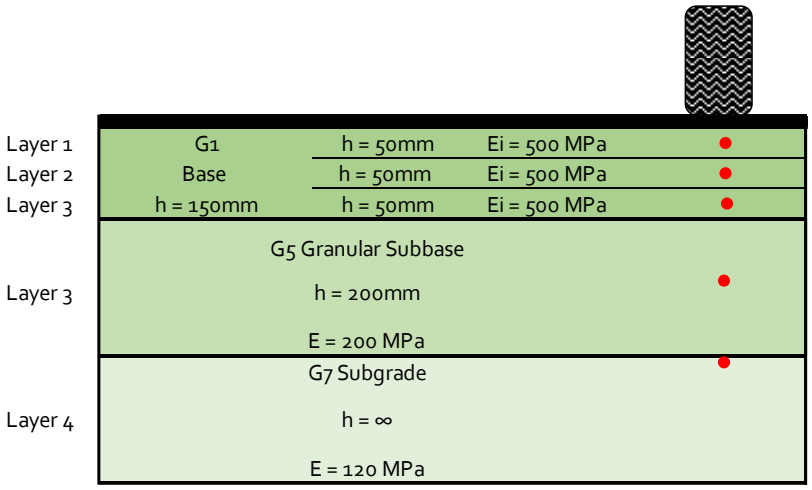

Figure 6-2: Reference Pavement A design layout with seed moduli

Reference Pavement B consists of a G1 unbound granular base course, which is placed on a C3 lightly cemented bound subbase layer followed by a G7 subgrade as shown in Figure 6-3. The layers are

colour coded to easily identify the parent material of each layer. An unbound granular material is indicated in green, with the intensity of colour increasing as the quality of the material increases. The lightly cemented bound material is coloured in grey, with RCA being an orange colour.

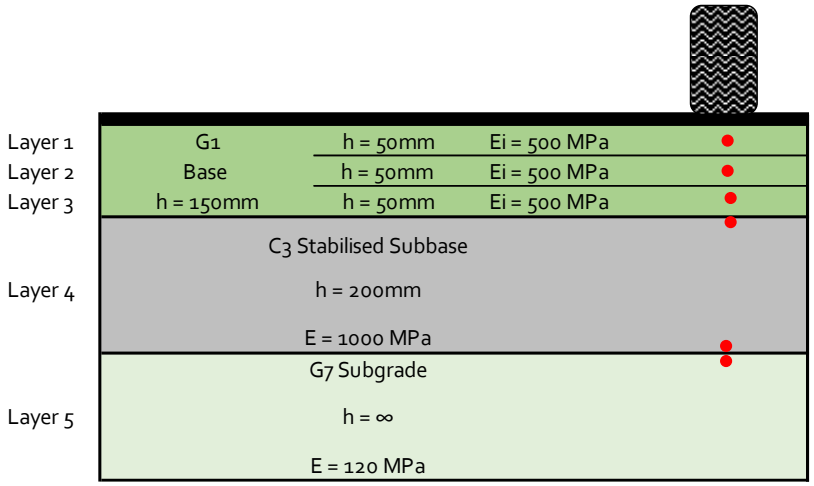

Figure 6-3: Reference Pavement B design layout with seed moduli

Reference Pavement C consists of a G4 unbound granular base, which is placed on an unbound G5 granular subbase, followed by a G7 subgrade, as seen in Figure 6-4. This structure is chosen so that the RCA material can be compared to a typical G4 material Although the material shows potential to perform equal to that of a higher quality material in practice it will most probably not be accepted (especially at first) to be "equivalent'" to a G1 to G3 material. .This decision was made taking cognisance of discussions in the current "Working group for the establishment of draft guidelines on RCA and RCM". In these discussions the group came to conclusion that the use of this material in higher end applications will not be practical.

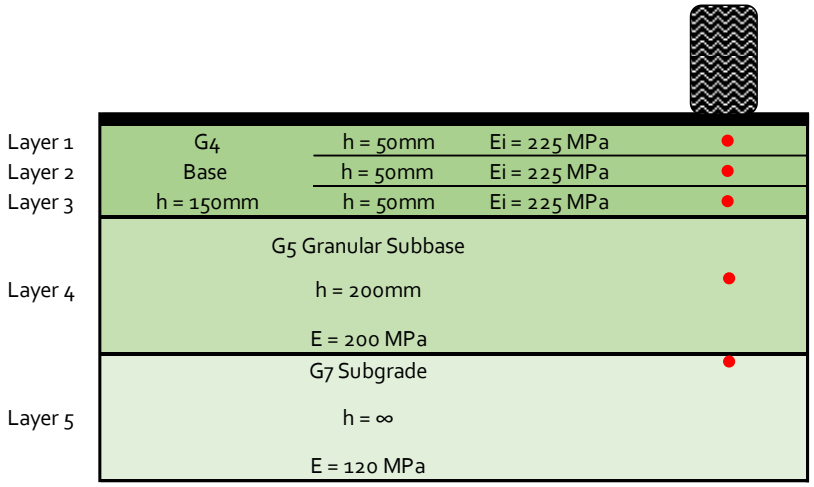

Figure 6-4: Reference Pavement C design layout with seed moduli

Three pavement structures that contain RCA were also analysed and compared to the reference pavement structures. Pavement 1 consists of a RCA base layer that is subdivided into three layers of equal thicknesses in order to simulate the stress dependent stiffness that changes with depth. A C3 lightly cemented bound layer provides a strong support so that the performance of the base layer can be analysed with minimal influence factors. Followed by a G7 subgrade that is used throughout all the pavement structures. Pavement 1 is shown in Figure 6-5.

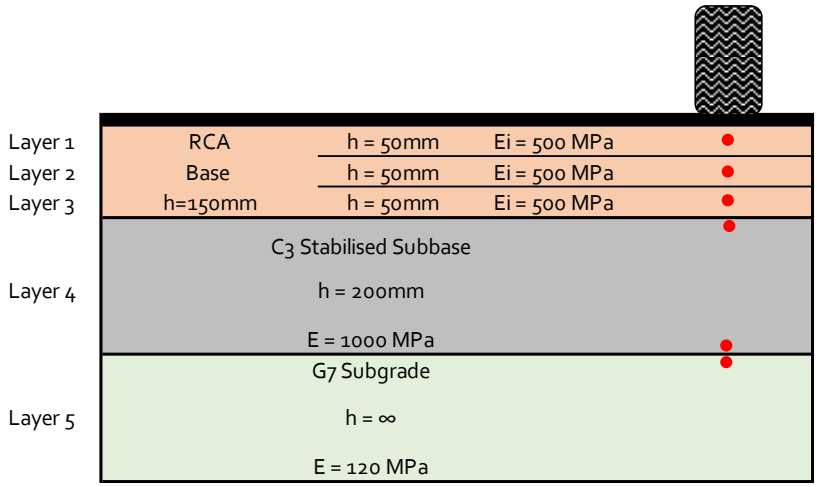

Figure 6-5: Pavement 1 design layout with seed moduli

Pavement 2 has a similar structure to Pavement 1 but with a different subbase material. As shown in Figure 6-6. Pavement 2 consists of the same RCA base layer that is sub-divided into three layers followed by a G5 unbound granular subbase layer, this is a weaker subbase layer that will not provide the same support for the RCA layer. The same G7 subgrade is used as in all pavement structures.

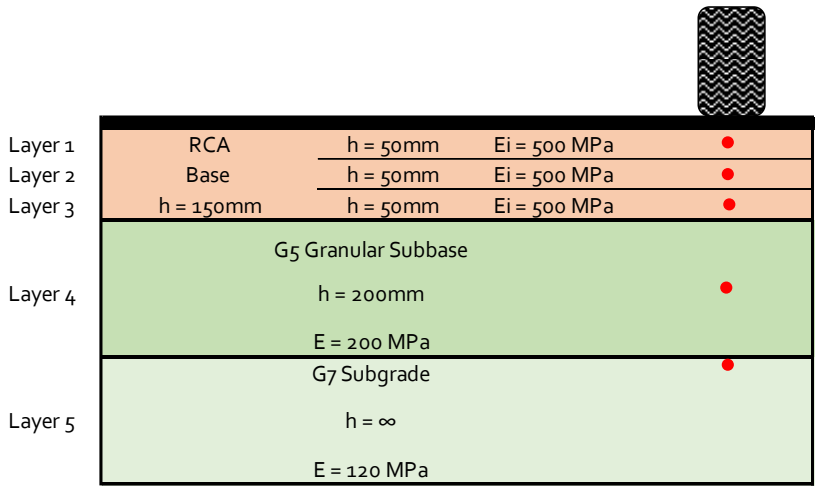

Figure 6-6: Pavement 2 design layout with seed moduli

Pavement 3 consists of a G1 unbound granular material that is placed on a RCA subbase layer, the RCA subbase is sub-divided into three layers to simulate the stress dependent stiffness that changes with depth. The pavement structure is built on a G7 subgrade as seen in Figure 6-7.

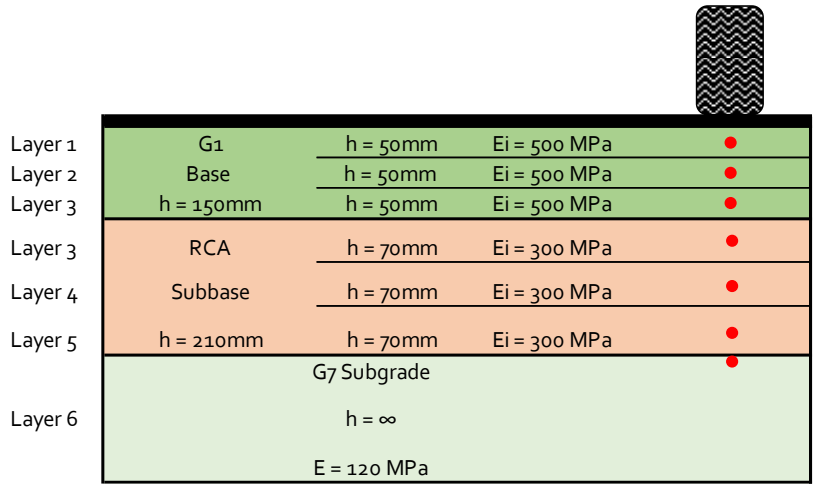

Figure 6-7: Pavement 3 design layout with seed moduli

All stiffness values for standard materials were obtained from SAPEM (SANRAL, 2014b). For the stiffnesses that are denoted by an E_i, this is the initial assumed stiffness. These stiffness will change using an iterative process together with the Mr-θ model in order to calculate new stiffnesses that include the stress dependence of the stiffness. Once the iterative process has been completed a modular ratio approach is used to limit the maximum values of the stiffness of each layer for the granular and RCA materials. This process if followed to ensure that the pavement is representative of the achievable stiffnesses. The linear-elastic software and the Mr-θ model does not take the stiffness of the supporting layer into consideration and therefore the model may yield stiffnesses that are improbable given the support conditions

6.3 Design Wheel Load

The standard axle load used for pavement design in South Africa is an 80 kN axle with super single tyres at the wheel loads(SANRAL, 2014b). This is known as the standard load, and any other applied loads are converted into equivalent standard axles or more commonly known as E80's. Many large vehicles have dual wheels on each side of the axle, however this complicates the pavement analysis as stresses and strains must then be obtained beneath and between the wheels. In order to simplify the problem, one wheel load on each side of the axle is considered, each wheel carries a load of 40 kN to meet the E80 standard axle load as seen in Figure 6-8 .

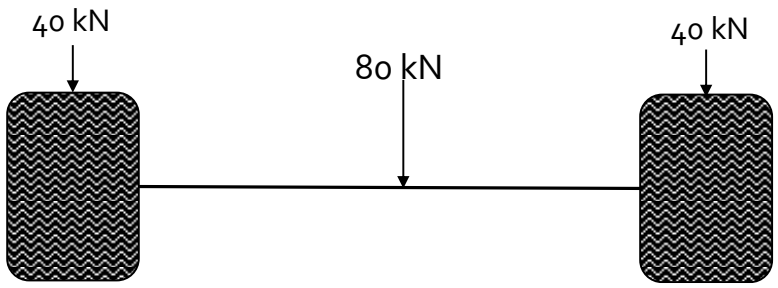

Figure 6-8: Super single E80 axle configuration

Theyse and Muthen (2000) suggested that a contact pressure of 520 kPa should be taken for a standard design load of 40 kN dual tyre. However, due to the advancements in technology of both large trucks as well as the tyres they use it has been found that the tyres can perform at higher pressures and the trucks can carry an increased load. Morton *et al*. (2004) conducted a study that found that axle loading can be as high as 9.45 tonnes per axle and that the tyre pressure has increased to between 700 kPa to 825kPa, this was found on a national highway namely the N3.

In this analysis it is assumed that the axles are not overloaded and that a standard super single E80 axle is used. To take the advancements in technology of truck tyres into account, the tyre pressure used in this analysis will be 720 kPa. This decision was based on applying a value representative of the suggested range by Morton *et al*. (2004).This results in a tyre radius of 133 mm. This deviates slightly from the SAMPDM which suggests a value of 750 kPa.

6.4 Pavement Modelling

The linear-elastic modelling software mePADS written by the CSIR in South Africa was be used to calculate the stresses and strains at each analysis point which will be used to iterate to obtain the resilient moduli of granular layers. The iterative process will focus on the RCA and granular layers in order to calculate the stress dependent layer stiffnesses. For the RCA as well as the G1 material in the base an initial stiffness value of 500 MPa is assumed, for the RCA subbase layer an initial stiffness of 300 MPa is assumed. The Mr-θ model is used to calculate the Resilient Modulus of each layer in the iterative process. The k_1 and k_2 values as defined for a G1 material by Maree *et al.* (1982) is used. Due to the fact that no resilient modulus tests were performed in this research typical k_1 and k_2 values as determined by Rudman and Jenkins (2015) at Stellenbosch University will be used as a representative for RCA. The parameters for RCA and G1 are presented in Table 6-1.

Table 6-1: Mr-θ model parameters for RCA and G1 material

Material	Mr-θ model parameters	
	k_1	k_2
RCA	18.81	0.515
G1	9.7	0.66

These values in conjunction with the shear parameters determined for RCA material at 0 month, as discussed in Chapter 4.2.1.1, and will be used in the pavement mechanistic design. A comparison between the stresses and strains for each pavement will be made to see influence of the different material types. In the next section the pavement life of each structure will also be calculated using these stresses and strains obtained in this section.

The iterative process to predict the Resilient Modulus was done for 6 iterations for each design until the Resilient Moduli converged. If needed more iterations were performed. The initial stiffnesses are imported to mePADS and the pavement is evaluated, the applicable stresses are taken from the output into a programmed worksheet to calculate the stress dependent resilient modulus for each sublayer. The new Resilient Moduli are exported to mePADS and a second pavement analysis is completed. This is the iterative loop, and is performed until the Mr values converged.

A detailed sheet for each pavement's iterative process can be found in Annexure E. For each pavement structure a summary table is compiled that includes the principal stresses and the Resilient Modulus for each layer. It is important to remember the concept of modular ratio's as some of the layer stiffnesses of the granular and RCA materials will be reduced in order to comply with modular ratio principles. With the granular material, a clear maximum stiffness is also set by SAPEM (2014b) and the maximum stiffness of granular materials will thus be limited. A maximum value for the RCA is unknown but for comparative purposes the same maximum stiffness applied to a G1 material will be used.

It is important to note that the sign convention as well as the naming convention followed in mePADS is in direct contravention of the normal conventions as stipulated by SAPEM. Normal convention states that for a compressive stress a "+" sign is used and for a tensile stress a "-" sign is used. According to mePADS a "+" sign denotes a tensile stress and a "-" sign denotes a compressive stress. When looking at principal stresses, σ_1 is the major principal stress in the vertical direction and σ_2 and σ_3 are the major principal stresses in the horizontal direction. According to MePADS σ_3 is the major principal stress in the vertical direction. In the report of the results in tables the SAPEM sign convention and definition of principal stresses is used.

6.4.1 Reference Pavement A

Reference Pavement A consists of a G1 granular base and G5 granular subbase. The base layer is split into three equal layers of 50 mm each. The iterative process as explained earlier will be used to find the Resilient Modulus of each sublayer.

From Table 6-2 the final resilient moduli for the G1 granular base layer for Scenario 1 with 3 sublayers is presented. The first Mr column shows the calculated Resilient Modulus using the stresses and the

Mr-θ model. Here it can be seen that the stiffness obtained using the Mr-θ model yields unrealistic results and stiffness values limited using the modular ratio concept. The second column shows the limit of the Resilient Modulus using the modular ratio. The third layer is built upon a G5 layer which has a modular ratio of 1.8, therefore the maximum stiffness it can reach is the 200 MPa of the G5 multiplied by the 1.8 which is 360. The second layer has a modular ratio of 2, thus the stiffness 360 MPa multiplied by 2 give 720 MPa but the maximum stiffness a G1 can achieve is 700 MPa, thus the stiffness is limited at 700 MPa.

Table 6-2: Resilient Modulus results for the granular base layer of Reference Pavement A with 3 sublayers

Sublayer	Software Output (kPa)[1]				k_1	k_2	mePADS	Mod Ratio
	σ_1	σ_2	σ_3	θ			Mr (MPa)	Mr (MPa)
1	639.13	722.54	722.54	2138.2			1530	700
2	515.63	54.27	54.27	624.17	9.7	0.66	679	700
3	324.18	-157.87	-157.87	481.98			572	360

Notes:

1: SAPEM Sign Convention

It should be noted that the third sublayer reports negative horizontal values. This implies that the material is in tension. This is not possible and realistic and a consequence of bad support conditions, and the shortcomings of the linear-elastic analysis. However, an adjustment is made by only taking σ_1 and σ_2 into account (Flexible Pavement Design, 2017). It does not occur in all of the pavements analysed but one should be aware of this shortcoming when presented.

6.4.2 Reference Pavement B

Reference Pavement B consists of a G1 granular base layer and a C3 lightly cemented subbase layer. Table 6-3 shows the iterative process for the Reference Pavement 2.

Table 6-3: Resilient Modulus results for the granular base layer of Reference Pavement B

Sublayer	Software output (kPa)[1]				k_1	k_2	mePADS	Mod Ratio
	σ_1	σ_2	σ_3	θ			Mr (MPa)	Mr (MPa)
1	707.86	579.90	579.90	1867.67			1399	700
2	597.72	123.49	123.49	844.70	9.7	0.66	829	700
3	460.71	127.85	127.85	332.85			448	448

Notes:

1: SAPEM Sign Convention

The granular layer is subdivided into three sublayers, and it is placed on a lightly cemented layer. The lightly cemented provides a very strong anvil for compaction and the modular ratio for a cemented material is very high. Therefore in this pavement structure modular ratios will not play a significant role, however the maximum limit of the G1 material is still applicable.

6.4.3 Reference Pavement C

Reference Pavement C consists of a G4 granular base layer placed on a G5 granular subbase layer. The base layer is subdivided into three sublayers, so that the effect of stress dependency on the resilient moduli are included in the layers. Although a G4 is seen as a weak layer to be used as a base layer, this is common in roads with a lower reliability index and also a lower category, such as municipal roads. The G4 material is used so that a comparison between the behaviour of an RCA and G4 base can be done. In industry it is realistic that RCA material will be compared to natural gravels such a G4 material. The iterative process followed to obtain the resilient moduli of the sublayers of the base is shown in Table 6-4.

Table 6-4: Resilient Modulus results for the granular base layer of Reference Pavement C

Sublayer	Software output (kPa)[1]				k_1	k_2	mePADS	Mod Ratio
	σ_1	σ_2	σ_3	θ			Mr (MPa)	Mr (MPa)
1	693.14	722.31	722.31	1529.50			1530	375
2	515.70	54.50	54.50	624.70	9.7	0.66	679	375
3	324.18	-157.84	-157.84	482.03			482	360

Notes:

1: SAPEM Sign Convention

Maree (1982) suggested that the k_1 and k_2 values for high quality crushed stone bases should be 9.7 and 0.66 respectively. A G4 material does not classify as a crushed stone, but rather as a natural gravel, the challenge is that there are no defined k_1 and k_2 for this material. It is therefore decided to use the values for a crushed stone, it is important to understand that this assumption will lead to the over estimation of the resilient moduli of the sublayers of G4 material. A way to counter act this, is by using the modular ratio approach. The bottom sublayer of G4 material is placed on a G5 subbase, which has a modular ratio of 1.8, and the maximum stiffness of this layer is then limited to 360 MPa. For the top and middle sublayer, the maximum stiffness of a G4 material is 375, and both layers will be limited to this value. It should be noted that these values are significantly lower than that obtained by the iterative process, which is explained by using the coefficients of the crushed stone.

6.4.4 Pavement 1

Pavement 1 consist of a RCA base layer, which is constructed on a lightly cemented C3 subbase layer. The initial stiffness of the three sublayers are assumed to be 500 MPa. The stresses and strain are calculated for each layer and the resilient moduli for each of three sublayers of the base are calculated through the iterative process as described earlier. The final iterations resulted in the stresses and resilient moduli as seen in Table 6-5.

Table 6-5: Resilient Modulus results for the RCA base layer of Pavement 1

Sublayer	Software output (kPa)[1]				k_1	k_2	mePADS	Mod Ratio
	σ_1	σ_2	σ_3	θ			Mr (MPa)	Mr (MPa)
1	715.59	514.06	514.06	1743.7			879	700
2	632.51	202.39	202.39	1037.29	18.81	0.515	672	672
3	488.98	134.34	134.34	757.657			572	572

Notes:

1: SAPEM Sign Convention

From Table 6-5 it can be seen that the modular ratio principle does not play a role in Pavement structure 1. This can be attributed to the fact that a C3 lightly cemented material has a modular ratio of 3 and a very high stiffness of 1000 MPa. The base sublayers never reach a high enough stiffness to be affected by the modular ratio. This is one of the advantages of building a granular base on a lightly cemented subbase. The high stiffness achieved by the RCA can be attributed to the self-cementation of the material, but also in this case by the good support conditions. . However in order to be conservative one cannot assume that the RCA material will have a continuous increase in strength and therefore a limiting value must be implemented. It is decided to use the same limiting value as for G1 materials which is 700 MPa.

The graphs of the various stresses and strains at different depths within the pavement structure can be drawn. From these graphs the development of the stresses and strains over the different layers can be observed. It is beneficial to compare these stresses and strains with Reference Pavement B. Both Pavement 1 and Reference Pavement B consists of a C3 lightly cemented subbase. This will give a good indication as to difference in stress development between the granular material and the RCA material.

Figure 6-9 shows the vertical and horizontal stresses developed at different depths within the pavement for both Pavement 1 and Reference Pavement B. From this it can be deduced that the RCA material behaves very similar to the G1 material in terms of stress development. There are only slight differences in the third sublayer of the base layer, further the RCA material behaves identically to a G1 material.

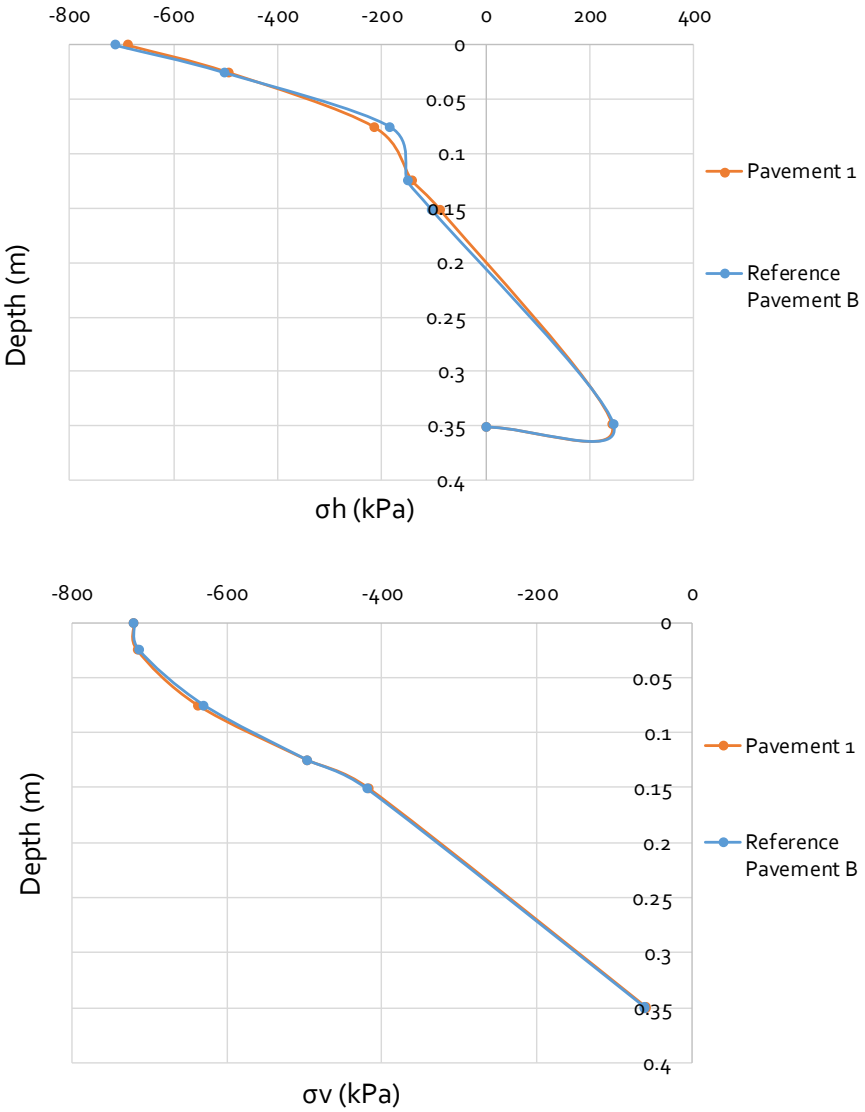

Figure 6-9: Comparison of horizontal (σ_h) and vertical (σ_v) stress at different depths for Pavement 1 and Reference Pavement B

Figure 6-10 shows the comparison of the vertical and horizontal strain as developed at different depths within the pavement for both Pavement 1 and Reference Pavement B. With regards to the strain development it can be seen that in the base between depths 0 to 150 mm, there are some minor variations in the development of horizontal strain. In the bottom sublayer of the base it can be seen that the vertical strain development is slightly different. Below the base in the cemented layer the strain development is again nearly identical.

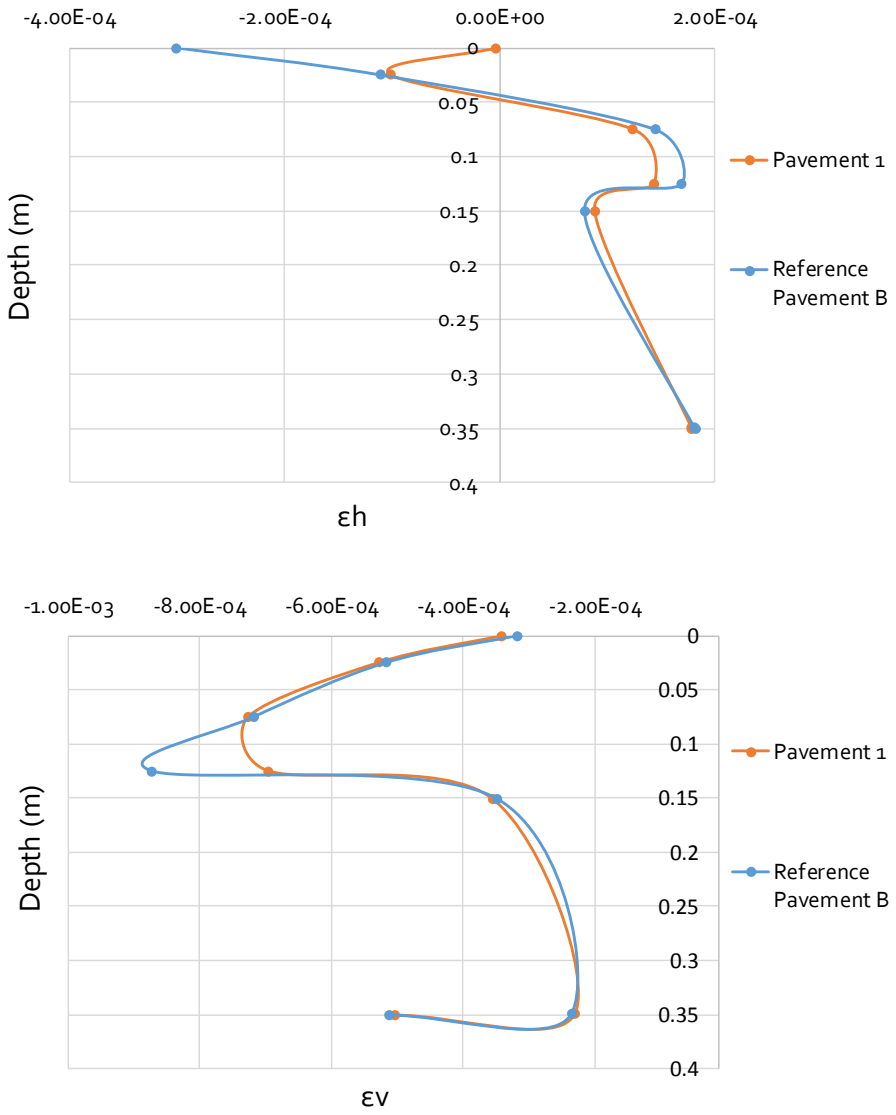

Figure 6-10: Comparison of horizontal (ε_h) and vertical (ε_v) strain at different depths for Pavement 1 and Reference Pavement B

6.4.5 Pavement 2

Pavement 2 consists of a RCA base layer which is placed on a G5 granular material subbase layer. This pavement will not have the same stiff subbase as Pavement 1. The initial stiffness of each of the three sublayers are assumed to be 500 MPa. The iterative process is completed to obtain the resilient moduli for each layer. The stresses for the final iteration and the resilient moduli for each layer is presented in Table 6-6.

From Table 6-6 it can be seen that the stiffness of the third base layer of the RCA has to be reduced in order to keep with modular ratio principles. The third base layer is placed on a G5 material with a maximum stiffness of 200 MPa and a modular ratio of 1.8, thus the maximum stiffness is 360 MPa. The second and first layer has a modular ratio of 2 which they both comply to and therefor remain constant.

Table 6-6: Resilient Modulus results for the RCA base layer of Pavement 2

Sublayer	Software output (kPa)[1]				k_1	k_2	mePADS	Mod Ratio
	σ_1	σ_2	σ_3	θ			Mr (MPa)	Mr (MPa)
1	699.34	654.21	654.21	2007.75			945	700
2	543.31	87.01	87.01	717.50	18.81	0.515	556	556
3	360.68	-94.81	-94.81	455.49			440	360

Notes:

1: SAPEM Sign Convention

Graphs comparing the stresses and strain of Pavement 2 and Reference Pavement A are compiled. It is beneficial to compare these two pavement structures as both Pavement 2 and Reference Pavement A have G5 granular subbase layers. This comparison will give a clear indication of the difference in behaviour of the RCA material when compared to the behaviour of a G1 base material. The stress distribution of the RCA material gives a good indication of the load spreading ability of the material.

Figure 6-11 shows the development of vertical and horizontal stress at different depths within Pavement 2, Reference Pavement A and Reference Pavement C. Both the vertical and horizontal stress development for the Pavement 2 and Reference Pavement A are identical. Reference Pavement C is used to compare the stresses that develop in a G4 base and in the RCA base. The observed behaviour in terms of the vertical stress shows similarities to that of the G1 material, in the subbase and subgrade the behaviour is identical which is to be expected as it is the same materials. For the horizontal stresses on can see that the G4 material has more horizontal induced stresses than either of the other two materials. In terms of vertical stress development in the first sublayer of the base, both Reference Pavement A and Pavement 1 has higher developed stresses, this can be attributed to the fact that stiffer material attracts higher stresses. The G4 base layer has a significantly lower stiffness and therefore lower stresses induced in the upper layer.

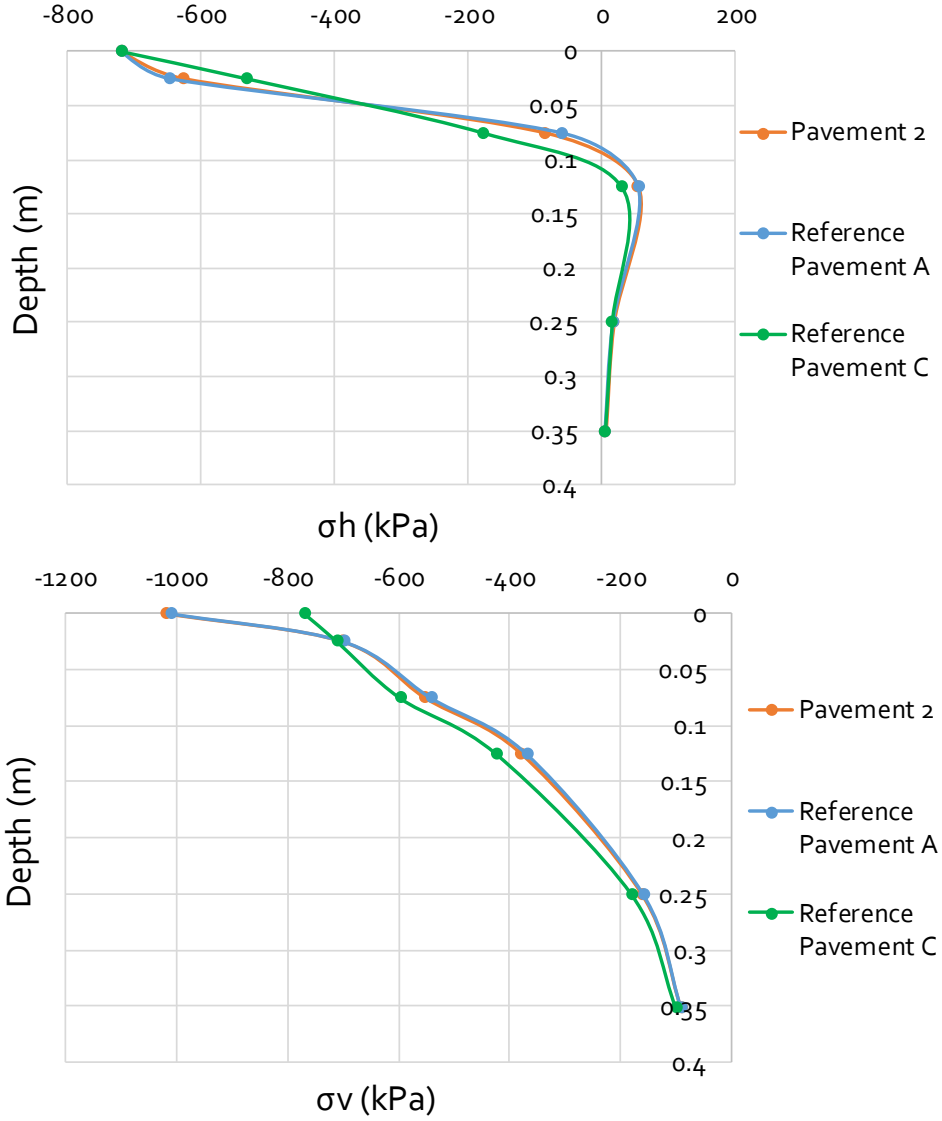

Figure 6-11: Comparison of horizontal (σ_h) and vertical (σ_v) stress at different depths for Pavement 2, Reference Pavement A and Reference Pavement C

Figure 6-12 shows the development of vertical and horizontal strain at different depths for Pavement 2, Reference Pavement A and Reference Pavement C. The horizontal strain development for Reference Pavement A and Pavement 2 is near identical except for the initial strain induced at the top of the pavement structure. Reference Pavement 2 has less initial induced horizontal strain. For the vertical strain development Reference Pavement A and Pavement 2 has very similar behaviour, however the magnitude of the strains are slightly larger for Pavement 2.

The horizontal strain development for the RCA and the G4 material is near identical. The significant difference can be seen when analysing the vertical strain in Reference Pavement C. The upper and middle sublayers of the base has significantly higher induced vertical strains, in the middle of the bottom sublayer of the base the strains are equal, and the again the strains in Reference Pavement C is higher in the subbase and subgrade layer. The difference in the bottom layer strains, may be

attributed to the fact that the load is spread poorly through the material due to the low stiffnesses. Therefore the subbase and subgrade are carrying a higher loads than in the other two pavement structures.

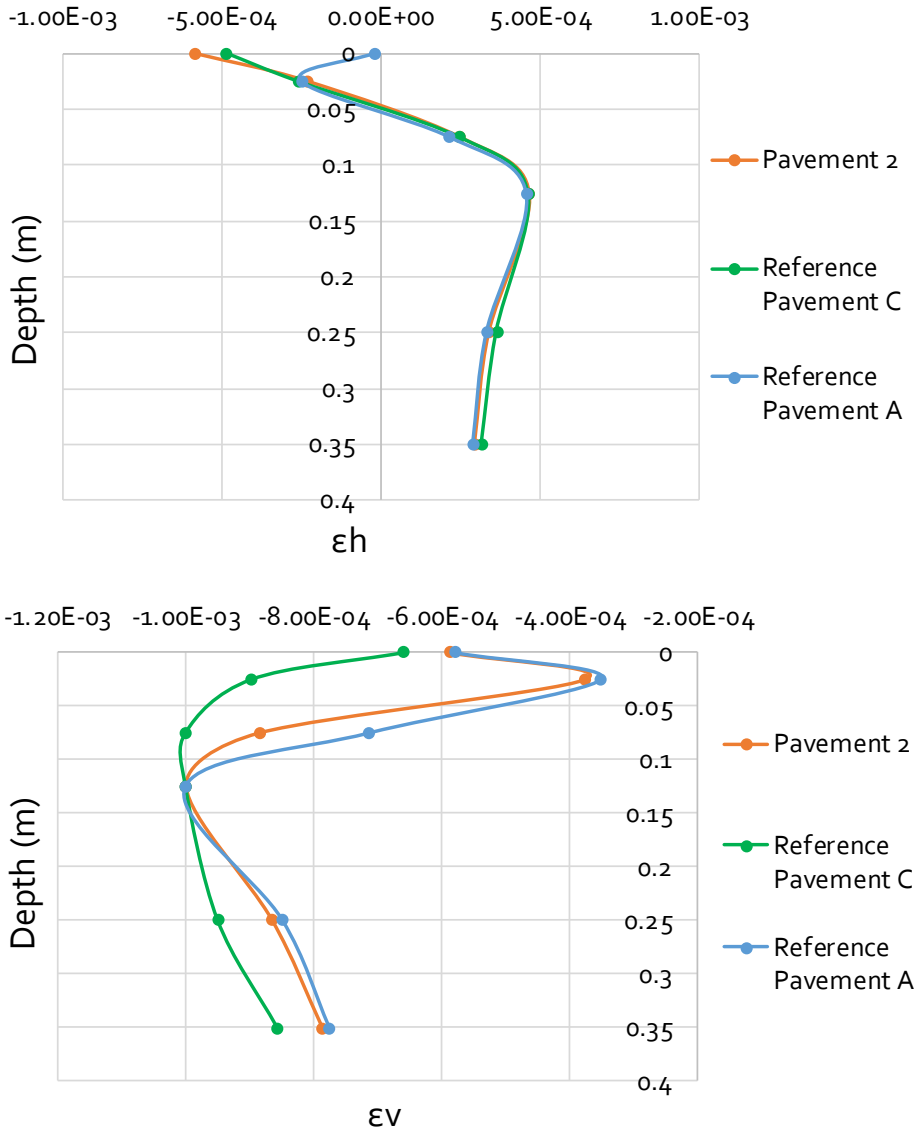

Figure 6-12: Comparison of horizontal (ε_h) and vertical (ε_v) strain at different depths for Pavement 2, Reference Pavement A and Reference Pavement C

6.4.6 Pavement 3

Pavement 3 consists of a G1 material base layer that is placed on top of a RCA material subbase layer. The RCA subbase is divided into three sublayers in order to simulate the stress dependency of the stiffness with depth. The initial stiffness of all three sublayers are assumed to be 300 MPa, and the iterative process as previously described will be used to find the stiffnesses of the three sublayers of RCA material. The base is subdivided into two sublayers and the same iterative process is followed to obtain the stiffness of the granular material.

Table 6-7 shows the final iteration of the resilient moduli for the G1 base layer of Pavement 3. The base layer was subdivided into three layers, the third layer is built on top of the RCA subbase which provides a relatively strong foundation, a modular ratio of 2 is used for RCA and therefor the resilient modulus stays the same. For the first and second layer of the G1 material a modular ratio of two is applied but a maximum value of 700 MPa is achievable for a G1 material, and therefore it is limited to this value.

Table 6-7: Resilient Modulus results for the G1 granular base layer of Pavement 3

Sublayer	Software output (kPa)[1]				k_1	k_2	mePADS	Mod Ratio
	σ_1	σ_2	σ_3	θ			Mr (MPa)	Mr (MPa)
1	695.126	677.35	677.35	2049.83			1488	700
2	533.99	43.19	43.19	620.37	9.7	0.66	676	676
3	368.32	-14.29	-14.29	382.61			402	402

Notes:

1: SAPEM Sign Convention

Table 6-8 shows the last iteration for the three sublayered RCA subbase layer of Pavement 3. The initial assumed stiffness was 300 MPa and it can be seen that the final values are very close to this estimation. The modular ratio process played no role in the determination of the stiffnesses for the RCA subbase in this case. It can be seen that the RCA material performs worse in the subbase than what was observed in the base layer, this is due to the fact that there is no confinement in the subbase material according to the mePADS calculations. The σ_2 and σ_3 for all three sublayers are positive which indicates a tension force, resulting in no confinement, although RCA behave counter intuitively with confinement pressure, some confinement pressure is still needed in order to provide cohesion and strength.

Table 6-8: Resilient Modulus results for the RCA subbase layer of Pavement 3

Sublayer	Software output (kPa)[1]				k_1	k_2	mePADS	Mod Ratio
	σ_1	σ_2	σ_3	θ			Mr (MPa)	Mr (MPa)
1	230.84	-35.26	-35.26	266.11			334	334
2	138.12	-35.39	-35.39	173.50	18.81	0.515	268	268
3	88.41	-37.10	-37.10	112.51			227	227

Notes:

1: SAPEM Sign Convention

To compare the stress and strain development of the different material graphs are compiled to compare the two parameters at different depths within the pavement. Pavement 3 and Reference Pavement A are compared as both of these structures consists of a granular G1 base, the RCA material and the transfer function thereof is based on the assumption that the material at 0 months behaves similar to a granular material. Therefore Pavement 3 is compared to a granular base and granular subbase pavement structure.

Figure 6-13 shows the development of the vertical and horizontal stress within the two pavement structures. It can be seen that the overall form of the stress distribution is similar for both materials with only a small difference in magnitude.

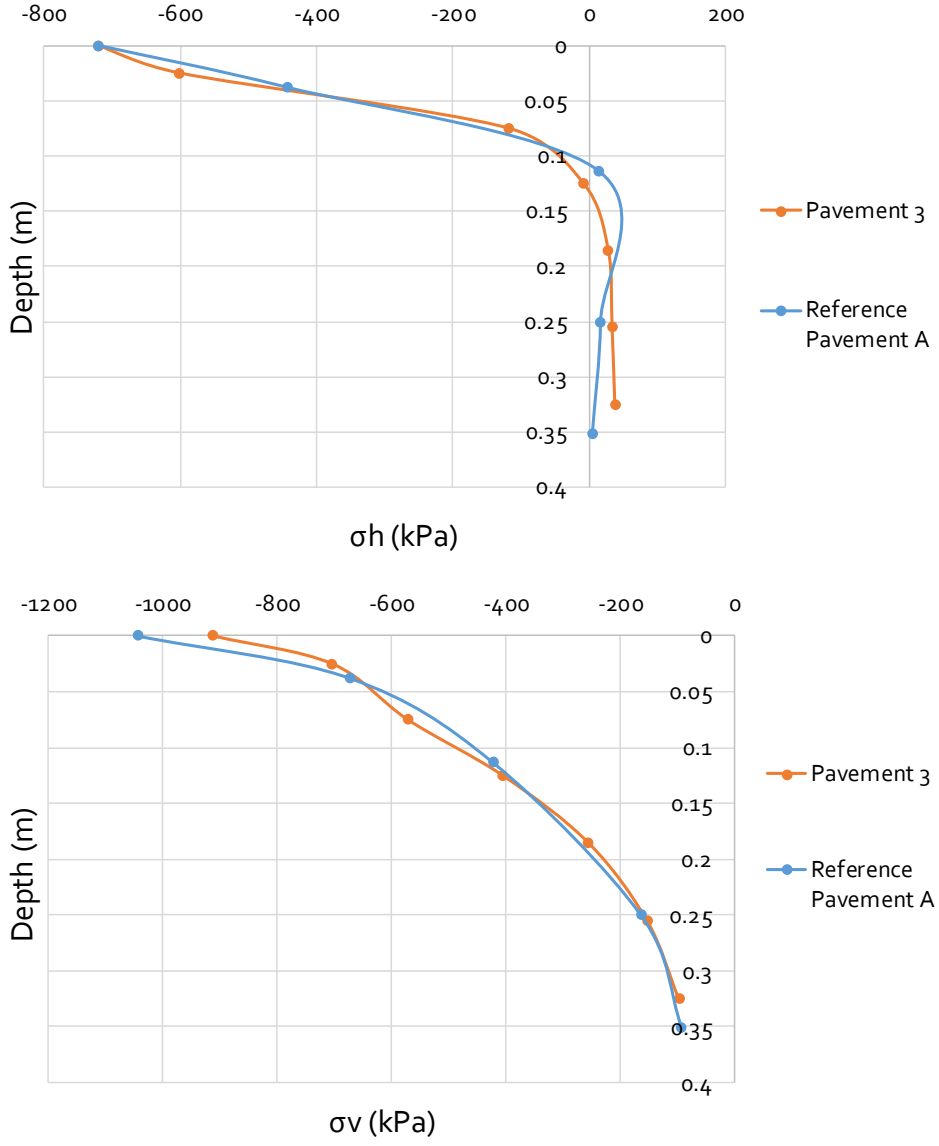

Figure 6-13: Comparison of horizontal (σ_h) and vertical (σ_v) stress at different depths for Pavement 3 and Reference Pavement A

Figure 6-14 shows the development of the vertical and horizontal strain within the two pavement structures. Here it can be seen that the two strain distributions differ vastly for the two pavement structures. This may attributed to the fact that for Reference Pavement A the subbase was not subdivided and iterated, the multiple layer approach results in more accurate strain measurements and this allows for the analysis at different points within the same layer. It would be beneficial to investigate Reference Pavement A with the subbase also subdivided, however that falls outside the scope of the research as the stress dependency of granular materials is not the focus of the research.

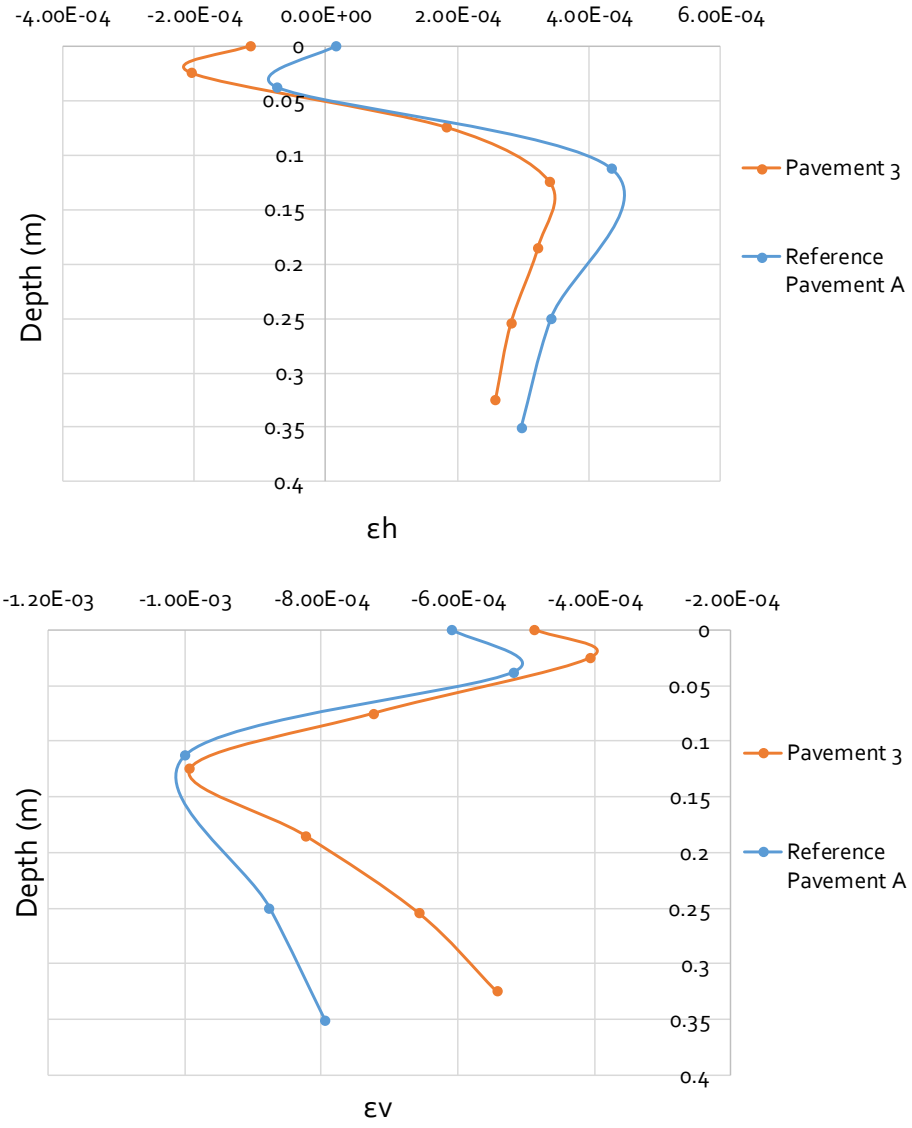

Figure 6-14: Comparison of horizontal (ε_h) and vertical (ε_v) strain at different depths for Pavement 3 and Reference Pavement A

6.5 Pavement Life

The structural analysis of the various pavements are performed to determine the stresses and strains for each layer within the pavement structure. These stresses and strains have been used in the previous section to compare the material behaviour of various pavement materials. To calculate the pavement life of each layer within the pavement structure the transfer functions as per SAPEM (2014b) are used in conjunction with the transfer function for RCA material as determined in this research. The critical points at which the stresses and strains must be calculated are indicated in red dots on each of the pavement structures in Figure 6-2 to Figure 6-7, and are as follows:

- The principal stresses that cause permanent deformation must be determined in the middle of the unbound granular layers;
- The principal stresses that results in permanent deformation must be determined in the middle of the RCA layer;
- The vertical stresses causing crushing must be determined at the top of the lightly cemented bound layer;
- The horizontal strain causing effective fatigue must be determined at the bottom of the lightly cemented bound layer;
- The vertical strain causing deformation must be determined at the top of the subgrade.

According to Theyse *et al*. (1996) a transfer function shows the relationship between the value of the critical parameter and the number of load repetitions that can be accommodated, given the critical parameter before a specific material will fail in a specific mode of failure. The transfer functions as given in SAPEM (2014b) Chapter 10 will be used and are as follows:

Granular Unbound Material

$$N = 10^{(\alpha F + \beta)} \qquad 6\text{-}1$$

Where:

N: Number of equivalent standard axles

α, β: Constants dependent on the Road category and Reliability

F: Factor that is based on the stress ratio, defined in Equation 6-2

For a Category B road with a 90% reliability the constants alpha and beta can be used as follows alpha is 2.605122 and beta is 3.707667.

6-2

$$F = \frac{\sigma_3 \cdot \varphi_{term} + C_{term}}{(\sigma_1 - \sigma_3)}$$

Where:

σ_1, σ_3: Major and Minor principle stresses acting in the middle of the granular layer[1]

φ_{term}: Value based on the friction angle as given in SAPEM (2014b) and Table 6-9

C_{term}: Value based on the cohesion as given in SAPEM (2014b) and Table 6-9

Notes: If the minor principal stress is negative (tensile stress), then σ_3 must be equal to zero and σ_1 is increased by a value of σ_3. This means that $(\sigma_1 - \sigma_3)$ will stay the same although σ_3 will be taken as zero SAPEM (2014b).

Table 6-9: Shear input parameters for the granular material transfer function

Material	Moisture Conditions					
	Dry		Moderate		Wet	
	φ_{term}	C_{term}	φ_{term}	C_{term}	φ_{term}	C_{term}
G1	8.61	392	7.03	282	5.44	171
G4	5.5	223	4.4	160	3.47	109
G5	3.60	143	3.30	115	3.17	83
EG4	4.02	140	3.50	120	3.12	100

RCA Material

$$logN = 5.85 + 0.01933\ (P_{vib}) - 0.44118(MC) - 21.753(DSR)^{3.358} + 0.8929(PS) \qquad 6\text{-}3$$

Where:

P_{vib}: Vibratory hammer density (%)

MC: Moisture content (%)

DSR: Deviator Stress Ratio

PS: Plastic Strain

Lightly Cemented Bound Material

Crushing

$$N_{ci/ca} = 10^{a\left(1-\frac{\sigma_v}{b \cdot UCS}\right)} \qquad 6\text{-}4$$

Where:

$N_{ci/ca}$: Standard axles until crack initiation takes place

a, b: constants dependent on the stage of cemented material failure

UCS: Unconfined Compressive Stress

σ_v: Vertical compressive stress

Given that all the lightly cemented materials used in this research was of a C3 quality, the UCS is given as 2250 KPa and the strain at break is 125 με.

Effective Fatigue

$$N_{eff} = SF \cdot 10^{c\left(1-\frac{\varepsilon}{d\cdot\varepsilon_b}\right)} \quad 6\text{-}5$$

Where:

N_{eff}: Effective fatigue life

ε: Horizontal tensile strain at the bottom of layer

ε_b: Strain at break

c,d: constants for effective fatigue of cemented layer

SF: Shift Factor for crack propagation as given in Equation 6-6

$$SF = 10^{(0.00285t-0.293)}\text{, with } 102 < t < 319 \text{ mm} \quad 6\text{-}6$$

Where:

t: Thickness of cemented layer

The values for the constants as used in Equations 6-4 and 6-5 are given in Table 6-10 as follows:

Table 6-10: Crushing and Fatigue constants for the cemented transfer function

Road	Crush Initiation		Advanced Crushing		Effective Fatigue	
Category	a	b	a	b	c	d
B	7.506	1.10	8.184	1.2	6.84	7.63

Subgrade

$$N_{PD} = 10^{(a-10\log\varepsilon_v)} \quad 6\text{-}7$$

Where:

N_{PD}: Standard axles to a predetermined level of permanent deformation

a: Constant dependent on the road category and reliability

ε_v: Vertical compressive strain at the top of the layer

The constant, a is influenced by the amount of terminal rutting that is permitted in the pavement structure as well as the road category. Given that the pavement structures are analysed as Category B road structures, and with a reliability of 90% this indicates the importance of the road. It is needed to limit the amount of rutting on important infrastructure, and therefore a terminal rut of 10mm is assumed. Given the following two assumptions the value for constant a is 33.47.

Moisture plays an integral role in the performance and durability of a pavement structure. With the ingress of moisture various problems such as rutting, pumping, increased permanent deformation, and potholing occurs. For the pavement analysis performed in this research the analysis where applicable will take into account three climatic condition, namely arid, moderate and wet. The climatic conditions will affect the amount of rainfall and indirectly the amount of moisture the pavement is subjected to.

6.5.1 Reference Pavement A

The pavement life for each layer in Reference Pavement A is calculated using the transfer functions as provided. Reference Pavement A consists of a granular base and granular subbase on a G7 quality subgrade. When analysing granular materials, moisture plays a big role in the performance of the material. The pavement life is calculated at dry, moderate and wet conditions for the granular layers by using the different cohesion and friction angle terms as shown in Table 6-9. The calculated pavement life for each layer is shown in Table 6-11. It is important to note here, that the critical factor has the same sign convention as what is used in SAPEM, this is to allow for easier substitution into the transfer function.

Table 6-11: Calculated pavement life for each layer of Reference Pavement A

Layer	Material	Sublayer	Critical Factor		N (arid)	N (mod)	N (wet)
Base	G1	1	σ_1 (kPa)	698.11	4.3E302	7.4E245	5.3E188
			σ_3 (kPa)	646.21			
		2	σ_1 (kPa)	540.85	4.11E8	3.21E7	2.47E6
			σ_3 (kPa)	59.71			
		3	σ_1 (kPa)	368.08	1.32E6	2.78E5	5.76E4
			σ_3 (kPa)	-55.01			
Subbase	G5		σ_1 (kPa)	157.74	6.88E5	2.36E5	8.79E4
			σ_3 (kPa)	-17.18			
Subgrade	G7		ε_v (με)	795		3.77E4	

Note:

Although the pavement life for the base layer is analysed at different points within the layer, only the point resulting in the most critical scenario is taken further as the pavement life for that layer

The base layer and the subbase layer show markedly lower pavement lives. The reason for the reduction in the pavement life, probably is as a result of poor confinement that can in part be attributed to weaker supporting layers. When considering a balanced and economical pavement design, the current weakness of the subgrade will have to be reconsidered as this is not realistic. However, as discussed the main objective is to compare between pavements. This approach allows for the worst case scenario and should be considered only with this perspective in mind.

From Table 6-11 the effect of moisture on the pavement life of granular materials can be seen. In dry conditions the base layer can withstand 1 million load cycles, and in wet conditions the lower base layer can withstand about 50 000 load cycles. The moisture conditions lead to a 95% reduction in the pavement life of the base layer. The critical layer in this pavement is the subgrade, however both the lower base and the subbase in wet conditions show low pavement lives.

In Reference Pavement A the subgrade is the critical layer within the pavement as shown in red. A solution to this problem would be to build up the subgrade by adding a selected subgrade layer. By doing this for all the pavement structures one would have the best case scenario and the pavements will show good performance in terms of pavement life. It was decided to continue with only the weak subgrade layer in order to get some comparison. This will give a less conservative view of the comparison of the performance of granular materials and RCA.

6.5.2 Reference Pavement B

The pavement life for each layer in Reference Pavement B is calculated using the respective transfer function for each material. Reference Pavement B consists of a G1 base material and a lightly

cemented C3 subbase layer. The pavement lives as calculated are presented in Table 6-12.Although the table shows 3 pavement lives for the sublayers of the base, this is purely just a numerical exercise as the most critical stress situation is the one you would apply from a logical path.

Table 6-12: Calculated pavement life for each layer of Reference Pavement B

Layer	Material	Sublayer	Critical Factor		N (arid)	N (mod)	N (wet)
Base	G1	1	σ_1 (kPa)	713.77	1.47E62	19.31E50	4.96E39
			σ_3 (kPa)	503.22			
		2	σ_1 (kPa)	630.34	1.62E15	7.52E12	3.37E10
			σ_3 (kPa)	183.56			
		3	σ_1 (kPa)	496.32	2.41E16	5.88E13	1.38E11
			σ_3 (kPa)	150.10			
Subbase	C3	Crushing Initiation	σ_3 (kPa)	419.70		1.71E6	
		Advanced Crushing	σ_3 (kPa)	419.70		6.55E5	
		Effective Fatigue[1]	ε_h (με)	181		8.16E6	
		Equivalent Granular[2]	σ_1 (kPa)	160.02	4.22E5	2.25E5	1.20E5
			σ_3 (kPa)	-30.15			
Subgrade	G7		ε_v (με)	513		2.33E6	

Notes:

1: First order analysis

2: Second order analysis

The cemented subbase provides a very stiff support for the base layer and thus high pavement life values for the base layer is obtained. The subbase consists of a lightly cemented layer which is investigated for both crushing and fatigue, although crushing is not a critical parameter it is still worthwhile to investigate. A cemented material performs in a unique way, as it starts as a bound layer, when exposed to repeated loading it starts to crack into first large pieces followed by breaking of the material into smaller pieces, if this process occurs the layer has not failed, however it will now perform as an equivalent granular material. Cemented materials must be analysed in two phases, the first phase is the number of load cycles up to the point where the bound cemented layer fails, and the second phase is the number of load cycles the equivalent granular materials can withstand before failure.

The cemented layer will fail due to fatigue after 8 million cycles, after which it will be act as a granular material, In order to calculate the remaining pavement life after the material transitions to an equivalent granular material, a second order analysis must be performed. From the second order analysis it can be seen that for moderate moisture conditions the equivalent granular layer can withstand a further 225 000 cycles before failure. The critical layer within the pavement structure is the subgrade which will fail after 2.3 million cycles. The critical parameters are highlighted in red. From the table it can be seen why an upside down pavement is preferred in a South African context, as all the layers within the material has a relatively long pavement life. The solution to extending the pavement life of the subgrade would be to add an additional selected subgrade layer which will support the subgrade.

6.5.3 Reference Pavement C

The pavement life for each layer in Reference Pavement C is calculate using the respective transfer function for each material. Reference Pavement C consists of a G4 base material and a G5 granular subbase layer. The pavement lives as calculated are presented in Table 6-13.

Table 6-13: Calculated pavement life for each layer of Reference Pavement C

Layer	Material	Sublayer	Critical Factor		N (arid)	N (mod)	N (wet)
Base	G4	1	σ_1 (kPa)	709.40	1.75E50	4.61E40	3.97E32
			σ_3 (kPa)	532.85			
		2	σ_1 (kPa)	596.77	1.7E11	4.08E9	1.8E8
			σ_3 (kPa)	178.86			
		3	σ_1 (kPa)	422.83	9.84E4	4.26E4	2.17E4
			σ_3 (kPa)	-29.16			
Subbase	G5		σ_1 (kPa)	179.42	4.20E5	1.77E5	6.60E4
			σ_3 (kPa)	-15.09			
Subgrade	G7		ε_v (με)	856		1.39E4	

Due to a weaker subbase layer as well as a weaker base layer the support of this pavement structure is weak. A weak support structure results in reduced or no confinement in the pavement layers which have a detrimental effect on the pavement life. The base performs poorly and can withstand 42 600 cycles for moderate moisture conditions. As discussed earlier this is not realistic for pavement design purposes, and would have to be reconsidered in its entirety. Both of these results in the base and subbase can be attributed to the fact that the pavement does not provide sufficient support for the layer that is above. This even after the modular ratio has been applied. However, the critical layer in this pavement structure is the subgrade, which will fail after 14 000 cycles, this is due to poor load

spreading ability in the upper layers which results in high induced strains in the subgrade layer. Another contributing factor is that only 10mm of rutting is allowed in the subgrade which is very stringent conditions and is only applicable to high volume roads.

6.5.4 Pavement 1

The pavement life for each layer in Pavement 1 is calculated using the respective transfer functions. Pavement 1 consists of a RCA base layer that is placed on a C3 lightly cemented subbase layer. The pavement life for each layer is shown in Table 6-14. To incorporate the climatic conditions into the transfer function for the RCA base layer the research of Emery (1988) is used. Emery (1988) synthesised a ratio between the equilibrium moisture content (EMC) and the optimum moisture content (OMC) for different climatic conditions. According to his thesis an EMC/OMC ratio of 53% for arid conditions, 63% for moderate conditions and 72% for wet conditions are applicable for a base layer.

Table 6-14: Calculated pavement life for each layer of Pavement 1

Layer	Material	Sublayer	Critical Factor		N (arid)	N (mod)	N (wet)
Base	RCA	1	DSR (%)	3.64	2.50E11	9.03E10	3.62E10
		2	DSR (%)	11.73	2.40E11	8.71E10	3.49E10
		3	DSR (%)	12.03	2.40E11	8.68E10	3.48E10
Subbase	C3	Crushing Initiation	σ_3 (kPa)	416.72		1.75E6	
		Advanced Crushing	σ_3 (kPa)	416.72		8.33E6	
		Effective Fatigue[1]	ε_h (με)	178		6.88E5	
		Equivalent Granular[2]	σ_1 (kPa)	157.42	4.49E5	2.37E5	1.25E5
			σ_3 (kPa)	-30.14			
Subgrade	G7		ε_v (με)	495		3.38E6	

In order to use the transfer function as synthesised in this research values for the moisture content, density and plastic strain must be assumed. A moisture content of added moisture and hygroscopic moisture of 10% is used. A density of 100% of vibratory hammer is used and the with the plastic strain

it is assumed that the full allowable 10 mm deformation take place in the base layer, yielding a strain of 6.667%.

The transfer function for RCA gives realistic although high values for all three sublayers of the base layer. When comparing the pavement life obtained in both Reference Pavement B and Pavement 1 it can be seen that similar values are obtained. Due to the stiff support of the lightly cemented layer the pavement life obtained for the base is high. The cemented subbase layer performs in a similar way to that of Reference Pavement B, the critical layer in Pavement 1 is the cemented layer that will fail after 925 000 cycles including both effective fatigue and the equivalent granular phase.

6.5.5 Pavement 2

The pavement life for each layer of Pavement 2 is calculated using the respective transfer functions for each material. Pavement 2 consists of a RCA base layer and a G5 granular subbase layer. It is beneficial the compare the pavement lives obtained for Pavement 2 and Reference Pavement A. The pavement life for each layer can be found in Table 6-15.

The transfer function used for the RCA base layer yields plausible yet very high values. The RCA base outperforms the granular base with a significantly higher pavement life. In both cases the subbase does not perform well and this can be attributed to the fact that a weak material was used. It may be beneficial to use a better aggregate for the subbase or to use a cemented subbase. In Pavement 2 the subgrade is the critical layer and is highlighted in red.

Table 6-15: Calculated pavement life for each layer of Pavement 2

Layer	Material	Sublayer	Critical Factor		N (arid)	N (mod)	N (wet)
Base	RCA	1	DSR (%)	1.031	2.50E11	9.04E10	3.62E10
		2	DSR (%)	18.91	2.07E11	7.50E10	3.01E10
		3	DSR (%)	25.25	1.53E11	5.52E10	2.21E10
Subbase	G5		σ_1 (kPa)	161.01	6.27E5	2.44E5	8.33E4
			σ_3 (kPa)	-17.28			
Subgrade	G7		ε_v (με)	786		3.26E4	

6.5.6 Pavement 3

The pavement life for each layer of Pavement 3 is calculated using the respective transfer function for each material. Pavement 3 consists of a G1 granular base that is placed on a RCA subbase layer. The calculated pavement life of each layer is shown in Table 6-16.

When comparing Pavement 3 and Reference Pavement A, it can be seen that the RCA layer provides a far superior subbase to that of the G5 granular material. For Reference Pavement A the subbase layer could withstand 236 000 cycles at moderate moisture conditions, whereas the RCA subbase can withstand 2.67E9 cycles. Depending on the moisture condition the critical layer in this pavement structure varies. If arid moisture conditions is considered the subgrade layer will be the weakest layer with a pavement life of 1.3 million cycles. If moderate or wet conditions are considered the base layer will be the critical layer as it can withstand less than 1 million cycles. Due to this both the subgrade and base is highlighted in red.

Table 6-16: Calculated pavement life for each layer of Pavement 3

Layer	Material	Sublayer	Critical Factor		N (arid)	N (mod)	N (wet)
Base	G1	1	σ_1 (kPa)	703.85	6.22E52	2.26E43	7.10E33
			σ_3 (kPa)	600.57			
		2	σ_1 (kPa)	571.12	9.11E6	1.36E6	1.99E5
			σ_3 (kPa)	118.08			
		3	σ_1 (kPa)	404.71	5.48E6	8.57E5	1.32E5
			σ_3 (kPa)	8.08			
Subbase	RCA	1	DSR (%)	15.55	7.37E9	2.67E9	1.07E9
		2	DSR (%)	10.14	7.93E9	2.87E9	1.15E9
		3	DSR (%)	7.33	8.05E9	2.92E9	1.17E9
Subgrade	G7		ε_v (με)	696		1.34E6	

6.5.7 Pavement Life Summary

When looking at the stresses that are induced in the pavement layers, it is beneficial to calculate the Deviator Stress Ratio. This will give another indication as to the pavement life, as each material has a maximum deviator stress ratio that the material can withstand. Figure 6-15 shows the DSRs that

are induced in the granular base layers as well as in the layers comprising of RCA. The granular layers are coloured in green and the RCA layers are indicated in orange. From this it can be seen that granular layers have a higher DSR's than that of the RCA layers. Another finding is that the DSR in a layer is significantly lower when it is constructed on a stiff subbase layer. Reference Pavement A that consists of a G5 subbase has extremely high induced stresses in the lower base layer, due to the fact that the layer does not have sufficient support. Reference Pavement B, which has a lightly cemented subbase layer, has markedly lower DSR's for all three base layers. In Reference Pavement C which consists of the worst quality base layer, a DSR of more than 200% is induced due to poor load spreading ability. The RCA material performs very well in terms of DSR, even Pavement 2 which is built on a weaker G5 subbase, has low DSR in each layer. However, when comparing Pavement 1 and Pavement 2, one can see the difference that a stiffer subbase creates (less DSR induced in the lower base sublayer).

Here the benefits of using an RCA subbase compared to a granular subbase can be seen, although the subgrade is weaker the RCA material yield much higher pavement life than that of the granular subbasses. The fact that the subgrade is performing poorly can be addressed by adding a selected subgrade, however for the purpose of this study it would not give the holistic view of the performance of RCA materials when placed on weaker layers.

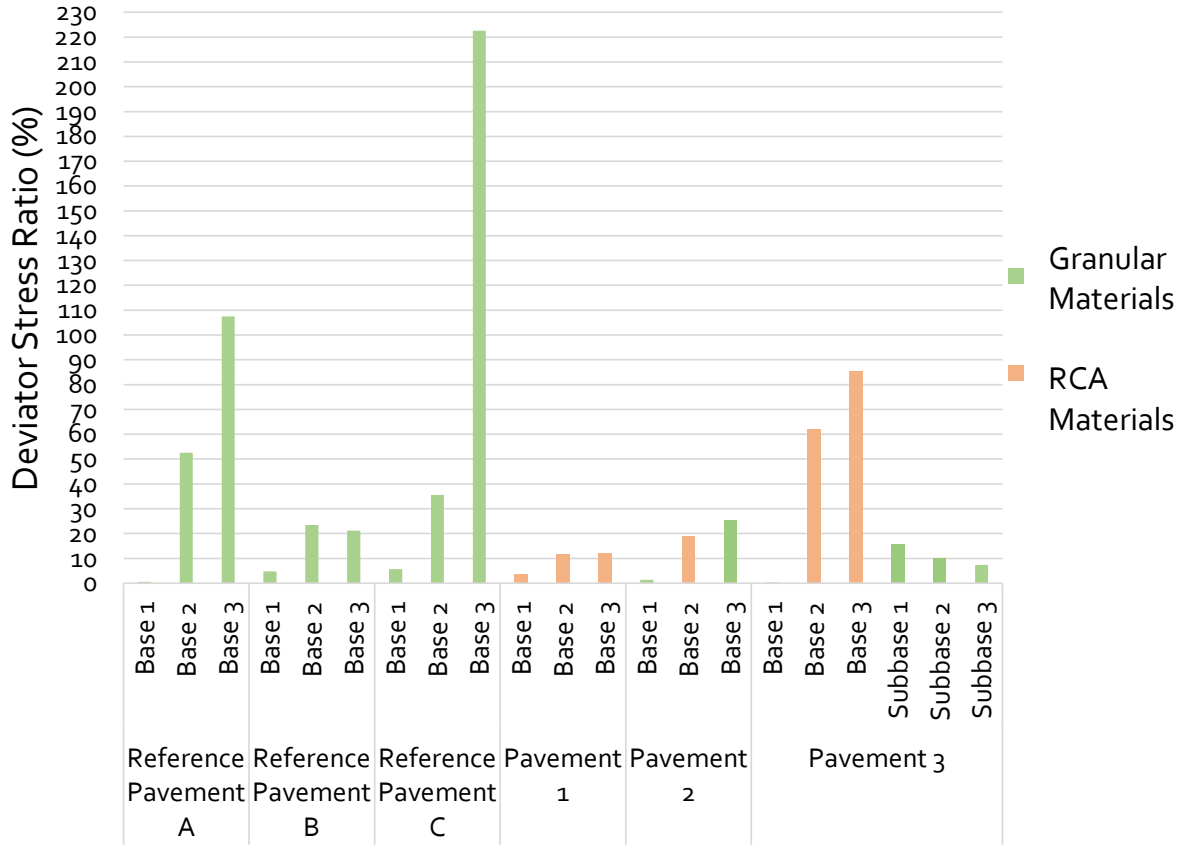

Figure 6-15: Summary of Deviator Stress Ratio of granular layers

Figure 6-16 is a summary of all 5 pavement structures that are analysed and the pavement life for each layer within the pavement structure. Where multiple sublayers existed for a layer, the pavement life representing the most critical path was taken, and all pavement lies for the moderate climatic condition are presented. The colours are the same as what is used in the presentation of the various pavement structure to allow for each material layer classification. The orange bars are indicative of RCA material, the grey bars shows a C3 lightly cemented material. The green bars show the granular materials, the bars are colour coded in chromatic order, with the darkest colour representing the best quality aggregate namely G1 and the lightest green bar representing the weakest granular material namely a G7 material.

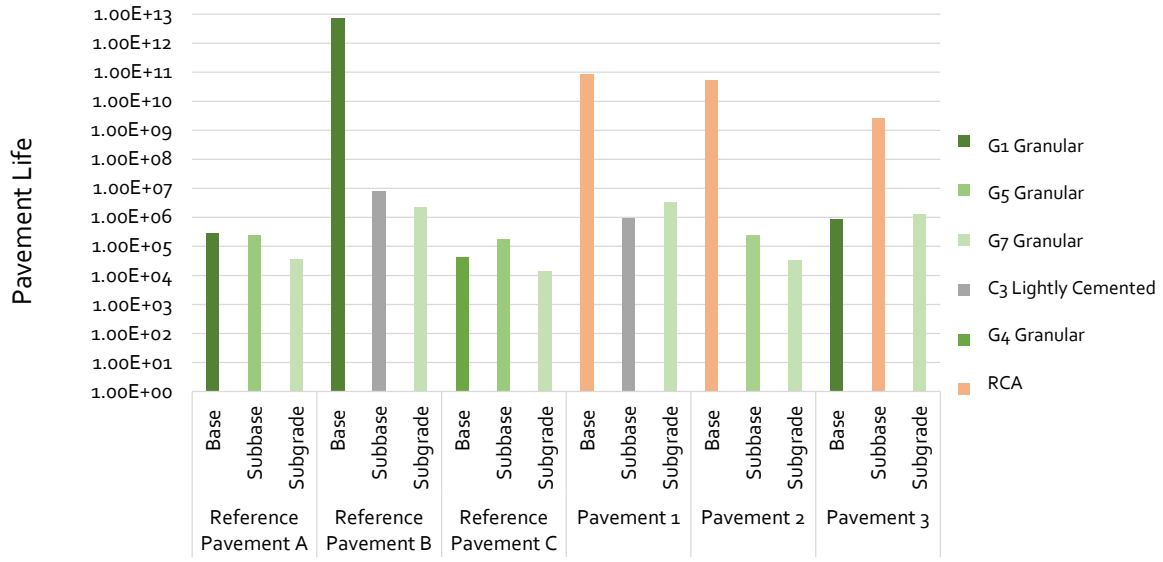

Figure 6-16: Summary of all pavement structures and the respective layer's pavement life

6.6 Conclusion

Pavement analyses were performed by using different pavement structures that include RCA material. This was compared against reference structures that comprise of traditional pavement materials. From these analysis it can be concluded that the RCA material performs very well as either a base or subbase layer within the pavement structure. As a subbase material RCA far outperforms its granular counterpart and as a base layer it results in a more predictable and realistic pavement life. By comparing the RCA material in the base to a G4, it can be seen that the RCA material performs better in terms of pavement life as well as stress and strain development. When comparing the RCA material to a G1 material in the base they show very similar performances in terms of stress and strain development. One should however recognise the limitations of this analysis and include how the transfer function is developed for this material. In addition, there are shortcomings of the current linear-elastic analysis. This was highlighted in that it showed some negative results for confinement

which is not possible. This of course was more prominent due to the choice of a relatively weak subbase and the architecture of the software programme. Nonetheless, the comparison of results revealed that RCA has significant potential.

The mechanistic empirical analysis method used for this analysis chapter only takes the structural performance of the material into account. This analysis type does not take into account the permeability of the material, although some pavement life's of the material was calculated for different moisture conditions. The durability and achievable compaction are other variables that play a very important role in the performance of a pavement structure but it is not included in the process. In order to investigate the durability the transfer function for Unexposed RCA material must be developed.

Chapter 7: Conclusions and Recommendations

7.1 Conclusions

In order to achieve the objectives of this research as outlined in Chapter 1.2, different test procedures and analyses were carried out as explained in Chapter 3 to Chapter 6. The results obtained in this research were based on the testing and modelling performed on Exposed and Unexposed RCA material. The material that was obtained from the N2 highway in close proximity to the Cape Town International Airport.

Chapter 3 of this study described the material preparation as well as provided a methodology for the for the laboratory tests that were to be carried out in the experimental design. Chapter 4 provided the results of the experimental design, which was completed to investigate the shear properties and the permanent deformation behaviour of the material. The tests were only performed for a limited number of cycles in order to gain a better understanding of long term behaviour the results were modelled. The modelled results were also included in Chapter 4. In order to compare RCA to traditional pavement materials an analysis including the pavement life was performed. This was done through the development of a transfer function which was undertaken in Chapter 5. Chapter 6 was dedicated to the practical application of the results, by using the transfer function to calculate the pavement life of the material in various situations.

This Chapter provides the general conclusions and recommendations, as the specific details are discussed in the individual Chapters as highlighted above. The success of the research as well as the limitations and shortcomings will be highlighted here. Therefore, based on the results and analysis completed in this study the following conclusions can be drawn regarding the behaviour of RCA and the performance:

RCA Performance:

- The shear parameters of RCA material is not an accurate indicator to predict the permanent deformation behaviour of the material. For Exposed RCA the material showed very high shear parameters but the deviator stress ratios at which the material failed is significantly lower than that of the Unexposed RCA.
- An increase in the deviator stress ratio causes an increase in deformation in the material, Due to the magnitude of the shear parameters, and increase in DSR results in a disproportional increase in applied stress (σ_1). When the applied stress reaches a certain point it starts to crush the cementitious bonds, which contributes to the strength of the specimen. The material can no longer rely on cementitious bonds and relies only on matrix interlock.

- Curing a specimen for 1 month increases the material strength and reduces the amount of permanent axial strain induced in the material.
- Intermittent tests performed illustrated the benefit of self-cementing. A sample that shows unstable behaviour and reaches a certain amount of predetermined plastic strain, can show stable behaviour subsequently due to self-cementation and an increase in strength after 1 month of curing.
- Although self-cementing occurs, none of the samples presented cracking.
- The Exposed material showed a smaller reduction in permanent axial strain between 0 and 1 month of curing when compared to the Unexposed material. This alludes to the fact that the Exposed material still has some self-cementing potential, but less than that of the Unexposed RCA.
- The strength and weaknesses of each model, namely the Barksdale, Sweere, Paute, Wolff and Visser and Huurman models was illustrated. The applicability of the model can be linked to the ranges identified by the Shakedown Theory. The best model for each range is as follows. Range A, the model developed by Paute (1996), for Range B the model developed Wolff and Visser (1994) and for Range C the model as developed by Huurman (1997).
- The Huurman (1997) model was used to model all the data used in the synthesis of the transfer function. It was chosen as it is able to model both stable and unstable permanent deformation behaviour.

Durability:

- The durability of RCA was investigated by testing two materials, Exposed and Unexposed RCA material. The self-cementing potential of RCA creates durability issues such as shrinkage cracking and carbonation.
- By exposing RCA material, and reducing the amount of latent cement the material cannot withstand high DSR's and the material behaviour is more variable and unpredictable. Unexposed RCA material performed much better in permanent deformation and shows no sign of shrinkage cracking at the end of the test cycles.
- From the conclusions regarding the self-cementing properties of RCA it is evident that the correct curing period of RCA material is of the utmost importance. By curing the material for 1 month and allowing for self-cementation to take place, it increases the strength and reduces the amount plastic strain develops which will result in stable behaviour once the pavement is trafficked.

Transfer Function:

- The transfer function for RCA material was based on the waterbound macadam transfer function which takes into account the failure mechanisms of granular materials. It was assumed that the failure mechanisms for RCA at 0 month of curing is similar to granular materials.
- Specimens at 1 month of curing had undergone large amounts of self-cementation which increases the strength of the material and reduces the amount of permanent axial strain in the material as previously stated. The transfer function is unable to handle very low plastic strains, and therefore the transfer function is not applicable to predict the behaviour of 1 month old samples.
- The DSR is the most significant factor that influences the number of load cycles to failure. Therefore, the DSR term is raised to a variable power in order to account for the large influence it has. After the iterative process the power function had a value of 3.358.
- The transfer function predicts unrealistic values when it used beyond 40 million cycles, due to the fact that the transfer function starts to predict an exponential relationship between observed and calculated values, instead of the linear relationship on which the transfer function is base. Therefore a limitation must be set.
- A reliability analysis completed to build in a surety in the application of the transfer function, the higher the reliability of the transfer function the more the transfer function under-predicts the pavement life.

Pavement Analysis:

Pavement analysis shows that Unexposed RCA can be used to replace a granular subbase layer for a Category B road, yielding good performance when compared of a G4 granular material when considering the poor subgrade that is implemented.

In general it is concluded that this is a material with high variability. More so when exposed. This is an important factor to consider when guidelines are proposed.

7.2 Recommendations

The results from this research yielded important information on the performance of RCA materials, by looking at the conclusions the following recommendations can be made for future research endeavours:

- Various sources of RCA should be investigated to be able to compare and establish a more comprehensive range of parameters for this material.
- More tests on materials with variable curing times should be done.
- Further research should be conducted on the permanent deformation behaviour of RCA materials when subjected to longer tests that comprises of larger number of load cycles.
- Additional research on the confinement pressures and at which point the confinement pressure changes from a beneficial factor in which the confinement results in a reduction of plastic strain. Trends of this nature was observed but not explicitly concluded as additional research is needed to confirm this.
- Investigations into the magnitude of the applied stress and what effect this has on the cementitious bonds, as well as the effect the shear parameters has on the magnitude of the applied stress.
- Investigate the applicability of permanent deformation models not included in this study, with particular interest the models that are based on stress conditions
- Other forms of the variables in the transfer function should be considered.
- A transfer function with two terms should be synthesised that allows for the incorporation of unstable behaviour of the material.
- Future research should consider two parameters including percentage of OMC, a value that indicates the proportional hygroscopic moisture. However, the current transfer function still provide valuable insight on the response of different variables
- Investigate the effect on the transfer function of the various factors that influence the deviator stress ratio as stated in Section 5.2.2.
- Further investigations into the nature of the material should be undertaken to define how the material is likely to behave. The transfer function can then be calibrated for a variety of materials to improve the reliability of the function.
- More materials should be tested in order to improve the calibration process of the coefficients for the transfer function. The current transfer function is only applicable to one material and one moisture content.
- A term that includes the pH of the material should be investigated as an addition to the transfer function, this will potentially allow for the incorporation of the both the Exposed and Unexposed RCA test results as input data for the transfer function.
- More pavement structures should be analysed to gain a better understanding of the effect of various factors such as density, moisture, plastic strain limit and subgrade quality plays on the performance of RCA material as both a base and subbase layer.

- In service test section should be constructed that includes RCA as both base and subbase layers on roads with high traffic counts. This will allow for observation of crack formation, stiffness increases due to self-cementation as well as the importance of the curing period and the resistance to permanent deformation.
- A Life Cycle Cost Analysis to investigate the feasibility of usage of RCA material compared to traditional granular materials.

Bibliography

Agnello, N. 2017. The modelling of shrinkage behaviour of Recycled Concrete Aggregate and Cement Stabilised Materials. Unpublished thesis dissertation. Stellenbosch: University of Stellenbosch.

Allen, J. 1973. The effect of non-constant lateral pressure of the resilient response of granular materials. Published doctoral dissertation. Chicago: University of Illinois.

Arm, M. 2000. Self-cementing properties of crushed demolishing concrete in unbound layers: results from triaxial tests and field tests. *Waste Management Series*. 1(C):579–587.

Arnold, G.K. 2004. Rutting of Granular Pavements. Published doctoral dissertation. Nottingham: University of Nottingham.

Arulrajah, A., Disfani, M.M., Horpibulsuk, S., Suksiripattanapong, C. & Prongmanee, N. 2014. Physical properties and shear strength responses of recycled construction and demolition materials in unbound pavement base/subbase applications. *Construction and Building Materials*. 58 (I): 245–257.

Barisanga, F. 2014. Material Characterisation and Response Modelling of Recycled Concrete and Masonry in Pavements. Published thesis dissertation. Stellenbosch: University of Stellenbosch.

Barksdale, R.D. 1972. Laboratory evaluation of rutting in basecourse materials. *3rd International Conference on Structural Design of Asphalt Pavements*. 161–174. London UK.

Barksdale, R.D. & Itani, S.Y. 1989. Influence of Aggregate Shape on Base Behavior. *Transportation Research Record*. 173- 182.

Bierman, C.R. 2017. A design function for Bitumen Stabilised Material performance based on laboratory and field evaluation. Unpublished thesis dissertation. Stellenbosch: University of Stellenbosch.

Bribian, I., Capilla, A. & Uson, A. 2011. Life cycle assessment of building materials: Comparaitive analysis of energy and environmental impacts and evaluation of eco-efficiency imporvent potential. *Building and Environment*. 46(I):1133–1140.

Brown, S.F. & Hyde, A.F.L. 1975. Significance of cyclic confining stress in repeated-load triaxial testing of granular materials. *Transportation research record*. 537(I):49–58.

Cameron, D.A., Gabr, A.G., Andrews, R. & Michell, P.W. 2013. The Use of Recycled Aggregates in Unbound Road Pavements. *18th International Conference on Soil Mechanics and Geotechnical Engineering*. Paris: 3187–3190.

Cheung, L. W. 1994. Laboratory assessment for pavement foundation materials. Published doctoral dissertation. Nottingham: University of Nottingham.

Cleghorn, A. 2015. The Self-Cementing Performance Properties of Recycled Concrete in Road Pavement Materials. Published thesis dissertation. Stellenbosch: University of Stellenbosch.

Colto. 1998. *COLTO: Standard Specifications for Road and Bridge Works for State Road Authorities*.

Deloitte. 2015. Screening template for Construction and Demolition Waste management in The Netherlands. [Online], Available: http://ec.europa.eu/environment/waste/studies/deliverables/CDW_The Netherlands_Factsheet_Final.pdf. [2016, July 26].

Department of Environmental Affairs. 2012. *National Waste Information Baseline Report*. Pretoria.

Emery, S.J. 1988. *The Prediction of Moisture Content in Untreated Pavement Layers and an Application to design in Southern Africa*. Pretoria.

Erkens, S. 2002. Asphalt Concrete Response (ACRe)- Determination, modelling and Prediction. Published doctoral dissertation. Delft: Delft Univeristy of Technology.

Federal Highway Administration Research and Technology. 2007. *Long-term Pavement Performance Project Laboratory Materials Testing and Handling Guide*. [Online], Available: https://www.fhwa.dot.gov/publications/research/infrastructure/pavements/ltpp/07052/pro46/002.cfm. [2016, September 25]

Gottfredsen, F.R. & Thogersen, F. 1994. Recycling of Concrete in Aggressive Enivronment. *International RILEM Symposium on Demolition and Reuse of Concrete and Masonry*. Denmark.

Hoff, I., Bakløkk, L.J. & Aurstad, J. 2003. Influence of Laboratory Compaction Method on Unbound Granular Materials. *6th International Symposium on Pavements Unbound*. 1-11.

Huurman, M. 1997. Permanent deformation in concrete block pavements. Published doctoral dissertation. Delft: Delft Univeristy of Technology.

Jenkins, K. 2016. *Hitchiker's Guide to Pavement Engineering*. Stellenbosch: University of Stellenbosch.

Jenkins, K & Molenaar, A.A. Flexible Pavement Design (2017) Unpublished postgraduate course notes (Civil Engineering) at the University of Stellenbosch.

Karlsson, M. 1998. Reactivity in recycled concrete aggregate. *2th International PhD Symposium in Civil Engineering*. Budapest. 1–7.

Khedr, S. 1985. Deformation Characteristics of Granular Base Course in Flexible Pavements. *Transportation Research Record*. 1043: 131- 138.

Kolisoja, P. 1998. Large scale dynamic triaxial tests. Published doctoral dissertation. Tampere Finland: University of Tampere.

Kotze, N. 2014. Toets van Granulêre Materiale. Published project. Stellenbosch: University of Stellenbosch.

Leek, C. & Siripun, K. 2010. Spesification and performance of recycled materials in road pavements. Perth: University of Curtin.

Lekarp, F. & Dawson, A. 1997. Analysis of permanent deformation behaviour of unbound granular materials. In New Brunswick *International Symposium on Thin Pavements, Surface Treatments and Unbound Roads*. New Brunswick.

Lekarp, F. & Dawson, A. 1998. Modelling permanent deformation behaviour of unbound granular materials. *Construction and Building Materials*. 12(1):9–18.

Lekarp, F., Isacsson, U. & Dawson, A. 2000a. State of the Art. II: Permanent Strain Response of Unbound Aggregates. *Journal of Transportation Engineering*. 126:76–83.

Lekarp, F., Isacsson, U. & Dawson, A. 2000b. State of the Art. I: Resilient Response of Unbound Aggregates. *Journal of Transportation Engineering*. 126:66–75.

Li, L., Liu, J. & Zhang, X. 2010. *Resilient Modulus Characterization of Alaskan Granular Base Materials*. Fairbanks. 39:655-664

Maree, J.H. 1982. Aspects of design and behaviour of road pavements with granular material. Published doctoral dissertation. Pretoria: University of Pretoria.

Meulen, M.J. Van Der, Gessel, S.F. Van & Veldkamp, J.G. 2005. Aggregate resources in the Netherlands. *Netherlands journal of Geoscience.* 84(IV):379–387.

Morgan, J. 1966. The response of granular materials to repeated loading. In *3rd Proceedings of the Australian Road Research Board*. Sydney: 1178–1192.

Morton, B., Luttig, E., Horak, E. & Visser, A. 2004. The Effect of Axle Load Spectra and Tyre Inflation Pressures on Standard Pavement Design Methods. *8th Conference on Asphalt pavements for Southern Africa*. Sun City.

Munro, M. & Mohajerani, A. 2016. Possible cause of instability of bulk carriers transporting iron ore fines: shear strength failure under cyclic loading. *Transportation geotechnics*.

Nataatmadja, A. & Tan, Y.L. 2001. Resilient Response of Recycled Concrete Road Aggregates. *Journal of Transportation Engineering*. 450–453.

Paige- Green, P. 2010. A preliminary evaluation of the reuse of cementitious materials. In Pretoria *A nnual Southern African Transport Conference*. Pretoria: 520-529.

Pappin, J.W. 1979. Characteristics of granular material for pavement analysis. Published doctoral dissertation. Nottingham: University of Nottingham.

Paute, J.L., Hornych, P. & Benaben, J.P. 1996. Repeated load triaxial testing of granular materials in the French network of Laboratories des Ponts et Chausees. *Proceedings of European Symposium on Flexible Pavements*. Rotterdam: 53–64.

Paute, J.L., Thom, N.H. & Dawson, A.R. 1996. Mechanical characteristics of unbound granular materials as a function of condition. *Proceedings of European Symposium on Flexible Pavements*. Nottingham: 35–44.

Poon, C.S. & Chan, D. 2006. Feasible use of recycled concrete aggregates and crushed clay brick as unbound road sub-base. *Construction and Building Materials*. 20(VIII):578–585.

Rudman, C. & Jenkins, K. 2015. *Self-Cementing Mechanisms of Recycled Concrete and Masonry Aggregate*. Unpublished paper. Stellenbosch.

Rudman, C. & Jenkins, K. 2017. *Aspects of Self-Cementing using Recycled Concrete Aggregate in Pavement Layers*. Unpublised paper. Stellenbosch.

SANRAL. 2011. *Revision of the South African Pavement Design Method (SAPDM) - Proposed Protocol for Resilient Modulus and Permanent Deformation Characteristics of Unbound and Bound Granular Materials*. Pretoria.

SANRAL. 2014a. *South African Pavement Engineering Manual- Chapter 3*. Pretoria.

SANRAL. 2014b. *South African Pavement Engineering Manaul - Chapter 10*. Pretoria.

Sharp, Y. 1997. *Investiagtion Into The Use of Recycled Crushed Concrete For Road Base Use, Technical Note*. Australia.

Sharp, R.W. & Booker, J.R. 1984. Shakedown of Pavements Under Moving Surface Loads. *Journal of Transportation Engineering*. 110(I):1– 14.

Strauss, P.J. & Van der Walt, N. 1989. Stress absorbing membranes and flexible asphalt overlays to prevent reflection cracking at joints or cracks in stiff pavements . *5th Conference on Asphalt pavements for Southern Africa (capsa 89)*. Swaziland: 31-35.

Sweere, G.T.H. 1990. Unbound Granular Bases for Roads. Published doctoral dissertation. Delft: Delft University of Technology.

Tao, M., Mohammad, L.N., Nazzal, M.D., Zhang, Z. & Wu, Z. 2010. Application of Shakedown Theory in Characterizing Traditional and Recycled Pavement Base Materials. *Journal of Materials in Civil Engineering*. 136(III):214–222.

Theyse, H.L. & Muthen, M. 2000. *Pavement Analysis and Design Software (PADS) based on the South African Mechanistic-Empirical Design Method*. Pretoria.

Theyse, H.L., De Beer, M. & Rust, F.C. 1996. Overview of South African Mechanistic Pavement Design Method. *Transportation Research Record*. (I):6–17.

Theyse, H.L., Legge, F.T.H., Pretorius, P.C. & Wolff, H. 2007. A Yield Strength Model for Partially Saturated Unbound Granular Material. *Road and Pavement Materials*. 8(3).

Theyse, H.L., Sadzik, E. & Notnagel, J.P. 2000. A Design Model for Waterbound Macadam based on Heavy Vehicle Simulator and Laboratory test results. *South African Transport Conference*. Pretoria.

Thom, N.H. & Brown, S.F. 1987. Effect of Moisture on the Structural Performance of a Crushed-Limestone Road Base. *Transportation Research Record*. 1121:50–56.

Thom, N.H. & Brown, S.F. 1988. The effect of grading and density on the mechanical properties of a crushed dolomitic limestone. *14th ARRB Conference*. 94–100.

Thom, N.H. & Brown, S.F. 1989. The mechanical properties of unbound aggregates from various sources. *Unbound Aggregates in Roads: Proceedings of the 5th International Symposium on Unbound Aggregates in Roads*. Nottingham: 130–142.

Tredoux, C. 2017. Response and Durability aspects of Recycled Concrete Aggregate as alternative to Standard Materials. Published project. Stellenbosch: University of Stellenbosch.

TRH 14. 1985. *TRH14 Road Construction Materials*. Pretoria.

Tutumluer, E. & Pan, T. 2008. Aggregate Morphology Affecting Strength and Permanent Deformation Behaviour of Unbound Aggregate Materials. *Journal of Materials in Civil Engineering*. 20(IX):617–627.

Uthus, L. 2007. Deformation Properties of Unbound Granular Aggregate. Published doctoral dissertation. Trondheim: Norwegian University of Science and Technology.

Van Niekerk, A.A. 2002. Mechanical Behaviour and Performance of Granular Bases and Sub-bases in Pavements. Published doctoral dissertation. Delft: Delf University of Technology.

Van Tonder, W. 2017. Resilient Response of Recycled Concrete and Masonry as Alternative to

Standard Materials. Published project. Stellenbosch: University of Stellenbosch.

Van Zyl, E.B. 2015. Influence of Specimen Geometry and Grading Curve on the Performance of an Unbound Granular Material. Published thesis dissertation. Stellenbosch: University of Stellenbosch.

Van Zyl, S. 2015. Permanent deformation behaviour of concrete demolition waste. Published project. Stellenbosch: University of Stellenbosch.

Veverka, V. 1979. Raming van de spoordiepe bij wegen met een bitumineuze verhardhing. *De Wegentechniek*. 24(III):25–45.

Werkmeister, S. 2003. Permanent Deformation Behaviour of Unbound Granular Materials in Pavement Construction. Published doctoral dissertation. Dresden: Dresden University of Technology.

Werkmeister, S.; Dawson, A R & Wellner, F. 2004. Pavement Design Model for Unbound Granular Materials. *Journal of Transportation Engineering*. 130(V):665–674.

Western Cape Government. 2016. *No Title*. [Online], Available: https://www.westerncape.gov.za/news/roadworks-n2-between-borcherdsquarry-%0Aroad-and-r300%0A [2018, January 01].

Wolff, H. 1992. The elasto-plastic behaviour of granular pavement layers i South Africa. Published doctoral dissertation. Pretoria: University of Pretoria.

Wolff, H. & Visser, A.T. 1994. Incorporating elasto-pasticity in granular layer pavement design. *Proceedings of Institution of Civil Engineering Transportation*. Pretoria: 259–272.

Annexure A: Simple Triaxial Setup

This section describes the preparation to conduct a Simple Monotonic Triaxial test to determine the shear strength properties from large specimens (152mm in diameter and 300mm height).

Stellenbosch University's Pavement Laboratory Material Testing System (MTS 810, Model 318.10) is used to perform simple triaxial tests. The MTS has the capability to simulate real life conditions by applying a vertical force (vehicle wheel loading) and confinement pressure around the specimen by means of air pressure, as the material in the pavement is already supported by other material that undergoes all around pressures.

It is also important to be aware of the MTS constraints. It has a maximum vertical load of 100kN and a maximum confinement pressure of 250kPa.

Specimen preparation for testing:

The specimen preparation and setup is not complex, but must be done accurately as it influences the reliability of results, seen in Figure A-5. For starters, the apparatus and all its components must be clean before setting up the specimen for testing.

Figure A- 1: MTS and specimen setup

Simple Triaxial Procedure:

Step 1: Remove the plastic bag and elastic band from the specimen that was used to cure the specimen for 1 day. The plastic bag allows for minimal amounts of moisture to be lost as shown in Figure A-2

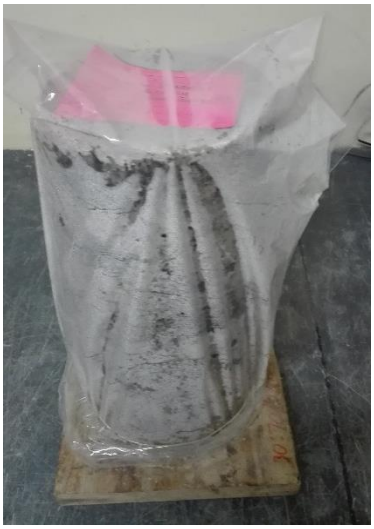

Figure A-2: Specimen covered for 1 day of curing

Step 2: Carefully fit the specimen into the rubber membrane shown in Figure A-3 which has an uninflated internal diameter of 160mm (±5mm) and height of 330mm, fitted with an inflation valve. The inflatable rubber bladder is used to apply the confining pressure. Care need to be exercised not to damage the edges of the specimen.

Figure A-3: Manufactured rubber membrane

Step 3: Place specimen that is covered with the inflatable membrane on the pedestal of the baseplate.

Step 4: The steel confining cylinder is placed over the specimen and positioned in the middle of the base plate, taking care not to damage the edges of the specimen. Fasten the triaxial cell (confining cylinder) to the base plate.

Step 5: Carefully position the top loading disc on the specimen. It is important that the specimen and the loading disc is correctly positioned and aligned with the base plate, as well as the tip of the MTS machine's loading pin. This will allow the sample to be loaded perpendicularly and only induce principal stresses.

Step 6: The bottom actuator is set (MTS program) to -45mm (Figure A-5) to ensure no variability between tests. The top loading pin is manually lowered to where it just makes contact with the loading disc (seating load < 0.4kN). Monitor the load cell reading to prevent loading of the specimen during this process.

Step 7: Ensure that the loading pin is in the middle of the loading disc before attaching the triaxial cell (confining cylinder) and base plate to each other by using the rods and nuts. Once done, all must be locked in place.

Step 8: Connect the air supply to the inflation valve protruding through the confining cylinder. Adjust the pressure regulator to inflate the bladder to the required pressure. Setup is shown in Figure A-4

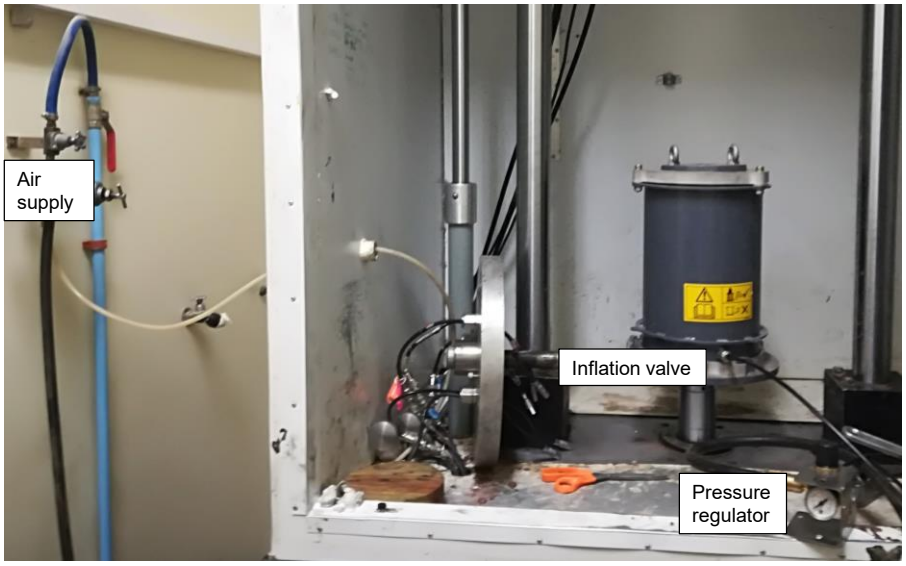

Figure A-4: Pressure supply to the specimen (σ_3)

The complete assembly of the specimen within the MTS machine, when ready for testing, is shown in Figure A-5.

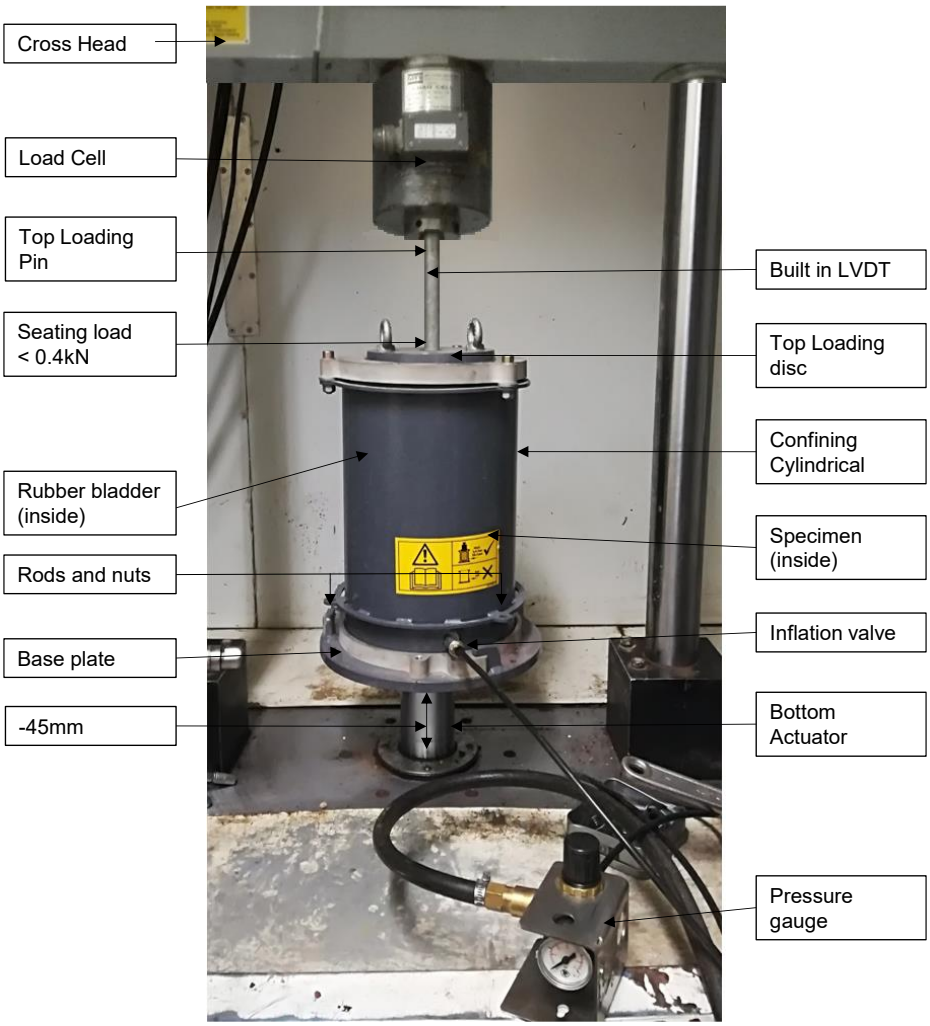

Figure A-5: Complete assembly before testing

Annexure B: Triaxial Input Data

Table B-1: Triaxial input data for Unexposed RCA

Triaxial input data						
Confinement pressure (kPa)	$\sigma_{1,f}$ (kPa)	$\sigma_{d,f}$ (kPa)	% Deviator stress	σ_d (kPa)	σ_1 (kPa)	Force (kN)
			12.50	269.200	319.200	5.792
			37	796.832	846.832	15.366
			45	969.120	1019.120	18.493
50	2203.600	2153.600	50	1076.800	1126.800	20.447
			37	878.232	953.232	17.297
			45	1068.120	1143.120	20.743
75	2448.600	2373.600	50	1186.800	1261.800	22.896
			37	959.632	1059.632	19.228
			45	1167.120	1267.120	22.993
100	2693.600	2593.600	50	1296.800	1396.800	25.346
			37	1122.432	1272.432	23.089
			45	1365.120	1515.120	27.493
150	3183.6	3033.6	50	1516.800	1666.800	30.245

Table B-2: Triaxial input data for Exposed RCA

Triaxial input data						
Confinement pressure (kPa)	$\sigma_{1,f}$ (kPa)	$\sigma_{d,f}$ (kPa)	% Deviator stress	σ_d (kPa)	σ_1 (kPa)	Force (kN)
			17	361.120	411.120	7.460
			22	467.332	517.332	9.387
			27	573.544	623.544	11.315
50	2174.237	2124.237	37	785.968	835.968	15.169
			17	426.811	526.811	9.559
			22	552.344	652.344	11.837
			27	677.876	777.876	14.115
100	2610.653	2510.653	37	928.942	1028.942	18.671
			17	492.502	642.502	11.659
			22	637.355	787.355	14.287
150	3047.068868	2897.068868	27	782.209	932.209	16.916

Annexure C: Individual Intermittent test results

C1: Unexposed RCA

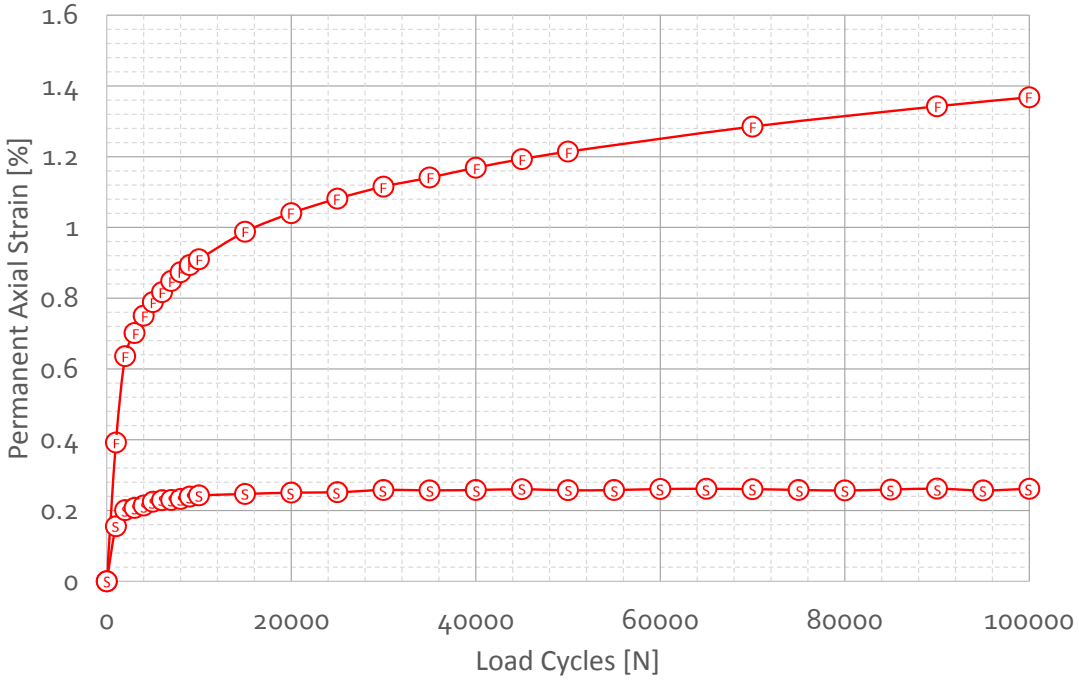

Figure C-1: First (F) and Second (S) Intermittent result for 50/37 Unexposed RCA

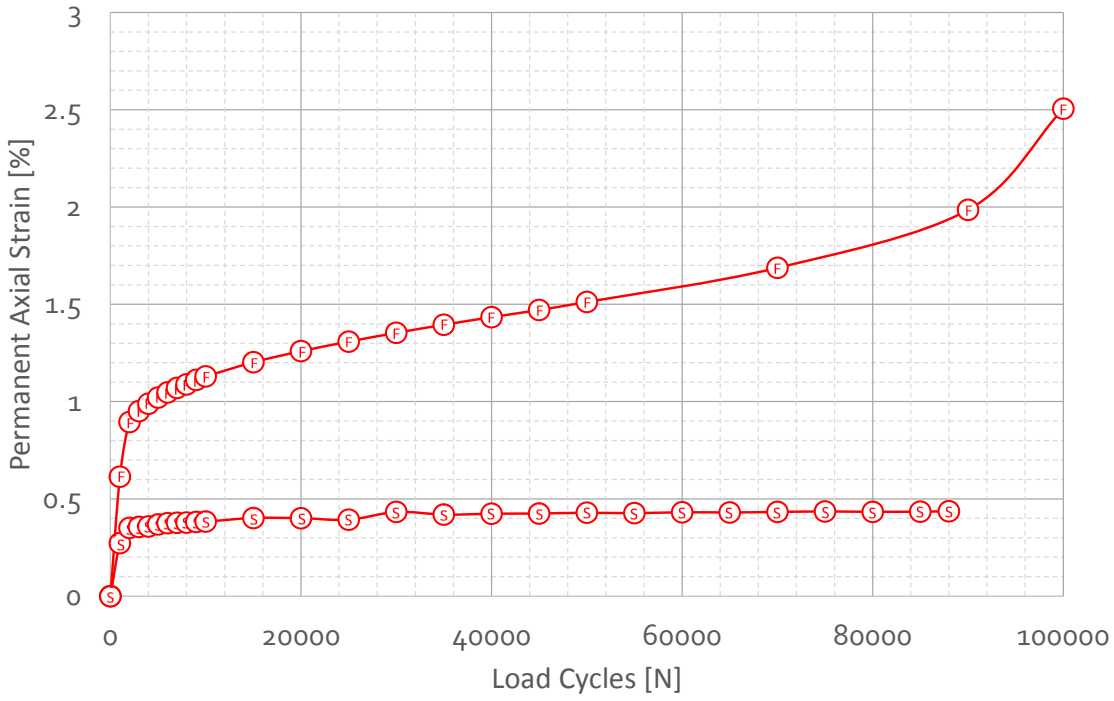

Figure C-2: First (F) and Second (S) Intermittent results for 50/45 Unexposed RCA

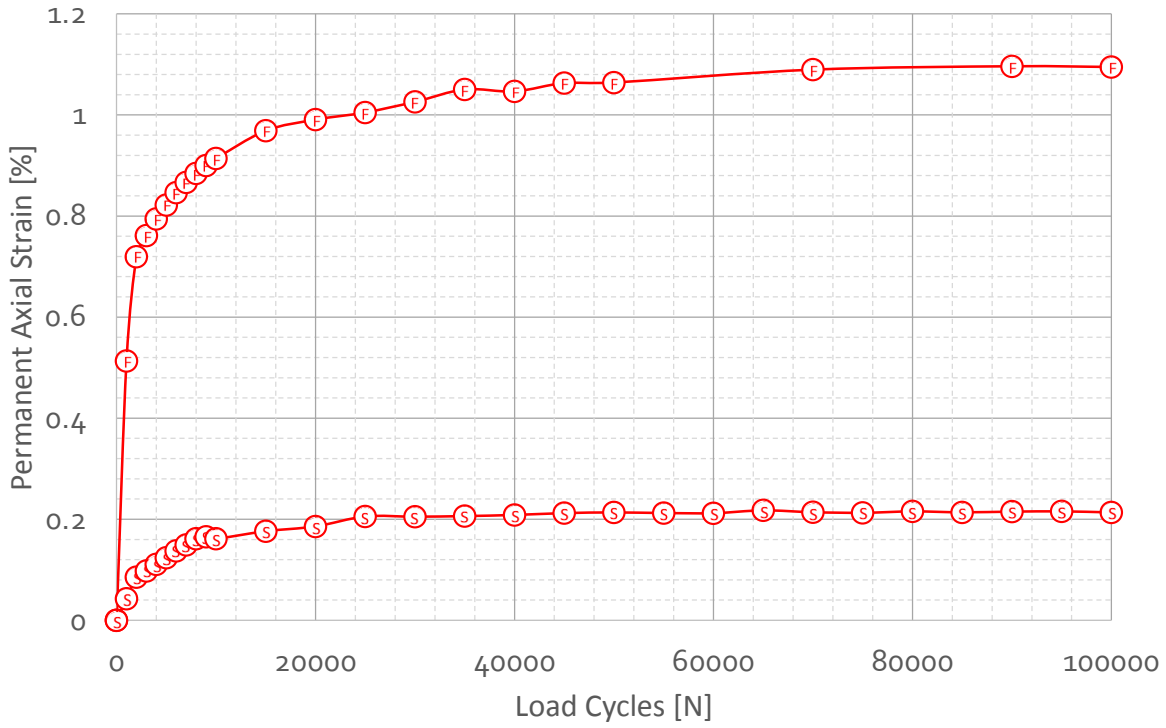

Figure C-3: First (F) and Second (S) Intermittent results for 50/50 Unexposed RCA

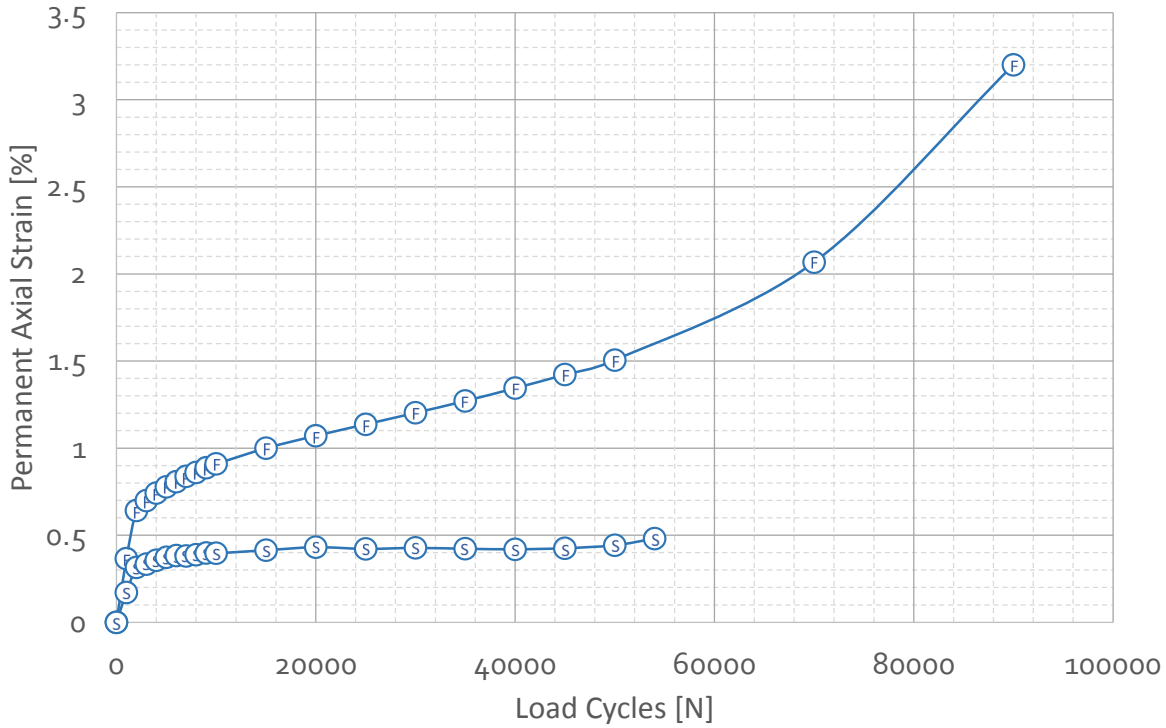

Figure C-4: First (F) and Second (S) Intermittent results for 75/37 Unexposed RCA

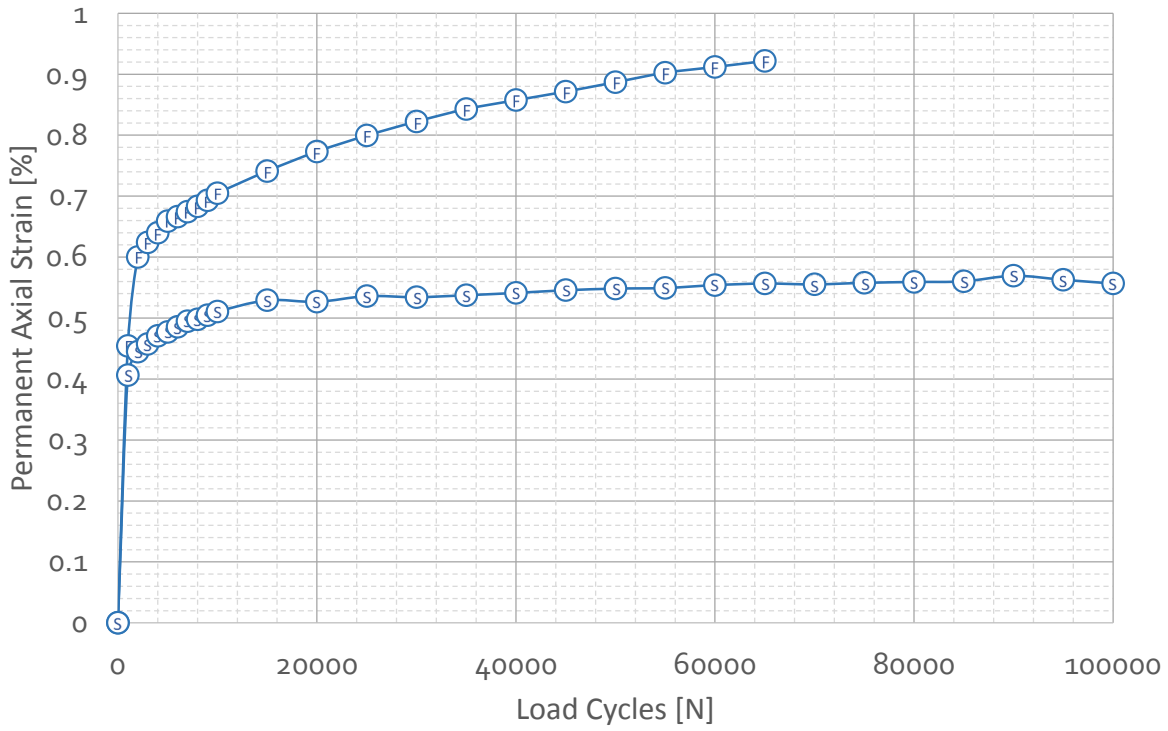

Figure C-5: First (F) and Second (S) Intermittent results for 75/45 Unexposed RCA

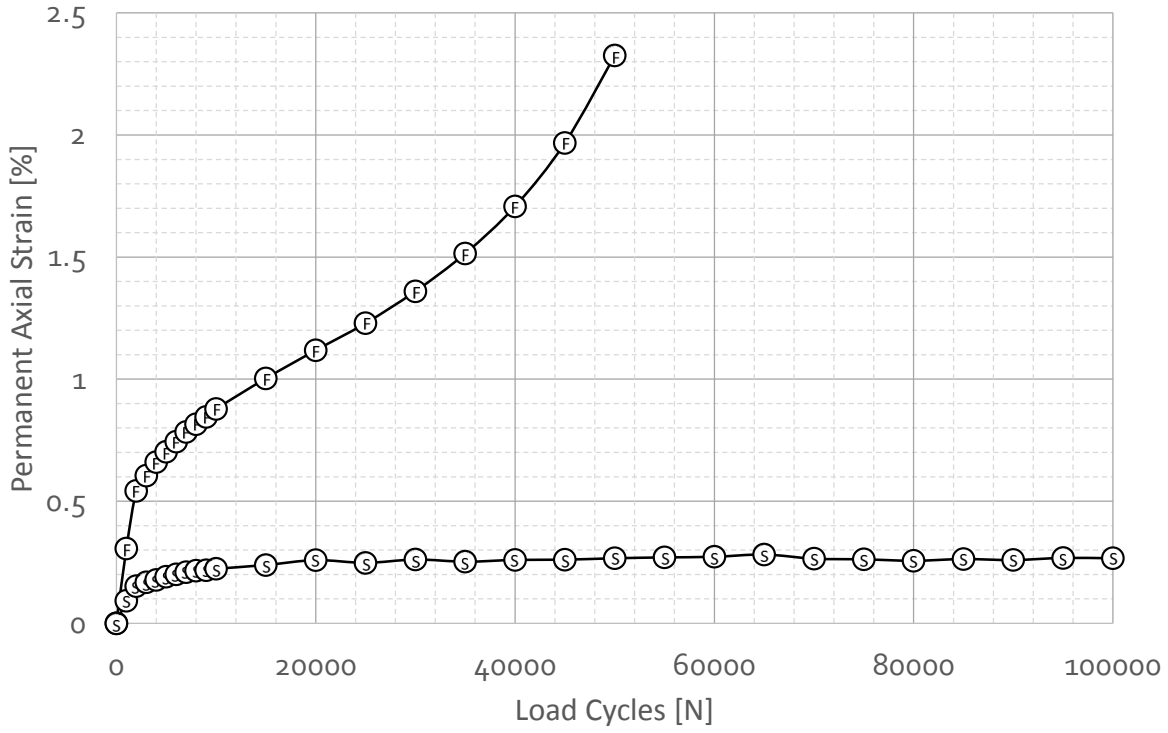

Figure C-6: First (F) and Second (S) Intermittent results for 100/37 Unexposed RCA

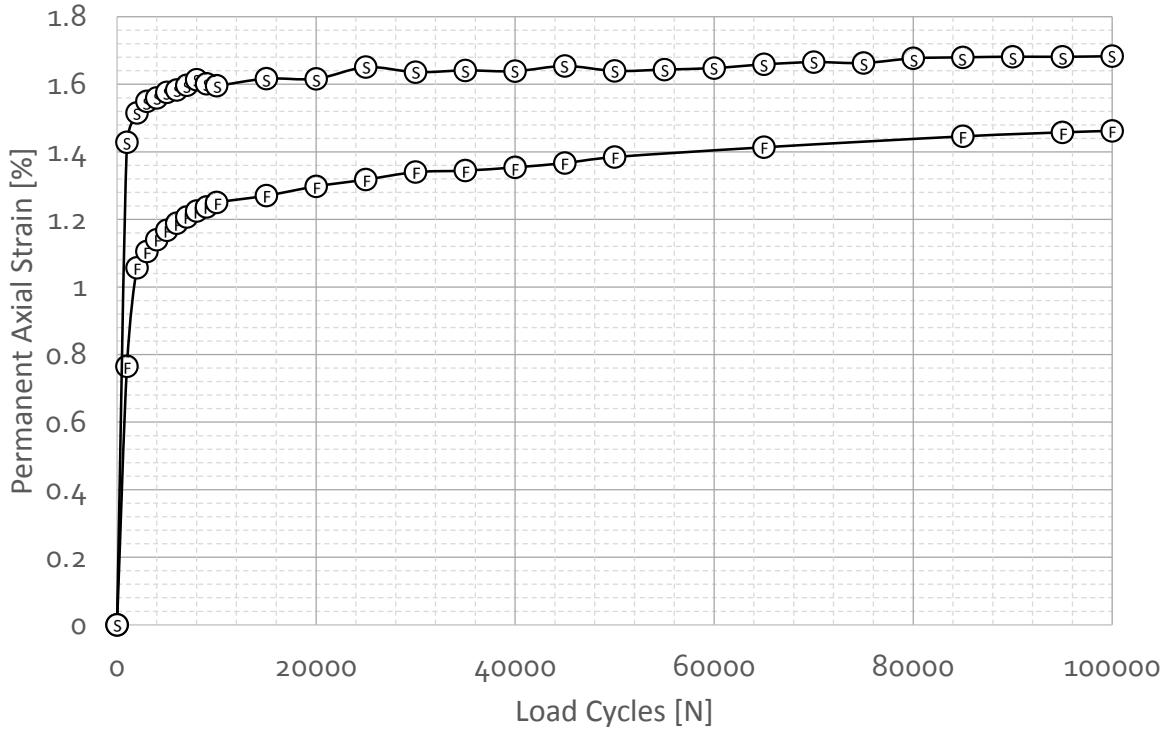

Figure C-7: First (F) and Second (S) Intermittent results for 100/45 Unexposed RCA

C2: Exposed RCA

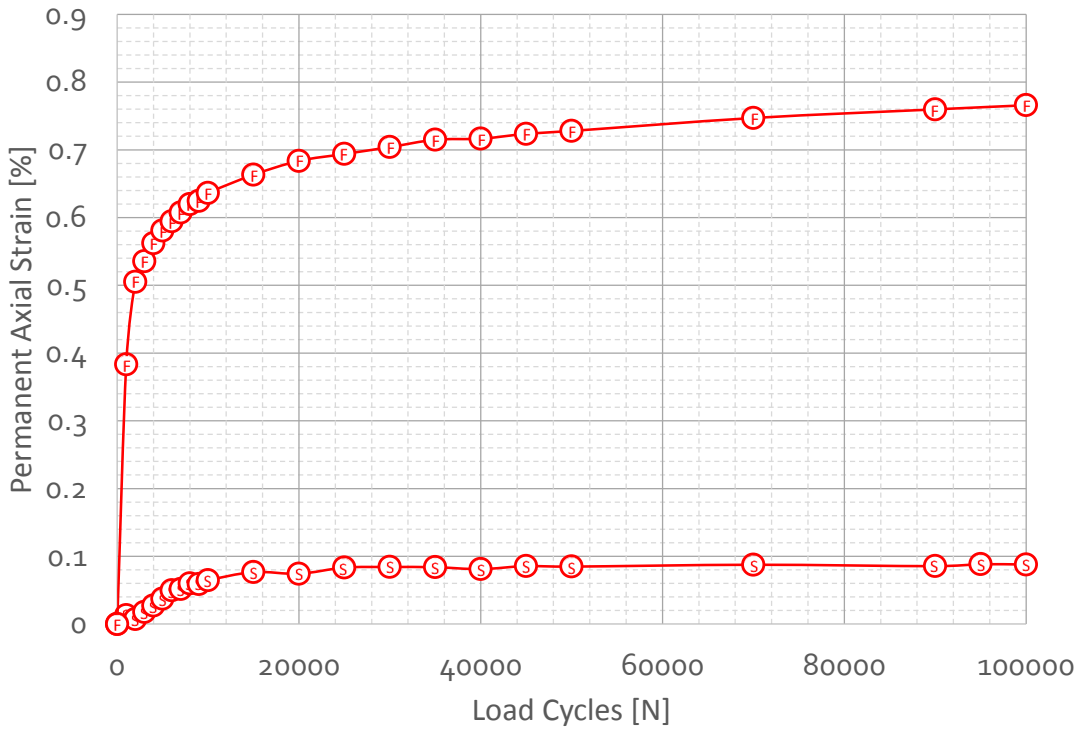

Figure C-8: First (F) and Second (S) Intermittent results for 50/17 Exposed RCA

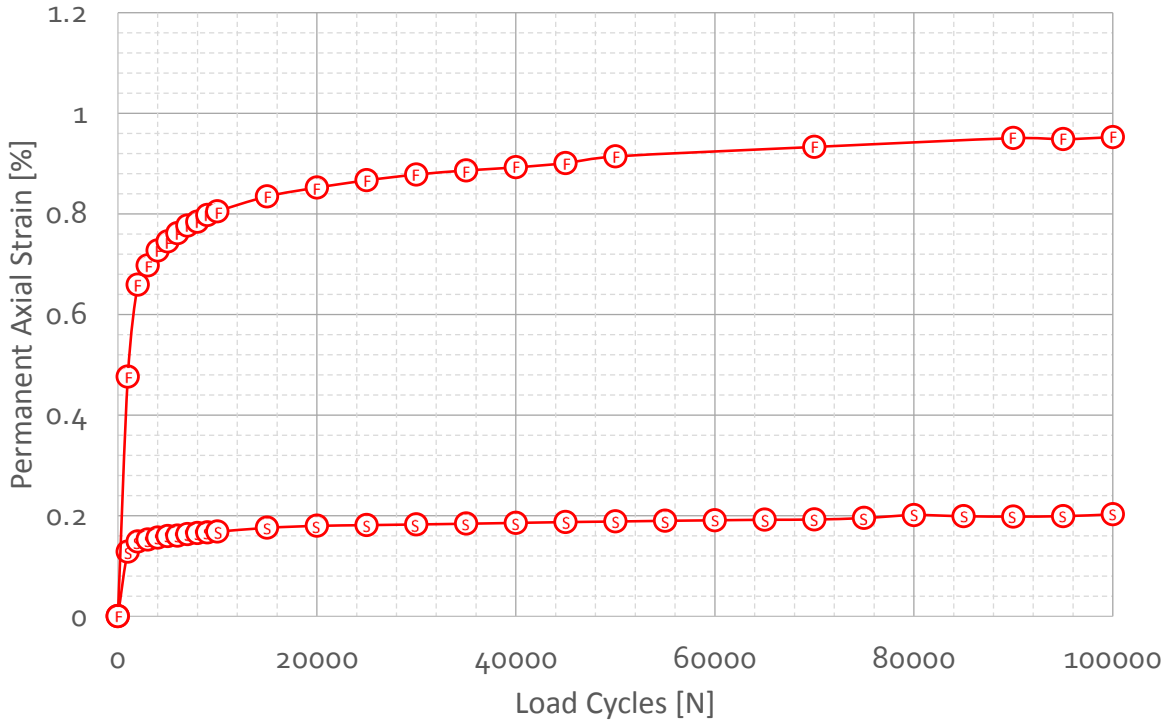

Figure C-9: First (F) and Second (S) Intermittent results for 50/22 Exposed RCA

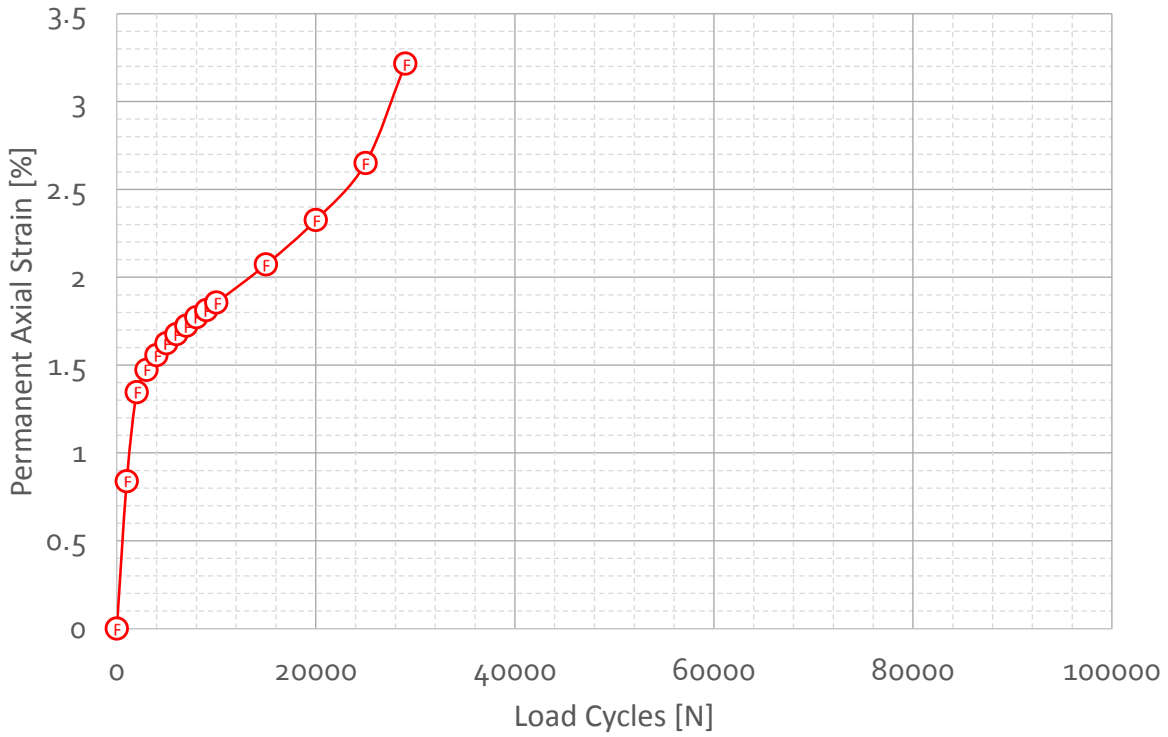

Figure C-10: First (F) Intermittent result for 50/27 Exposed RCA

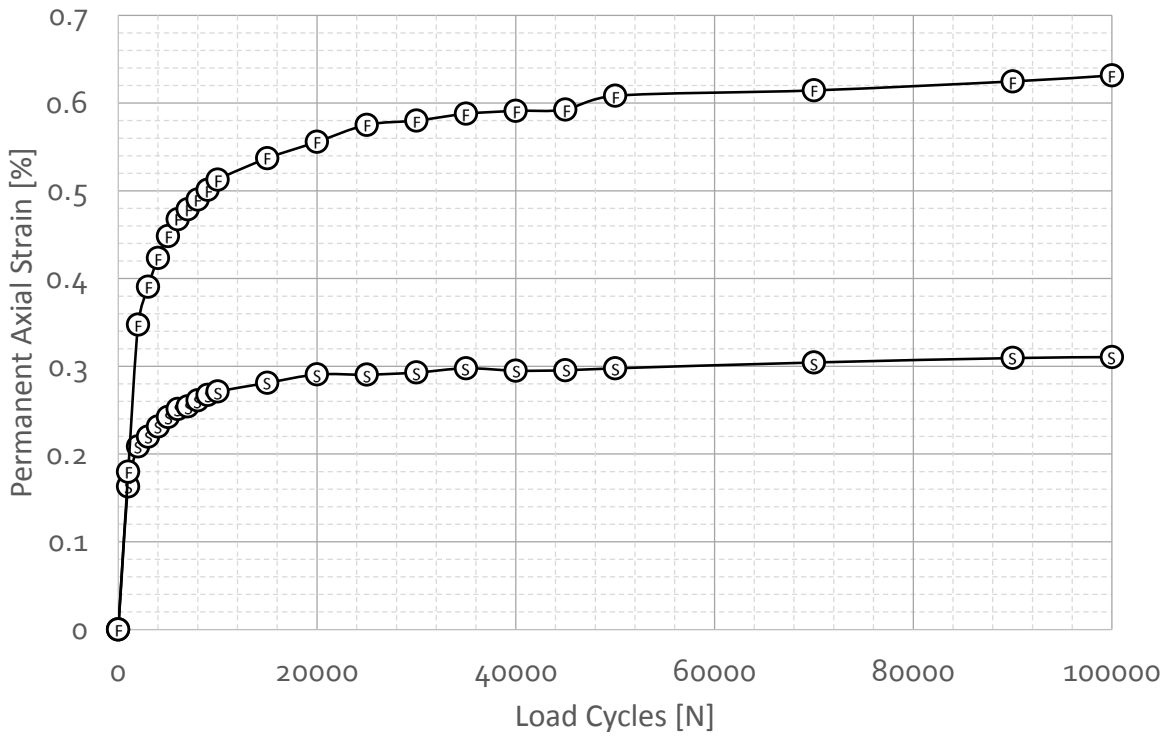

Figure C- 11: First (F) and Second (S) Intermittent results for 100/17 Exposed RCA

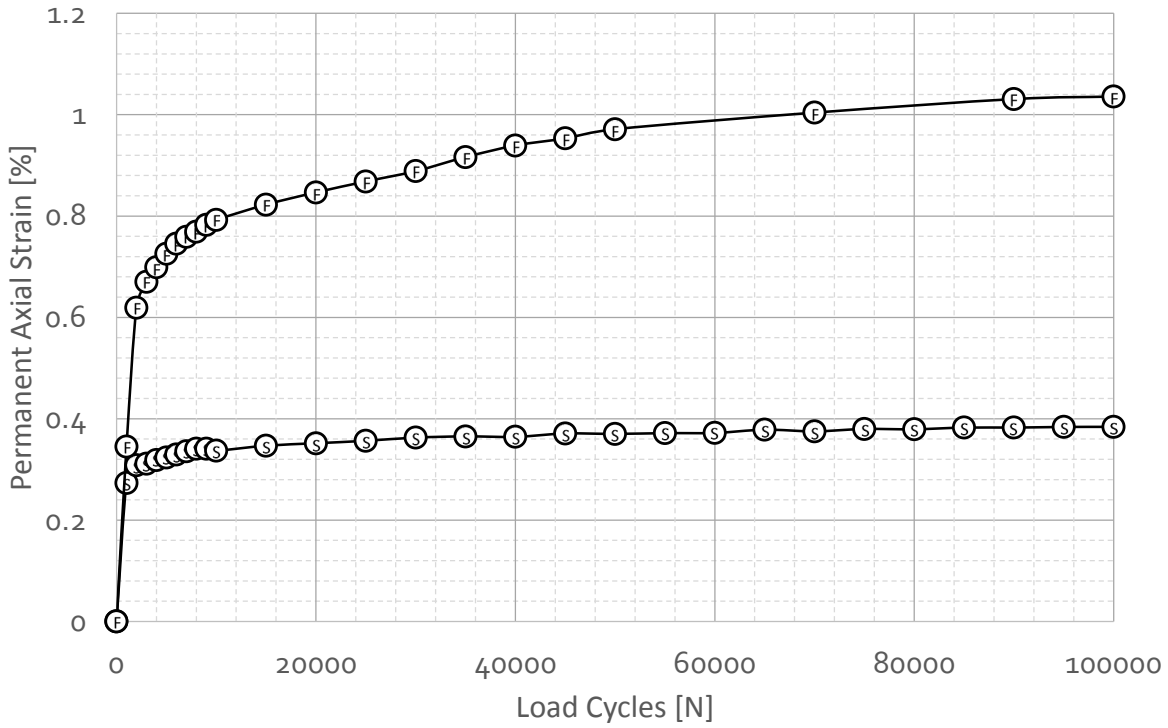

Figure C-12: First (F) and Second (S) Intermittent results for 100/22 Exposed RCA

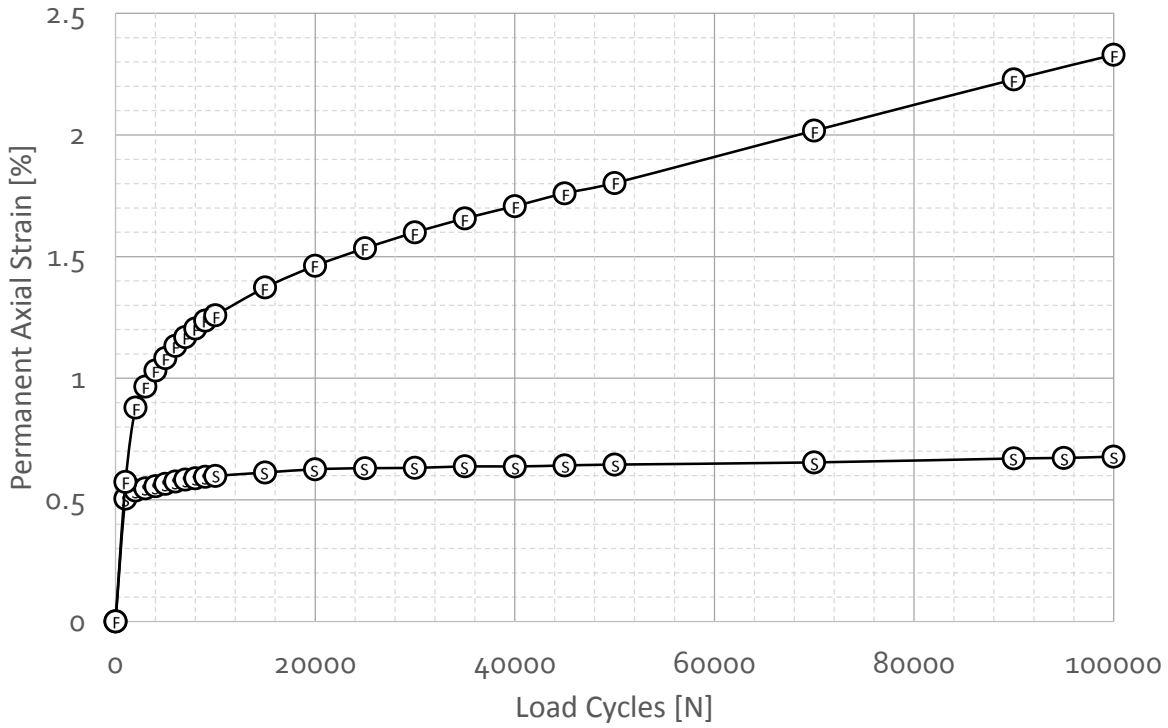

Figure C-13: First (F) and Second (S) Intermittent results for 100/27 Exposed RCA

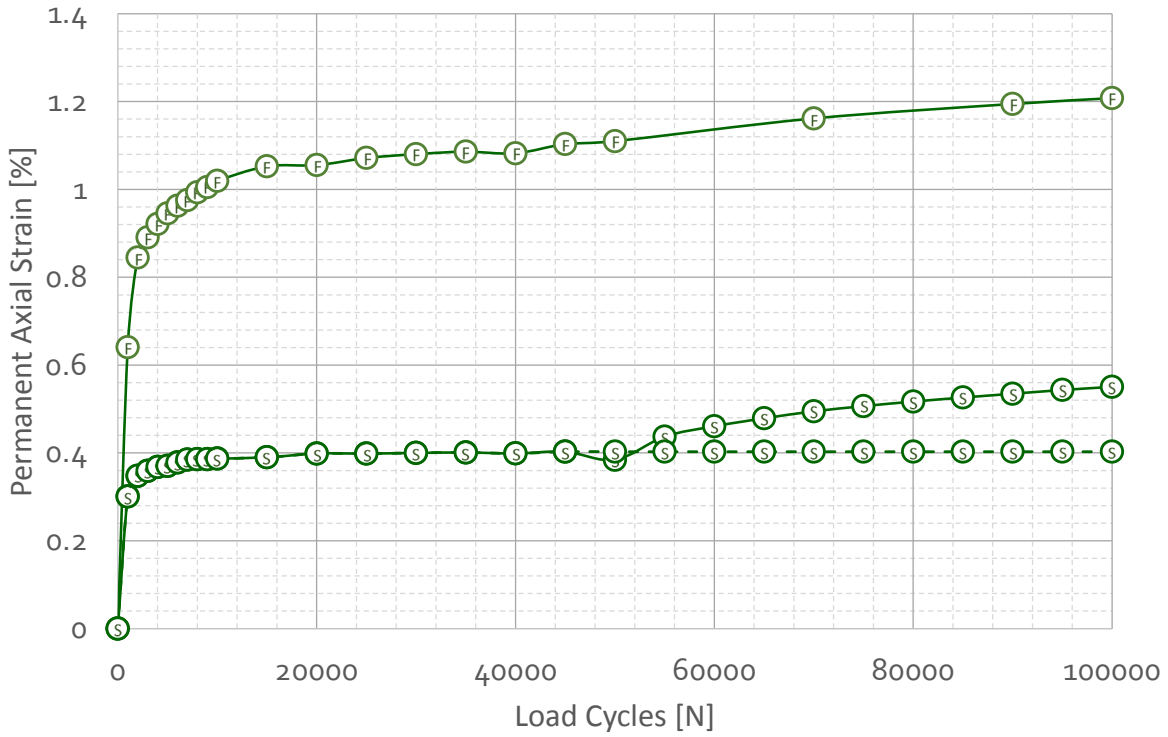

Figure C-14: First (F) and Second (S) Intermittent results for 150/17 Exposed RCA

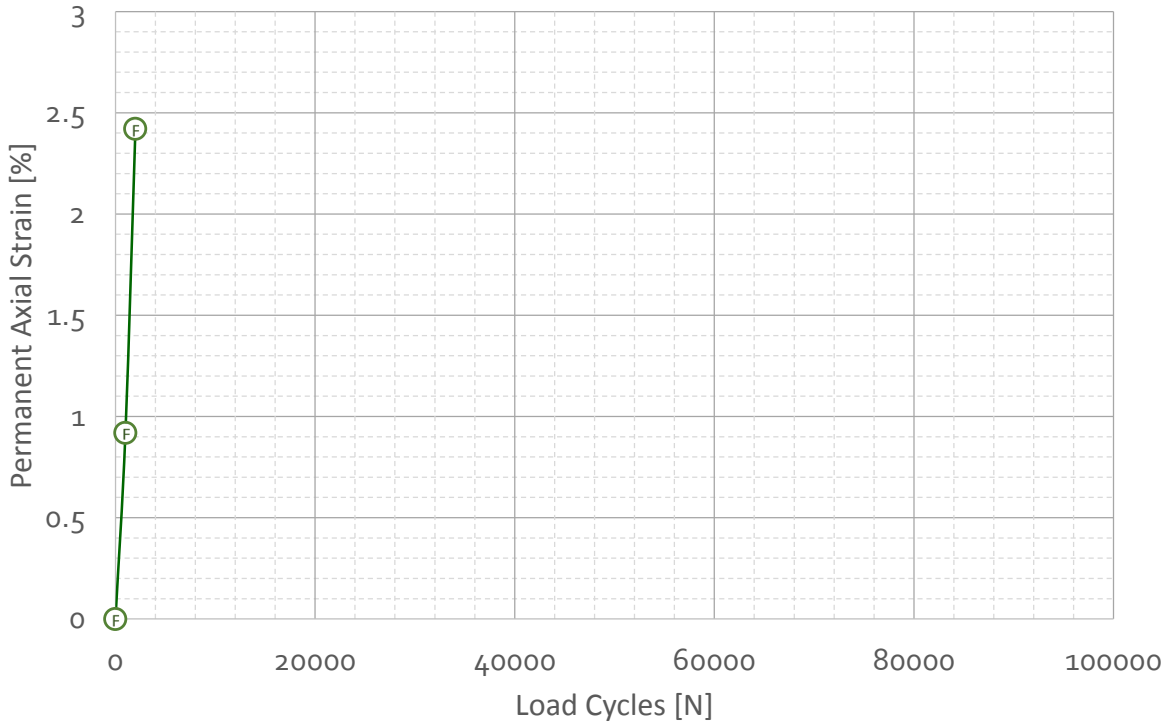

Figure C- 15: First (F) Intermittent result for 100/27 Exposed RCA

Annexure D: Modelling of Measured Data

Unexposed RCA

Basic

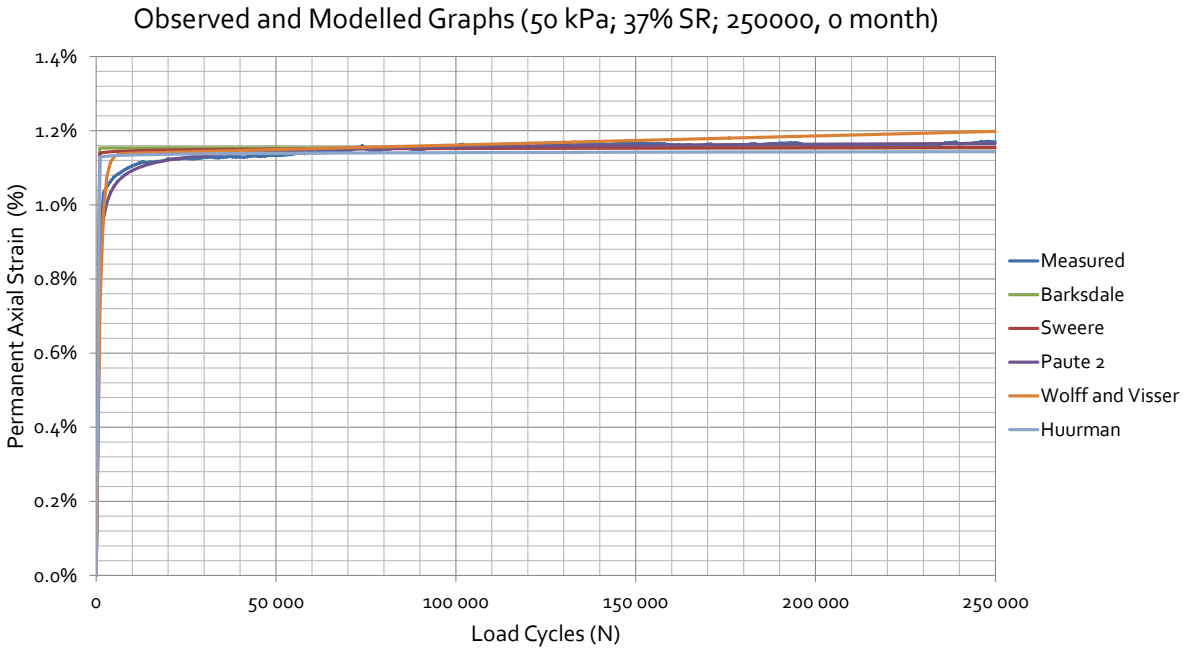

Figure D-1: Modelled Curves for Unexposed Basic 50/37

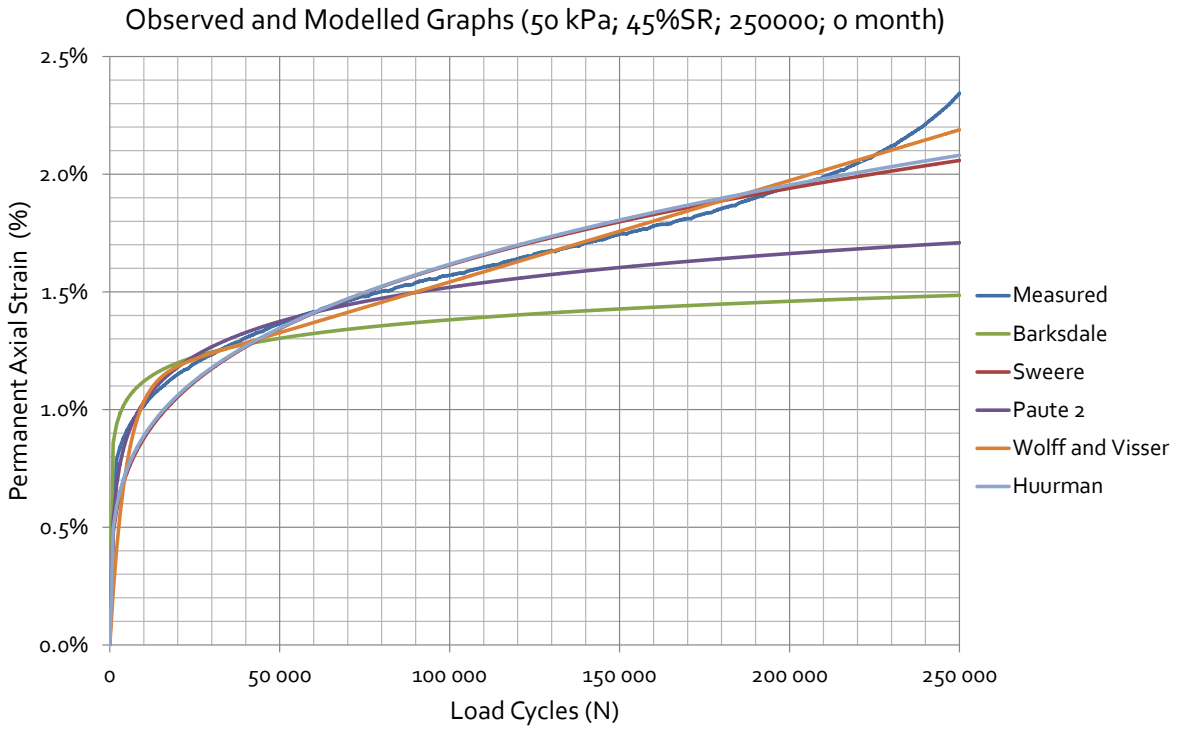

Figure D-2: Modelled Graphs for Unexposed Basic 50/45

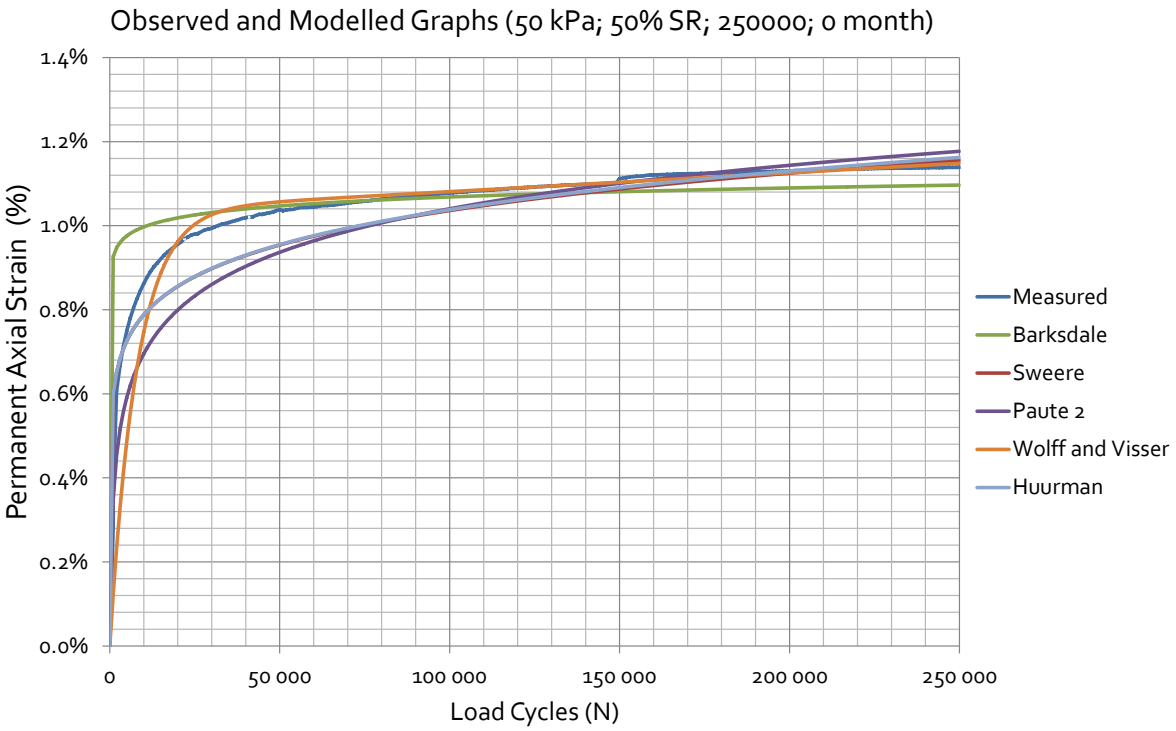

Figure D-3: Modelled Graphs for Unexposed Basic 50/45

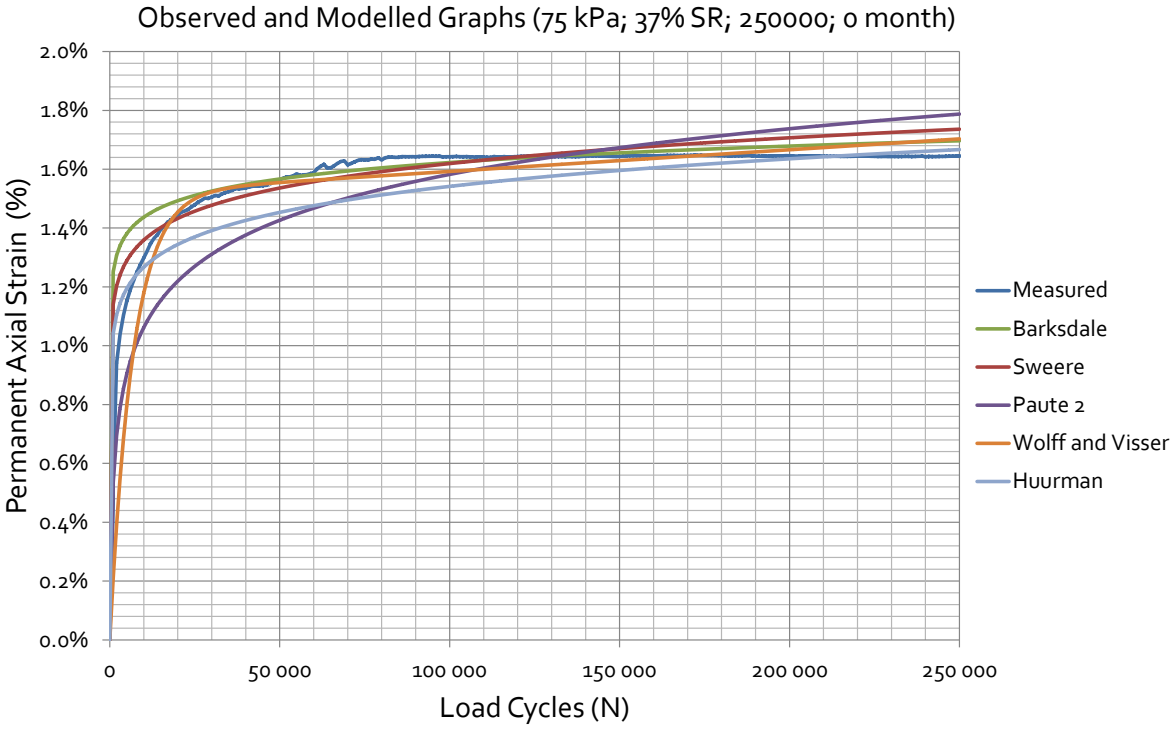

Figure D-4 Modelled Graphs for Unexposed Basic 75/37

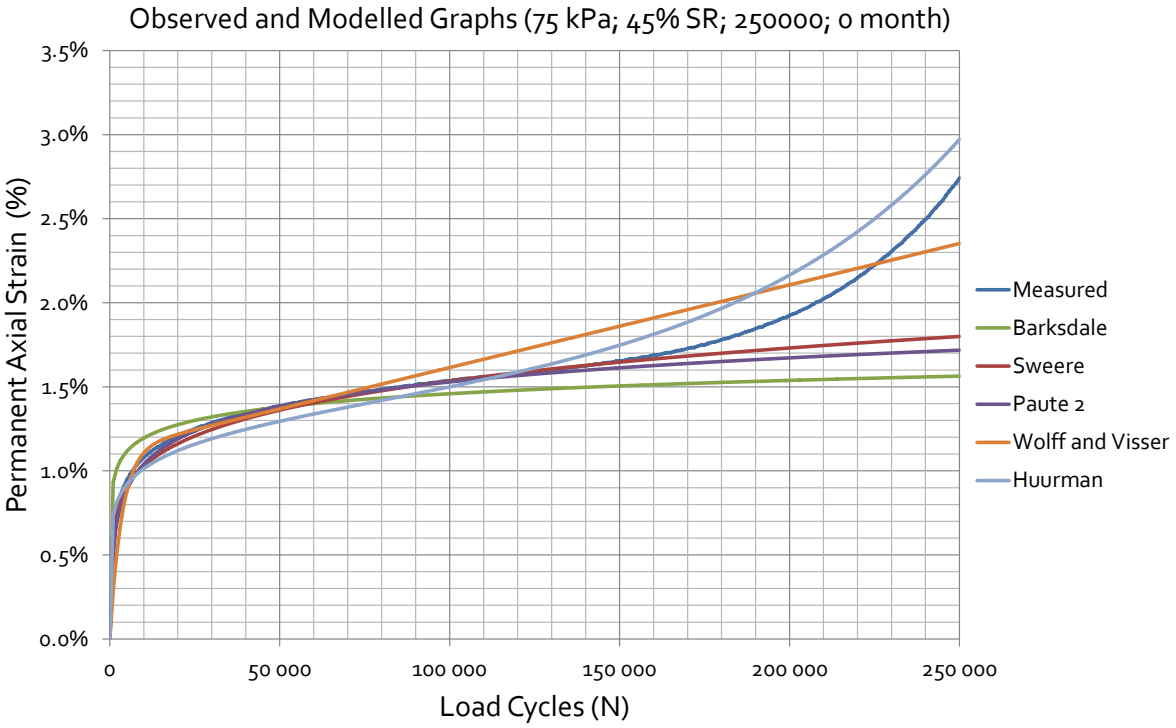

Figure D-5: Modelled Graphs for Unexposed Basic 75/45

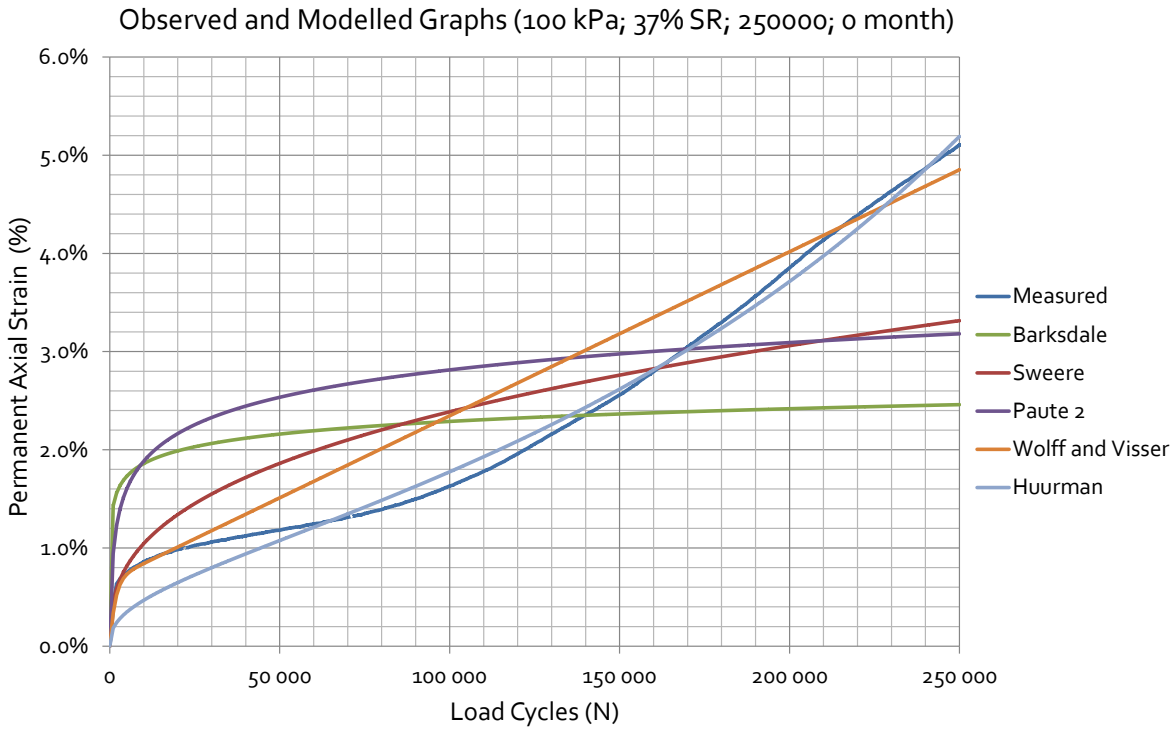

Figure D-6: Modelled Graphs for Unexposed Basic 50/45

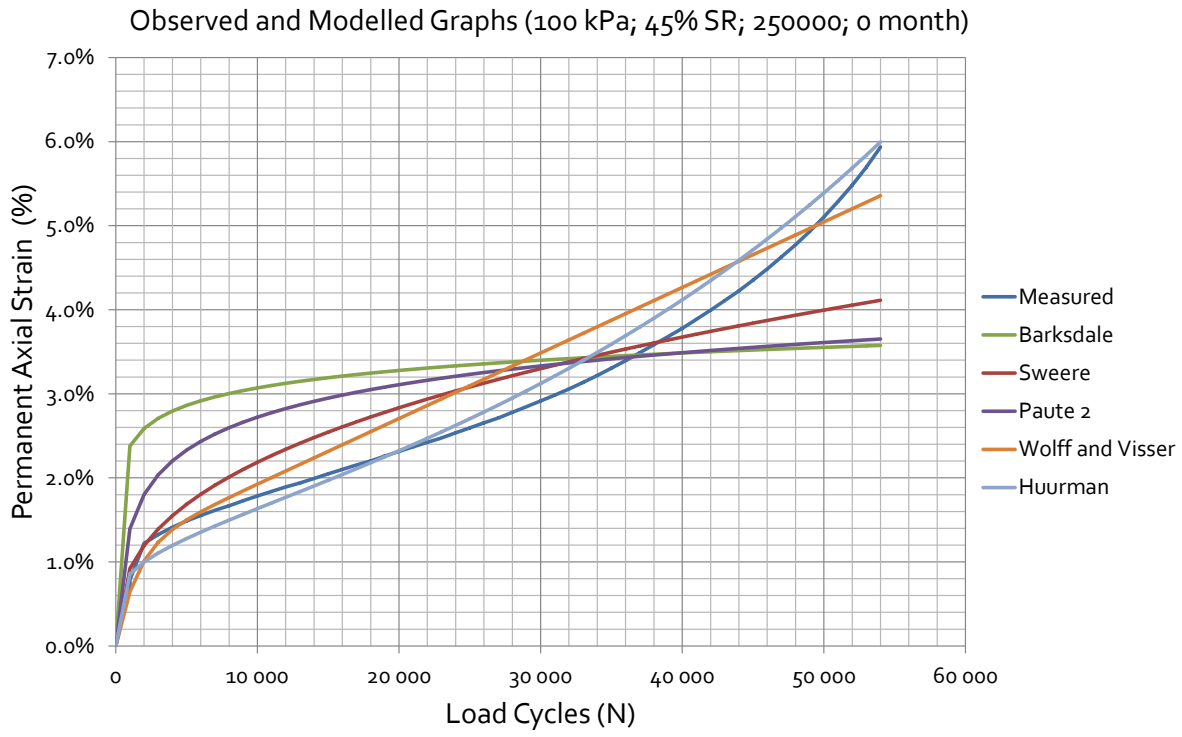

Figure D-7: Modelled Graphs for Unexposed Basic 100/45

Intermittent:

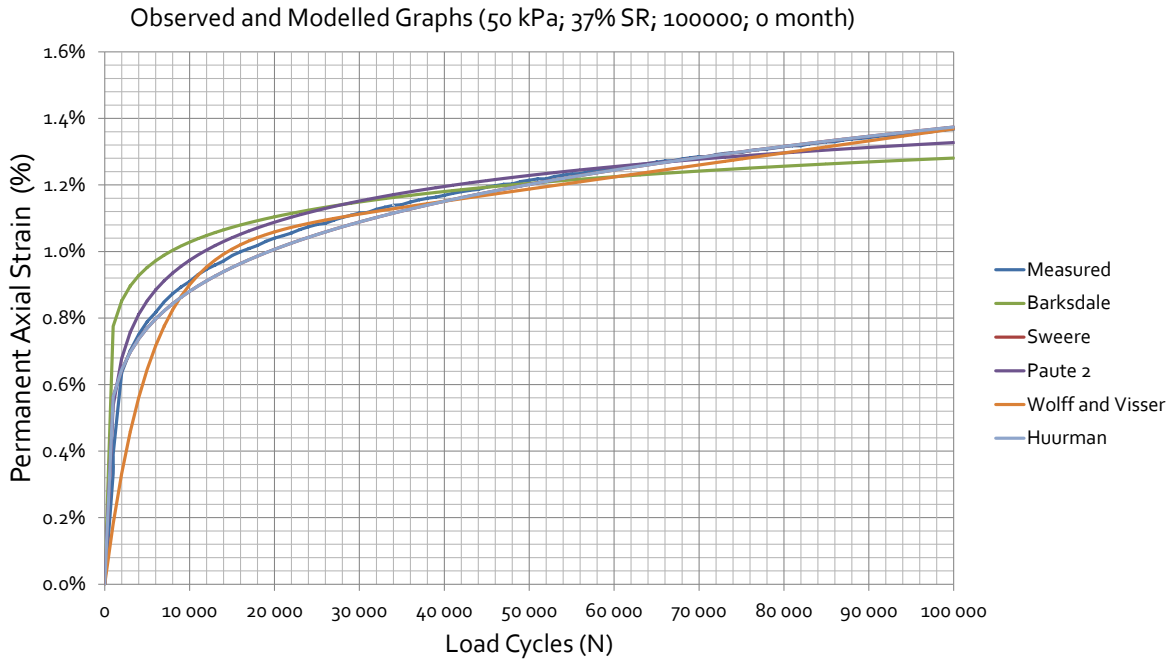

Figure D-8: Modelled Graphs for Unexposed Intermittent 50/37 for 0 month

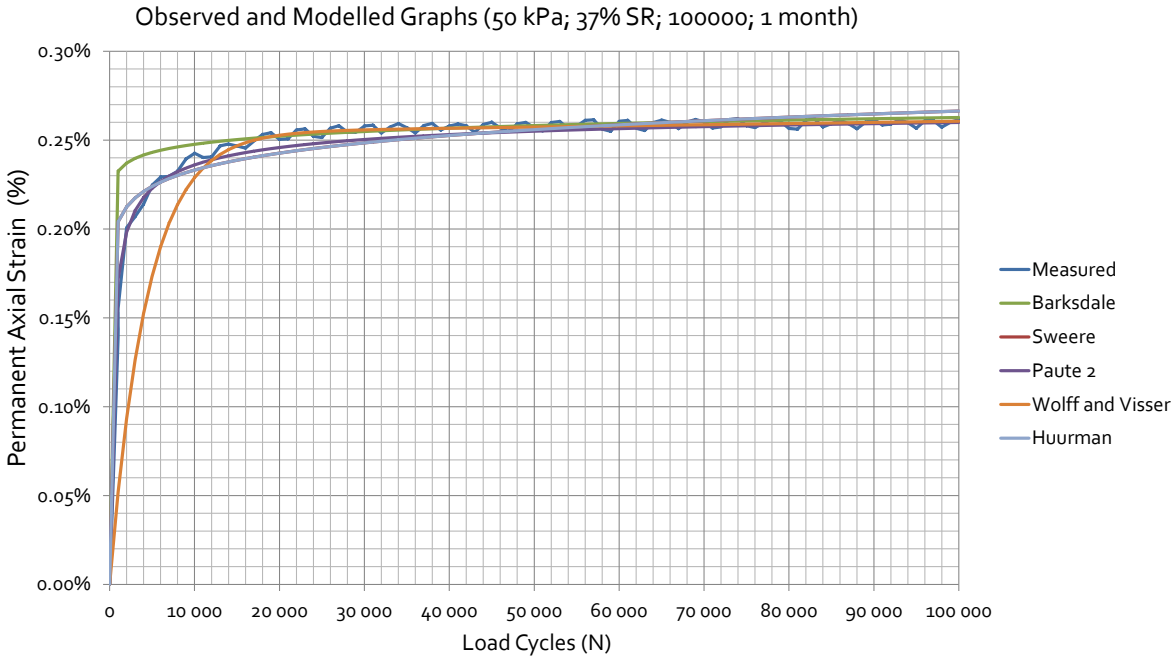

Figure D-9: Modelled Graphs for Unexposed Intermittent 50/37 for 1 month

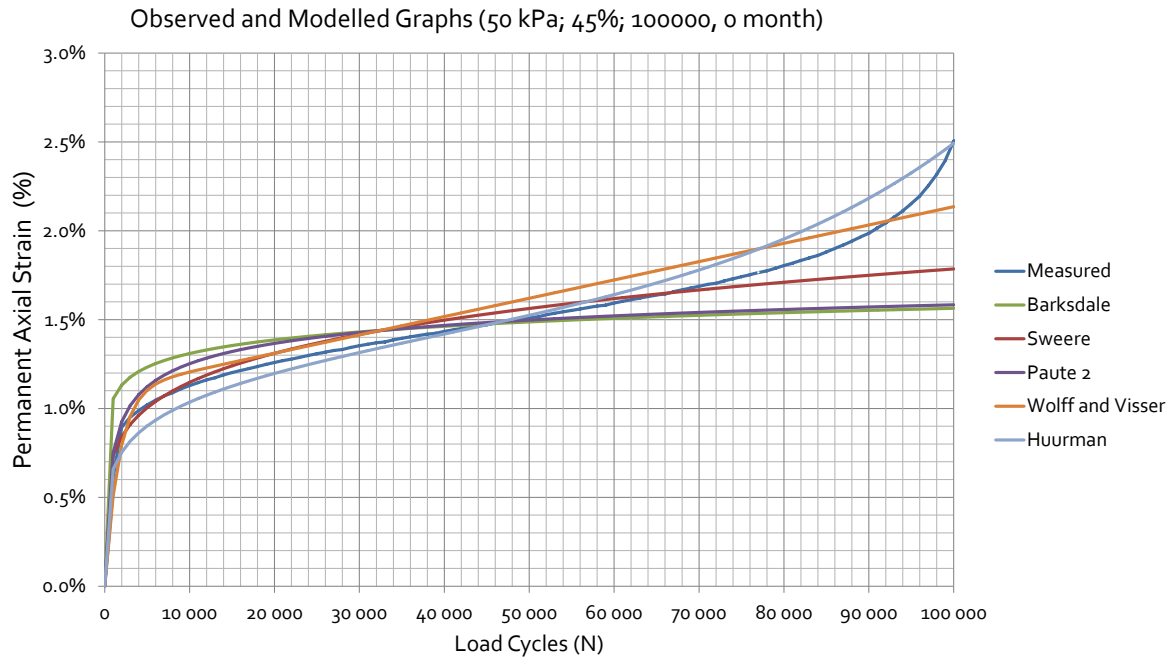

Figure D-10: Modelled Graphs for Unexposed Intermittent 50/45 for 0 month

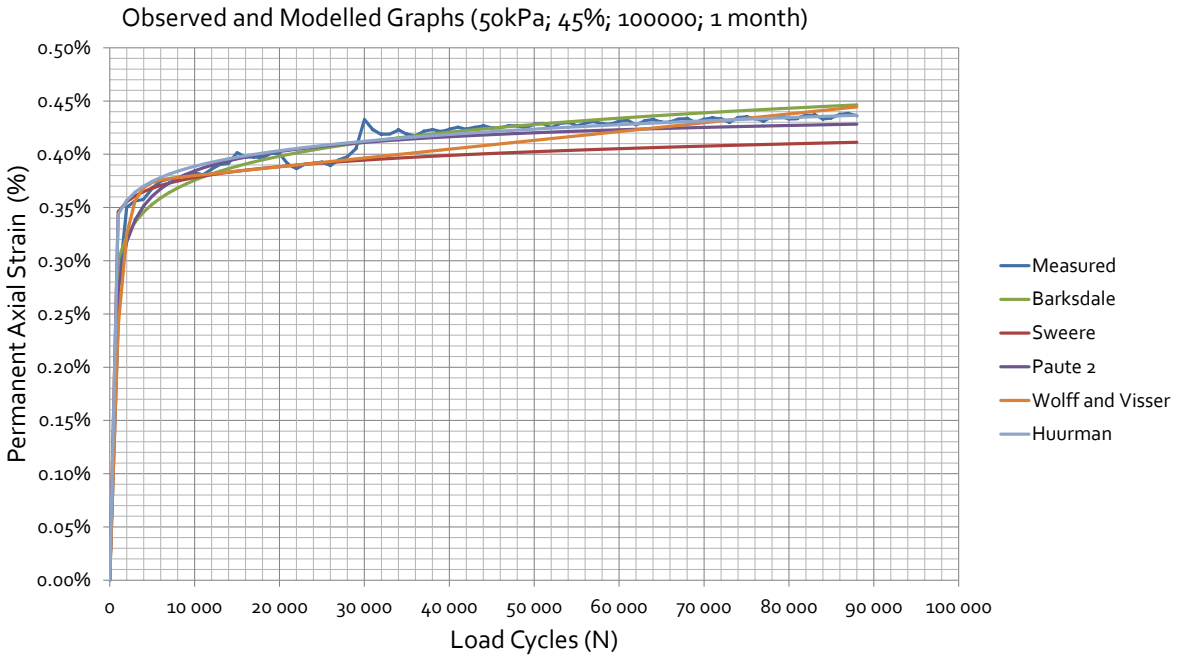

Figure D-11: Modelled Graphs for Unexposed Intermittent 50/45 for 1 month

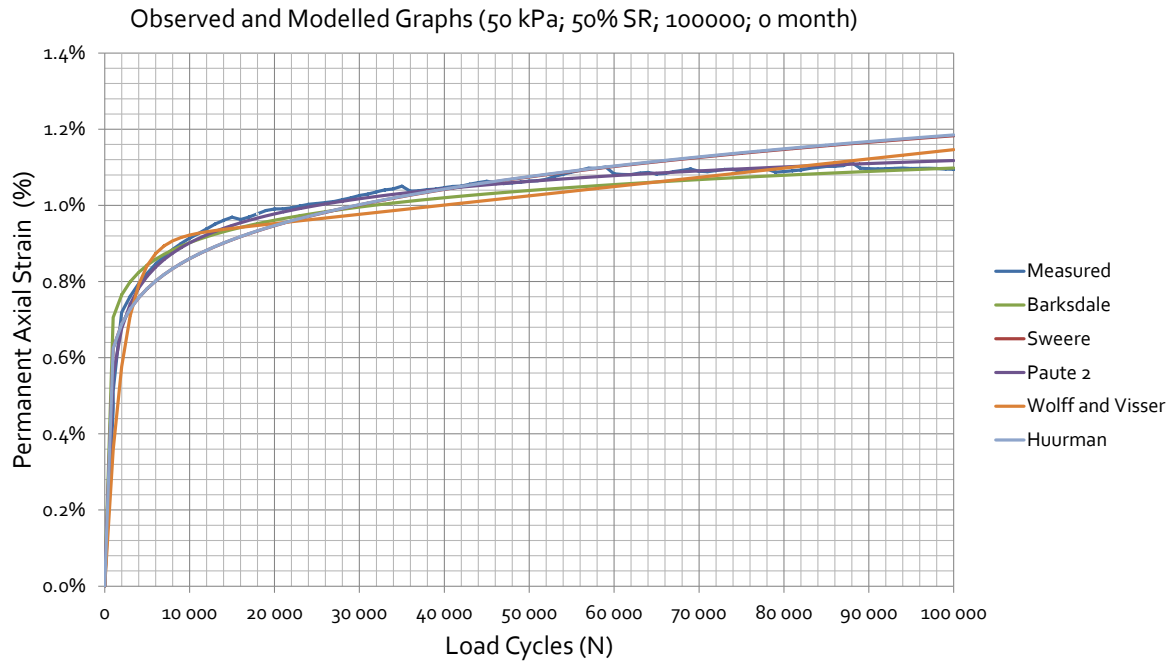

Figure D-12: Modelled Graphs for Unexposed Intermittent 50/50 for 0 month

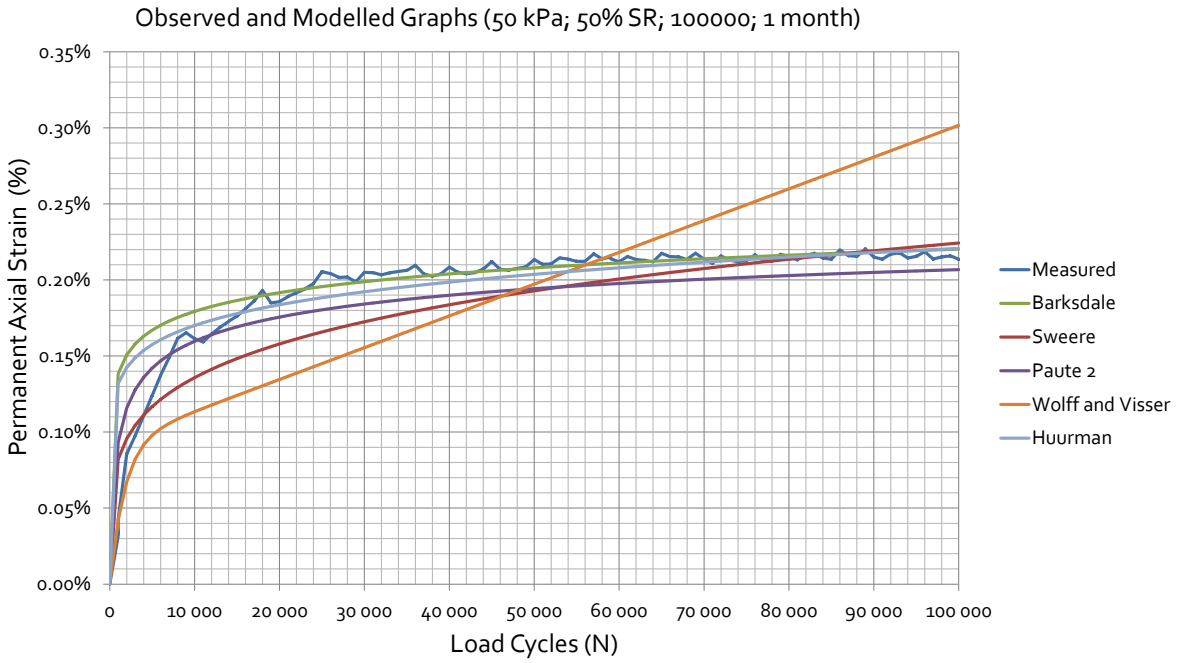

Figure D-13: Modelled Graphs for Unexposed Intermittent 50/50 for 1 month

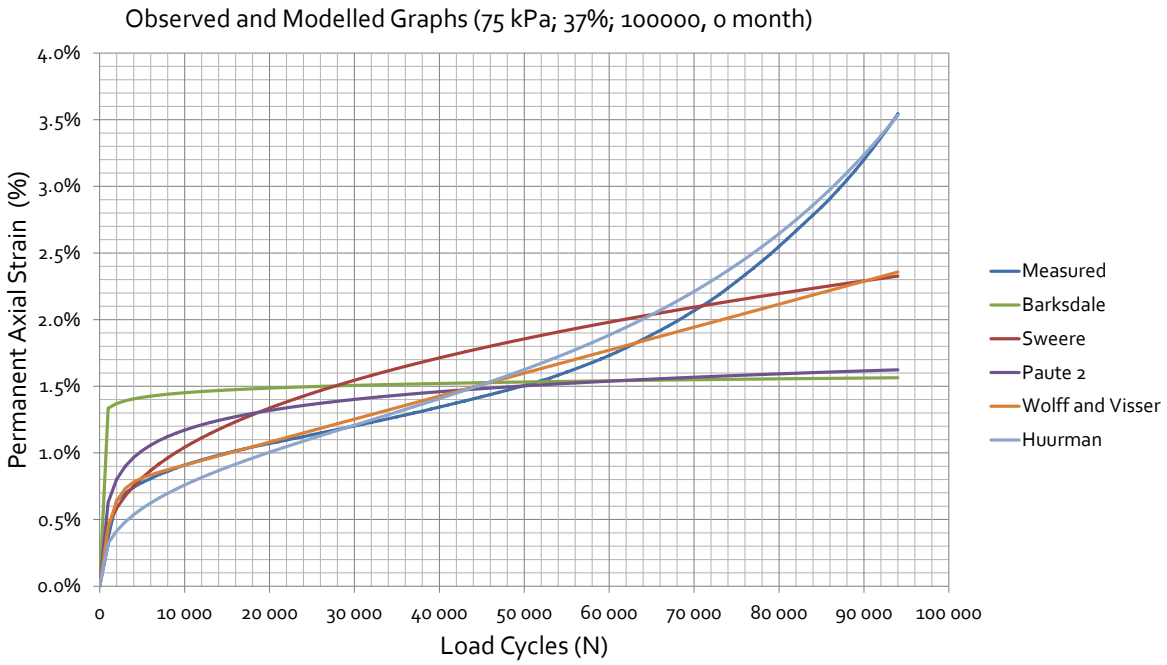

Figure D-14: Modelled Graphs for Unexposed Intermittent 75/37 for 0 month

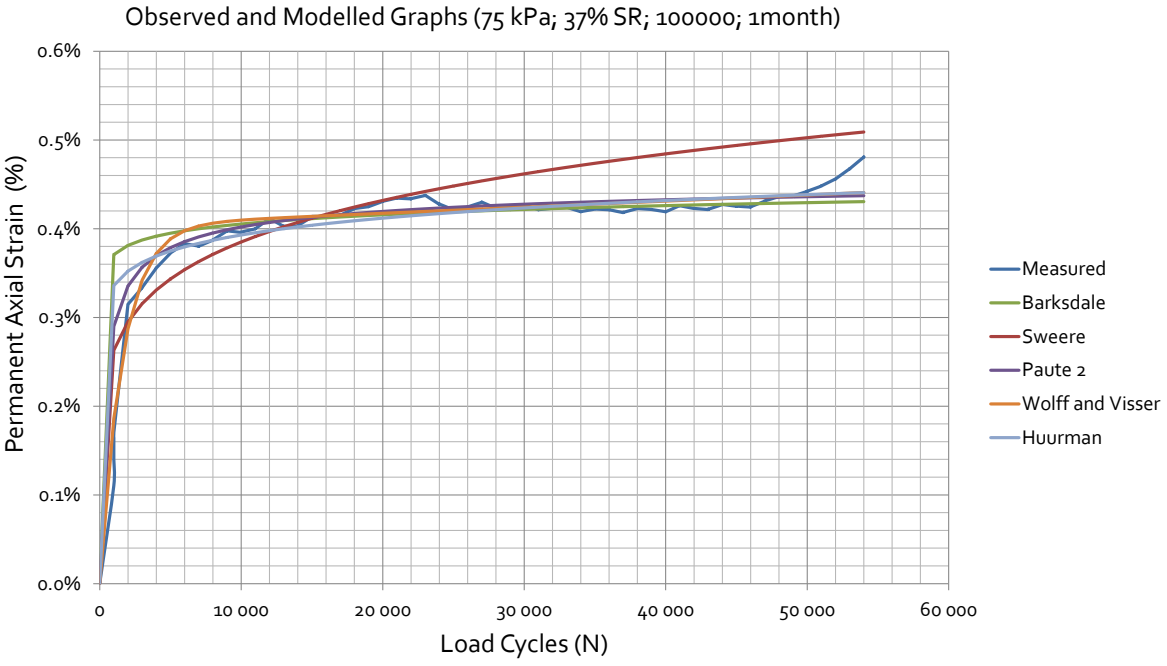

Figure D-15: Modelled Graphs for Unexposed Intermittent 75/37 for 1 month

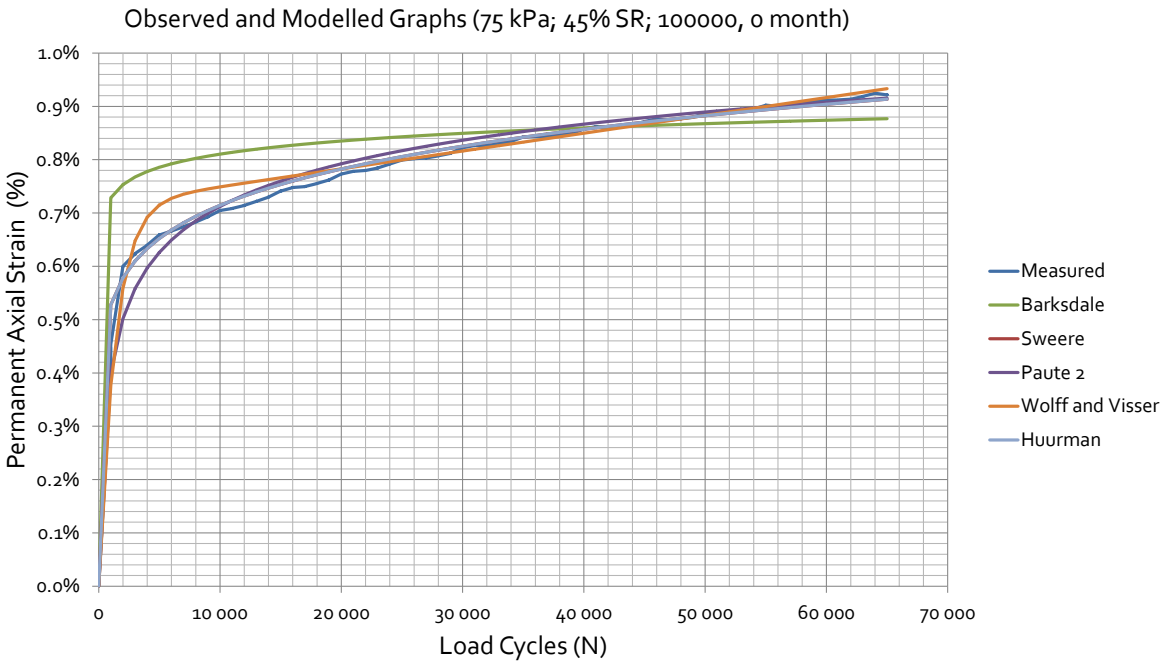

Figure D-16: Modelled Graphs for Unexposed Intermittent 75/45 for 0 month

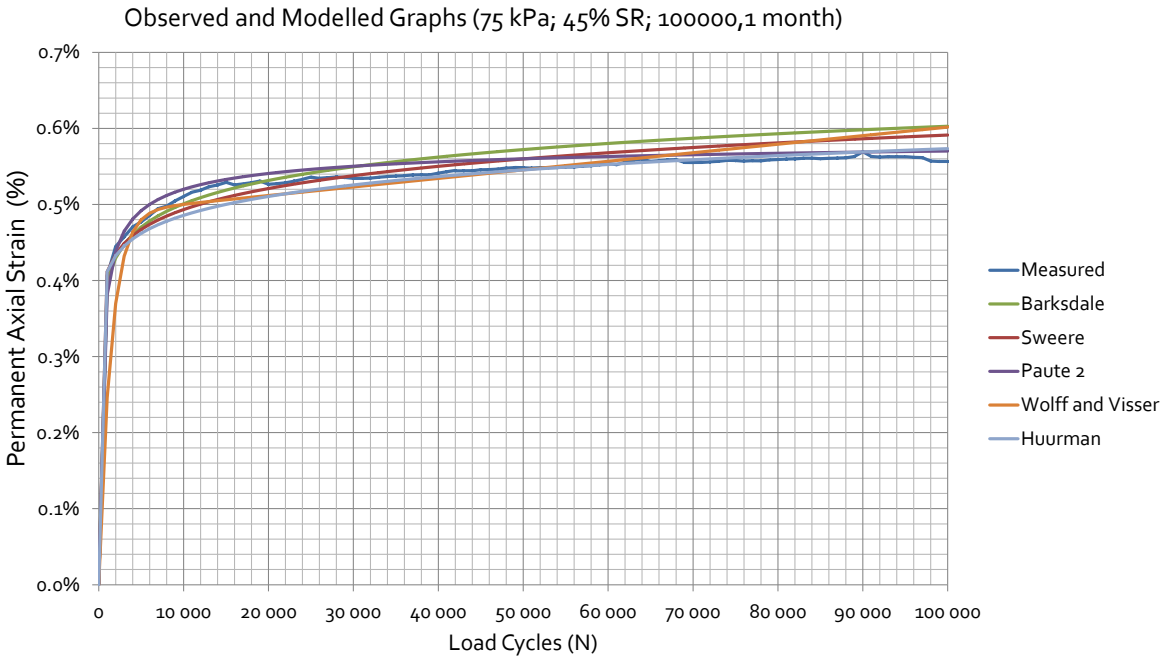

Figure D-17: Modelled Graphs for Unexposed Intermittent 75/45 for 1 month

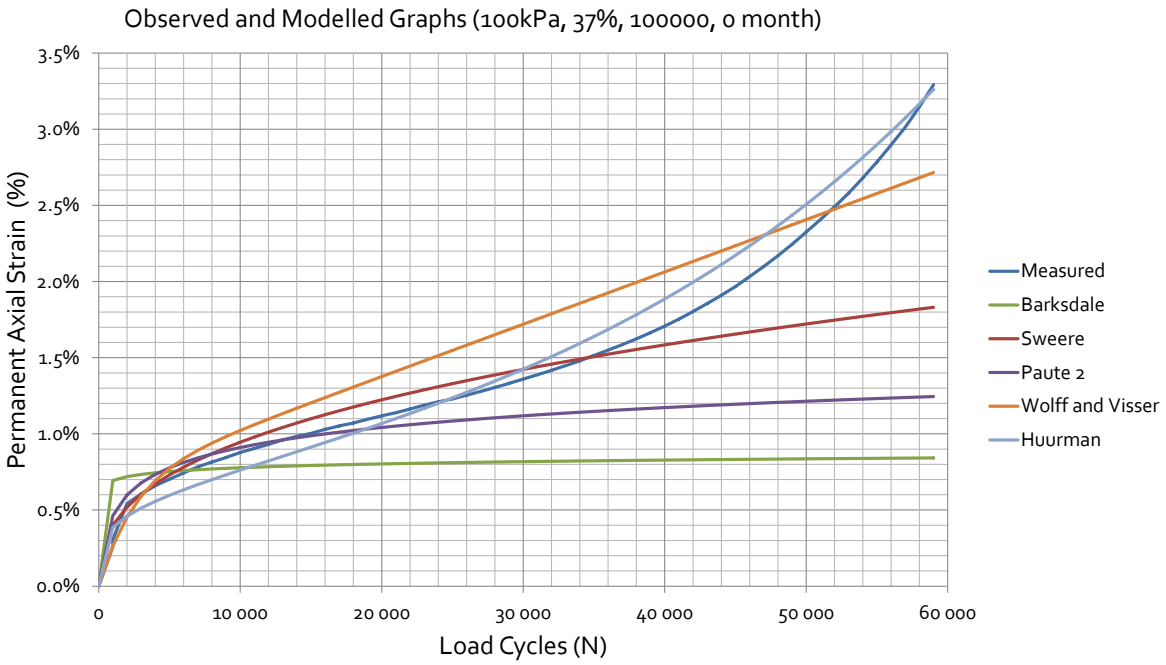

Figure D-18: Modelled Graphs for Unexposed Intermittent 100/37 for 0 month

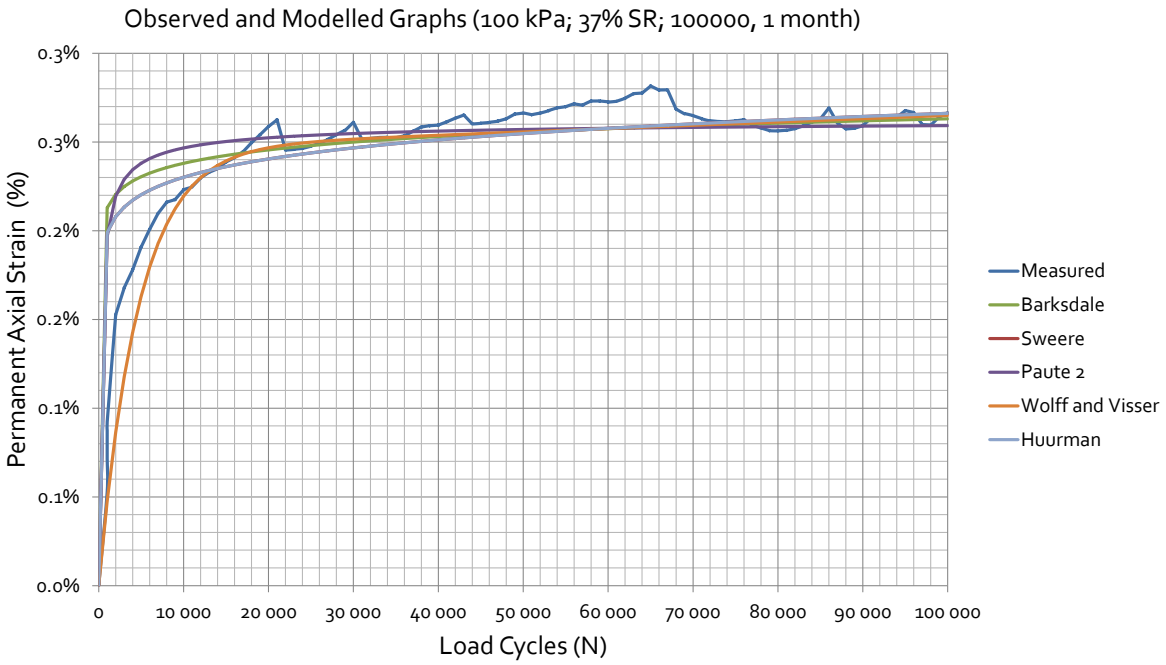

Figure D-19: Modelled Graphs for Unexposed Intermittent 100/37 for 1 month

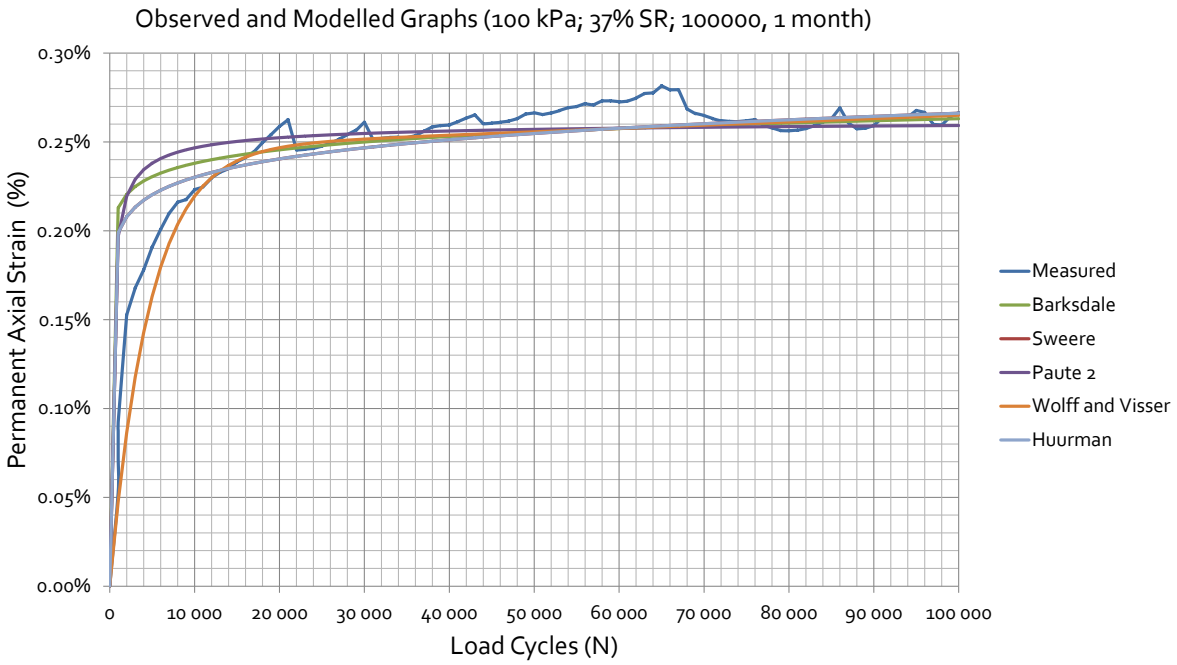

Figure D-20: Modelled Graphs for Unexposed Intermittent 100/45 for 0 month

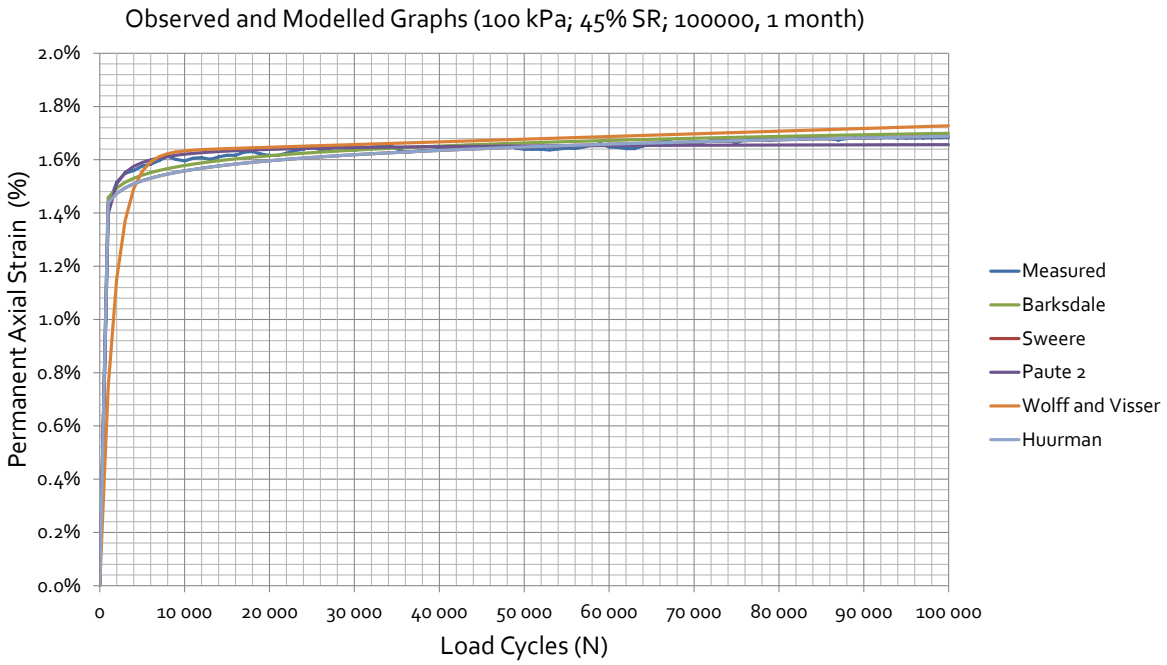

Figure D-21: Modelled Graphs for Unexposed Intermittent 100/45 for 1 month

Annexure E: Stress Dependent Iterative process for Pavement Design

Table E-1: Iterative Process for base layers in Reference Pavement A

Base Layer 1						
Iteration	E-mod	σ_1	σ_2	σ_3	θ	Mr
1	500	-704.576	-581.176	-581.176	1866.928	1398.67
2	1398.67	-738.184	-738.184	-692.116	2168.484	1543.96
3	1543.96	-709.943	-460.237	-460.237	1630.417	1279.05
4	1279.05	-753.377	-753.377	-691.796	2198.55	1558.05
5	1558.05	-711.169	-711.169	-693.456	2115.794	1519.09
6	1519.09	-722.535	-722.535	-693.128	2138.198	1529.69

Base Layer 2						
Iteration	E-mod	σ_1	σ_2	σ_3	θ	Mr
1	500	-572.658	-131.565	-131.565	835.788	822.915
2	822.915	-508.763	-25.239	-25.239	559.241	631.229
3	631.229	-613.827	-307.318	-307.318	1228.463	1061.09
4	1061.09	-503.878	-19.121	-19.121	542.12	618.407
5	618.407	-519.159	-65.149	-65.149	649.457	696.715
6	696.715	-515.629	-54.271	-54.271	624.171	678.691

Base Layer 3						
Iteration	E-mod	σ_1	σ_2	σ_3	θ	Mr
1	500	-398.295	43.197	43.197	441.492	540.034
2	540.034	-320.395	146.545	146.545	466.94	560.382
3	560.382	-421.931	87.376	87.376	509.307	593.442
4	593.442	-311.834	163.808	163.808	475.642	567.253
5	567.253	-328.033	154.55	154.55	482.583	572.703
6	572.703	-324.117	157.867	157.867	481.984	572.233

Table E-2: Iterative Process for base layers in Reference Pavement B

Base Layer 1						
Iteration	E-mod	σ_1	σ_2	σ_3	θ	Mr
1	500	-718.803	-455.292	-455.292	1629.387	1278.52
2	1278.52	-706.959	-585.577	-585.577	1878.113	1404.2
3	1404.2	-707.882	-579.589	-579.589	1867.06	1398.74
4	1398.74	-707.863	-579.895	-579.895	1867.653	1399.03
5	1399.03	-707.862	-579.903	-579.903	1867.668	1399.04
6	1399.04	-707.862	-579.904	-579.904	1867.67	1399.04

Base Layer 2						
Iteration	E-mod	σ_1	σ_2	σ_3	θ	Mr
1	500	-654.287	-228.852	-228.852	1111.991	993.57
2	993.57	-594.185	-120.259	-120.259	834.703	822.21
3	822.21	-597.83	-123.551	-123.551	844.932	828.846
4	828.846	-597.723	-123.499	-123.499	844.721	828.71
5	828.71	-597.72	-123.496	-123.496	844.712	828.704
6	828.704	-597.718	-123.489	-123.489	844.696	828.694

Base Layer 3						
Iteration	E-mod	σ_1	σ_2	σ_3	θ	Mr
1	500	-518.007	-160.433	-160.433	357.574	469.887
2	469.887	-457.113	-125.87	-125.87	331.243	446.754
3	446.754	-460.867	-128.011	-128.011	332.856	448.189
4	448.189	-460.712	-127.856	-127.856	332.856	448.189
5	448.189	-460.707	-127.852	-127.852	332.855	448.188
6	448.188	-460.707	-127.854	-127.854	332.853	448.186

Table E-3: Iterative Process for base layers in Reference Pavement C

Base Layer 1						
Iteration	E-mod	σ_1	σ_2	σ_3	θ	Mr
1	500	-714.196	-466.656	-466.656	1647.508	1287.89
2	1287.89	-742.705	-742.705	-691.742	2177.152	1548.03
3	1548.03	-708.541	-708.541	-693.394	2110.476	1516.57
4	1516.57	-724.708	-724.708	-693.025	2142.441	1531.69
5	1531.69	-721.356	-721.356	-693.159	2135.871	1528.59
6	1528.59	-722.331	-722.331	-693.136	2137.798	1529.5

Base Layer 2						
Iteration	E-mod	σ_1	σ_2	σ_3	θ	Mr
1	500	-626.216	-188.146	-188.146	1002.508	927.876
2	927.876	-506.046	-12.058	-12.058	530.162	609.37
3	609.37	-519.497	-64.041	-64.041	647.579	695.384
4	695.384	-514.81	-51.096	-51.096	617.002	673.536
5	673.536	-515.982	-55.281	-55.281	626.544	680.393
6	680.393	-515.698	-54.499	-54.499	624.696	679.068

Base Layer 3						
Iteration	E-mod	σ_1	σ_2	σ_3	θ	Mr
1	500	-472.168	-50.805	-50.805	421.363	523.655
2	523.655	-319.512	138.631	138.631	458.143	553.391
3	553.391	-329.481	149.383	149.383	478.864	569.786
4	569.786	-323.52	157.212	157.212	480.732	571.252
5	571.252	-324.546	157.365	157.365	481.911	572.176
6	572.176	-324.184	157.844	157.844	482.028	572.268

Table E-4: Iterative Process for base layers in Pavement 1

Base Layer 1						
Iteration	E-mod	σ_1	σ_2	σ_3	θ	Mr
1	500	-718.803	-455.292	-455.292	-1629.387	848.362
2	848.362	-715.593	-512.324	-512.324	-1740.241	877.612
3	877.612	-715.474	-514.519	-514.519	-1744.512	878.721
4	878.721	-715.585	-514.061	-514.061	-1743.707	878.512
5	878.512	-715.576	-514.095	-514.095	-1743.766	878.527
6	878.527	-715.589	-514.055	-514.055	-1743.699	878.51

Base Layer 2						
Iteration	E-mod	σ_1	σ_2	σ_3	θ	Mr
1	500	-654.287	-228.852	-228.852	-1111.991	696.837
2	696.837	-633.144	-208.288	-208.288	-1049.72	676.459
3	676.459	-632.13	-201.53	-201.53	-1035.19	671.621
4	671.621	-632.494	-202.21	-202.21	-1036.914	672.197
5	672.197	-632.467	-202.197	-202.197	-1036.861	672.179
6	672.179	-632.512	-202.39	-202.39	-1037.292	672.323

Base Layer 3						
Iteration	E-mod	σ_1	σ_2	σ_3	θ	Mr
1	500	-518.007	-160.433	-160.433	-838.873	602.688
2	602.688	-488.478	-132.356	-132.356	-753.19	570.157
3	570.157	-488.785	-134.435	-134.435	-757.655	571.895
4	571.895	-489.015	-134.426	-134.426	-757.867	571.978
5	571.978	-488.988	-134.407	-134.407	-757.802	571.953
6	571.953	-488.983	-134.337	-134.337	-757.657	571.896

Table E-5: Iterative Process for base layers in Pavement 2

Base Layer 1						
Iteration	E-mod	σ_1	σ_2	σ_3	θ	Mr
1	500	-706.804	-576.529	-576.529	-1859.862	908.179
2	908.179	-698.577	-664.262	-664.262	-2027.101	949.357
3	949.357	-699.44	-653.163	-653.163	-2005.766	944.198
4	944.198	-699.32	-654.416	-654.416	-2008.152	944.776
5	944.776	-699.336	-654.184	-654.184	-2007.704	944.668
6	944.668	-699.334	-654.208	-654.208	-2007.75	944.679

Base Layer 2						
Iteration	E-mod	σ_1	σ_2	σ_3	θ	Mr
1	500	-579.628	-180.008	-180.008	-939.644	638.947
2	638.947	-539.128	-79.751	-79.751	-698.63	548.499
3	548.499	-543.82	-88.564	-88.564	-720.948	557.454
4	557.454	-543.23	-86.948	-86.948	-717.126	555.93
5	555.93	-543.323	-87.127	-87.127	-717.577	556.11
6	556.11	-543.311	-87.095	-87.095	-717.501	556.08

Base Layer 3						
Iteration	E-mod	σ_1	σ_2	σ_3	θ	Mr
1	500	-390.982	94.6	94.6	-485.582	454.793
2	454.793	-355.417	101.507	101.507	-456.924	440.766
3	440.766	-361.075	94.972	94.972	-456.047	440.33
4	440.33	-360.572	94.948	94.948	-455.52	440.068
5	440.068	-360.684	94.812	94.812	-455.496	440.056
6	440.056	-360.675	94.811	94.811	-455.486	440.051

Table E-6: Iterative Process for base and subbase layers in Pavement 3

Base Layer 1						
Iteration	E-mod	σ_1	σ_2	σ_3	θ	Mr
1	500	-710.451	-536.525	-536.525	1783.501	1357.1
2	1357.1	-697.059	-692.889	-692.889	2082.837	1503.43
3	1503.43	-694.931	-681.244	-681.244	2057.419	1491.3
4	1491.3	-695.259	-676.151	-676.151	2047.561	1486.58
5	1486.58	-695.105	-678.088	-678.088	2051.281	1488.36
6	1488.36	-695.126	-677.353	-677.353	2049.832	1487.67

Base Layer 2						
Iteration	E-mod	σ_1	σ_2	σ_3	θ	Mr
1	500	-602.203	-195.527	-195.527	993.257	922.215
2	922.215	-534.926	-58.004	-58.004	650.934	697.76
3	697.76	-532.069	-40.095	-40.095	-612.259	670.114
4	670.114	-534.591	-45.344	-45.344	-625.279	679.486
5	679.486	-533.761	-42.509	-42.509	-618.779	674.816
6	674.816	-533.992	-43.191	-43.191	-620.374	675.963

Base Layer 3						
Iteration	E-mod	σ_1	σ_2	σ_3	θ	Mr
1	500	-428.744	12.121	12.121	440.865	539.527
2	539.527	-358.869	53.517	53.517	412.386	418.091
3	418.091	-364.538	24.164	24.164	388.702	405.547
4	405.547	-368.633	15.294	15.294	383.927	402.974
5	402.974	-368.06	14.53	14.53	382.59	402.251
6	402.251	-368.322	14.287	14.287	382.609	402.261

Subbase Layer 1						
Iteration	E-mod	σ_1	σ_2	σ_3	θ	Mr
1	300	-275.981	4.257	4.257	280.238	342.661
2	342.661	-222.984	35.446	35.446	258.43	328.659
3	328.659	-227.991	37.033	37.033	265.024	332.951
4	332.951	-231.123	34.844	34.844	265.967	333.561
5	333.561	-230.69	35.26	35.26	265.95	333.55
6	333.55	-230.843	35.263	35.263	266.106	333.651

Subbase Layer 2						
Iteration	E-mod	σ_1	σ_2	σ_3	θ	Mr
1	300	-164.907	30.563	30.563	195.47	284.639
2	284.639	-132.883	37.323	37.323	170.206	265.058
3	265.058	-136.391	36.801	36.801	173.192	267.443
4	267.443	-138.389	34.673	34.673	173.062	267.339
5	267.339	-138.065	35.211	35.211	173.276	267.509
6	267.509	-138.119	35.384	35.384	173.503	267.69

Subbase Layer 3						
Iteration	E-mod	σ_1	σ_2	σ_3	θ	Mr
1	300	-100.324	62.462	62.462	162.786	259.043
2	259.043	-83.901	48.394	48.394	132.295	232.8
3	232.8	-87.143	42.879	42.879	130.022	230.732
4	230.732	-88.41	38.102	38.102	126.512	227.503
5	227.503	-88.354	37.28	37.28	125.634	226.688
6	226.688	-88.408	37.098	37.098	125.506	226.569